Uncoupling of growth and defence in the *Arabidopsis thaliana* mutant *chs3-2D*, by optimization of chemicals and identification of putative receptors

Martine Wilhelmina Maria Keijzer

Dissertation zur Erlangung der Würde des Doktors der Naturwissenschaften der Fakultät

Mathematik, Informatik und Naturwissenschaften, Fachbereich Biologie

der Universität Hamburg

vorgelegt von

Martine Wilhelmina Maria Keijzer aus Jacobswoude

Hamburg, 2023

Vorsitzender der Prüfungskommission:	PD Dr. Hartwig Lüthen
1. Gutacher:	Prof. Dr. Stefan Hoth
2. Gutachterin:	Prof. Dr. Lars Voll
Datum der Disputation:	22.11.2023

Table of Contents

Abbreviations		///
1 Introduction		1
1.1 The immu	ne response in plants	1
	gered immunity in plants	
1.1.2 Effector-trig	gered immunity in plants	3
1.1.3 The auto-im	mune mutant CHILLING SENSITIVE 3-2D	4
1.2 Immunity and	growth are coupled via molecular pathways	6
1.3 The use of che	mical biology to discover Ro8-4304	10
2 Aim of the projec	t	11
3 Materials and me	ethods	12
3.1 Suppliers used	in this thesis	12
	methods for the organic synthesis of Ro8-4304 and its analogues	
	eagents, and solvents	
_	f the spectra	
	al synthesis of the building blocks for synthesis of Ro8-4304	
	al synthesis of Ro8-4304 and the Ro8-4304 derivatives	
_	synthesis of some small molecules used in this thesis	
	methods for biological experiments	
	ial and growth conditions	
•	chain reaction	
	ection assay	
• •	fication	
3.3.5 SA analysis .		49
	on of the chemical activity of Ro8-4304	
4.2 Organic chemi	cal modification of Ro8-4304	56
•	is of Ro8-4304	
	ue that binds to DADPA activated agarose	
_	ue that binds to NHS activated agarose (Ro-A07 and Ro-A08)	
	is of the analogues Ro-A09 to Ro-A12	
4.2.5 The synthes	is of the analogues Ro-A13 to Ro-A18	68
4.3 Biological activ	rity of the Ro8-4304 analogues	70
4.3.1 The effect o	f the analogues on the fresh weight of chs3-2D	70
	f Ro8-4304 analogues on the expression of immunity genes in <i>chs3-2D</i>	
	f Ro-A03 on immunity in <i>chs3-2D</i> mutants	
4.3.4 The effect o	f Ro-A03 on the methylosome in <i>chs3-2D icln2</i> double mutants	82
4.4 The determina	tion of Ro8-4304 binding proteins	83
4.4.1 Identificatio	n of putative binding proteins using matrix-bound Ro8-4304	83
4.4.2 Identificatio	n of putative binding proteins by literature search	85
4.5 A pharmacolog	gical analysis of Ro8-4304 activity	85
	emical bikinin alter the brassinosteroid signalling in the Ro8-4304 treated chs	

4.5.2 Does the NMDA antagonist ifenprodil influence the effect of Ro8-4304 in the chs3-2D seedlings? 87	7
4.5.3 Do calcium levels influence the effect of Ro8-4304 in the chs3-2D seedlings? 88	3
4.5.4 Does the NMDA antagonist DNQX influence the effect of Ro8-4304 in the chs3-2D seedlings? 90	
4.5.5 Does the NMDA agonist BMAA influence the effect of Ro8-4304 in the chs3-2D seedlings? 91	
4.5.6 Does calcium signalling influence the effect of Ro8-4304 in the chs3-2D seedlings?	<u>)</u>
4.5.7 Do the substrates of NMDA (spermine and spermidine) influence the effect of Ro8-4304 in the	
chs3-2D seedlings?	
4.5.8 Does ABA influence the effect of Ro8-4304 in the <i>chs3-2D</i> seedlings?	
4.5.9 Does GSH influence the effect of Ro8-4304 in the <i>chs3-2D</i> seedlings?	ō
4.5.10 Does GDA, an inhibitor of HSP90 protein, influence the effect of Ro8-4304 in the <i>chs3-2D</i>	
seedlings?)
4.5.11 Does UPC, an inhibitor of CDC48 protein, influence the effect of Ro8-4304 in the <i>chs3-2D</i>	
seedlings?	2
4.5.12 Do the natural substrates of NMDA receptors influence the effect of Ro8-4304 in the <i>chs3-2D</i>	
seedlings?	5
4.6 Generation and characterization of double mutants between chs3-2D and mutants lacking	
the respective gene encoding putative Ro8-4304 binding proteins105	5
	_
5 Discussion and conclusion114	ļ
5.1 Characterization of properties and chemical optimization of Ro8-4304114	ļ
5.1.1 Important properties of Ro8-4304 affecting growth and immunity of chs3-2D seedlings	
5.1.2 Ro8-4304 derivatives with novel properties have distinct effects on the performance of <i>chs3-2D</i>	
seedlings	5
5.1.3 The effect of Ro8-4304 and Ro-A03 on the methylosome mutant chs3-2D icln2	5
5.2 May the identified putative binding proteins play a role in Ro8-4304 activity? 117	7
5.2.1 The possible role of GLRs in Ro8-4304 activity	
5.2.2 The role of the putative binding protein CDC48A in Ro8-4304 activity	
5.2.3 The role of the putative binding protein CDC46A in Ro8-4304 activity	
5.2.4 The role of the putative binding protein GAPC in Ro8-4304 activity	
5.2.5 The role of the putative binding protein HSC in Ro8-4304 activity	
5.2.6 The role of the putative binding protein HSP90 in Ro8-4304 activity	
5.2.7 The role of the putative binding proteins GSTF2 and/ or GSTF7 in Ro8-4304 activity	
5.3 A model for the action of Ro8-4304131	L
5.4 Conclusive summary135	5
7 Literature	5
8 Abstract	5
9 German summary / Deutsche Zusammenfassung157	
10 Declaration of Oath158	3
11 Acknowledgment159)

Abbreviations

ABA Abscisic acid ACN Acetonitrile

AcOH Glacial acetic acid

ADP Adenosine-5'-diphophate
AFB AUXIN SIGNALLING F-BOX

AMPA α-AMINO-3-HYDROXY-5-METHYL-4-ISOXAZOLEPROPIONIC ACID RECEPTOR

ARF AUXIN RESPONSE FACTOR
At Arabidopsis thaliana
ATD Amino terminal domain
ATP Adenosine-5'-triphosphate

AtSR1 ARABIDOPSIS SINGAL RESPONSIVE 1

AUX/IAA AUXIN-INDUCIBLE/INDOLE-3-ACETIC ACID INDUCIBLE

BAK1 BRI1-ASSOCIATED RECEPTOR KINASE 1

BES1 BRI1-EMS-SUPRESSOR 1
bHLH Basic HELIX-LOOP-HELIX
BIK1 BOTRYTIS INDUCED KINASE 1
BIN2 BRIDGING INTEGRATOR 2

BIR1 BAK1-INTERACTING RECEPTOR LIKE KINASE

BMAA β -methylamino-L-alanine Boc₂O Di-tert-butyl-dicarbonate

Bp Base pairs
BR Brasinosteroid

BRI1 LRR-RK BRASSINOSTEROID-INSENSITIVE 1

BSO Buthionine sulfoximine
BSU BRI1 SUPPRESSOR 1
BTH Benzothiadiazole

BZR1 BRASSINAZOLE-RESISTANT 1

Ca²⁺ Calcium²⁺

CaCl₂ Calcium chloride

CaM CALMODULIN receptors

CAMTA3 CALMODULIN-BINDING TRANSCRIPTIONAL ACTIVATOR 3

CAPX CYTOSOLIC ASCORBATE PEROXIDASE

CBP60 CBP60 transcription factor

CC COILED COIL

CDC48 CELL DIVISION CYCLE 48

CDPKs CALCIUM-DEPENDENT PROTEIN KINASES
CERK1 CHITIN ELICITOR RECEPTOR KINASE 1

CFU Colony forming units
CHS1-3 CHILLING SENSITIVE 1 to 3

CNGC CYCLIC NUCLEOTIDE GATED CHANNEL

COI1 CORONATINE INSENSITIVE 1

CUL1 CULLIN1

CUL E3 CULLIN 3 UBIQUITIN E3 ligase

DAMPS Danger associated molecular patterns

DCC Dicyclohexylcarbodiimid

DCM Dichloromethane

DEG Differential expressed gene

DMSO Dimethylsulfoxide
DNA Deoxyribonucleic acid

DNQX 6,7-dinitroquinoxaline-2,3-dione

DTT Dithiothreitol

E4P Erythrose-4-phosphate

EDS1-90 ENHANCED DISEASE SUSCPETIBILITY 1-90 EFR ELONGATION FACTOR TU RECEPTORS

EGTA Ethylene glycol-bis-(β-aminoethyl ether)-N,N,N',N'-tetra-acetic acid

ER Endoplasmic reticulum
ETI Effector triggered immunity

EtOAc Ethyl acetate
EtOH Ethanol
Eq Equivalents

FLS2 LRR-RK-FLAGELLIN SENSING 2

G Gram

GA Gibberellins

GADPH Glyceraldehyde-3-phosphate dehydrogenase

GAPC GLYCERALDEHYDE-3-PHOSPHATE DEHYDROGENASE C SUBUNIT

GDA Geldanamycin gDNA Genomic DNA

GID1 GA INSENSITIVE DWARF 1

Gln L-glutamine
Glu L-glutamate
Gly L-glycine

GLRs Plant GLUTAMATE-LIKE RECEPTOR homologs

GR GLUCOCORTICOID RECEPTOR

GSH L-glutathione reduced

GSK3 GLYCOGEN SYNTHASE KINASE 3

GSTF2&7 GLUTATHIONE-S-TRANSFERASES 2 & 7

GO Gene ontology
GOI Gene of interest

H Hour H₂O Water

H₂O₂ Hydrogen Peroxide

HBI1 HOMOLOG OF BEE2 INTERACTING WITH IBH 1

HCl Hydrochloric acid

Hpa Hyaloperonospora arabidopsis

HR Hypersensitive response

HRS Hours

HSC70.1 HEAT SHOCK COGNATE 70.1 HSP81-2/90.2 HEAT SHOCK PROTEIN 81-2/90.2 ICS1 ISOCHORISMATE SYNTHASE 1

iGluRS Mammalian ionotropic glutamate receptors

JA Jasmonic acid

JAZ JASMONATE ZIM DOMAIN

Kb Kilobase kDa Kilodalton

KEGG Kyoto Encyclopaedia of Genes and Genomes

K₂CO₃ Kalium carbonate LBD Ligand Binding Domain

LIM LIN-11, ISL-1 and MEC-3 domain

LP Left primer

LRR LEUCINE RICH REPEAT

MAPKS MITOGEN ACTIVATED PROTEIN KINASES

MeOH Methanol
Met L-Methionine
Mg Milligram
MHz Mega hertz
Min Minutes

miR393 MicroRNA 393

mL Millilitre

½ MS½ Murashige and SkoogMSMass spectrometryMWMolecular weight

MYC MYC transcription factor M/Z Mass to charge ratio NAHCO₃ Sodium bicarbonate NaOH Sodium hydroxide Na₂SO₄ Sodium sulphate NB Nucleotide Binding NC Negative control

NDR1 NON-RACE-SPECIFIC DISEASE RESISTANCE 1
NIMIN1 NIM1 INTERACTING (NIM1 is allelic to NPR1)

NLRS NB and LRRs containing protein

NMDA N-METHYL-D-ASPARTATE RECEPTOR (an ionotropic glutamate receptor)

NMR Nuclear magnetic resonance

NO Nitric oxide

NPR1 NONEXPRESSOR OF PATHOGENESIS-RELATED GENES1

O₂ Superoxide radical
OH Hydroxyl radical
O/N Overnight

PAD4 PHYTOALEXIN DEFICIENT 4

PAGE Polyacrylamide gel electrophoresis

PAMPS Pathogen associated molecular patterns

PBS Phosphate buffered saline

PC Positive control

PCR Polymerase chain reaction

PDB Protein databank
PE Petroleum ether
PEPR1 PEP1 RECEPTOR 1
PLT1/PLT2 PLETHORA 1 and 2

PIFS PHYTOCHROME INTERACTING FACTORS

PIN2 PINFORMED 2

PR PATHOGENESIS RELATED

Pro L-proline

PRRS PATTERN RECOGNITION receptors
Pst Pesudomonas syringae pv tomato

PTI PAMP-triggered immunity

PTP-F 4-(4-fluorophenyl-1,2,3,6- tetrahydropyridine • HCl

qRT-PCR Quantitative real-time PCR

RAR1 REQUIRED FOR MLA12 RESISTANCE 1

RBOHD RESPIRATORY BURST OXIDASE HOMOLOG D

RK RECEPTOR KINASES
RLKs RECEPTOR-LIKE KINASES
RLPS RECEPTOR-LIKE PROTEINS

RNA Ribonucleic acid RNA-seq RNA sequencing

Ro8-4304 4-{3-[4-fluoro-phenyl-3, 6-dihyrdro-1(2H)-pyridyl]-2-hydoxy-propoxy}-

benzamide

ROS Reactive oxygen species

RP Right primer

RPM Rounds per minute
R proteins Resistance proteins
RPS RIBOSOMAL PROTEIN S2

RPT3 PROTEASOMAL REGULATORY PARTICLE AAA-ATPASE-3

RT Room temperature

RT-PCR Reverse transcription PCR

SA Salicylic acid

SAG101 SENESCENCE-ASSOCIATED GENE101 SAR Structure activity relationship study

SAR Systemic acquired resistance

SAUL1 SENESCENCE ASSOCIATED E3 UBIQUITIN LIGASE 1
SCF SKP-CULLIN-F-BOX E3 ubiquitin ligase complex

SE Standard error

SGT1b SUPPRESSOR OF THE G2 ALLELE OF SKP1, b

SKP1 S-PHASE KINASE PROTEIN 1

SLY1 SLY1, SLEEPY 1

SNC1-4 SUPPRESSOR OF *npr1-1*, CONSTITUTIVE 1-4

SRIP1 AtSR1 INTERACTING PROTEIN 1

TEA Triethylamine

TGA TGACG SEQUENCE-SPECIFIC BINDING PROTEIN

THF Tetrahydrofuran

TIR TOLL-INTERLEUKIN-1 RECEPTOR
TIR1 TRANSPORT INHIBITOR RESISTANT 1

TKL1 TRANSKETOLASE 1
TFA Trifluoroacetic acid
TFP Trifluoperazine·HCl
TFs Transcription factors

TPL TOPLESS

TTSS THE TYPE III SECRETION SYSTEM

 $\begin{array}{ll} \mu L & Micro-liter \\ \text{UPC} & \text{UPCDC30245} \\ \text{VOL} & \text{Volume} \end{array}$

WRKY DNA-BINDING PROTEIN

Weeks

WT Wild-Type

WKS

1 Introduction

Plants developed unique systems to survive, because of their inability to move. For example, their immune system was especially adapted so that plants can defend themselves against harmful pathogens on the spot. Plants growing on the field are constantly at risk of being invaded by pathogens and the global loss of crops is considerable ^{1,2}. However, plant immunity is an intricate process, and research in this area is vital if we want to maintain healthy crops in future harvests.

1.1 The immune response in plants

1.1.1 Pattern-triggered immunity in plants

The immunity pathway is activated when a pathogen tries to invade a plant. The pathogen is recognized as invader by the plant through microbial elicitors. These pathogen-associated molecular patterns (PAMPs) are identified by receptor proteins known as PATTERN RECOGNITION RECEPTORS (PRRs) ³. These receptors can be classified into two types, RECEPTOR-LIKE KINASES (RLKs) and RECEPTOR-LIKE-PROTEINS (RLPs) ⁴.

PAMPs are fundamental parts of the pathogen typical examples include flagellin or fungal chitin ⁴. In fact, any unfamiliar protein, carbohydrate, lipid or small molecules may be recognized as PAMP ⁵. Additionally, cell wall damage and cuticular fragments caused by the pathogen, are recognized as endogenous molecules, and these are termed danger-associated molecular patterns (DAMPs) ⁶.

Currently, the best researched PRRs are the receptor kinase FLAGELLIN SENSING 2 (FLS2) ⁷ and EF-TU RECEPTOR (EFR) ⁸. FLS2 is a typical LEUCINE-RICH-REPEAT (LRR) protein ⁷, which binds elicitors, like flagellin ⁹. After binding the receptor associates with a BRI1-ASSOCIATED RECEPTOR KINASE 1 (BAK1) to form an active signalling complex ^{10,11} this complex in turn phosphorylates the BOTYRIS INDUCED KINASE 1 (BIK1) ^{12,13}, to induce the PAMP-Triggered Immunity (PTI) ^{14,15}.

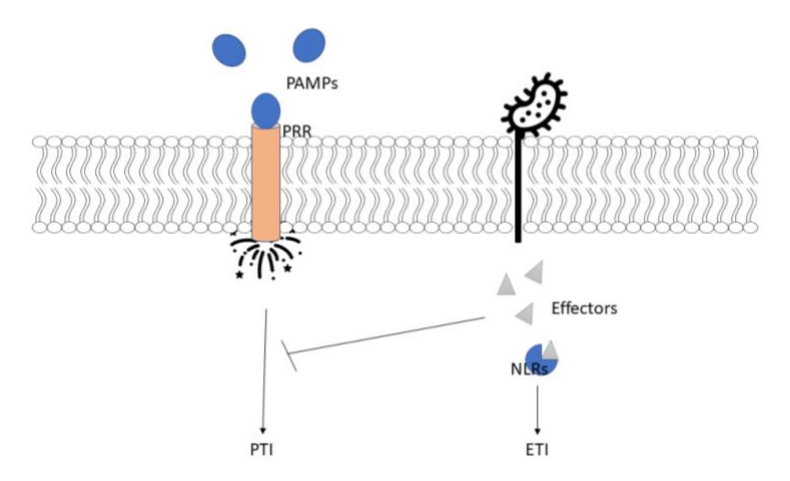


Figure 1. Elementary schematic representation of the plant immune system. PAMPs are recognized by PRR. This induces a signalling cascade resulting in PTI. Some pathogens are able to secrete effectors which are able to inhibit the immunity signalling. Nonetheless, effectors and changes mediated by these molecules can be recognized by NLRs leading to the onset of ETI.

One of the earliest events upon this induction is a transient elevation in cytosolic Ca^{2+} 16,17 . Several plasma membrane PRRs that interact with BAK1 have been implicated in Ca^{2+} release during plant-microbe interactions, including CHITIN ELICITOR RECEPTOR KINASE 1 (CERK1), FLS2, EFR, and PEP1 RECEPTOR 1 (PEPR1) $^{16,18-20}$. The calcium is probably transported into the cytosol via Ca^{2+} permeable channels such as the CYCLIC NUCLEOTIDE GATED CHANNEL (CNGC) and GLUTAMATE RECEPTOR-LIKE CHANNELS (GLR) 21 . The *cngc2*-null mutant defence no death1 and the *glr3.3-1* mutant have been demonstrated to be important for immunity $^{20,22-26}$.

The rise of cytosolic calcium results in the activation of MAP KINASES (MAPKs), and CALCIUM-DEPENDENT PROTEIN KINASES (CDPKs) $^{27-29}$. CPK5 was shown to phosphorylate RESPIRATORY BURST OXIDASE HOMOLOG D (RBOHD) 30 , hereby regulating the activity of downstream immune signalling. The phosphorylation and activation of these MAPKs further causes the activation of WRKY type transcription factors 31 . These transcription factors activate the expression of defence genes and also induce transcription of other WRKY factors 31,32 . Additionally, BIK1 directly interacts with and phosphorylates the RBOHD complex 33,34 . The activation of the RBOHD complex leads to the generation of reactive oxygen species (ROS) 35,36 , which include hydrogen peroxide (H_2O_2), superoxide radical (O_2 -), and hydroxyl radical (OH-). Previous research already indicated that the signalling of these molecules is vital during abiotic stresses. The ROS use a network comprising 152 genes to induce the immune signalling cascade 37,38 . Moreover, ROS are able to directly act as antimicrobial compounds, to reinforce the cell by cross-linking of cell wall components 33,34 . This may also induce the strengthening of the cell wall by deposition of callose and lignin $^{39-41}$.

One small molecule vital for the immune response is salicylic acid (SA). SA has a critical role in plant immunity by inducing systemic acquired resistance ⁴². Pathogen attack induces a rise of cytosolic Ca^{2+ 16,17,43}. This Ca²⁺ signal directly activate SA biosynthesis through the transcriptional activation of ISOCHORISMATE SYNTHASE 1 (ICS1) 44 via the CALMODULIN (CaM) BINDING transcription factor CBP60 ⁴⁵, ensuing an increase in SA levels. Wu et al. (2012) demonstrated that NONEXPRESSOR OF PATHOGENESIS-RELATED GENES1 (NPR1) directly binds SA ⁴⁶. However, recent research indicated that the NPR1 protein does not have considerable SA binding activity ⁴⁷. But the nuclear translocation of NPR1 is controlled through cellular redox change ⁴⁷. Normally, NPR1 remains in the cytoplasm as an oligomer through redox sensitive bonds. After pathogen attack, the disulphide bonds are reduced, resulting a conformational change, monomerization and translocation to the nucleus of NPR1 ⁴⁶. Here, NPR1-SA interacts with the enhanceosome by binding the BTB/POZ domain ^{48,49}. This interaction inhibits the molecular function of the TGA2 repression domain by excluding TGA2 oligomers from cognate DNA ^{48,49}. Removal of the TGA2 repression results in activation of the PATHOGENESIS RELATED 1 defence gene (PR1) ⁴⁸. The transcriptional activation of *PR* genes induces the production of lytic enzymes (chitinases), anti-microbial proteins (defensins) or anti-microbial secondary metabolites (phytoalexins) 50,51, which prevent the spread of pathogens. Interestingly, NPR1 is degraded by the proteasome in the nucleus to reduce the defence response, NPR1 is phosphorylated at an ικβ-like phosphodegron motif, ubiquitinylated by CULLIN 3 UBIQUITIN E3 (CUL E3) ligases and degraded to sustain maximum levels of active target gene expression ⁵². This degradation is controlled by the NPR1 paralogues NPR3 and NPR4 53. Both NPR3 and 4 function as adaptors of the CUL E3 in the absence of SA ⁵³. High amounts of SA disrupt the accessibility of NPR3 and NPR4 to NPR1, and via this system SA regulates the availability of NPR1 in the nucleus ^{53,54}.

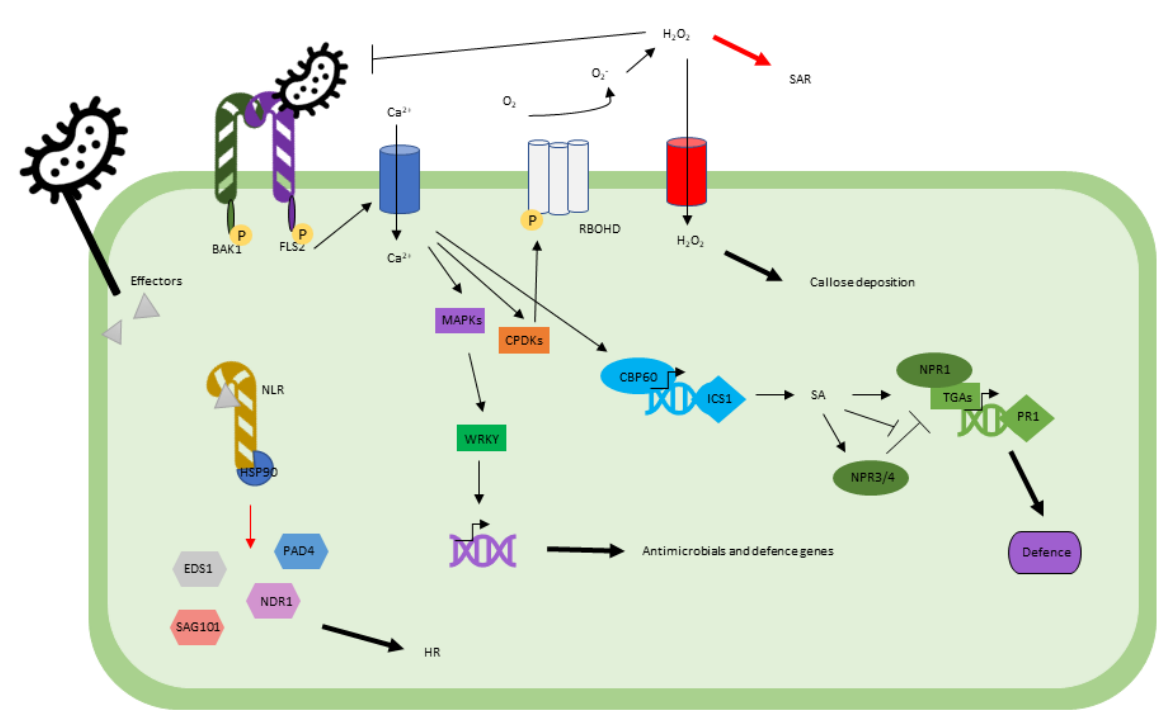


Figure 2. Schematic representation of the immunity pathway in plants, as explained in Sections 1.1.1 and 1.1.2. Arrows and blunted lines represent positive and negative regulations. Double helices with arrows represent a global transcriptional re-programming. The black lines indicate known connections, whereas red lines indicate unknown connections or missing steps between components of the pathway.

1.1.2 Effector-triggered immunity in plants

To suppress PTI, pathogens have a collection of harmful factors such as bacteria that uses virulent components like the phytotoxin coronatine 55. But also, fungal and oomycete effectors have been demonstrated ⁵⁵. Most of the known effectors are proteins and these are secreted into the plant through the TYPE III SECRETION SYSTEM (TTSS) ^{56–58}. These bacterial effectors contribute to pathogen virulence, often by mimicking or inhibiting eukaryotic cellular functions ^{56–58}. For example, the bacterial effector HopBF1 from Pseudomonas syringae inactivates eukaryotic HEAT SHOCK PROTEIN 90 (HSP90) 59. The effector HopBF1 is mimicking as HSP90 client, which results in the phosphorylation and inactivation of the HSP90 chaperone, and this prevents activation of intracellular immune receptors ⁵⁹. To defend themselves against these effectors, plants acquired through evolution immune receptors, which are called RESISTANCE (R) proteins. The R proteins may recognise the pathogen effectors directly or by a protection mechanism; in case of the latter, they recognize the disruption of innate proteins ^{56,60}. The guard hypothesis implies that R proteins indirectly recognize pathogen effectors by monitoring the integrity of their cellular targets. The R receptor proteins are NUCLEOTIDE-BINDING LEUCINE-RICH REPEAT proteins (NLRs) that consist of a NUCLEOTIDE-BINDING (NB) domain and a LEUCINE-RICH-REPEAT (LRR) domain. In addition, they may contain a N-TERMINAL TOLL-INTERLEUKIN-1 RECEPTOR (TIR) or a COILED-COIL (CC) domain ^{56,60}. The mechanism of activation seems to vary substantially between the different NLRs ⁶¹. However, in most cases the N-terminal domains is responsible for activating cell death pathways, and the NBS and LRR domain are generally known to regulate the activity of the R protein ^{61–63}. Activation of these receptors directly or via a guardee initiates a second layer of defence, known as effector-triggered

immunity (ETI) ⁶³. Signalling through these proteins requires NON-SPECIFIC DISEASE RESISTANCE 1 (NDR1), ENHANCED DISEASE SUSCEPTIBILITY 1 (EDS1), PHYTOALEXIN-DEFICIENT 4 (PAD4) and SENESCENCE ASSOCIATED GENE 101 (SAG101) ^{64,65}.

PTI responses are normally transient and quite mild, in comparison with ETI. This immune response is stronger, longer lasting, and results more often in a hypersensitive response (HR) ^{66–68}. This is a highly localized programmed cell death, which eradicates the cell along with the invading pathogen. This cell death is characterized by a shrinking of the plant protoplast, which is accompanied by chromatin condensation, cytochrome c release, chloroplast disruption, ion leakage, vacuolization and finally lysis of the plasma membrane ⁶⁹. However, the signalling cascade that activates HR is not yet known ⁷⁰. Although, it has been demonstrated that bursts of ROS and nitric oxide (NO) are vital for the initiation of HR ⁷¹, as well as Ca²⁺ signalling ^{23,43}. Furthermore, the generation of ROS was found to be influenced by the Ca²⁺ signalling ⁴³. Genes required for ETI include MLA12 RESISTANCE 1 (RAR1), SUPPESSOR OF THE G2 ALLELE OF SKP1 (SGT1), HEAT SHOCK PROTEIN (HSP90) and the R-gene itself 72. These genes have also been demonstrated to be important regulators of HR and have been shown to interact with the E3 UBIQUITING LIGASES S-PHASE KINASE PROTEIN 1 (SKP1) and CULLIN 1 (CUL1) ⁷³. The function of E3 enzymes is to add ubiquitin to specific proteins and thereby target them for degradation with the 26S proteasome 74. Hence, it could be hypothesized that cell death suppressors are ubiquitinated by this complex, in order to initiate HR. Another hypothesis states that generation of ROS species leads to the activation of caspase-like proteins, and this activity may ultimately lead to tonoplast rupture ^{70–72} and HR lesions ^{75–77}.

1.1.3 The auto-immune mutant CHILLING SENSITIVE 3-2D

Many of the characteristics discussed above have been discovered using auto-immune mutants of *Arabidopsis thaliana*. In general, autoimmune phenotypes have constitutive defence responses, at chilling temperatures ^{78–80}. This can be recognized by necrosis and/or yellowing of the leaves due to HR, and by a dwarfed morphology, due to slow growth ⁸⁰. Early studies showed that newly synthesized chloroplast localized proteins fail to accumulate after chilling ⁸¹. And later studies confirmed that the stability, function and oligomerization of the co-chaperones HSP90, RAR1, and SGT1b that assist in the folding of proteins change at chilling and elevated temperatures ^{82,83}. Additionally, immune responses have a direct effect on the seed development, and auto-immune mutants normally have reduced fertility. The auto-immune mutant pre-dominantly used in this study is *Arabidopsis thaliana chilling sensitive 3-2D (chs3-2D)*.

The CHILLING SENSITIVE 3 (CHS3) gene encodes a TIR-NB-LRR protein with a C-terminal zinc-binding LIN-11, ISL-1 and MEC-3 (LIM) domain. The G to A dominant gain-of-function mutation in chs3-2D, causes a C1340 to Y1340 substitution close to this LIM domain ⁸⁴. It has been proposed that the LIM domain keeps the NLR protein in its native inactive state ^{84–86}, so disruption of this domain results in a constitutive immune phenotype at chilling temperatures. At low temperatures the chs3-2D mutant is severely stunted and displays curled leaf morphology. Additionally, it constitutively expresses PATHOGENESIS-RELATED (PR) genes, accumulates salicylic acid, and shows enhanced resistance to the virulent oomycete isolate Hyaloperonospora arabidopsidis (H.a.) Noco2 ⁸⁴. A suppressor screen indicated that SAG101, EDS1-90, SGT1b, and HEAT SHOCK PROTEIN 81-2 (HSP81-2)

also known as HSP90.2) are positive regulators of the defence signalling in *chs3-2D* ^{87,88}. It is proposed that the CHS3 protein has two states, a resting and an active state (Figure 3). A pathogen infection or mutation induces the active state. This is facilitated by the chaperone HSP90, and the two co-chaperones SGT1b and RAR1 ^{88,89}. The activated CHS3 protein triggers cell death and defence signalling via EDS1 and SAG101 ⁸⁹.

Pathogen attack or chilling conditions LIM LIM LRR SGT1B effector TIR HSP90 Defence response

Figure 3. Proposed working model for the CHS3-mediated defence pathway. The LIM domain was proposed to repress CHS3 activities in the absence of pathogens. A mutation in the LIM domain (*chs3-2D*) or an immune activation triggered by an effector activates the CHS3 protein. This is only possible when HSP90 and SGT1b form a chaperone complex and properly assemble the receptor. The immune signalling pathway appears to primarily rely on SAG101 and EDS1- 90. Figure was adapted from Kadota et al. (2009), Bao et al. (2014) and Xu et al. (2015) 34,89,90.

1.2 Immunity and growth are coupled via molecular pathways

In plants, immunity and growth are often coupled. This is evident from auto-immune mutants, which have a high expression of immune marker genes but also a dwarfed morphology, due to reduced growth 80 . Additionally, prolonged treatment of a plant with a PAMP resulted in constitutively active PTI and growth inhibition 8 . In 1981, it was demonstrated in barley, that an immune response results in a decreased grain yield 91 . Additional reports support the presence of a negative effect on plant growth when immunity is induced $^{92-97}$.

In the early times it was believed that this growth reduction was due to a limited number of resources 98 , and allocation of resources toward defence occurred at the expense of plant fitness. This suggested that defence related products were auto toxic 99 or that the resistance was energetically costly 91,100,101 . Using radio-labelled carbon or nitrogen it was demonstrated that pathogen attack alters the normal metabolic flux, to the incorporation of carbon and nitrogen into defence related small molecules 102,103 . Later molecular research demonstrated a regulatory crosstalk of the hormones and signalling cascade involved in the growth and immunity trade-off 104 .

Antagonistic interactions have been observed between growth promoting hormones and small molecules induced in pathogen responses. Auxin inhibits immunity by suppressing SA biosynthesis and signalling. It was demonstrated that enhancing auxin signalling by transgenic overexpression of the AUXIN SIGNALLING F-BOX 1 (AFB1) gene resulted in a reduction of pathogen induced SA biosynthesis ¹⁰⁵. On the other hand, PTI was demonstrated to inhibit auxin signalling by repressing the expression of the auxin receptor TRANSPORT INHIBITOR RESISTANT 1 (TIR1) and this in turn stabilized the AUX-IAA proteins and decreased auxin signalling 106,107. Interestingly, the proteins TIR1 and AFB1 were recognized and ubiquitinated by the SKP-CUL1-F-BOX (SCF) E3 ubiquitin ligase complex 108-¹¹⁰. Normally when the auxin concentration reaches a certain threshold, the auxin directly facilitates SCFTIR1/AFB binding to AUX/IAA proteins, resulting in the ubiquitination and degradation of AUX/ IAA repressors via the 26S proteasome thereby derepressing ARFdependent transcription of auxin-regulated genes ¹¹¹. The HSP90 protein is a crucial component of immunity ⁷² as well as an important chaperone of the E3 ubiquitin ligases SKP1 and CUL1 73. Moreover, SGT1b has been demonstrated to be necessary for the SCF-TIR1 mediated auxin response ¹⁰⁹. So, it is quite likely that the higher amount of HSP90 and SGT1b may ubiquitinate AUX/IAA repressors by chaperoning of SCF, hereby reducing the expression of auxin genes and inducing a smaller phenotype ¹¹².

An antagonistic interaction has also been reported for the growth promoting hormone brassinosteroid (BR) ¹¹³. Both BR and the PAMP flagellin are recognized by the kinases BRI1 and FLS2, and these kinases both act on the same co-receptor BAK1 ^{113–115}. Moreover, the downstream basic-HELIX-LOOP-HELIX (bHLH) transcription factor HOMOLOG OF BEE2 INTERACTING WITH IBH 1 (HBI1) functions as a critical crosstalk node for immunity and growth ⁹⁶. While PTI responses repressed HBI1 and overexpression of HBI1 slightly abolished immune responses ⁹⁶. Research on the target genes revealed that HBI1 activates growth-related genes and suppresses defence related genes ⁹⁶. Moreover, WRKY transcription factors are known to be important regulators of the defence response ^{31,32}. Lozano-Durán et al. (2013) demonstrated that the BR-induced transcription factor BRASSINAZOLE-RESISTANT 1 (BZR1) physically interacts with WRKY40 to supress PTI responses ¹¹⁶, indicating another coupling of these pathways. Furthermore, it has been

demonstrated that BR signalling and localization of BRIDGING INTEGRATOR 2 (BIN2) was dependent on HSP90 117 .

SA mediated defences also have been demonstrated to affect gibberellins (GA). Loss of SA was demonstrated to restore gene induction and growth enhancement in response to exogenous GA ¹¹⁸. It is believed that suppression of GA by SA via EDS1 increases the stability of the transcription factor DELLA ^{119,120}. In the presence of growth signalling, a conformational change resulted in the binding of GA INSENSITIVE DWARF 1 (GID1) to DELLA ¹²¹. This binding enhanced the interaction of the E3 UBIQUITIN LIGASE SCF and resulted in the ubiquitination of DELLA. This ubiquitination released the bHLH transcription factors PHYTOCHROME INTERACTING FACTORS (PIFs) ¹²², and this in turn promoted GA-mediated gene expression and growth ^{122,123}. Moreover, the BR- and GA-mediated signalling pathways have been demonstrated to act synergistically ^{124,125}. This relationship is due to the formation of BZR1/PIF4 heterodimers, and the DELLA transcription factors that can inhibit BZR1, PIF4, and the heterodimer ¹²⁶.

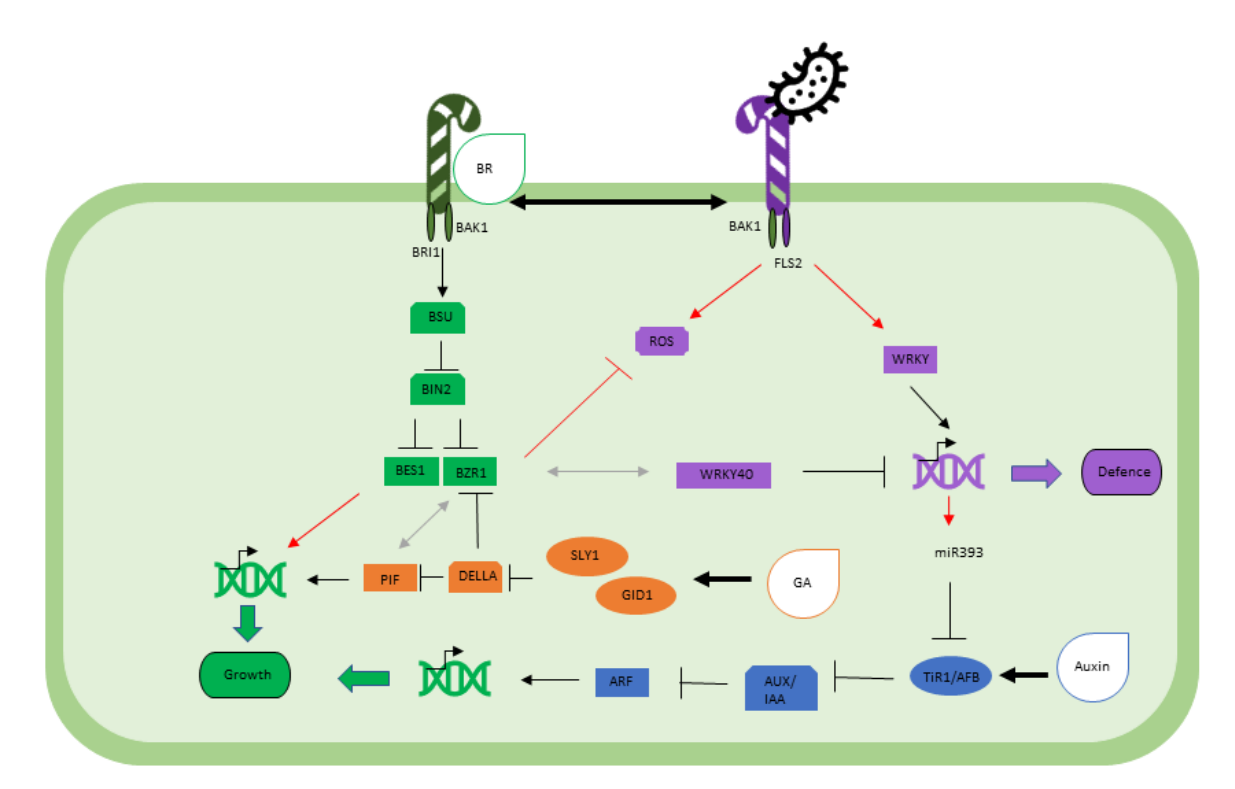


Figure 4. Schematic representation of the known signalling pathway contributing to the growth-defence trade-off between PTI-mediated defence, and auxin-, brassinosteroid (BR)- and gibberellin (GA)-mediated growth, as discussed in Section 1.2. Arrows and blunted lines represent positive and negative regulations. Double helices with arrows represent a global transcriptional re-programming. The black lines indicate known connections, whereas red lines indicate unknown connections or missing steps between components of the pathway. Grey lines indicate protein-protein interactions. Adapted from Huot et al. (2014) 127.

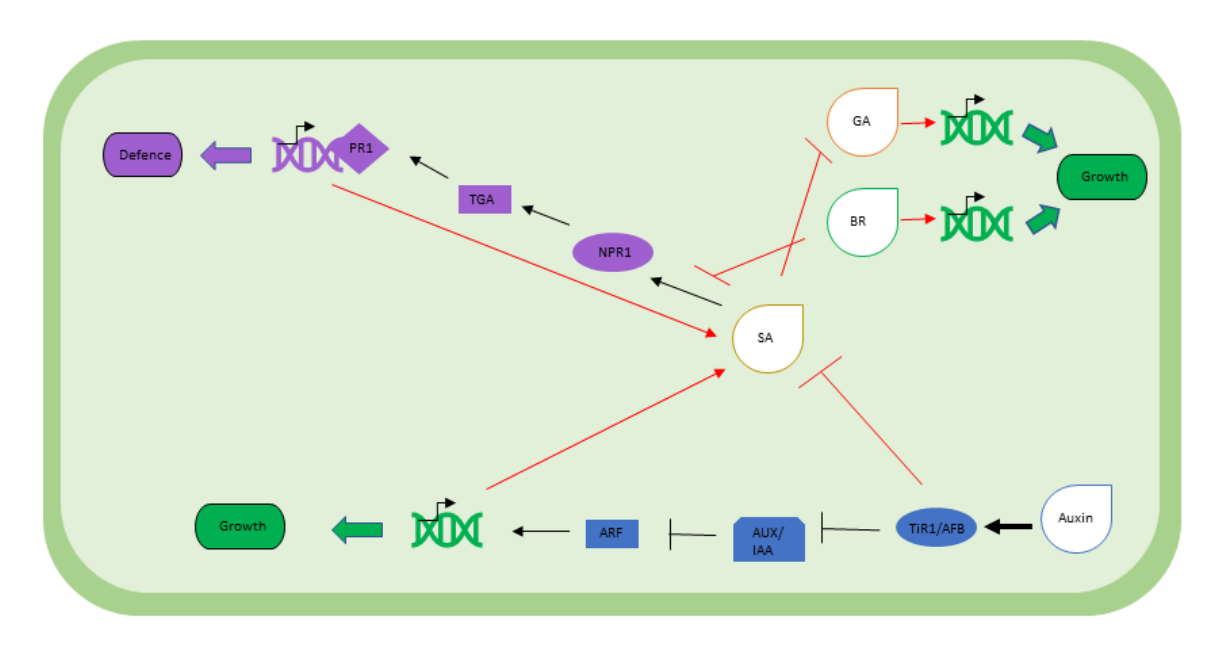


Figure 5. Schematic representation of the known signalling pathway contributing to the growth-defence trade-off between salicylic acid (SA)-mediated defence, and auxin-, brassinosteroid (BR)- and gibberellin (GA)-mediated growth, as discussed in Section 1.2. Arrows and blunted lines represent positive and negative regulations. Double helices with arrows represent a global transcriptional re-programming. The black lines indicate known connections, whereas red lines indicate unknown connections or missing steps between components of the pathway. Adapted from Huot et al. (2014) 127.

Another small molecule important for the growth defence trade-off is jasmonic acid (JA), a lipid derived molecule that regulates the immune response when the plant is invaded with a necrotrophic pathogen ¹²⁸. Besides, JA is also known to affect reproductive development and primary and secondary metabolism ^{128,129}. Jasmonoyl isoleucine is perceived by a co-receptor complex consisting of the F-BOX protein CORONATINE INSENSITIVE 1 (COI1) and the transcription repressor JASMONATE ZIM DOMAIN (JAZ)¹³⁰. Normally, JAZ recruits a co-repressor TOPLESS (TPL) and this complex binds MYC transcription factors, to repress expression of JA responsive genes ^{131–133}. Interestingly, similar to TIR1, JAZ repressor proteins are ubiquitinated with SCF and degraded with the 26S proteasome to relieve the repression on MYC transcription factors and to induce the expression of JA responsive genes ¹³². Furthermore, physical association of JAZ proteins with MYC2 was demonstrated to be required for the nuclear localization of JAZ repressors ¹³⁴.

Adding JA to growth medium results in severe growth inhibition ¹³⁵. This is due to the effect of JA on auxin, BR and GA. JA influences the auxin distribution by suppressing the expression and membrane accumulation of the auxin efflux carrier PINFORMED 2 (PIN2) ¹³⁶. Moreover, the transcription factors PLETHORA (PLT1 and PLT2), which are import regulators of auxin metabolism, are negatively regulated by MYC2 ¹³⁷. Conversely, auxin has been demonstrated to induce expression of JAZ1, and hereby suppresses the JA signalling pathway ¹³⁸. A crosstalk between JA and BR has also been demonstrated in mutants of *Arabidopsis thaliana* ¹³⁹, and in tomato ¹⁴⁰. However, the most studied crosstalk of JA is with GA. High amounts of JA reduces growth in *Nicotiana attenuata*, and this is due to a reduced GA biosynthesis ¹⁴¹. Stabilization of the DELLA transcription factors result in MYC2-dependent hypersensitivity to JA ^{142,143}, this is due to a direct physical interaction between JAZ and DELLA ^{142–144}. The binding of JAZ to DELLA blocks the interaction of DELLAs to PIFs, and relieving this inhibition promoted GA dependent growth ¹⁴⁴.

More recently, researchers have been able to identify another component involved in this crosstalk, the $Ca^{2+}/CALMODULIN$ DEPEDENTENT ARABIDOPSIS SINGAL RESPONSIVE 1 (AtSR1)/CAMTA3 transcription factor 96,97 . AtSR1 has been demonstrated to be a negative regulator of plant immune responses 145,146 . Following pathogen attack, AtSR1 was targeted for ubiquitination by the AtSR1 INTERACTING PROTEIN 1 (SRIP1) and degradation, releasing the repression of NDR, EDS1 and NPR1. Moreover, this transcription factor has also been demonstrated to serve as a positive regulator of plant growth and development 147 . Meanwhile, global gene expression analysis demonstrated that AtSR1 negatively regulates the immune-related genes and also regulates several of the plant growth genes like auxin and BR 147 .

Even though a lot is already known about the regulatory crosstalk, the complete mechanism remains elusive. While the signalling cascade between immunity and growth is an intricate one. E.g., SA and JA antagonize not only stereotypical growth-related hormones like auxin, and BR, but also one another ^{127,148}. Therefore, more research is necessary to completely characterize the hormonal network. At the time of writing, the definite justification of a growth drawback during an immune response is still lacking.

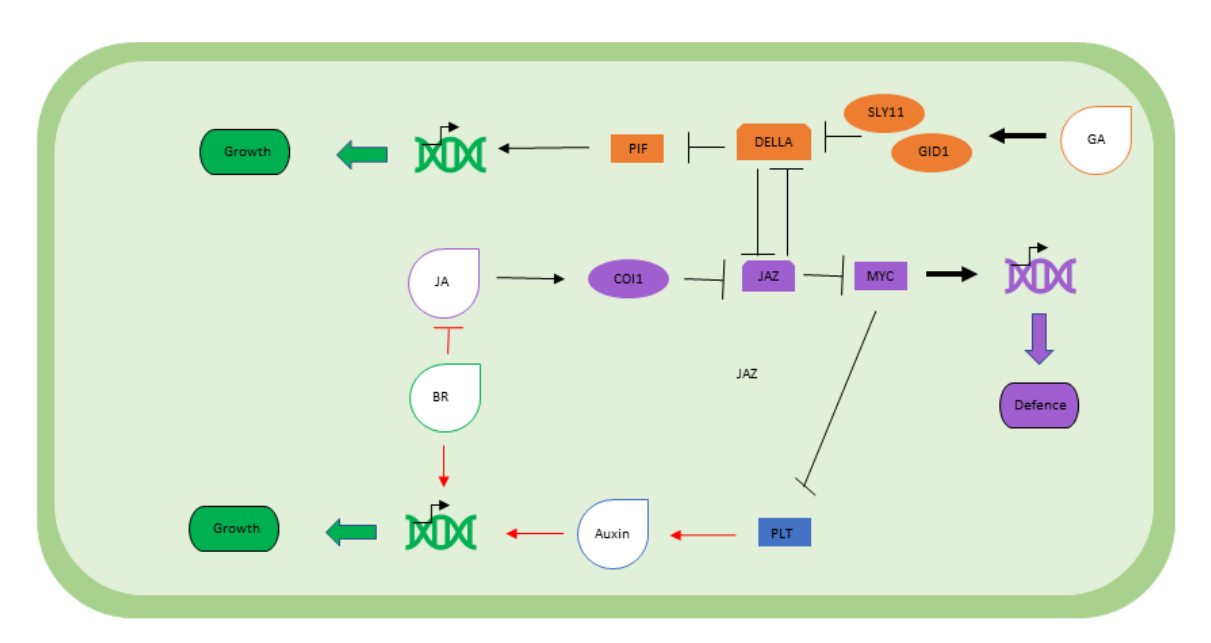


Figure 6. Schematic representation of the known signalling pathway contributing to the growth-defence trade-off between jasmonate (JA)-mediated defence, and auxin-, brassinosteroid (BR)- and gibberellin (GA)-mediated growth, as discussed in Section 1.2. Arrows and blunted lines represent positive and negative regulations. Double helices with arrows represent a global transcriptional re-programming. The black lines indicate known connections, whereas red lines indicate unknown connections or missing steps between components of the pathway. Adapted from Huot et al. (2014) 127.

1.3 The use of chemical biology to discover Ro8-4304

In chemical biology, organic compounds are used to permeate and understand biological systems. Alterations resembling genetic mutations are induced by application of a small molecule that can selectively bind and modulate a protein or members of a protein family. Moreover, this method has the advantage that it can overcome the issue of classical genetics e.g., gene redundancy, lethality and pleiotropy. Additionally, the chemical can be added at a precise time, and in a reversible or dose dependent matter. However, a small molecule needs to be identified before the chemical biology method is usable. Two methods are commonly used to discover new compounds: the forward genetic screening and the reverse genetic screening. In the forward chemical genetic screen, quantitative or qualitative screening is done to identify a molecule, hereafter the compound is characterized, and the target identified. In the reverse genetic screening, a protein of interest is selected, and chemical hit screening is done against this protein.

This chemical biology method was groundbreakingly used by Park et al. (2009) to identify the abscisic acid (ABA) receptor of *Arabidopsis thaliana* ¹⁴⁹. In their research, they used a forward chemical genetic screen to discover the small molecule pyrabactin4 which employed as a probe binds the ABA receptor PYR1 ¹⁴⁹. Their success led to the start and identification of many more small molecules useful for molecular biology in various research areas e.g., growth ^{150,151}, immunity ^{152–156} and flowering ^{157,158}.

Treatment of plants with synthetic chemicals can induce resistance to pathogen attack ¹⁵⁹ also known as priming. This induction of resistance can lead to direct activation of defences or to a priming state of the cell resulting in a stronger and faster elicitation of immune response after pathogen attack ¹⁶⁰. Indicating that chemical biology is a critical aspect of plant immunity. Moreover, priming has been demonstrated to be an interesting way to prepare the defence response while it doesn't necessary stunt plant growth ^{161–163}. Buswell et al. (2018) demonstrated that application of (R)-b-homoserine induced the defence without stunting plant growth ¹⁶⁴, and also the compound 5-(cyclopropylmethyl)-6-methyl-2-(2-pyridyl) pyrimidin-4-ol was able to induce defence responses without a negative effect on fresh weight ¹⁶⁵. Hence, inducing immunity without affecting growth using chemical elicitors is achievable.

Huang et al. (2016) performed a chemical screening in the *Arabidopsis thaliana* auto-immune mutant *chs3-2D* ¹⁶⁶. They reported a chemical, Ro8-4304 (Figure 7) which was able to reverse the growth of *chs3-2D* to normal WT levels ¹⁶⁶. But the chemical had a negative effect on the expression of the defence marker genes *PR1* and *PR2*. Moreover, they demonstrated that the methylosome is important for the *chs3-2D* phenotype and the action of this chemical ¹⁶⁶. However, more research is necessary if Ro8-4304 is to be applied more universally.

$$H_2N$$

Figure 7. The chemical structure of Ro8-4304.

2 Aim of the project

Plants are sessile organisms, and therefore they developed various defence mechanisms ^{56–58}. However, the high resistance often comes with a cost. Plants with a high resistance are often smaller due to a molecular linkage of growth and defence ^{96,97,104}. Conversely, it has been shown that plants with a high yield have low levels of chemical defence, and for this reason an increased susceptibility to herbivory and pathogen attack ^{93,94}. Additionally, previous research indicates that during the evolution of plants, through breeding and crop improvement, there has been a gradual loss of defence-related traits

This is a huge problem, and it would be beneficial if those trade-offs could be uncoupled. Moreover, research in this area is vital. Knowledge is necessary if we want to grow a healthy plant with a sufficient yield in the future. This aim should not be an impossible objective, while priming with small molecules, induced resistance dependent on SA, but this priming did not affect the growth significantly ^{161–164}.

^{92,95,167,168}. Presumably, when farmers and breeders selected for the fastest growing plants

with the highest yields, they sacrificed the expression of costly defence genes.

Hence, chemical biology has been demonstrated to be an attractive way to tackle this problem ^{152–156}. Huang et al. (2016) used a forward chemical screening to discover a chemical that could rescue the immune phenotype of *chs3-2D* ¹⁶⁶. The identified small molecule, Ro8-4304, rescued the *chs3-2D* phenotype to normal growth levels, but this rescue mounted a reduction in the expression of defence marker genes *PR1* and *PR2*. Additionally, at the moment Ro8-4304 only has an active response in this particular *Arabidopsis thaliana* mutant. So, before this compound can be used more universally, it needs to be improved. Since this chemical rescued one characteristic, we thought it to be a good starting point for chemical optimization. Additionally, for more regular use, we need to understand the direct mode of action. And this will hopefully also lead to more insight into the growth and immunity trade-off.

In this project, we aimed to identify the target protein of Ro8-4304 by using affinity purification, and literature research. However, to bind Ro8-4304 to a matrix, first the structure needed to be altered. Using organic chemistry, we aimed to synthesis analogues which would give us more insight about the active site, and which would be able to bind activated matrixes. The validity of the discovered proteins would be tested using chemical biology and genetic methods. This research would give us more insight about the chemical Ro8-4304 and will hopefully lead to an improved variant, which could be used as marker molecule in plant immunity and growth research.

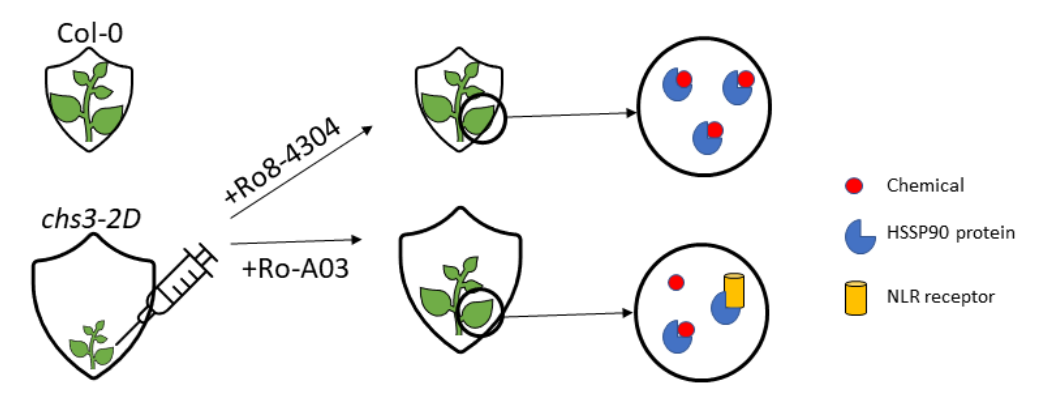


Figure 8. A graphical abstract of the dissertation.

3 Materials and methods

3.1 Suppliers used in this thesis

Company name	City	Country
abcr GmbH & Co. KG	Karlsruhe	Germany
Across organics	Geel	Belgium
Alfa Aesar GmbH & Co. KG	Karlsruhe	Germany
Agilent Technologies Inc.	Santa Clara, California	United States of America
Analytik Jena	Jena	Germany
Apollo Scientific	Stockport	United Kingdom
AppliChem GmbH	Darmstadt	Germany
Bayer Cropscience	Monheim	Germany
Biogazelle	Zwijnaarde	Belgium
Biomol GmbH	Hamburg	Germany
Bio-Rad	Hercules, California	United States of America
Bruker	Billerica, Massachusetts	United States of America
Carl Roth GmbH & Co. KG	Karlsruhe	Germany
Cayman Chemical Company	Ann Arbor, Michigan	United states of America
Chemsolute; Th. Geyer GmbH &	Hamburg	Germany
Co. KG Niederlassung	G	•
Duchefa	Haarlem	The Netherlands
Eppendorf	Hamburg	Germany
Eurofins	Hamburg	Germany
Eurofins Genomics	Anzinger	Germany
Fibo ExClay	Lahmstedt	Germany
Fluorochem	Hadfield	United Kingdom
Glentham Life Sciences	Corsham	United Kingdom
Grüssing GmbH	Filsum	Germany
Heraeus Deutschland GmbH &	Hanau	Germany
Co. KG		•
Hoffmann-La Roche	Basel	Switzerland
J&K Scientific	Pforzheim	Germany
Matrix Scientific	Planegg	Germany
Merck	Darmstadt	Germany
MestReNova software	Santiago de Compostela	Spain
Mestrelab Research		
Molekula GmbH	München	Germany
Neudorff	Emmerthal	Germany
Nottingham Arabidopsis Stock	Loughborough	United Kingdom
Centre		
Novogene (UK) Company Limited	Cambridge	United Kingdom
Percival Scientific	Perry, Iowa	United States of America
Phenomenex	Torrance, California	United States of America
Qiagen	Venlo	The Netherlands
Salk Institute for Biological	La Jolla, San Diego	United States of America
Studies	_	

Santa Cruz Biotechnology Inc.	Dallas, Texas	United States of America
Sarstedt AG & Co. KG	Nümbrecht	Germany
Sartorius AG	Göttingen	Germany
SIA Enamine	Riga	Latvia
Sigma-Aldrich Chemie GmbH	Taufkirchen	Germany
Serva Electrophoresis GmbH	Heidelberg	Germany
Thermo Fisher Scientific	Waltham, Massachusetts	United States of America
VWR International GmbH	Darmstadt	Germany
Wilsaflor	Neulehe	Germany

3.2 Materials and methods for the organic synthesis of Ro8-4304 and its analogues

3.2.1 Chemicals, reagents, and solvents

All commercially available chemicals and reagents were used without any purification. Solvents were distilled before use, in contrast to dry solvents bought from Acros Organics.

3.2.2 Recording of the spectra

The spectra were recorded at the chemistry department of Universität Hamburg. The NMR spectra were taken in the NMR section under guidance of Dr. Thomas Hackl und Dr. Young-Joo Lee. The mass spectra were taken in the mass spectrometry section under guidance of Dr. Maria Riedner.

The 1H-, 13C-, 19F-, and 2D-NMR spectra were recorded on the following Bruker instruments: Fourier-300 (300 MHz/75 MHz), AV-400 (400 MHz/100 MHz), DRX-500 (500 MHz/125 MHz), and AVIII6000 (600 MHz/150 MHz). Chemical shifts were referenced to the solvent: Chloroform-d (δ = 7.26 ppm in 1H-NMR, δ = 77.16 ppm in 13C-NMR), Methanol-d4 (δ = 3.31 ppm and 4.87 ppm in 1H-NMR, δ = 79.00 ppm in 13C-NMR), DMSO-d6 (δ = 2.50 ppm and 3.33 ppm in 1H-NMR, δ = 39.52 ppm in 13C-NMR), D₂O (δ = 4.79 ppm in 1H-NMR). Data was analysed with the MestReNova software [Mestrelab Research] and multiplicities are abbreviated as: s = singlet, d = doublet, dd = doublet of doublets, ddd = doublet of doublets, td = triplet of doublets, dq = doublet of quartets, t = triplet, tt = triplet of triplets, quint = quintet and m = multiplet.

ESI-MS spectra were recorded on an Agilent 6224 ESI-TOF Mass spectrometer attached to an Agilent HPLC 1200 Series [Agilent Technologies]. The EI-MS spectra were recorded on a Thermo ISQ LT EI attached to a Thermo Trace 1300 [Thermo Fisher Scientific]. The data was processed using MestReNova [Mestrelab Research].

3.2.3 The chemical synthesis of the building blocks for synthesis of Ro8-4304

BB01; 4-oxiranylmethoxy benzamide

The synthesis of 4-oxiranylmethoxy benzamide was done according to US patent no. 3,674,799, 1972 169 . 4-hydroxybenzamide (3 mmol) [Fluorochem] was added to a solution of 1 Eq of sodium hydroxide (NaOH) (3 mmol) [Grüssing GmbH] in 5 ml of water (H₂O). The mixture was treated with 3 Eq of epichlorohydrin (9 mmol) [J&K Scientific] and stirred at room temperature (RT) overnight (O/N). The precipitated 4-oxiranylmethoxy benzamide was filtered and washed with H₂O. The compound was retrieved in a yield of 499 mg (86%) and was used without further purification.

HRMS m/z (ESI) 194.082, consistent with empirical formula $C_{10}H_{11}NO_3$ with an accuracy of 0.0081 ppm (accepted as $[M+H]^+$).

¹H NMR: (500 MHz, MeOH- d_4) δ 7.90-7.83 (m, 2H, H-2, H-4), 7.10-7.01 (m, 2H, H-3, H-5), 4.41 (dd, J=11.3, 2.5 Hz, 1H, H-6), 3.95 (dd, J=11.4, 6.2 Hz, 1H, H-6), 3.38 (ddt, J=6.7, 4.4, 2.6 Hz, 1H, H-7), 2.91 (dd, J=5.0, 4.2 Hz, 1H, H-8), 2.78 (dd, J=5.0, 2.7 Hz, 1H, H-8).

¹³C NMR: (101 MHz, MeOH- d_4) δ 130.67, 115.35, 70.39, 49.85, 49.54.

BB02; 4-(4-bromophenyl)-1,2,3,6-tetrahydropyridine

Method 1

The synthesis of 4-(4-bromophenyl)-1,2,3,6-tetrahydropyridine was done according to Conway et al. (2012) 170 . 4-(4-bromopenyl-4-piperidinol) (1g, 3.9 mmol) [Sigma-Aldrich Chemie GmbH], and 30 ml 6 M aqueous hydrochloric acid (HCl) [VWR International GmbH] were mixed, and heated at reflux (\sim 85°C) O/N. The solution was allowed to slowly cool down to RT, and this was left alone over the day. Crystals were formed. These were filtered, washed with H₂O, diethyl ether, and dried O/N on the vacuum pomp. This yielded 313 mg (34%) of pink crystals. So, the H₂O layer was checked, by NMR. Also, this layer contained (clean) product, although this was probably not pure enough for crystallisation. The H₂O was removed yielding 515 mg (56%) of a yellowish solid.

Method 2

Another method was tried, according to Junker et al. (2016) 171 . 3 ml trifluoroacetic acid (TFA) [Sigma-Aldrich Chemie GmbH] was placed in a round-bottom flask and 1 g 4-(4-bromophenyl-4-piperidinol) (3.9 mmol) [Sigma-Aldrich Chemie GmbH] was added. The mixture was stirred for 4-5 h at $\sim 90^{\circ}$ C. The solution was allowed to cool down to RT, and the TFA was removed, in vacuo, in combination with methanol (MeOH). This left a yellowish powder in a quantitative amount.

HRMS m/z (ESI) 238.022, consistent with empirical formula $C_{11}H_{12}BrN$ with an accuracy of 0.0067 ppm (accepted as $[M+H]^+$).

¹H NMR (500 MHz, DMSO- d_6) δ 9.36 (s, 2H, H-7), 7.62–7.55 (m, 2H, H-1), 7.48–7.41 (m, 2H, H-2), 6.25 (tt, J=3.5, 1.6 Hz, 1H, H-3), 3.73 (q, J=2.4 Hz, 2H, H-4), 3.29 (t, J=6.0 Hz, 2H, H-5), 2.67 (tq, J=6.3, 2.0 Hz, 2H, H-6).

 13 C NMR (126 MHz, DMSO- d_6) δ 138.32, 133.62, 131.83, 127.26, 121.38, 118.15, 41.73, 40.28, 23.30.

BB03; 4-(4-hydroxy-phenyl)-1,2,3,6-tetrahydropyridine

Method 1

The synthesis of 4-(4-hydroxy-phenyl)-1,2,3,6-tetrahydropyridine was done according to Gessner et al. (1985) 172 . 4-piperidone monohydrate (2 mmol) [Apollo Scientific] and phenol (2 mmol) [Grüssing GmbH] were dissolved in 5 ml of glacial acetic acid (AcOH) [VWR International GmbH]. Gaseous HCl was passed through the solution for 3 min, according to Arnáiz (1995) 173 . The mixture was heated at reflux (\sim 85°C) for 1 h, and the mixture was

allowed to cool down to RT. Gaseous HCl was passed again through the solution for 3 min, and the mixture was re-heated to reflux for 1 h. The mixture was allowed to cool down to RT. The AcOH was removed in vacuo giving a yellow/orange solid. This was purified in reverse phase on a flash chromatograph with an eluent of 100% H₂O to 100% acetonitrile (ACN). Appropriate fractions were combined, and the solvent of these fractions was removed in vacuo, leaving a Colourless powder in a yield of 65 mg (21%).

Method 2

4-piperidone monohydrate (2 mmol) [Apollo Scientific] and phenol (2 mmol) [Grüssing GmbH] were dissolved in 5 ml of ethanolic HCl (1M). The mixture was heated to reflux (\sim 85°C). After two hours, 2 ml ethanolic HCl was added, and this was repeated three times with 1 h intervals, the next day this was again repeated 3 times. So, in total 12 ml ethanolic HCl was added at six different time points. On day two, the heating was stopped, and the mixture was allowed to cool down to RT. The ethanolic HCl was removed in vacuo giving a yellow/orange solid. The product was purified in reverse phase on a flash chromatograph with an eluent of 100% H_2O to 100% ACN. Appropriate fractions were combined, and the solvent of these fractions was removed in vacuo, leaving a Colourless powder in a yield of 143 mg (41%).

HRMS m/z (ESI) 176.106, consistent with empirical formula $C_{11}H_{13}NO$ with an accuracy of 0.0003 ppm (accepted as $[M+H]^+$).

¹H NMR: (500 MHz, D₂O) δ 7.32 (d, J=8.2 Hz 2H, H-2), 6.82 (d, J=8.2 Hz, 2H, H-3), 5.95 (dq, J=3.8, 1.7 Hz, 1H, H-6), 3.74 (q, J=2.6 Hz, 2H, H-7), 3.38 (t, J=6.2 Hz, 2H, H-4), 2.67 (td, J=6.3, 3.5 Hz, 2H, H-5).

 13 C NMR: (101 MHz, D₂O) δ 155.57, 134.46, 131.32, 126.56, 115.44, 113.97, 42.13, 40.97, 23.23.

BB04; 4-phenyl-1,2,3,6-tetrahydropyridine

The synthesis of 4-phenyl-1,2,3,6-tetrahydropyridine was done according to Method 2, described in BB02. 3 ml TFA [Sigma-Aldrich Chemie GmbH] was placed in a round-bottom flask and 1 g 4-phenyl-4-piperidinol (5.6 mmol) [Sigma-Aldrich Chemie GmbH] was added. The mixture was stirred O/N at \sim 90°C. The solution was allowed to cool down to RT, and the TFA was removed, in vacuo, in combination with MeOH. This left beige crystals in quantitative amounts.

HRMS m/z (ESI) 160.113, consistent with empirical formula $C_{11}H_{13}N$ with an accuracy of 0.0082 ppm (accepted as $[M+H]^+$).

¹H NMR (400 MHz, MeOH- d_4) δ 7.52–7.45 (m, 2H, H-1), 7.44–7.34 (m, 2H, H-2), 7.38–7.29 (m, 1H, H-3), 6.17 (tt, J=3.5, 1.7 Hz, 1H, H-4), 3.87 (dt, J=3.6, 2.5 Hz, 2H, H-5), 3.49 (t, J=6.1 Hz, 2H, H-6), 2.83 (tq, J=5.6, 2.0 Hz, 2H, H-7).

 13 C NMR (101 MHz, MeOH- d_4) δ 139.01, 135.77, 128.30, 127.89, 124.76, 115.58, 42.09, 40.85, 23.51.

BB05; 4-[4-(trifluoromethyl)-phenyl]-1,2,3,6-tetrahydropyridine

The synthesis of 4-[4-(trifluoromethyl)-phenyl]-1,2,3,6-tetrahydropyridine was done according to **Method 2**, described in BB02. 2 ml TFA [Sigma-Aldrich Chemie GmbH] was placed in a round-bottom flask and 0.1549 g 4-[4-(trifluoromethyl)phenyl]4-piperidinol (0.63 mmol) [Matrix Scientific] was added. The mixture was stirred for 2.5 h at \sim 90°C. The solution was allowed to cool down to RT, and the TFA was removed, in vacuo, in combination with MeOH. This resulted in a dark orange oil in quantitative amounts. HRMS m/z (EI) 228.100, consistent with empirical formula $C_{12}H_{12}F_3N$ with an accuracy of 0.0078 ppm (accepted as [M+H]⁺).

¹H NMR (500 MHz, DMSO- d_6) δ 7.85–7.71 (m, 6H, H-6, H-7, H-1), 6.43 (s, 0H, H-5), 3.36 – 3.30 (m, 2H, H-4), 2.25 – 2.15 (m, 2H, H-3), 1.84 (d, J=14.1 Hz, 2H, H-2).

 13 C NMR (126 MHz, DMSO- d_6) δ 159.10, 158.76, 158.48, 153.13, 127.86, 125.97, 125.87, 125.60, 125.56, 125.53, 125.49, 120.00, 68.72, 42.05, 34.48, 23.41.

¹⁹F NMR: (565 MHz, DMSO- d_6) δ -77.64 (3F).

BB06; tert-Butyl(4-hydroxybenzyl)carbamate

4-aminomethyl phenol (2.5 mmol) [Sigma-Aldrich Chemie GmbH] was suspended in 10 ml dichloromethane (DCM). 2.5 Eq of triethylamine (TEA) (6.25 mmol) [Grüssing GmbH], and 1.2 Eq of di-tert-butyl-dicarbonate (Boc₂O) (3 mmol) [Sigma-Aldrich Chemie GmbH] were added. Everything dissolved after 5 min of stirring, and the solution was stirred O/N at RT. The next day, the organic layer was washed with H_2O , brine, and H_2O , hereafter the organic layer was dried with sodium sulphate (Na₂SO₄) and evaporated in vacuo. The resulting oil was purified by Column chromatography (eluent: petroleum ether (PE)/ethyl acetate (EtOAc) 7/3), yielding 309 mg (55%) of product (Colourless oil).

HRMS m/z (ESI) 246.110, consistent with empirical formula $C_{12}H_{17}NO_3$ with an accuracy of 0.000 ppm (accepted as $[M+Na]^+$).

¹H NMR: (400 MHz, CDCl₃) δ 7.04 (d, J=7.8 Hz, 2H, H-2), 6.74-6.66 (m, 2H, H-3), 4.74 (s, 1H, H-5), 4.15 (d, 2H, H-4), 1.38 (s, 9H, H-6).

 $^{13}\text{C NMR:}$ (101 MHz, CDCl₃) δ 209.15, 189.12, 179.39, 155.18, 130.73, 129.84, 128.97, 115.47, 54.86, 46.90, 44.22, 28.44.

BB07; 4-oxiranylmethoxy-[tert-Butyl(4-hydroxybenzyl)carbamate]

4-oxiranylmethoxy-[tert-Butyl(4-hydroxybenzyl)carbamate] was synthesized comparable to BB01. However, the solvent was changed to MeOH. BB06 (2.5 mmol) was added to a solution of 1 Eq of NaOH (2.5 mmol) [Grüssing GmbH] in 5 ml of MeOH. The mixture was treated with 3 Eq of epichlorohydrin (7.5 mmol) [J&K Scientific], and stirred at RT O/N. The solvent was removed in vacuo. The residue was partitioned between DCM, and H₂O. The DCM layer was separated, washed three times with H₂O, and dried with Na₂SO₄, before the solvent was evaporated in vacuo. This was purified by Column chromatography (eluent: DCM/EtOAc, 9/1). A Colourless oil was obtained, which turned into a Colourless solid in a couple of hours, in a yield of 203 mg (29%).

HRMS m/z (ESI) 302.136, consistent with empirical formula $C_{15}H_{21}NO_4$ with an accuracy of 0.0003 ppm (accepted as $[M+Na]^+$).

¹H NMR: (600 MHz, CDCl₃) δ 7.13 (d, J=8.1 Hz, 2H, H-5), 6.83-6.78 (m, 2H, H-4), 4.71 (s, 1H, H-2), 4.17 (d, J=5.8 Hz, 2H, H-3), 4.14 (dd, J=11.0, 3.2 Hz, 1H, H-6), 3.88 (dd, J=11.0, 5.6 Hz, 1H, H-6), 3.28 (ddt, J=5.8, 4.1, 2.9 Hz, 1H, H-7), 2.83 (dd, J=4.9, 4.1 Hz, 1H, H-8), 2.68 (dd, J=4.9, 2.6 Hz, 1H, H-8); 1.39 (s, 9H, H-1).

¹³C CNMR: (101 MHz, DMSO- d_6) δ 157.82, 155.85, 131.66, 128.89, 114.75, 105.03, 93.02, 69.86, 68.81, 50.15, 45.96, 45.76, 44.72, 44.13, 29.70, 28.42.

BB08; 2-[(4-fluorophenoxy)methyl]-oxirane

2-[(4-fluorophenoxy)methyl]-oxirane was synthesized comparable to BB01. 4-fluorophenol (2 mmol) [Grüssing GmbH] was added to a solution of 1 Eq of NaOH (2 mmol) [Grüssing GmbH] in 3 ml of H_2O . The mixture was treated with 3 Eq of epichlorohydrin (6 mmol) [J&K Scientific], and stirred at RT O/N. A yellow oil was visible in the H_2O layer. This was extracted into diethyl ether. The organic layer was separated, washed with a 5% NaOH solution, and H_2O . The organic layer was dried with Na_2SO_4 , and the solvent was evaporated in vacuo. The obtained clear yellow oil was purified by Column chromatography (eluent: DCM/PE 8/2). The product, a Colourless oil, was obtained in a yield of 165 mg (49%).

HRMS m/z (EI) 168.10, consistent with empirical formula $C_9H_9FO_2$ with an accuracy of 0.0413 ppm (accepted as $[M]^{-+}$).

 1 H NMR (600 MHz, CDCl₃) δ 6.94–6.87 (m, 2H, H-1), 6.83–6.76 (m, 2H, H-2), 4.13 (dd, J=11.0, 3.0 Hz, 1H, H-3), 3.84 (dd, J=11.0, 5.7 Hz, 1H, H-3), 3.27 (ddt, J=5.7, 4.1, 2.8 Hz, 1H, H-4), 2.84 (dd, J=4.9, 4.1 Hz, 1H, H-5), 2.68 (dd, J=4.9, 2.7 Hz, 1H, H-5).

¹³C NMR (151 MHz, CDCl3) δ 158.33, 156.75, 154.64, 154.62, 115.96, 115.81, 115.78, 115.72, 69.46, 51.28, 46.96, 45.00, 44.64.

¹⁹F NMR: (565 MHz, CDCl₃) δ -123.4 (1F).

$$\begin{array}{c|c}
1 & 2 & 0 & 4 \\
\hline
 & 1 & 2 & 0
\end{array}$$

BB09; (2-phenoxymethyl)-oxirane

(2-phenoxymethyl)-oxirane was synthesized comparable to BB01. Phenol (2 mmol) [Grüssing GmbH] was added to a solution of 1 Eq of NaOH (2 mmol) [Grüssing GmbH] in 3 ml of H_2O . The mixture was treated with 3 Eq of epichlorohydrin (6 mmol) [J&K Scientific], and stirred at RT O/N. A Colourless oil was visible in the H_2O layer. This was extracted into diethyl ether. The organic layer was separated, washed with a 5% NaOH solution, and H_2O . The organic layer was dried with Na_2SO_4 , and the solvent was evaporated in vacuo. The obtained Colourless oil was purified by Column chromatography (eluent: DCM/PE, 8/2). The product, a Colourless oil, was obtained in a yield of 127 mg (42%).

HRMS m/z (EI), 150.12, consistent with empirical formula $C_9H_{10}O_2$ with an accuracy of 0.0519 ppm (accepted as $[M]^{-+}$).

¹H NMR (600 MHz, CDCl₃) δ 7.26–7.19 (m, 2H, H-1), 6.90 (tt, J=7.4, 1.1 Hz, 1H, H-3), 6.88–6.83 (m, 2H, H-2), 4.14 (dd, J=11.0, 3.3 Hz, 1H, H-4), 3.90 (dd, J=11.0, 5.6 Hz, 1H, H-4), 3.29 (ddt, J=5.7, 4.0, 2.9 Hz, 1H, H-5), 2.84 (dd, J=4.9, 4.1 Hz, 1H, H-6), 2.69 (dd, J=4.9, 2.7 Hz, 1H, H-6).

 13 C NMR (151 MHz, CDCl₃) δ 158.47, 129.53, 121.24, 114.63, 68.67, 68.40, 50.17, 44.78.

BB10; 4-oxiranylmethoxy-4-hydroxy acetophenon

4-oxiranylmethoxy-4-hydroxy acetophenone was synthesized comparable to BB01. 4-hydroxyacetophenon (3 mmol) [Merck, Darmstadt, Germany] was added to a solution of 1 Eq of NaOH (3 mmol) [Grüssing GmbH] in 5 ml of H_2O . The mixture was treated with 3 Eq of epichlorohydrin (9 mmol) [J&K Scientific], and stirred at RT O/N. A Colourless oil was visible in the H_2O layer. This was extracted into EtOAc. The organic layer was separated, washed twice with H_2O , and once with brine. The organic layer was dried with Na_2SO_4 , and the solvent was evaporated in vacuo. The product was purified by Column chromatography (eluent: EtOAc/PE 5/5). A Colourless oil was obtained in a yield of 490 mg (85%). HRMS m/z (EI) 192.11, consistent with empirical formula $C_{11}H_{12}O_3$ with an accuracy of 0.0314 ppm (accepted as $[M]^{-+}$).

 1 H NMR (400 MHz, CDCl₃) δ 7.91–7.82 (m, 2H, H-2), 6.93–6.84 (m, 2H, H-3), 4.25 (dd, J=11.1, 3.0 Hz, 1H, H-4), 3.93 (dd, J=11.1, 5.8 Hz, 1H, H-4), 3.30 (ddt, J=5.7, 4.1, 2.8 Hz, 1H, H-5), 2.86 (dd, J=4.9, 4.1 Hz, 1H, H-6), 2.77–2.67 (m, 1H, H-6), 1.97 (s, 3H, H-1).

 $^{13}\text{C NMR}$ (126 MHz, CDCl₃) δ 197.17, 197.13, 196.27, 171.56, 162.69, 162.49, 131.30, 131.16, 131.04, 131.00, 114.68, 114.63, 70.06, 69.25, 69.09, 60.78, 50.29, 46.24, 44.97, 26.74, 21.43, 14.58.

BB11; 4-oxiranylmethoxy-4-ethyl phenol

4-oxiranylmethoxy-4-ethyl phenol was synthesized comparable to BB01. 4-ethylphenol (3 mmol) [Sigma Aldrich] was added to a solution of 1 Eq of NaOH (3 mmol) [Grüssing GmbH] in 5 ml of H_2O . The mixture was treated with 3 Eq of epichlorohydrin (9 mmol) [J&K Scientific], and stirred at RT O/N. A Colourless oil was visible in the H_2O layer. This was extracted into DCM. The organic layer was separated, washed twice with H_2O , and once with brine. The organic layer was dried with Na_2SO_4 , and the solvent was evaporated in vacuo. The obtained yellow oil was purified by Column chromatography (eluent: DCM/PE 8/2). A clear yellow oil was obtained in a yield of 162 mg (30%).

HRMS m/z (EI) 178.11, consistent with empirical formula $C_{11}H_{14}O_2$ with an accuracy of 0.0106 ppm (accepted as [M]⁻⁺).

¹H NMR (500 MHz, CDCl₃) δ 7.18–7.11 (m, 2H, H-3), 6.91–6.85 (m, 2H, H-4), 4.21 (dd, J=11.0, 3.3 Hz, 1H, H-5), 3.98 (dd, J=11.1, 5.6 Hz, 1H, H-5), 3.37 (ddt, J=5.8, 4.0, 3.0 Hz, 1H, H-6), 2.93 (dd, J=5.0, 4.1 Hz, 1H, H-7), 2.78 (dd, J=5.0, 2.6 Hz, 1H, H-7), 2.62 (q, J=7.6 Hz, 2H, H-2), 1.24 (t, J=7.6 Hz, 3H, H-1).

 $^{13}\text{C NMR}$ (126 MHz, CDCl₃) δ 187.91, 156.97, 137.44, 129.17, 114.96, 69.27, 50.64, 45.18, 28.38, 16.24.

BB12; 4-(3-bromo-ethoxy)-benzamide

The synthesis 4-(3-bromoethoxy)-benzamide was done according to Kubota et al. (2003) and patent no. WO 2008096093/A1 174,175 . 4-hydroxybenzamide (3 mmol) [Fluorochem] was dissolved in 10 ml ACN. Kalium carbonate (K_2CO_3) (1.5 Eq, 4.5 mmol) [Grüssing GmbH], and 1,2-dibromoethane (5 Eq, 15 mmol) [Merck] were added. This mixture was stirred at ~80°C O/N. The ACN was removed in vacuo, and the leftover product was participated between H_2O and EtOAc. The organic layer was separated, washed with H_2O , a 5% NaOH solution, H_2O , and brine. After this the organic layer was dried with H_2O , and the solvent was removed in vacuo. The resulting product was purified by Column chromatography (eluents: EtOAc/MeOH 9.5/0.5), yielding 147 mg (30%) of product (Colourless solid).

HRMS m/z (ESI) 244.000, consistent with empirical formula $C_9H_{10}BrNO_2$ with an accuracy of 0.0105 ppm (accepted as $[M+H]^+$).

 1 H NMR (600 MHz, CDCl₃) δ 7.73 (d, J=8.5 Hz, 2H, H-2), 6.89 (d, J=8.4 Hz, 2H, H-3), 6.04 (s, 1H, H-1), 5.77 (s, 1H, H-1), 4.28 (t, J=6.2 Hz, 2H, H-4), 3.59 (t, J=6.2 Hz, 2H, H-5).

¹³C NMR (151 MHz, CDCl₃) δ 129.51, 125.85, 114.53, 67.89, 28.62.

BB13; 4-(3-bromopropoxy)-benzamide

The synthesis of 4-(3-bromopropoxy)-benzamide was done as described in BB12. On a 5 mmol scale, using 1,3-dibromopropane (5 Eq. 25 mmol) [Alfa Aesar GmBH & Co KG], instead of 1,2-dibromoethane. The resulting product was purified by Column chromatography (eluent: EtOAc), yielding 886 mg (69%) of product (Colourless solid).

HRMS m/z (ESI) 258.995, consistent with empirical formula $C_{10}H_{12}BrNO_2$ with an accuracy of 0,9899 ppm (accepted as $[M+H]^+$).

¹H NMR (600 MHz, CDCl₃) δ 7.77–7.72 (m, 2H, H-2), 6.88 (d, J=8.4 Hz, 2H, H-3), 6.06 (s, 1H, H-1), 4.10 (t, J=5.8 Hz, 2H, H-4), 3.54 (t, J=6.4 Hz, 2H, H-6), 2.28 (h, J=6.1 Hz, 2H, H-5). ¹³C NMR (151 MHz, CDCl₃) δ 207.58, 169.32, 162.10, 134.06, 129.59, 124.81, 115.21, 114.68, 114.44, 80.97, 65.65, 65.54, 34.87, 32.12, 31.11, 29.70, 29.49.

BB14; 4-(3-bromobutoxy)-benzamide

The synthesis of 4-(3-bromobutoxy)-benzamide was done as described in BB12. On a 3 mmol scale, using 1,4-dibromobutane (5 Eq, 15 mmol) [Merck], instead of 1,2-dibromoethane. The resulting product was purified twice by Column chromatography (eluents: EtOAc/MeOH 9.5/0.5; EtOAc/MeOH 9.75/0.25), yielding 251 mg (31%) of product (Colourless solid).

HRMS m/z (ESI) 272.007, consistent with empirical formula $C_{11}H_{14}BrNO_2$ with an accuracy of 0.0138 ppm (accepted as $[M+H]^+$).

¹H NMR (500 MHz, CDCl₃) δ 7.81–7.73 (m, 2H, H-2), 6.91–6.84 (m, 2H, H-3), 6.46 (s, 2H, H-1), 3.99 (t, J=6.0 Hz, 2H, H-4), 3.42 (t, J=6.5 Hz, 2H, H-7), 2.01 (dddd, J=12.0, 10.0, 6.1, 2.3 Hz, 2H, H-5), 1.98–1.87 (m, 2H, H-6).

 13 C NMR (126 MHz, CDCl₃) δ 182.72, 176.55, 170.25, 130.17, 115.55, 114.90, 89.91, 77.67, 67.60, 33.63, 33.50, 28.12, 28.04.

BB15; 4-(3-bromopentoxy)-benzamide

The synthesis of 4-(3-bromopentoxy)-benzamide was done as described in BB12. On a 3 mmol scale, using 1,5-dibromopentane (5 Eq, 15 mmol) [Alfa Aesar GmbH & Co KG], instead of 1,2-dibromoethane. The resulting product was purified by Column chromatography (eluents: EtOAc/MeOH 9.5/0.5), yielding 498 mg (58%) of product (Colourless solid).

HRMS m/z (ESI) 286.048, consistent with empirical formula $C_{12}H_{16}BrNO_2$ with an accuracy of 0.0122 ppm (accepted as $[M+H]^+$).

¹H NMR (400 MHz, CDCl₃) δ 7.84 (d, J=8.5 Hz, 2H, H-2), 6.96 (d, J=8.3 Hz, 2H, H-3), 6.41 (s, 2H, H-1), 4.05 (t, J=6.3 Hz, 2H, H-4), 3.48–3.43 (m, 2H, H-5), 2.03–1.93 (m, 2H, H-6), 1.87 (ddt, J=14.6, 8.3, 3.8 Hz, 2H, H-8), 1.73–1.60 (m, 2H, H-7).

 13 C NMR (101 MHz, CDCl₃) δ 129.67, 115.16, 114.65, 114.46, 86.58, 78.79, 67.89, 33.49, 33.26, 32.40, 31.87, 24.76.

BB16; 4-oxiranylethoxy benzamide

4-oxiranylethoxy benzamide was synthesized comparable to BB01. 4-hydroxybenzamide (2 mmol) [Fluorochem] was added to a solution of 1 Eq of NaOH (2 mmol) [Grüssing GmbH] in 3 ml of H_2O . The mixture was treated with 3 Eq of 2-(chloroethyl)oxirane (6 mmol) [SIA Enamine, Riga, Latvia], and stirred at RT O/N. A Colourless precipitate was visible, on the stirrer. This was filtered, scrapped off, and washed with H_2O , yielding 197 mg (48%) of a Colourless solid.

HRMS m/z (EI) 246.071, consistent with empirical formula $C_{11}H_{13}NO_3$ with an accuracy of 0.0184 ppm (accepted as $[M+K]^+$).

¹H NMR (300 MHz, DMSO- d_6) δ 7.89–7.78 (m, 3H, H-2, H-1), 7.18 (s, 1H, H-1), 7.04–6.93 (m, 2H, H-3), 5.22–5.14 (m, 1H, H-4), 4.05–3.90 (m, 3H, H-4, H-5), 3.77 (ddd, J=7.9, 5.9, 1.7 Hz, 2H, H-7), 1.92 (tdd, J=14.1, 10.1, 5.9 Hz, 1H, H-6).

¹³C NMR (75 MHz, DMSO- d_6) δ 167.85, 161.38, 129.80, 126.99, 114.38, 72.43, 65.99, 42.56, 36.96.

BB17; 4-[(2-methyl-2-oxiranyl)methoxy]-benzamide

4-[(2-methyl-2-oxiranyl)methoxy]-benzamide was synthesized comparable to BB01. 4-hydroxybenzamide (2 mmol) [Fluorochem] was added to a solution of 1 Eq of NaOH (2 mmol) [Grüssing GmbH] in 3 ml of H_2O . The mixture was treated with 3 Eq of 2-(chloromethyl)-2-methyloxirane (6 mmol) [Fluorochem], and stirred at RT O/N. A Colourless precipitate was visible. This was filtered, and washed with H_2O , yielding 228 mg (55%) of a Colourless solid.

HRMS m/z (EI) 208.081, consistent with empirical formula $C_{11}H_{12}NO_3$ with an accuracy of 0.0085 ppm (accepted as $[M+H]^+$).

¹H NMR (400 MHz, MeOH- d_4) δ 7.90–7.81 (m, 2H, H-2), 7.08–6.99 (m, 2H, H-3), 4.23 (d, J=10.9 Hz, 1H, H-4), 3.98 (d, J=10.9 Hz, 1H, H-4), 2.90 (d, J=4.8 Hz, 1H, H-5), 2.76 (d, J=4.8 Hz, 1H, H-5), 1.48 (s, 3H, H-6).

 13 C NMR (126 MHz, DMSO- d_6) δ 167.74, 167.70, 161.41, 161.04, 129.70, 127.18, 126.96, 114.38, 72.49, 71.77, 70.70, 55.58, 51.13, 22.49, 18.52.

3.2.4 The chemical synthesis of Ro8-4304 and the Ro8-4304 derivatives

Ro8-4304; (4-{3-[4-fluoro-phenyl-3, 6-dihyrdro-1(2H)-pyridyl]-2-hydoxy-propoxy}-benzamide)

The synthesis of **Ro8-4304** was adapted from US patent no. 3,674,799, 1972 169 . 4-(4-fluorophenyl-1,2,3,6- tetrahydropyridine • HCl (PTP-F) (0.5 mmol) [Acros Organics] was dissolved in 5 ml of ethanol (EtOH). 2 Eq (1 mmol) of TEA [Grüssing GmbH] was added, and the mixture was stirred for 5 min before the addition of BB01 (0.5 mmol). This mixture was stirred at reflux (\sim 78°C) for 4 h. The reaction mixture was allowed to cool down, and a beige precipitate separated out. This was filtered and washed with EtOH. The leftover product was treated with 3 ml ethanolic HCl (1 M). This was stirred for 2 h, filtered, and washed with EtOH, giving 84 mg of beige compound (45.6%). The residual EtOH was removed in vacuo, and the product was used without further purification.

Ethanolic HCl (1 M) is created by slowly adding acetyl chloride (0.71 ml) [Merck] to cooled EtOH (9.29 ml, \sim 0°C).

HRMS m/z (ESI) 371.178, consistent with empirical formula $C_{21}H_{23}FN_2O_3$ with an accuracy of 0.0087 ppm (accepted as $[M+H]^+$).

¹H NMR (600 MHz, DMSO- d_6) δ 10.54 (s, 0H), 10.43 (s, 1H), 7.90 –7.83 (m, 3H, H-1, H-2), 7.59-7.52 (m, 2H, H-13), 7.27–7.20 (m, 2H, H-12), 7.21 (s, 1H, H-1), 7.05–6.99 (m, 2H, H-3), 6.19 (q, J=3.3, 2.9 Hz, 1H, H-11), 6.05 (s, 1H, H-7), 4.59–4.34 (m, 1H, H-5), 4.12 (d, J=16.4 Hz, 1H, H-4), 4.07 (d, J= 4.9 Hz, 2H, H-4, H-6), 3.95–3.88 (m, 1H, H-10), 3.80 (d, J=11.9 Hz, 1H, H-10), 3.68 (d, J=12.4 Hz, 1H, H-6), 3.49–3.39 (m, 1H, H-9), 3.31 (ddd, J=17.6, 13.3, 7.2 Hz, 1H, H-9), 2.95–2.87 (m, 1H, H-8), 2.76 (t, J=14.9 Hz, 1H, H-8).

 13 C NMR (151 MHz, DMSO- d_6) δ 167.78, 163.16, 161.53, 161.06, 135.25, 135.23, 129.86, 127.42, 127.36, 116.73, 116.49, 115.91, 115.76, 114.46, 106.85, 70.67, 64.50, 64.29, 57.84, 57.72, 51.72, 50.00, 49.88, 48.50, 24.07, 23.75.

¹⁹F NMR: (565 MHz, DMSO- d_6) δ -114.72 (1F).

Ro-A01; 4-[3-[4-(4-bromophenyl)-3,6-dihydro-1(2H)-pyridinyl]-2-hydroxypropoxy]-benzamide

Ro-A01 was synthesized on a 0.5 mmol scale using BB01, and BB02. The synthesis was performed as described in Ro8-4304. However, the reaction was stirred at reflux O/N, and the work-up was changed. The precipitate could not be filtered after cooling down to RT, while it was too fine. So, the solvent was removed in vacuo, and the product was treated

with 3 ml ethanolic HCl (1M). This was stirred for 3 h, and the solvent was again removed in vacuo. The leftover compound dissolved in MeOH, but not in DCM, so recrystallization was tried, with two solvents. A light beige solid precipitated out of a yellow solution. This was filtered and washed with DCM. This gave the product in an amount of 79 mg (37%). HRMS m/z (ESI) 431.0973, consistent with empirical formula $C_{21}H_{23}BrN_2O_3$ with an accuracy of 0.0081 ppm (accepted as $[M+H]^+$).

¹H NMR (400 MHz, DMSO- d_6) δ 7.90–7.81 (m, 3H, H-2), 7.63–7.57 (m, 2H, H-13), 7.51–7.42 (m, 2H, H-12), 7.20 (s, 1H, H-1), 7.05–6.98 (m, 2H, H-2), 6.27 (s, 1H, H-11), 4.44 (s, 1H, H-4), 4.06 (d, J=5.0 Hz, 2H, H-10), 3.88 (d, J=43.8 Hz, 1H, H-5), 3.00 (s, 3H, H-9), 2.97–2.59 (m, 2H, H-6), 1.21 (dt, J= 12.2, 7.0 Hz, 2H, H-8).

¹³C NMR (101 MHz, DMSO- d_6) δ 167.78, 131.95, 129.86, 127.45, 114.46, 70.61, 49.06.

Ro-A02; (4-{3-[4-hydroxy-phenyl-3,6-dihyrdro-1(2H)-pyridyl]-2-hydoxy-propoxy}-benzamide)

Ro-A02 was synthesized on a 0.3 mmol scale using BB01, and BB03. The synthesis was performed as described in Ro8-4304. This reaction yielded 47 mg (42%) of a yellow solid. This was used without further purification.

HRMS m/z (ESI) 369.152, consistent with empirical formula $C_{21}H_{24}N_2O_4$ with an accuracy of 0.0216 ppm (accepted as [M+H]⁺).

¹H NMR (400 MHz, DMSO- d_6) δ 10.33 (d, J=45.7 Hz, 1H), 7.86 (d, J=8.2 Hz, 2H, H-2), 7.32 (d, J=8.6 Hz, 2H, H-13), 7.23–7.19 (m, 2H, H-1), 7.01 (dt, J=9.0, 2.0 Hz, 2H, H-3), 6.78 (d, J=8.6 Hz, 2H, H-12), 6.02 (s, 1H, H-11), 4.69–4.38 (m, 1H, H-4), 4.06 (d, J=4.8 Hz, 2H, H-10), 3.47–3.26 (m, 2H, H-8), 3.05 (dd, J=7.3, 4.8 Hz, 1H, H-5), 2.98–2.58 (m, 2H, H-6), 1.20 (t, J=7.3 Hz, 1H, H-4), 1.05 (t, J=7.0 Hz, 2H, H-9).

 ^{13}C NMR (101 MHz, DMSO- d_6) δ 167.30, 160.55, 129.36, 125.94, 115.24, 113.95, 113.03, 112.80, 70.16, 63.99, 63.75, 45.33.

Ro-A03; 4-[3-(3,6-dihydro-4-phenyl-1(2H)-pyridinyl)-2-hydroxypropoxy]-benzamide

Ro-A03 was synthesized on a 1 mmol scale using BB01, and BB04. The synthesis was performed as described in Ro8-4304. However, the reaction was stirred at reflux O/N, and the work-up was changed. The next day, a red precipitate was visible, and the solution was slowly allowed to cool down to RT. Hereafter, the solution was treated with ethanolic HCl

(1M) till the pH reached 2-3. This was stirred for 3 h. The precipitate re-appeared, and was filtered, washed with EtOH, and placed on the vacuum pomp for drying. The beige product was obtained in an amount of 240 mg (68%).

HRMS m/z (ESI) 353.187, consistent with empirical formula $C_{21}H_{24}N_2O_3$ with an accuracy of 0.0083 ppm (accepted as [M+H]⁺).

¹H NMR (500 MHz, DMSO- d_6) δ 7.91–7.82 (m, 2H, H-2), 7.85 (s, 1H, H-1), 7.54–7.49 (m, 2H, H-12), 7.44–7.37 (m, 2H, H-13), 7.38–7.31 (m, 1H, H-14), 7.20 (s, 1H, H-1), 7.06–6.98 (m, 2H, H-3), 6.22 (s, 1H, H-11), 6.01 (s, 1H, H-7), 4.43 (d, J=15.4 Hz, 1H, H-5), 4.17–4.03 (m, 3H, H-10, H-4), 3.94 (s, 1H, H-4), 3.85–3.66 (m, 1H, H-6), 3.60–3.57 (m, 1H, H-6), 3.08 (dd, J=7.3, 4.8 Hz, 0H, H-9), 2.93 (d, J = 11.4 Hz, 0H, H-9), 2.84–2.74 (m, 2H, H-8), 1.26–1.16 (m, 1H). ¹³C NMR (126 MHz, DMSO- d_6) δ 167.67, 160.94, 129.76, 128.98, 128.38, 125.19, 114.36, 70.52, 61.68, 56.39, 46.00, 28.99, 18.92.

Ro-A04; 4-[3-[3,6-dihydro-1(2H)-pyridinyl]-2-hydroxypropoxy]-benzamide

Ro-A04 was synthesized on a 1 mmol scale using BB01, and 1,2,3,6-tetrahydropyridine • HCl [abcr GmbH & Co. KG]. The synthesis was performed as described in Ro8-4304. However, the reaction was stirred at reflux O/N. The next day, this was slowly cooled down to RT. A yellow solution was visible. EtOH was removed in vacuo, and the product was purified in reverse phase on a flash chromatograph with an eluent of 100% H_2O to 100% ACN. Appropriate fractions were combined, and the solvent of these fractions was removed in vacuo, leaving a Colourless powder in a yield of 69 mg (25%).

HRMS m/z (ESI) 277.133, consistent with empirical formula $C_{15}H_{28}N_2O_3$ with an accuracy of 0.0144 ppm (accepted as [M+H]⁺).

¹H NMR (500 MHz, DMSO- d_6) δ 7.87–7.80 (m, 2H, H-2), 7.82 (s, 1H, H-1), 7.16 (s, 1H, H-1), 7.01–6.95 (m, 2H, H-3), 5.73–5.60 (m, 2H, H-10), 4.90 (d, J=4.8 Hz, 1H, H-4), 4.05 (dd, J=9.7, 3.6 Hz, 1H, H-4), 4.02–3.96 (m, 1H, H-5), 3.93 (dd, J=9.7, 6.0 Hz, 1H, H-6), 3.32 (s, 1H, H-7), 3.00–2.94 (m, 2H, H-11), 2.64-2.52 (m, 2H, H-8), 2.44 (dd, J=12.7, 6.3 Hz, 1H, H-6), 2.08 (dh, J=7.5, 2.4 Hz, 2H, H-9).

¹³C NMR (126 MHz, DMSO- d_6) δ 167.78, 161.49, 159.11, 129.70, 126.77, 126.02, 125.16, 114.26, 71.58, 66.92, 61.39, 53.32, 50.64, 26.13.

Ro-A05; 4-[3-[4-(4-trifluoromethylphenyl)-piperidin-4-ol]-2-hydroxypropoxy]-benzamide

Ro-A05 was synthesized on a 1 mmol scale using BB01, and [4-(trifluoromethyl)phenyl]4-piperidinol (0.88 mmol) [Matrix Scientific]. The synthesis was performed as described in

Ro8-4304. However, the reaction was stirred at reflux O/N. The next day, this was slowly cooled down to RT. An orange solution was visible. EtOH was removed in vacuo, and the obtained product was purified by Column chromatography (eluent: EtOAc/MeOH 9/1). This left a beige solid, in a yield of 89 mg (21%).

HRMS m/z (ESI) 439.185, consistent with empirical formula $C_{22}H_{25}F_3N_2O_4$ with an accuracy of 0.0084 ppm (accepted as [M+H]⁺).

¹H NMR (600 MHz, DMSO- d_6) δ 7.93–7.87 (m, 2H, H-2), 7.88 (s, 1H, H-1), 7.76 (d, J=8.4 Hz, 2H, H-14), 7.73 (d, J=8.5 Hz, 2H, H-13), 7.23 (s, 1H, H-1), 7.09–7.03 (m, 2H, H-3), 4.93 (s, 1H, H-12), 4.14 (dd, J=9.8, 3.4 Hz, 2H, H-9), 4.06 (s, 1H, H-7), 4.01 (dd, J=9.8, 6.1 Hz, 2H, H-8), 2.82 (s, 1H, H-4), 2.76 (s, 1H, H-4), 2.60 (s, 1H, H-5), 2.51 (s, 2H, H-6, H-10), 2.06–1.98 (m, 2H, H-6, H-10), 1.64 (dd, J=13.8, 6.3 Hz, 2H, H-11).

 13 C NMR (151 MHz, DMSO- d_6) δ 167.87, 161.61, 129.95, 129.80, 127.30, 126.88, 126.21, 125.27, 125.24, 125.21, 114.40, 113.92, 104.44, 71.77, 70.16, 61.62, 58.51, 50.18, 40.52, 38.28.

¹⁹F NMR: (565 MHz, DMSO- d_6) δ -60.79 (3F).

Ro-A06; 4-[3-[4-(4-trifluoromethylphenyl)-3,6-dihydro-1(2H)-pyridinyl]-2-hydroxypropoxy]-benzamide

Ro-A06 was synthesized on a 0.6 mmol scale using BB01, and BB05. The synthesis was performed as described in Ro8-4304. However, the reaction was stirred at reflux O/N. The next day, this was slowly cooled down to RT. An orange solution was visible. EtOH was removed in vacuo, and the obtained product was purified by Column chromatography (eluent: EtOAc/MeOH 9/1). This left a yellow oil, in a yield of 16 mg (6%). This was still contaminated, however since the yield was so low, no further purification was done. HRMS m/z (ESI) 421.171, consistent with empirical formula $C_{22}H_{23}F_3N_2O_3$ with an accuracy of 0.0049 ppm (accepted as [M+H]⁺).

¹H NMR (600 MHz, DMSO- d_6) δ 7.89–7.81 (m, 2H, H-2), 7.71 (s, 2H, H-1), 7.70–7.64 (m, 2H, H-13), 7.19 (d, J=16.6 Hz, 2H, H-12), 7.04–6.95 (m, 2H, H-3), 6.35 (s, 1H, H-11), 4.22–4.10 (m, 1H, H-5), 4.12–4.06 (m, 2H, H-4), 3.97 (s, 1H, H-6), 3.17 (d, J=5.2 Hz, 1H, H-9), 2.74 (s, 1H, H-9), 1.99 (s, 4H, H-8, H-10).

¹³C NMR (151 MHz, DMSO- d_6) δ 167.83, 161.33, 129.85, 129.83, 114.44, 114.40, 113.92, 69.80, 67.77, 60.22, 21.23, 14.56.

¹⁹F NMR: (565 MHz, DMSO- d_6) δ -73.38 (3F).

Ro-A07 & Ro-A08; 4-[3-[4-(4-fluorophenyl)-3,6-dihydro-1(2H)-pyridinyl]-2-hydroxypropoxy]-benzylamine

Ro-A07 was synthesized on a 1 mmol scale using BB07, and PTP-F. The synthesis was performed as described in Ro8-4304. However, the reaction was stirred at reflux O/N, and the work-up was changed. After refluxing, the solution was allowed to cool down to RT. EtOH was removed in vacuo, and a small amount of material was taken this is Ro-A08. To the remaining material, 8 ml ethanolic HCl (1M) was added, and the solution was stirred at reflux for 6 h. The solution was slowly allowed to cool down to RT, and a yellow precipitate separated out. This was filtered and washed with EtOH. Residual solvent was removed in vacuum O/N. A beige solid was obtained in a yield of 128 mg (36%). This was used without further purification.

HRMS Ro-A07 m/z (ESI) 357.1997, consistent with empirical formula $C_{21}H_{25}FN_2O_2$ with an accuracy of 0.0097 ppm (accepted as $[M+H]^+$).

HRMS Ro-A08 m/z (ESI) 479.2317, consistent with empirical formula $C_{26}H_{33}FN_2O_4$ with an accuracy of 0.0535 ppm (accepted as [M+Na]⁺).

¹H NMR Ro-A07 (600 MHz, DMSO- d_6) δ 10.58 (s, 1H), 10.47 (s, 1H), 8.37 (s, 3H, H-1), 7.59–7.51 (m, 2H, H-4), 7.47–7.40 (m, 2H, H-14), 7.27–7.19 (m, 2H, H-3), 7.04–6.97 (m, 2H, H-13), 6.19 (d, J=3.8 Hz, 1H, H-12), 6.07 (s, 0H, H-8), 6.02 (s, 0H, H-8), 4.51–4.43 (m, 1H, H-6), 4.09 (dd, J=34.5, 16.5 Hz, 1H, H-5), 4.01 (d, J=5.0 Hz, 2H, H-11), 3.95 (q, J=5.9 Hz, 3H, H-2, H-5), 3.79 (d, J=12.4 Hz, 1H, H-7), 3.68 (dt, J=11.3, 3.4 Hz, 1H, H-7), 3.49–3.39 (m, 1H, H-10), 3.29 (ddd, J=13.9, 11.2, 3.8 Hz, 1H, H-10), 2.98–2.84 (m, 1H, H-9), 2.76 (t, J=13.5 Hz, 1H, H-9). ¹H NMR Ro-A08 (600 MHz, DMSO- d_6) δ 9.77 (s, 2H), 9.12 (s, 1H), 8.28 (s, 3H, H-1), 7.54 (ddd, J=15.9, 8.9, 5.5 Hz, 2H, H-4), 7.45–7.38 (m, 2H, H-14), 7.23 (q, J=8.8 Hz 2H, H-3), 7.04–6.98 (m, 2H, H-13), 6.19 (s, 1H, H-12), 4.51–4.43 (m, 1H, H-6), 4.14-4.02 (m, 1H, H-5), 4.05-3.97 (m, 2H, H-11), 3.95 (d, J=5.9 Hz, 2H, H-5, H-7), 3.74 (d, J=4.7 Hz, 1H, H-7), 3.45 (t, J=7.0 Hz, 1H, H-10), 3.07 (qd, J=7.3, 4.8 Hz, 2H, H-2), 2.76 (t, J=15.9 Hz, 1H, H-9), 2.67 (s, 1H, H-9; 1.19 (t, J=7.3 Hz, 9H, H-0).

¹³C NMR Ro-A07 (151 MHz, DMSO-*d*₆) δ 161.53, 158.87, 135.22, 133.65, 133.35, 131.03, 127.41, 127.35, 126.88, 126.85, 116.73, 116.50, 115.92, 115.90, 115.78, 115.76, 115.07, 70.70, 64.54, 64.34, 57.87, 57.83, 51.64, 50.03, 49.80, 48.55, 45.84, 42.09, 24.05, 23.77, 8.91.

¹⁹F NMR Ro-A07 & Ro-A08: (565 MHz, DMSO- d_6) δ -114.56 (1F).

Ro-A09; 4-[3-[4-(4-fluorophenyl)-3,6-dihydro-1(2H)-pyridinyl]-2-hydroxypropoxy]-fluorophenyl

Ro-A09 was synthesized on a 0.75 mmol scale using BB08, and PTP-F. The synthesis was performed as described in Ro8-4304. However, the reaction was stirred at reflux O/N. The next day, this was slowly cooled down to RT, before placing it in the freezer O/N. A precipitate was visible. This was filtered and washed with EtOH. The obtained product was treated with 3 ml ethanolic HCl (1M), and this was stirred O/N. The ethanolic liquid was removed in vacuo, leaving a Colourless solid, in a yield of 142 mg (55%). This was used without further purification.

HRMS m/z (ESI) 346.178, consistent with empirical formula $C_{20}H_{21}F_2NO_2$ with an accuracy of 0.024 ppm (accepted as $[M+H]^+$).

¹H NMR (400 MHz, DMSO- d_6) δ 10.38 (s, 1H), 10.28 (s, 1H), 7.66–7.56 (m, 2H, H-2), 7.29 (t, J=8.8 Hz, 2H, H-1), 7.20 (t, J= 8.9 Hz, 2H, H-12), 7.05 (ddd, J=9.0, 4.3, 1.5 Hz, 2H, H-11), 6.24 (s, 1H, H-10), 4.54–4.44 (m, 1H, H-4), 4.12 (d, J=19.7 Hz, 1H, H-9), 4.03 (d, J=5.0 Hz, 2H, H-3), 3.96 (d, J=16.6 Hz, 1H, H-9), 3.84 (d, J=12.4 Hz, 1H, H-5), 3.79–3.67 (m, 0H, H-5), 3.52 (s, 1H, H-8), 3.40–3.32 (m, 1H, H-8), 2.94 (s, 1H, H-7), 2.86 (d, J = 20.6 Hz, 1H, H-7). ¹³C NMR (101 MHz, DMSO- d_6) δ 155.11, 133.70, 133.39, 127.44, 127.36, 116.72, 116.49, 116.44, 116.36, 116.25, 115.95, 115.73, 71.17, 64.52, 64.30, 57.86, 57.69, 51.80, 49.99, 49.93, 48.42, 45.94, 40.63, 40.42, 40.20, 39.99, 39.78, 39.56, 39.35, 24.06, 23.76. ¹⁹F NMR: (565 MHz, DMSO- d_6) δ -114.37, -123.53 (2F).

Ro-A10; 4-[3-[4-(4-fluorophenyl)-3,6-dihydro-1(2H)-pyridinyl]-2-hydroxypropoxy]-phenyl

Ro-A10 was synthesized on a 0.75 mmol scale using BB09, and PTP-F. The synthesis was performed as described in Ro8-4304. However, the reaction was stirred at reflux O/N. The next day, this was slowly cooled down to RT, before placing it in the freezer O/N. The precipitate was filtered and washed with EtOH. The obtained product was purified by Column chromatography (eluent: DCM/MeOH 9/1), and hereafter treated with 3 ml ethanolic HCl (1M). This was stirred O/N. The ethanolic liquid was removed in vacuo, leaving a Colourless solid, in a yield of 161 mg (66%).

HRMS m/z (ESI) 328.180, consistent with empirical formula $C_{20}H_{22}FNO_2$ with an accuracy of 0.0165 ppm (accepted as [M+H]⁺).

¹H NMR (400 MHz, DMSO- d_6) δ 10.27 (s, 1H), 10.19 (s, 0H), 7.65–7.57 (m, 2H, H-13), 7.42–7.30 (m, 2H, H-3), 7.34–7.24 (m, 2H, H-12), 7.02 (ddd, J=8.4, 6.9, 2.6 Hz, 3H, H-2, H-1), 6.24 (s, 1H, H-11), 4.49 (s, 1H, H-4), 4.25–4.05 (m, 1H, H-8), 4.08–4.01 (m, 2H, H-10), 3.97 (d, J=17.2 Hz, 1H, H-9), 3.89–3.68 (m, 1H, H-9), 3.62–3.39 (m, 1H, H-5), 2.94 (s, 1H, H-6), 2.88–2.81 (m, 1H, H-6).

¹³C NMR (101 MHz, DMSO-*d*₆) δ 158.71, 130.04, 127.45, 127.36, 121.43, 116.72, 116.44, 115.97, 115.75, 115.03, 70.41, 64.53, 64.29, 57.88, 57.66, 56.49, 51.85, 50.06, 49.87, 48.34, 24.07, 23.76.

¹⁹F NMR: (565 MHz, DMSO- d_6) δ -114.32 (1F).

Ro-A11; 4-[3-[4-(4-fluorophenyl)-3,6-dihydro-1(2H)-pyridinyl]-2-hydroxypropoxy]-phenyl ethanone

Ro-A11 was synthesized on a 1 mmol scale using BB10, and PTP-F. The synthesis was performed as described in Ro8-4304. However, 2.5 Eq of TEA was used, and the reaction was stirred at reflux O/N. The next day, this was slowly cooled down to RT. An orange solution was visible. The EtOH was removed in vacuo, and the product was purified by Column chromatography (eluent: EtOAc/ MeOH, 9/1), yielding 242 mg (66%) of product (beige solid).

HRMS m/z (ESI) 370.202, consistent with empirical formula $C_{22}H_{24}NO_3$ with an accuracy of 0.028 ppm (accepted as $[M+H]^+$).

¹H NMR (600 MHz, DMSO- d_6) δ 7.95–7.90 (m, 2H, H-3), 7.50–7.43 (m, 2H, H-13), 7.19–7.12 (m, 2H, H-12), 7.09–7.03 (m, 2H, H-2), 6.12 (dq, J=3.5, 1.8 Hz, 1H, H-11), 4.11 (dd, J=9.8, 3.5 Hz, 1H, H-9), 4.08–4.03 (m, 1H, H-9), 4.05–3.96 (m, 1H, H-8), 3.31 (s, 1H, H-8), 3.17 (q, J=3.1 Hz, 2H, H-10), 2.75 (dt, J=11.2, 5.6 Hz, 1H, H-4), 2.68 (dt, J=11.3, 5.7 Hz, 1H, H-4), 2.59 (dd, J=12.6, 6.1 Hz, 1H, H-5), 2.52 (s, 3H, H-1), 2.46 (dt, J=6.1, 3.3 Hz, 2H, H-6).

¹³C NMR (151 MHz, DMSO- d_6) δ 196.74, 163.15, 162.59, 160.98, 137.09, 137.07, 133.39, 130.95, 130.27, 126.91, 126.86, 122.61, 115.59, 115.45, 114.80, 113.92, 71.82, 67.09, 66.99, 61.11, 53.87, 51.02, 27.95, 26.87.

¹⁹F NMR: (565 MHz, DMSO- d_6) δ -115.93 (1F).

Ro-A12; 4-[3-[4-(4-fluorophenyl)-3,6-dihydro-1(2H)-pyridinyl]-2-hydroxypropoxy]-ethylphenoxy

Ro-A12 was synthesized on a 1 mmol scale using BB11, and PTP-F. The synthesis was performed as described in Ro8-4304. However, the reaction was stirred at reflux O/N. The next day, this was slowly cooled down to RT. A precipitate was visible. This was filtered and washed with a small amount of EtOH. The obtained product was treated with 3 ml ethanolic HCl (1M), and this was stirred for 1 h before removal in vacuo. This left a beige solid, in a yield of 52 mg (38%). This was used without any further purification.

HRMS m/z (ESI) 356.196, consistent with empirical formula $C_{22}H_{16}FNO_2$ with an accuracy of 0.0012 ppm (accepted as [M+H]⁺).

¹H NMR (600 MHz, DMSO- d_6) δ 10.22 (s, 0H), 10.13 (s, 1H), 7.59–7.52 (m, 2H, H-14), 7.27–7.20 (m, 2H, H-13), 7.14 (d, J=8.1 Hz, 2H, H-4), 6.91–6.86 (m, 2H, H-3), 6.19 (s, 1H, H-12), 6.00 (s, 1H, H-8), 5.95 (s, 0H, H-8), 4.41 (s, 1H, H-6), 4.14–4.01 (m, 1H, H-5), 4.00–3.86 (m, 3H, H-5, H-11), 3.78 (d, J=12.1 Hz, 1H, H-7), 3.69 (d, J=12.2 Hz, 1H, H-7), 3.50–3.34 (m, 1H, H-10), 3.30 (s, 1H, H-10), 2.94–2.86 (m, 1H, H-9), 2.76 (t, J=15.9 Hz, 1H, H-9), 2.54 (q, J=7.6 Hz, 2H, H-2), 1.15 (t, J=7.6 Hz, 3H, H-3).

¹³C NMR (151 MHz, DMSO- d_6) δ 161.54, 156.79, 136.67, 135.22, 133.70, 129.17, 127.43, 127.37, 116.73, 116.45, 115.92, 115.78, 114.92, 70.55, 64.53, 64.29, 57.90, 57.68, 51.85, 50.04, 49.85, 48.32, 27.92, 27.75, 24.07, 23.74, 16.42.

¹⁹F NMR: (565 MHz, DMSO- d_6) δ -114.3 (1F).

Ro-A13; 4-[3-[4-(4-fluorophenyl)-3,6-dihydro-1(2H)-pyridinyl]-ethoxy]-benzamide

Ro-A13 was synthesized on a 1 mmol scale using BB12, and PTP-F. The synthesis was performed as described in Ro8-4304. However, 2.5 Eq of TEA was used, and the reaction was stirred at reflux O/N. The next day, this was slowly cooled down to RT. The EtOH was removed in vacuo leaving an orange solution, this was treated with 3 ml ethanolic HCl (1M) and stirred for 1 h before removal in vacuo. The resulting product was purified by Column chromatography (eluent: DCM/MeOH 9/1), yielding 211 mg (62%) of product (light yellow solid).

HRMS m/z (ESI) 341.167, consistent with empirical formula $C_{20}H_{21}FN_2O_2$ with an accuracy of 0.0083 ppm (accepted as [M+H]⁺).

¹H NMR (600 MHz, DMSO- d_6) δ 9.79 (s, 2H, H-1), 7.88–7.83 (m, 2H, H-2), 7.56–7.50 (m, 2H, H-11), 7.25–7.19 (m, 2H, H-10), 7.02 (d, J=8.5 Hz, 2H, H-3), 6.17 (dq, J=3.5, 1.8 Hz, 1H, H-9), 3.74 (q, J=2.7 Hz, 2H, H-8), 3.30 (t, J = 6.0 Hz, 2H, H-7), 3.09 (s, 2H, H-4), 2.67 (tq, J=3.9, 2.0 Hz, 2H, H-5), 1.30 (s, 1H, H-6), 1.29 (ddd, J=12.8, 3.4, 0.0 Hz, 1H, H-6).

¹³C NMR (151 MHz, DMSO- d_6) δ 167.82, 133.78, 133.47, 129.83, 127.33, 127.27, 117.39, 115.91, 115.77, 115.65, 115.50, 114.40, 45.92, 41.88, 40.51,31.97, 23.67, 15.67, 8.98. ¹⁹F NMR: (565 MHz, DMSO- d_6) δ -114.54 (1F).

Ro-A14; 4-[3-[4-(4-fluorophenyl)-3,6-dihydro-1(2H)-pyridinyl]-propoxy]-benzamide

Ro-A14 was synthesized on a 1 mmol scale using BB13, and PTP-F. The synthesis was performed as described in Ro8-4304. However, 2.5 Eq of TEA was used, and the reaction was stirred at reflux O/N. The next day, this was slowly cooled down to RT. A beige precipitate was visible, in an orange solution. This was filtered and washed with EtOH. The obtained product was treated with 3 ml ethanolic HCl (1M), and this was stirred for 1 h before removal in vacuo. This left a lightly yellow solid, in a yield of 133 mg (38%). This was used without any further purification.

HRMS m/z (ESI) 355.189, consistent with empirical formula $C_{21}H_{23}FN_2O_2$ with an accuracy of 0.0146 ppm (accepted as $[M+H]^+$).

¹H NMR (400 MHz, DMSO- d_6) δ 10.74 (s, 1H), 7.91–7.81 (m, 2H, H-2), 7.61–7.51 (m, 2H, H-12), 7.28–7.18 (m, 2H, H-11), 7.19 (s, 1H, H-1), 7.04–6.96 (m, 2H, H-3), 6.19 (d, J=3.2 Hz, 1H, H-10), 4.16 (t, J=6.1 Hz, 2H, H-4), 4.04 (d, J=17.1 Hz, 1H, H-9), 3.87–3.59 (m, 0H, H-9), 3.70 (d, J=11.6 Hz, 1H, H-8), 3.39–3.30 (m, 2H, H-6), 3.25 (dd, J=14.3, 7.3 Hz, 1H, H-8), 2.96–2.84 (m, 1H, H-7), 2.75 (d, J=17.6 Hz, 1H, H-7), 2.27 (dd, J=10.7, 6.0 Hz, 2H, H-5).

¹³C NMR (101 MHz, DMSO-*d*₆) δ 167.81, 161.14, 161.04, 135.21, 135.17, 133.64, 129.85, 127.45, 127.37, 127.23, 116.75, 115.96, 115.74, 114.37, 65.60, 52.78, 50.10, 48.57, 24.22, 23.96, 21.81.

¹⁹F NMR: (565 MHz, DMSO- d_6) δ -114.34 (1F).

Ro-A15; 4-[3-[4-(4-fluorophenyl)-3,6-dihydro-1(2H)-pyridinyl]-butoxy]-benzamide

Ro-A15 was synthesized on a 1 mmol scale using BB14, and PTP-F. The synthesis was performed as described in Ro8-4304. However, 2.5 Eq of TEA was used, and the reaction was stirred at reflux O/N. The next day, this was slowly cooled down to RT. A yellow precipitate was visible. This was filtered and washed with EtOH. The obtained product was treated with 3 ml ethanolic HCl (1M), and this was stirred for 1 h before removal in vacuo. This left a beige solid, in a yield of 207 mg (61%). This was used without any further purification.

HRMS m/z (ESI) 369.207, consistent with empirical formula $C_{22}H_{25}FN_2O_2$ with an accuracy of 0.017 ppm (accepted as $[M+H]^+$).

¹H NMR (600 MHz, DMSO- d_6) δ 10.52 (s, 1H), 7.88–7.85 (m, 2H, H-2), 7.57–7.52 (m, 2H, H-13), 7.26–7.20 (m, 2H, H-12), 7.19 (s, 1H, H-1), 7.02–6.94 (m, 2H, H-3), 6.17 (p, J=2.2 Hz, 1H,

H-11), 4.07 (dt, J=11.2, 6.1 Hz, 2H, H-10), 4.00 (d, J=18.9 Hz, 1H, H-4), 3.80–3.69 (m, 1H, H-4), 3.65 (dd, J=10.7, 5.0 Hz, 1H, H-8), 3.24 (ddqd, J=15.8, 9.4, 5.8, 3.8, 3.0 Hz, 3H, H-7, H-8), 2.90–2.81 (m, 1H, H-9), 2.74 (d, J=17.5 Hz, 1H, H-9), 1.97–1.76 (m, 4H, H-5, H-6). ¹³C NMR (151 MHz, DMSO-d₆) δ 167.82, 161.53, 161.28, 135.22, 135.19, 133.63, 129.83, 127.42, 127.37, 127.01, 116.75, 115.92, 115.78, 114.34, 114.29, 67.47, 54.93, 50.03, 49.94, 48.49, 26.27, 24.16, 20.85, 8.94.

¹⁹F NMR: (565 MHz, DMSO- d_6) δ -114.36 (1F).

Ro-A16; 4-[3-[4-(4-fluorophenyl)-3,6-dihydro-1(2H)-pyridinyl]-pentoxy]-benzamide

Ro-A16 was synthesized on a 1 mmol scale using BB15, and PTP-F. The synthesis was performed as described in Ro8-4304. However, 2.5 Eq of TEA was used, and the reaction was stirred at reflux O/N. The next day, this was slowly cooled down to RT. The EtOH was removed in vacuo leaving an orange solution, this was treated with 3 ml ethanolic HCl (1M), and stirred for 1 h, before removal in vacuo. The resulting product was purified by Column chromatography (eluent: DCM/MeOH 9/1), yielding 115 mg (30%) of product (yellow solid). HRMS m/z (ESI) 383.214, consistent with empirical formula $C_{23}H_{27}FN_2O_2$ with an accuracy of 0.0083 ppm (accepted as [M+H]⁺).

¹H NMR (600 MHz, DMSO- d_6) δ 7.87–7.82 (m, 2H, H-3), 7.83 (s, 1H, H-1), 7.58–7.53 (m, 2H, H-14), 7.26–7.20 (m, 2H, H-13), 7.00–6.95 (m, 2H, H-2), 6.18 (s, 1H, H-12), 4.06 (t, J=6.3 Hz, 2H, H-11), 4.00 (d, J=16.9 Hz, 1H, H-4), 3.80–3.73 (m, 1H, H-9), 3.66 (d, J=12.1 Hz, 1H, H-9), 3.23 (d, J=11.2 Hz, 2H, H-10), 3.17 (s, 3H, H-4, H-5), 2.82 (s, 1H, H-6), 1.79 (s, 3H, H-6, H-7), 1.49 (p, J=7.7 Hz, 2H, H-8).

¹³C NMR (151 MHz, DMSO- d_6) δ 167.83, 133.67, 129.83, 127.45, 127.39, 116.78, 115.93, 115.79, 114.28, 67.74, 55.41, 55.14, 46.00, 23.50, 23.14, 8.99.

¹⁹F NMR: (565 MHz, DMSO- d_6) δ -114.35 (1F).

Ro-A17; 4-[3-[4-(4-fluorophenyl)-3,6-dihydro-1(2H)-pyridinyl]-2-hydroxybutoxy]-benzamide

Ro-A17 was synthesized on a 1 mmol scale using BB16, and PTP-F. The synthesis was performed as described in Ro8-4304. However, the reaction was stirred at reflux O/N. The next day, this was slowly cooled down to RT. An orange solution was visible. EtOH was removed in vacuo, and the obtained product was purified by Column chromatography (eluent: EtOAc/MeOH 9/1). However, the product was stuck on the Column, thus the eluent was changed to 100% MeOH. This gave a yellow solid, in a yield of 29 mg (9%). This was still

contaminated with PTP-F, however since the yield was so low, no further purification was done. Probably a reverse phase Column purification would have been better.

HRMS m/z (ESI) 385.192, consistent with empirical formula $C_{22}H_{25}FN_2O_3$ with an accuracy of 0.0071 ppm (accepted as [M+H]⁺).

¹H NMR (600 MHz, DMSO- d_6) δ 7.93–7.87 (m, 3H, H-2, H-1), 7.61–7.55 (m, 2H, H-14), 7.31–7.25 (m, 2H, H-13), 7.07–7.02 (m, 2H, H-3), 6.23 (td, J=3.6, 1.8 Hz, 1H, H-10), 4.19 (q, J=5.2 Hz, 1H, H-6), 4.05–3.94 (m, 4H, H-4, H-5), 3.76 (q, J=2.7 Hz, 2H, H-9), 3.32 (t, J=6.0 Hz, 2H, H-11), 3.23 (d, J=5.1 Hz, 2H, H-7), 2.80 (s, 1H, H-8), 2.73 (tt, J=6.2, 3.0 Hz, 2H, H-12).

 13 C NMR (151 MHz, DMSO- d_6)) δ 167.87, 161.49, 133.47, 129.81, 127.29, 127.24, 126.99, 126.94, 115.88, 115.74, 115.63, 115.49, 114.38, 113.92, 72.67, 67.60, 41.84, 40.51, 40.48, 23.76, 17.72.

¹⁹F NMR: (565 MHz, DMSO- d_6) δ -114.62 (1F).

Ro-A18; 4-[3-[4-(4-fluorophenyl)-3,6-dihydro-1(2H)-pyridinyl]-2-hydroxy-2-methyl-propoxy]-benzamide

Ro-A18 was synthesized on a 1 mmol scale using BB17, and PTP-F. The synthesis was performed as described in Ro8-4304. However, the reaction was stirred at reflux O/N. The next day, this was slowly cooled down to RT. A precipitate was visible. This was filtered and washed with a small amount of EtOH. The obtained beige product was purified by Column chromatography (eluent: EtOAc/MeOH 9/1). This left a beige solid, in a yield of 39 mg (10%). This was used without any further purification.

HRMS m/z (ESI) 385.196, consistent with empirical formula $C_{22}H_{25}FN_2O_3$ with an accuracy of 0.0111 ppm (accepted as $[M+H]^+$).

¹H NMR (600 MHz, DMSO- d_6) δ 7.92–7.86 (m, 2H, H-2), 7.87 (s, 1H, H-1), 7.54–7.47 (m, 2H, H-13), 7.21 (d, J=4.0 Hz, 1H, H-1), 7.21–7.16 (m, 2H, H-12), 7.06–7.03 (m, 2H, H-3), 6.17–6.13 (m, 1H, H-11), 4.12–4.06 (m, 1H, H-4), 4.00 (dd, J=18.8, 9.2 Hz, 2H, H-4, H-5), 3.87 (d, J=9.0 Hz, 1H, H-5), 3.33–3.23 (m, 2H, H-10), 2.85 (dt, J=11.3, 5.6 Hz, 1H, H-9), 2.79 (dt, J=11.3, 5.6 Hz, 1H, H-9), 2.45 (s, 2H, H-8), 1.27 (s, 3H, H-5).

¹³C NMR (151 MHz, DMSO- d_6) δ 167.88, 167.82, 162.54, 161.66, 161.50, 160.93, 137.08, 137.06, 133.22, 129.83, 129.79, 127.06, 126.94, 126.90, 126.84, 126.78, 123.16, 115.55, 115.41, 114.44, 114.44, 114.03, 113.92, 73.89, 73.67, 72.59, 72.31, 70.79, 64.45, 58.39, 55.20, 52.17, 40.52, 29.10, 28.08, 23.98, 22.60.

¹⁹F NMR: (565 MHz, DMSO- d_6) δ -116.01 (1F).

3.2.5 The organic synthesis of some small molecules used in this thesis

E1. N-hydroxy succinimide propanoate

The synthesis of N-hydroxy succinimide propanoate was adapted from keller et al. (2008), and Bonnitcha et al. (2010) 176,177 . The glassware used was flame dried under vacuum, and then purged with nitrogen prior to use. 5.5 mmol of dicyclohexylcarbodiimid (DCC, 1.1 Eq) [Acros Organics] in 2 ml of Tetrahydrofuran (THF) was added to a stirred, ice Cold, solution of propionic acid (5 mmol, 1 Eq) [Merck], and N-hydroxysuccinimide (5.5 mmol, 1.1 Eq) [Alfa Aesar]. The ice bath was removed after 2 h, and the stirring was continued overnight at RT. The Colourless solid (dicyclohexylurea, DCU) was removed by filtration, and the leftover solvent was Collected and subsequently removed in vacuo. The residue was partitioned between DCM, and H_2O . The organic layer was washed twice with a saturated sodium bicarbonate (NaHCO₃) solution, and was dried with Na₂SO₄, before the solvent was removed in vacuo. This gave a Colourless solid in a yield of 723 mg (84%). This was used without further purification.

HRMS m/z (EI) 171.06, consistent with empirical formula $C_7H_9NO_4$ with an accuracy of 0.0068 ppm (accepted as $[M]^{-+}$).

¹H NMR: (500 MHz, CDCl₃) δ 2.79-2.75 (m, 4H, H-3, H-4), 2.58 (q, J=7.5 Hz, 2H, H-2), 1.21 (t, J=7.5 Hz, 3H, H-1).

E2; 2-phenoxyacetic acid

The synthesis of 2-phenoxyacetic acid was done according to Yan et al. (2015), and He et al. (2015) 178,179 . Chloroacetic acid (4 mmol) [Abcr GmbH & Co. KG] was dissolved in stirred, ice Cold, H₂O (5 ml). Then, a NaOH solution (25% w/w) [Grüssing GmbH] was added dropwise until the pH reached 9-10. Hereby, creating a sodium chloroacetate solution. In another round bottom flask, NaOH (4 mmol) was dissolved in 5 ml H₂O, and phenol (4 mmol) [Grüssing GmbH] was added. This mixture was stirred for 20 min. Then, the sodium chloroacetate solution was dropwise added to the phenol solution. This mixture was stirred at reflux (\sim 105°C) O/N. The next day, the solution was allowed to cool down to RT, and the pH was adjusted to a value of 1, with a 5M HCl solution. The solution was left to settle down, and the precipitated 2-phenoxyacetic acid was filtered, washed with H₂O, and recrystallized from EtOH. This yielded 281 mg (46%) of light pink crystals. This was used without further purification.

HRMS m/z (EI) 152.07, consistent with empirical formula $C_8H_8O_3$ with an accuracy of 0.0227 ppm (accepted as $[M]^{-+}$).

¹H NMR: (400 MHz, DMSO- d_6) δ 12.83 (s, 1H, H-5), 7.34-7.24 (m, 2H, H-3), 7.01-6.86 (m, 3H, H-2, H-1), 4.66 (s, 2H, H-4).

¹³C NMR: (101 MHz, DMSO- d_6) δ 170.19, 157.68, 129.42, 120.93, 114.35, 64.33, 60.58, 43.68.

E3; 2-phenoxy ethanol

The synthesis of 2-phenoxy ethanol was done according to Huang et al. (2017) 180 . Phenol (4 mmol) [Grüssing GmbH] was dissolved in a NaOH solution (6 mmol, 10 ml) [Grüssing GmbH], and 2-bromoethanol (6 mmol) [abcr GmbH & Co. KG was added. The solution was heated to $\sim 90^{\circ}$ C, and stirred O/N. The next day, the solution was allowed to cool down to RT and diluted with H₂O. The product was extracted into DCM, and this layer was washed with a 5% NaOH solution, H₂O, and brine. The organic layer was dried with Na₂SO₄, before the solvent was evaporated in vacuo, yielding 115 mg (21%) of Colourless oil. This compound was used without further purification.

HRMS m/z (ESI) 161.099, consistent with empirical formula $C_8H_{10}O_2$ with an accuracy of 0.0417 ppm (accepted as [M+Na]⁺).

¹H NMR: (400 MHz, CDCl₃) δ 7.21 (dt, J=8.8, 7.0 Hz, 2H, H-3), 6.94-6.81 (m, 3H, H-1, H-2), 4.01 (dd, J=5.2, 3.8 Hz, 2H, H-4), 3.88 (dd, J=5.2, 3.8 Hz, 2H, H-5).

 $^{13}\text{C NMR:}$ (151 MHz, CDCl₃) δ 158.60, 129.56, 121.15, 114.57, 85.80, 69.08, 61.51.

E4; tert-butyl 4-(4-bromophenyl)-3,6-dihydropyridine-1(2H)-carboxylate

BB02 (3.9 mmol), was dissolved in 10 ml DCM, and 5 Eq of TEA was added (20 mmol) [Grüssing GmbH]. This mixture was stirred for 5 min. Hereafter, 2 Eq of Boc_2O was added (8 mmol) [Sigma-Aldrich]. This was stirred at RT for 36 h. The DCM was washed with H_2O three times. The organic layer was dried with Na_2SO_4 before the solvent was removed in vacuo. The resulting oil was purified by Column chromatography (eluent: PE/EtOAc, 9/1), yielding 757 mg (58%) of product (Colourless oil), which turned into a white solid O/N.

HRMS m/z (ESI) 360.062, consistent with empirical formula $C_{16}H_{20}BrNO_2$ with an accuracy of 0.0051 ppm (accepted as [M+Na]⁺).

¹H NMR (400 MHz, CDCl₃) δ 7.43–7.33 (m, 2H, H-1), 7.22–7.12 (m, 2H, H-2), 5.95 (s, 1H, H-3), 3.98 (q, J=2.9 Hz, 2H, H-4), 3.55 (t, J=5.6 Hz, 2H, H-5), 2.41 (s, 2H, H-6), 1.41 (s, 9H, H-7). ¹³C NMR (101 MHz, CDCl₃) δ 139.58, 131.48, 127.04, 126.55, 121.08, 79.79, 28.49, 28.03, 27.42.

$$\begin{array}{c|c}
 & & & & & 7 \\
 & & & & & & 7 \\
 & & & & & & & 7 \\
 & & & & & & & & 7 \\
 & & & & & & & & & & 7
\end{array}$$
Br $\begin{array}{c} & & & & & & & & & & 7 \\
 & & & & & & & & & & & 7 \\
 & & & & & & & & & & & & 7 \\
 & & & & & & & & & & & & & 7
\end{array}$

E5; N-acyl-(4-phenyl)-1,2,3,6,-tetrahydropyridine

This protection was adapted from Alekseyev et al. [2011] 181 . BB04 (3 mmol), was dissolved in 10 ml H₂O, and 2.4 Eq of K₂CO₃ was added (7.2 mmol) [Grüssing GmbH]. This mixture was stirred for 5 min, and then 5 ml DCM, and 1.05 Eq of acetyl chloride (3.15 mmol) [Merck] were added. This was stirred at RT O/N. The DCM was washed with H₂O, a 5% NaOH solution, and H₂O. The organic layer was dried with Na₂SO₄ before the solvent was removed in vacuo. Yielding 316 mg (52%) of product (clear yellow oil)

HRMS m/z (EI) 201.13, consistent with empirical formula $C_{13}H_{15}NO$ with an accuracy of 0.0146 ppm (accepted as $[M]^{-+}$).

¹H NMR (500 MHz, CDCl₃) δ 7.42–7.33 (m, 4H, H-6, H-7), 7.33–7.26 (m, 1H, H-8), 6.09 (s, 1H, H-5), 4.26 (s, 1H, H-2), 4.16 (s, 1H, H-2), 3.84 (s, 1H, H-3), 3.69 (s, 1H, H-3), 2.61 (d, J=11.8 Hz, 2H, H-4), 2.19 (s, 3H, H-1).

 $^{13}\text{C NMR}$ (126 MHz, CDCl₃) δ 169.80, 169.64, 140.68, 140.65, 137.22, 135.29, 128.89, 127.94, 127.81, 125.35, 125.32, 121.46, 119.74, 46.24, 43.79, 42.58, 38.72, 28.33, 27.54, 22.31, 21.90.

$$\begin{array}{c|c}
 & 6 & 7 & 8 \\
 & 3 & 6 & 7 \\
 & 2 & 6 & 7
\end{array}$$

E6; 4-(4-carboxyphenyl)piperidine

3 ml ethanolic HCl (1M) was placed in a round-bottom flask and 0.5 g 4 N-boc-4-(4-carboxyphenyl)piperidine (1.64 mmol) [Fluorochem] was added. The mixture was stirred for 2 h at \sim 80°C. The solution was allowed to cool down to RT, and the EtOH was removed, in vacuo. This left a light yellowish powder in a quantitative amount. The solid was partitioned between H₂O and EtOAc. The layers were separated, and the H₂O layer was washed twice with EtOAc. The H₂O was removed in vacuo, yielding a white solid in a quantitative amount. HRMS m/z (EI) 206.121, consistent with empirical formula C₁₂H₁₅NO₂ with an accuracy of 0.0107 ppm (accepted as [M+H]⁺).

1H NMR (600 MHz, MeOH- d_4) δ 8.01–7.96 (m, 2H, H-6), 7.42–7.36 (m, 2H, H-5), 3.51 (ddt, J=12.8, 3.8, 1.6 Hz, 2H, H-2), 3.15 (td, J=13.1, 3.0 Hz, 2H, H-2), 3.00 (tt, J=12.3, 3.6 Hz, 1H, H-4), 2.10 (dtt, J=14.2, 3.5, 2.0 Hz, 2H, H-3), 1.98–1.88 (m, 2H, H-3).

 13 C NMR (151 MHz, MeOH- d_4) δ 168.21, 149.23, 129.86, 129.56, 129.32, 126.56, 126.47, 85.38, 44.12, 39.60, 29.41.

36

3.3 Materials and methods for biological experiments

3.3.1 Plant material and growth conditions

The different lines used in this thesis are listed below (Table 1).

Table 1. Original Arabidopsis thaliana lines used in this thesis.

Stock-ID	Name	Affected gene	Reference
Wild type	Col-0		
	chs3-2D	AT5G17890	Bi et al. (2011) ⁸⁴
	chs3-1	AT5G17890	Yang et al. (2010) ⁸⁵
SALK_040458	glr3.3-1	AT1G42540	Qi et al. (2006) ²⁴
SALK_030186	gstf2-1K	AT4G02520	
GK-261D05	gstf7-1K	AT1G02920	
N69995	cdc48a4	AT3G09840	Copeland et al. (2016) ¹⁸²
SALK_038646	hsp90-2K	AT5G56030	Hubert et al. (2003) ¹⁸³
N68761	hsp90-2.7	AT5G56030	Hubert et al. (2009) ⁷²
salk_05023	icln-2	AT5G62290	Huang et al. (2016) ¹⁶⁶

Seeds were surface sterilized before use, using either ethanol or chlorine gas. In the ethanol method seeds were sterilized for 8 min at 950 rpm in 70% ethanol [ChemSolute, Th. Geyer GmbH & Co. KG Niederlassung]. This was replaced with 100% ethanol [ChemSolute], which was immediately removed. Using the chlorine method, seeds were incubated for 3 h in an exicator containing a beaker with 25 mL sodium hypochlorite [ChemSolute], and 2 mL 37% HCl [ChemSolute]. Before sowing, seeds were left to dry for 1 h, in a sterile environment. The seeds were sown on soil containing two parts Frustorfer Pikiersubstrat [Wilsaflor], one-part coarse-grained sand and one third part expanded clay Fibobau [Fibo ExClay]. Prior to sowing, soil was treated O/N with a Neudomuck ® [Neudorff] solution with a concentration of 2 ml L⁻¹. The next day, soil was treated with a Previcur® Energy [Bayer Cropscience] solution with a concentration of 2.5 mL L⁻¹.

Seeds sown in 96-well plates were grown on ½ MS-medium containing 0.245% Murashige and Skoog [Duchefa], 0.5% sucrose [Carl Roth GmbH & Co. KG], and 0.8% phytoagar [Duchefa]. Media was buffered to a pH of 5.7 and sterilized by autoclaving before use. Seeds were stratified by storing the pots, or plates at 4°C for at least 48 h in the dark. All plants were grown at controlled conditions in growth cabinets [Percival Scientific]. Plants for genotyping experiments were grown at 25°C. Plants for experiments were grown at the indicated temperatures. All plants were grown under long day conditions with 16 h light and 8 h dark, the light intensity was set between 90 to 100 μ mol m-2 s-1. Plants on plates were analysed after 21 days.

Various chemicals were added to the ½ MS media. The chemicals are listed in Table 2.

Table 2. The chemicals used for the pharmaceutical analysis. With the corresponding concentration, supplier, and CAS number.

Name	Abbreviation	Conc.	Dissolved in	Supplier	Cas Nr.
Abscisic acid	ABA	10 μΜ	DMSO	Sigma-Aldrich Chemie GmbH	14375- 45-2
Bikinin		15 μΜ	DMSO	Fluorochem	188011- 69-0
β-methylamino-L- alanine	BMAA	50 μΜ	ddH ₂ O	Santa Cruz Biotechnology Inc.	16012- 55-8
Calcium chloride	CaCl ₂	4 mM	ddH₂O	Merck	10043- 52-4
6,7- dinitroquinoxaline- 2,3-dione	DNQX	0.5 mM	DMSO	Cayman Chemical Company	2379-57- 9
Dithiothreitol	DTT	1 mM	ddH₂O	Applichem GmbH	3483-12- 3
Egtazic acid	EGTA	4 mM	ddH ₂ O	Applichem GmbH	67-42-5
Geldanamycin	GDA	10 μΜ	DMSO	Thermo Fisher Scientific	30562- 34-6
L-glutathione reduced	GSH	1 mM	ddH ₂ O	Carl Roth GmbH & Co. KG	70-18-8
Ifenprodil·hemitartate		0.5 mM	DMSO	Cayman Chemical Company	23210- 58-4
UPCDC 30245	UPC	50 μΜ	DMSO	Sigma-Aldrich Chemie GmbH	1883351- 53-4
Spermidine		100 μΜ	ddH₂O	Carl Roth GmbH & Co. KG	124-20-9
Spermine		100 μΜ	ddH₂O	Carl Roth GmbH & Co. KG	71-44-3
Trifluoperazine·HCl	TFP	50 μΜ	DMSO	Cayman Chemical Company	440-17-5
Buthionine sulfoximine	BSO	1 mM	DMSO	Sigma-Aldrich Chemie GmbH	83730- 53-4
L-glutamine	Gln	1 mM	ddH ₂ O	Glentham Life Sciences	56-85-9
L-proline	Pro	1 mM	ddH ₂ O	Applichem GmbH	147-85-3
L-glycine	Gly	1 mM	ddH_2O	Chemsolute	56-40-6
L-glutamate	Glu	1 mM	ddH₂O	Serva Electrophoresis GmbH	56-86-0

L-methionine Met 1 mM ddH₂O Carl Roth GmbH 63-68-3 & Co. KG

Stock solutions were made by dissolving the compound in either DMSO [VWR International GmbH], or ddH $_2$ O. The compounds dissolved in water were filter sterilized [Syringe filter, Filtropur S, PES, pore size: 0.45 μ m, Sarstedt AG & Co. KG] before use. Each well in the 96-wells plate contained 3 μ L from a stock solution and 147 μ L ½ MS-medium.

3.3.2 Polymerase chain reaction

To amplify specific deoxyribonucleic acid (DNA) fragments different polymerase chain reaction (PCR) setups were performed, including genotyping and quantitative PCR.

3.3.2.1 gDNA extraction

To determine the genotype of our plants, gDNA extraction was performed. For this, a small leaf was harvested, placed into a 1.5 mL reaction tube, and 400 μ L lysis buffer was added (Table 3). The leaf material was grounded using a pestle, and the sample was centrifuged for 5 min, 14000 rpm at RT. The supernatant was transferred to a new tube containing 300 μ L of isopropanol [ChemSolute], and precipitation was done at -20°C for 5 min. The samples were hereafter centrifuged for 8 min, 14000 rpm at RT, and the supernatant was discarded. The pellet was washed with 500 μ L of 70% ethanol [ChemSolute], by vortexing, and centrifugated for 3 min, 14000 rpm at RT. The supernatant was completely removed, and the pellet was dried at 50°C for 5 min. The pellet was dissolved in 50 μ L of ddH₂O, and incubated at 50°C for 5 min, 550 rpm. The gDNA was centrifuged one last time for 1 min, 14000 rpm, at RT, and was then stored at -20°C before use.

Table 3. Lysis buffer composition.

Component	Concentration	Supplier
Tris·HCl	200 mM	VWR International GmbH
NaCl	250 mM	ChemSolute
EDTA	25 mM	Carl Roth GmbH & Co. KG
SDS	0.5% (v/v)	Carl Roth GmbH & Co. KG

3.3.2.2 Genotyping and T-DNA insertion mutant analysis

The gDNA extracted was used to determine if plants are hetero- or homozygous. The PCR was performed using 2 μ L of gDNA, specific primers (Tables 6 and 7), and the DreamTaqtm polymerase [Thermo Fisher Scientific] (Tables 4 and 5). The PCR was done using a tabletop thermocycler [Eppendorf]. Primers for SALK lines were designed using the T-DNA Primer Design tool [The Salk Institute for Biological Studies]. Primers for point mutation mutants were taken from their respective publications. All gene specific primers were synthesized by Eurofins, and the primers were used in different combinations to detect either the wild type or mutant allele (Table 7, Figure 9). Visualization of the PCR fragments by separation was achieved using agarose gel electrophoresis. The agarose [VWR International GmbH]

concentration (1% or 3%) was chosen based on the expected fragment size. The agarose was dissolved in 1X TAE buffer using a microwave. The agarose gel was poured into the cast, and ethidium bromide [Carl Roth GmbH & Co. KG] was added to a concentration of 0.04 µg mL⁻¹. The Generulertm 1kb plus [Thermo Fisher Scientific] was used according to manufacturer's instructions. Separations was achieved by applying 120V to the gel, for 20-60 min, depending on the size of the gel, the concentration of the gel, and the size of the fragments. Bands were detected using the E-BOX VX2 gel documentation system [VWR International GmbH]. To determine the correct T-DNA insertion site in the plants, DNA was sequenced by Sanger sequencing. The primers were mixed with the corresponding gDNA in a reaction tube, according to the instructions, and Sanger sequencing was done by Eurofins Genomics [Anzinger].

Table 4. Composition of each PCR sample using the DreamTaq[™] polymerase.

Component	Volume (μL)
ddH₂O	14.7
DreamTaq™ buffer (10X)	2
DNTPs (10 μM)	0.4
Forward primer	0.4
Reverse primer	0.4
DreamTaq [™] polymerase	0.1
Template gDNA	2

Table 5. PCR program used for the DreamTag[™] polymerase.

Step	Temperature (°C)	Time (s)
1	95	30
2	95	20
3	Primer-dependent (~52)	20
4	72	90 (Step 2-4 were repeated 35X)
5	72	180
6	8	∞

Table 6. Primers used for genotyping and sequencing.

ID	Name	Gene	Sequence (5' to 3')	Reference
ML55	chs3-2D	AT5G17890	TTTCAGACTTAAGAGGAATG	Colleague
ML56	chs3-2D	AT5G17890	AAGGACCTCTAATCTTTAAC	Colleague
ML57	chs3-2D	AT5G17890	ATTAAGGACCTCTAATCTTTAAT	Colleague
MK_L Bb1.3			ATTTTGCCGATTTCGGAAC	SALK institute
MK17	icln-2	AT5G62290	TGGCTAAAGGATACGCAGTTG	Huang et al. (2016) ¹⁶⁶
MK18	icln-2	AT5G62290	TGAACCATCTCTTCAGCATCC	Huang et al. (2016) ¹⁶⁶
MK24	glr3.3-1	AT1G42540	GAAACCAAAAGTTGTGAAAATCGGT	Qi et al. (2006) ²⁴

MK25	glr3.3-1	AT1G42540	GACACATTGTCTCTTAGGTGGGCCT	Qi et al. (2006) ²⁴
MK48	cdc48a4	AT3G09840	CTTTTTCTTCTGTATCAAGGG	Copeland et al. (2016) ¹⁸²
MK49	cdc48a4	AT3G09840	CTTTTTCTTCTGTATCAAGGA	Copeland et al. (2016) ¹⁸²
MK50	cdc48a4	AT3G09840	CTTCAGCCAGCTTCATGTTC	Copeland et al. (2016) ¹⁸²
MK63	hsp90-2.7	AT5G56030	GATGATGAGGGAAAGCAACTGGTTGAT CTAAG	Hubert et al. (2009) ⁷²
MK64	hsp90-2.7	AT5G56030	GGGCCTTAAAATGGCCCCCATCA	Hubert et al. (2009) ⁷²
MK67	hsp90-2K	AT5G56030	TCCATAGGTTATTGCACTGGC	This thesis
MK68	hsp90-2K	AT5G56030	CACAAAAAGCTTCGCAACTTC	This thesis
MK73	gstf2-1K	AT4G02520	TTGGTTTTCATATCGGTGAGC	This thesis
MK74	gstf2-1K	AT4G02520	ATTTTTCCATCGAATTCCACC	This thesis
MK77	gstf7-1K	AT1G02920	AGAATTAGGGCAATGAGGTCATCG	This thesis
MK78	gstf7-1K	AT1G02920	TGTTGTCTTATCCAGCCA	This thesis
MK79	gstf7-1K	AT1G02920	ATAATAACGCTGCGGACATCTACATTTT	This thesis

Table 7. Primer combinations used for genotyping.

Gene	Primer 1	Primer 2	Allele type
chs3-2D	ML56	ML55	WT
chs3-2D	ML57	ML55	Mutant
icln-2	MK17	MK18	WT
icln-2	MK18	MK_LBb1.3	Mutant
glr3.3-1	MK24	MK25	WT
glr3.3-1	MK25	MK_LBb1.3	Mutant
cdc48a4	MK48	MK50	WT
cdc48a4	MK49	MK50	Mutant
hsp90-2.7	MK63	MK63	Digestion with HinIII to interpret WT and mutant
hsp90-2K	MK67	MK68	WT
hsp90-2K	MK68	MK_LBb1.3	Mutant
gstf2-1K	MK73	MK74	WT
gstf2-1K	MK74	MK_LBb1.3	Mutant
gstf7-1K	MK77	MK78	WT
gstf7-1K	MK78	MK79	Mutant

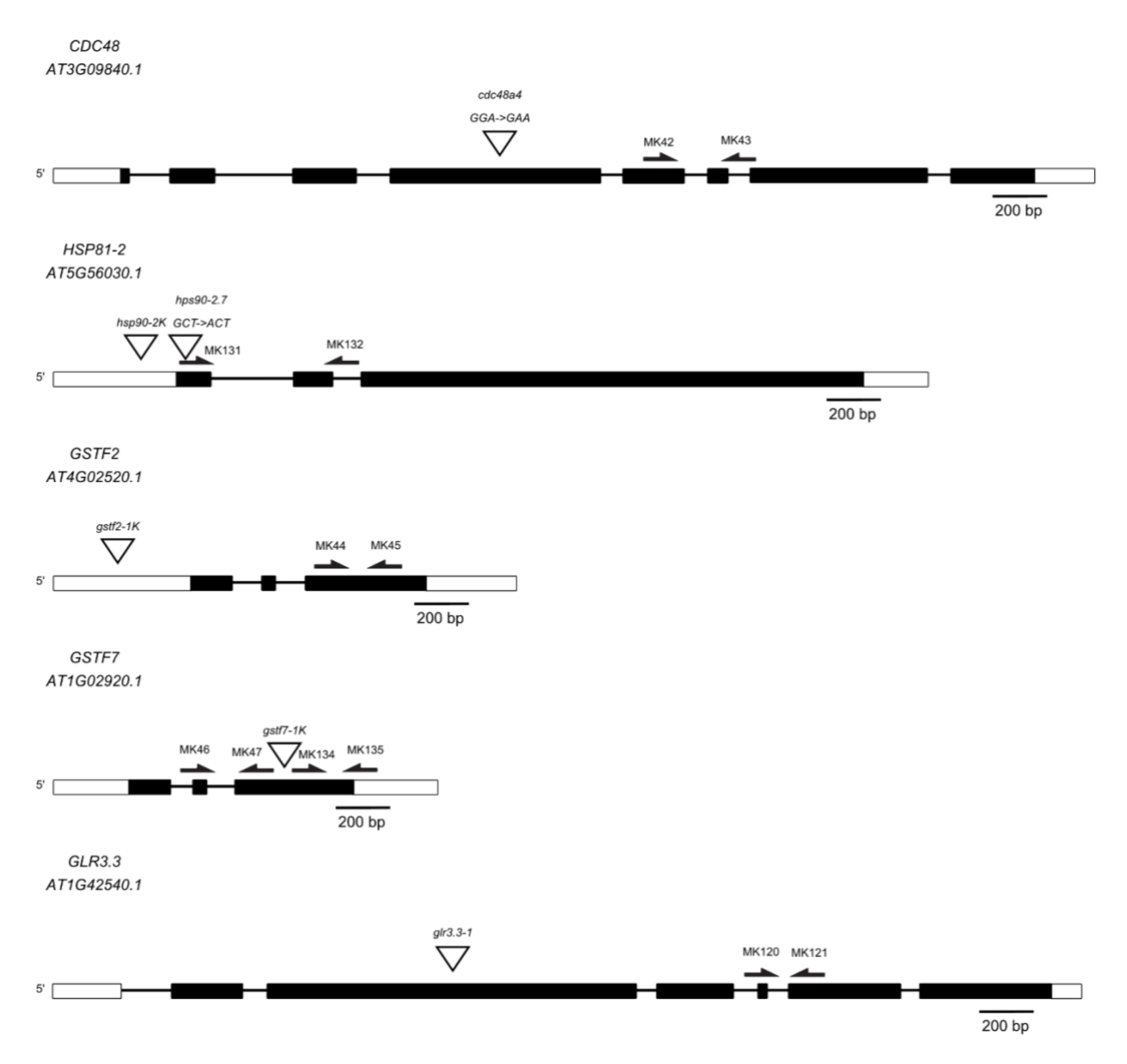


Figure 9. Insertion sites of the mutations of the different mutants used in this thesis. The white arrows indicate the insertions sites, while black arrows indicate the RT-qPCR primer binding sites.

3.3.2.3 Gene expression analysis

Plant material for real-time quantitative PCR (RT-qPCR) was Collected after 21 days of growth. The samples were immediately frozen in liquid nitrogen and stored at -80°C, until use. Samples were mechanically crushed using a Tissuelyser [Qiagen, Venlo, Netherlands] for 30 s at a frequency of 30 S $^{-1}$. RNA was isolated using the innuPREP plant RNA kit [Analytik Jena AG] according to manufacturer's instructions. RNA was stored at -80°C. The RNA was transformed to cDNA using the Qiagen quantitect® reverse transcription kit [Qiagen], according to the manufacturer's instructions. Samples were stored at -20°C. For analysis of immune gene expression, qPCR was performed on RT 2 SYBR 8 Green qPCR Mastermix [Qiagen] treated samples using a Rotor-Gene 8 Q [Qiagen] (Tables 8 and 9). Gene specific primers (Table 10) were synthesized by Eurofins. The RT-qPCR data was analysed using qbase $^+$ software, version 3.0 [Biogazelle, Zwijnaarde, Belgium] [www.qbaseplus.com]. All samples were standardized to transcription levels of reference genes $EF1\alpha$ (At5g60390) and

GAPDH (At1g13440) or *GADPH* and *CUL4* (At5G46210). Student's t-test analysis, or two-tailed anova was used to determine the significance of different values.

Table 8. Composition of each qRT-PCR sample.

Component	Volume (μL)
RT ² SYBR [®] Green qPCR Mastermix	5
Forward primer	0.5
Reverse primer	0.5
H₂O	2
Template cDNA	2

Table 9. PCR program used for the qRT-PCR.

Step	Temperature (°C)	Time (s)
1	95	300
2	95	10
3	60	30 (steps 2 and 3 were repeated 40X)
4	65-95	5 °C ⁻¹

Table 10. Primers used for qRT-PCR.

ID	Gene		ATG number	Sequence (5' to 3')
Н3	CUL4	LP	AT5G46210	GCTGGCTGTTTCCCTGTTTC
H4		RP		CAGCTCCTTGTCCTCTATGC
Н9	EIF1 $lpha$	LP	AT5G60390	TGAGCACGCTCTTCTTGCTTTCA
H10		RP		GGTGGTGGCATCCATCTTGTTACA
ML15	GADPH	LP	AT1G13440	GACTGGAGAGGTGGAAGAGC
ML16		RP		GGCAACACTTTCCCAACAGC
ML09	PR2	LP	AT3G57260	GCTTCCTTCAACCACACAG
ML10		RP		TGGACTTGGCAAGGTATCGC
ML11	PR1	LP	AT2G14610	CAACTACGCTGCGAACACG
ML12		RP		GGCACATCCGAGTCTCACTG
ML13	NIMIN1	LP	AT1G02450	AGGAGGAAATCTAACGGCGG
ML14		RP		AACCCGTACGACACTGAGAG
ML21	EDS1	LP	AT3G48090	CGTTCAAGCTGCATTAGAGGAAG
ML22		RP		ACCTCTCTTGCTCGATCAC
ML64	PAD4	LP	AT3G52430	CGGCTACCAACAACCAC
ML65		RP		CATTCCCGGAGGTAAGTTCG
JK45	SID2	LP	AT1G74710	TGGCAAGATCGCTGTTGAAT
JK46		RP		AGCCAACATTGAACTTCCACC
MK42	CDC48	LP	AT3G09840	ATTTCCACACTGCTCTCGGG
MK43		RP		TGGGTATTGAACAGTCTCCTGG
MK44	GSTF2	LP	AT4G02520	GGAACCAACCTTCTCCAAACC
MK45		RP		TGTGGTCAAGCCGTAGATGGA
MK46	GSTF7 set 1	LP	AT1G02920	CCACCTTGCTTTAAGAACAAAGTC
MK47		RP		TTGGAGCCAAGGGAGACAAGTTGG
MK120	GLR3.3	LP	AT1G42540	TCGCGCATAGAGAGAACACAG

MK121		RP		AAGAGAGCTGCTGAACCGTC
MK131	HSP90-2	LP	AT5G56030	CCAGTTGCTTTCCCTCATCATC
MK132		RP		CGAGCTTGCTCTTGTCCGTC
MK134	GSTF7 set 2	LP	AT1G02920	ACGAGCGTCCACATGTCAGT
MK135		RP		CACAGAGTGTATGAGAATTTGGC

3.3.3 Bacterial infection assay

Arabidopsis thaliana Col-0, and chs3-2D were grown for 14 days on ½ MS-medium at 20°C and long-day conditions. The growth media contained 50 μM DMSO, Ro8-4304 or A03, respectively. A liquid culture was made by inoculation of the NYG liquid containing tetracycline [Molekula GmbH] (Table 11) and subsequent incubation in a rotary shaker at 200 rpm at 28 °C for 48 h. On the day of the infection, 50 ml NYG liquid containing tetracycline [Molekula GmbH] was inoculated with 2.5 ml of the premade liquid culture. This was incubated in a rotary shaker at 200 RPM at 28 °C for 3 h. The culture was pelleted at 4500 rpm, for 20 min at RT [Heraeus Multifuge 3S-R, Heraeus Deutschland GmbH & Co. KG, Hanau, Germany] and the pellet was re-suspended in a sterile 10 mM MgCl₂ [Carl Roth GmbH & Co. KG] solution, hereafter the OD was measured. The 10 mM bacterial infiltration solution was prepared (Tables 12 and 13) and plants were vacuum infiltrated for 2 min, using a Concentrator Plus [Eppendorf], with the infiltration solution containing the fluorescent strain PstDC3000-GFP of *Pseudomonas syringae pv tomato* 184 at OD600 = 0.002. Plants were washed, and leaf discs were Collected 0 and 3 days after infection. These discs were grounded in a 1.5 ml tube containing 10 mM MgCl₂ solution. The bacterial solutions were serial diluted using 10 mM MgCl₂ and plated on NYG-agar plates containing tetracycline [Molekula GmbH]. The plates were incubated at 28°C for 48 h. Hereafter, Colony forming units were counted and tithers were calculated. Medium and solutions were sterilized by autoclaving before use.

Table 11. Composition of the NYG liquid medium.

Component	Concentration	Supplier
Peptone	0.5% (v/w)	Carl Roth GmbH & Co. KG
Yeast extract	0.3% (v/w)	Chemsolute
Glycerol	0.002% (v/v)	Chemsolute

Table 12. NYG agar media composition.

Component	Concentration	Supplier
NYG + Agar (Kobe I)	0.5% (v/w)	Carl Roth GmbH & Co. KG

Table 13. Composition of the bacterial infiltration solution. For the bacterial suspension an OD600 (=0.02) was used.

Component	Concentration	Supplier
MgCl ₂	10 mM	Carl Roth GmbH & Co. KG
Silwet L-77	0.0012% (v/v)	Chemsolute

3.3.4 Affinity purification

3.3.4.1 Arabidopsis thaliana protein lysate extraction

Arabidopsis thaliana *chs3-2D* was grown on ½ MS-medium at 22°C and long-day conditions. Plant material was Collected after 14 days, and immediately frozen in liquid nitrogen. Frozen material was pulverized in liquid nitrogen with mortar and pestle. Then, 4 mL extraction buffer (Tables 14 and 15) was added to 1 g of plant material (4X VOL), and the mixture was transferred to Eppendorf tubes. The cellular debris was separated by centrifugation for 20 min, at 4°C and 4000 rpm. The supernatant was transferred to a new tube, without disturbing the pellet, and this crude lysate was subjected to another round of centrifugation (10 min, at 4°C and 4000 rpm). The soluble fraction was transferred to a new tube and was used as the Arabidopsis protein lysate.

Table 14. Composition of 1X Phosphate Buffered Saline (PBS), pH 7.4.

Composition	Concentration (M)	Supplier
Sodium phosphate dibasic	0.01	Chemsolute
NaCl	0.137	Chemsolute
KCI	0.0027	VWR International GmbH
Potassium phosphate monobasic	0.0018	Applichem GmbH

Table 15. Composition of the extraction buffer.

Composition	Concentration	Supplier
PBS	1X	
DTT	1 mM	Applichem GmbH
Protease inhibitor cocktail tablets, c0mplete, EDTA free	1X	Hoffman-La Roche
Tween	0.5% (v/v)	Applichem GmbH

3.3.4.2 Affinity purification

Pierce® NHS-Activated Agarose Slurry, and Pierce® Centrifuge Columns, 2 mL [Thermo Fisher Scientific] were used for the affinity purification, according to the manufacturer's instructions (Figure 10). Solutions were always removed by gravity-flow. Solutions used in this Protocol are shown in Tables 16-21. The bottle of agarose slurry was inverted several times, before adding it to the spin Column. The agarose was equilibrated to RT, while the resin settled. The storage solution was removed, and the resin was washed with 2 mL of milli-Q H₂O, and 2 mL of coupling buffer. 2 mg of Ro-A07 was dissolved in 2 mL of coupling buffer, and this was added to the Column. The Column was incubated with end-over-end mixing at 4°C O/N. The next day, the flow through was removed, and the Column was washed 3 times with 1 mL of coupling buffer. Hereafter, 2 mL of quenching buffer was added, and this was incubated with end-over-end mixing at 4°C for 20 min. The buffer was removed, and the Column was washed with 6 mL of coupling buffer. The protein lysate was added (1-2 mL), and the Column was incubated with end-over-end mixing at 4°C for 2 h. The used lysate was removed and saved for analysing purposes. The Column was washed with 3

mL of binding buffer, and these washes were saved. The bound proteins were eluted by applying 8 mL of elution buffer, 1 mL fractions were Collected, and the pH of these fractions was adjusted by addition of 50 μ L neutralization buffer. Proteins in the fractions did not have an adequate stability, so 40 μ L of the fractions were combined with 10 μ L of SDS-PAGE Loading Buffer (5X) (1.8 mL SDS blue staining + 200 μ L DTT) [Carl Roth GmbH & Co. KG and Hoffman-La Roche], and this was incubated at 95°C, 500 rpm for 20 min.

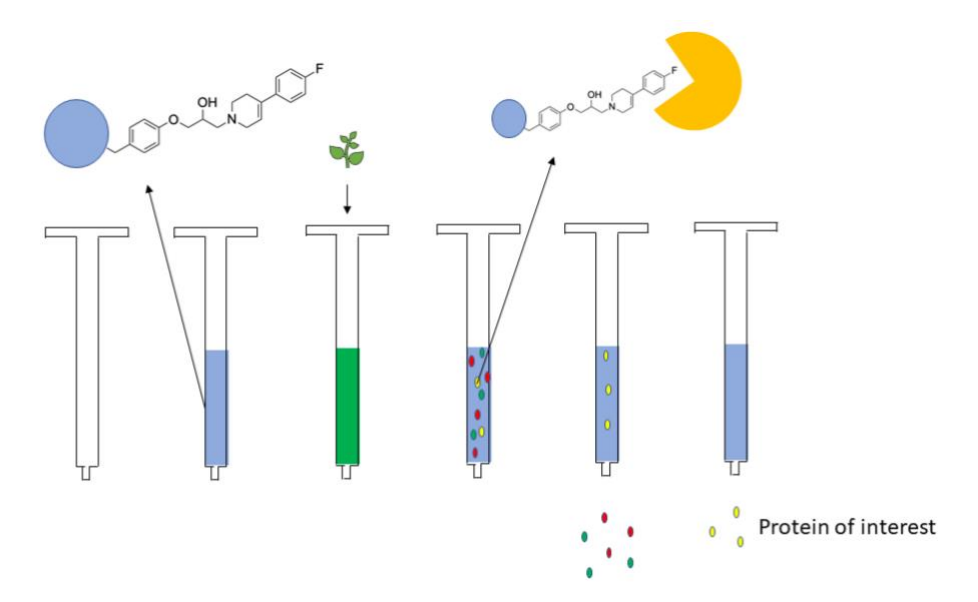


Figure 10. A schematic representation of the process of affinity purification.

Table 16. Composition of the coupling buffer, pH 7.2.

Composition	Concentration (M)	Supplier
Sodium phosphate dibasic	0.1	Chemsolute
NaCl	0.15	Chemsolute

Table 17. Composition of the Quenching buffer, pH 7.4.

Composition	Concentration (M)	Supplier
Ethanolamine	1	Sigma-Aldrich Chemie
		GmbH

Table 18. Composition of the binding and wash buffer.

Composition	Concentration	Supplier
PBS	1X	

Table 19. Composition of the elution buffer, pH 2.9.

Composition	Concentration (M)	Supplier
Glycine	0.1	Chemsolute
HCI	0.02	Chemsolute

Table 20. Composition of the neutralization buffer, pH 8.8.

Composition	Concentration (M)	Supplier
Sodium phosphate dibasic	1	Chemsolute

Table 21. Composition of the storage buffer.

Composition	Concentration	Supplier
PBS	1X	
Sodium azide	0.05% (v/v)	Sigma-Aldrich Chemie
		GmbH

3.3.4.3 Visualization of the proteins using sodium dodecyl sulphate-polyacrylamide gel electrophoresis (SDS-PAGE), and Colloidal Coomassie G-250 staining

To separate and visualize the bound proteins, sodium dodecyl sulphate-polyacyrylamide gel electrophoresis (SDS-PAGE) was used. Acrylamide gels were cast using the mini-protean® Tetra Handcast System [Bio-Rad]. Spacer plates with 0.75 mm integrated spacers were used. The PageRuler Prestained Protein Ladder [Thermo Fisher Scientific] was used according to manufacturer's instructions. Gels were run using a constant 60V for 3 h. Afterwards, the gels were washed three times for at least 10 min using ddH₂O. And gels were stained O/N with Colloidal Coomassie G-250 staining. Gels were de-stained at least two times with at least a 15 min interval using ddH₂O. Gels were documented using the ChemidocTM touch imaging system [Bio-Rad]. Composition of the SDS-PAGE gels, and staining used are given in Tables 22-26.

Table 22. Composition of the SDS-PAGE stacking gel.

Composition	Concentration	Supplier
Tris·HCl (pH 6.8)	130 mM	VWR International GmbH
Acryl/bisacrylamide mix (37.5:1)	5.1% (v/v)	Carl Roth GmbH & Co. KG
SDS	0.1% (v/v)	Carl Roth GmbH & Co. KG
APS	0.1% (v/v)	Th. Geyer GmbH & Co. KG
		Niederlassung
TEMED	0.001% (v/v)	Applichem GmbH

Table 23. Composition of the SDS-PAGE separating gel (10%).

Composition	Concentration	Supplier
Tris·HCl (pH 8.8)	382 mM	VWR International GmbH
Acryl/bisacrylamide mix (37.5:1)	10% (v/v)	Carl Roth GmbH & Co. KG
SDS	0.1% (v/v)	Carl Roth GmbH & Co. KG
APS	0.1% (v/v)	Th. Geyer GmbH & Co. KG
		Niederlassung
TEMED	0.001% (v/v)	Applichem GmbH

Table 24. Composition of the Colloidal Coomassie G-250.

Composition Concentration Supplie

Coomassie Brilliant Blue G-250	0.02% (v/v)	Gentham Life Sciences
Aluminium sulphate-(14-18)-	5% (v/v)	Carl Roth GmbH & Co. KG
hydrate		
Ethanol	10% (v/v)	Chemsolute
Phosphoric acid	2% (v/v)	Applichem GmbH

Table 25. Composition of the 10X running buffer.

Composition	Concentration	Supplier
Tris·HCl	0.25 M	VWR International GmbH
Glycine	1.92 M	Chemsolute
SDS	1% (v/w)	Carl Roth GmbH & Co. KG

Table 26. The volume load of the samples for the different combs used.

Comb	Load (μL)
5	55
10	20
15	12

3.3.4.4 Concentrating of protein samples

Fractions from the affinity purifications were not concentrated enough for distinct bands on the SDS-PAGE, therefore fractions were immediately concentrated after the affinity purification. Fractions 2-5 from the elution buffer were expected to have the protein of interest. So, these fractions were concentrated twice using the vivaspin 500 [Sartorius AG], for 30 min, 15000 g, at 4°C. Since the results, were not 100% satisfying, another method was used. Here, the 1 mL elution samples were added to 4 mL of Cold precipitation solution (Table 27), and these tubes were stored at -20°C for 2 h. The tubes were centrifuged for 10 min, 700 rpm, at 4°C. The supernatant was removed, and the precipitate was washed with Cold precipitation solution. The acetone was completely removed, and the dry pellet was dissolved in 80 mL PBS. SDS-PAGE Loading Buffer (5x) was added, and the samples were incubated as described before.

Table 27. Composition of the precipitation solution.

Composition	Concentration	Supplier
Acetone	90% (v/v)	Chemsolute
Methanol	10% (v/v)	Applichem GmbH
DTT	10 mM	Hoffmann-La Roche

3.3.4.5 Protein mass spectrometry

To identify and analyse interesting bands from the Affinity purification experiment, mass spectrometry (MS) measurements were realized. These were carried out by the *Molecular Plant Genomics* group of Julia Kehr (Institute of Plant Science and Microbiology, Hamburg,

Germany). The extraction, measurements, and final identification were conducted by Dr. Steffen Ostendorp.

3.3.5 SA analysis

Arabidopsis thaliana Col-0, and *chs3-2D* were grown for 5 days or 21 days on ½ MS-medium containing chemicals at 18°C and long-day conditions (Figure 11). The growth media contained 50 μ M DMSO, Ro8-4304 or A03, respectively. Leaf material was Collected after 21 days, for each sample 12 plants were harvested. The samples were immediately frozen in liquid nitrogen and stored at -80°C, until use. The sequencing was carried out by our Collaborators at by the *Molecular Plant Physiology* group of Lars Voll (Philipps-Universität Marburg, Marburg, Germany). The extraction, measurements, and final analysis were conducted by Julia Seufer.

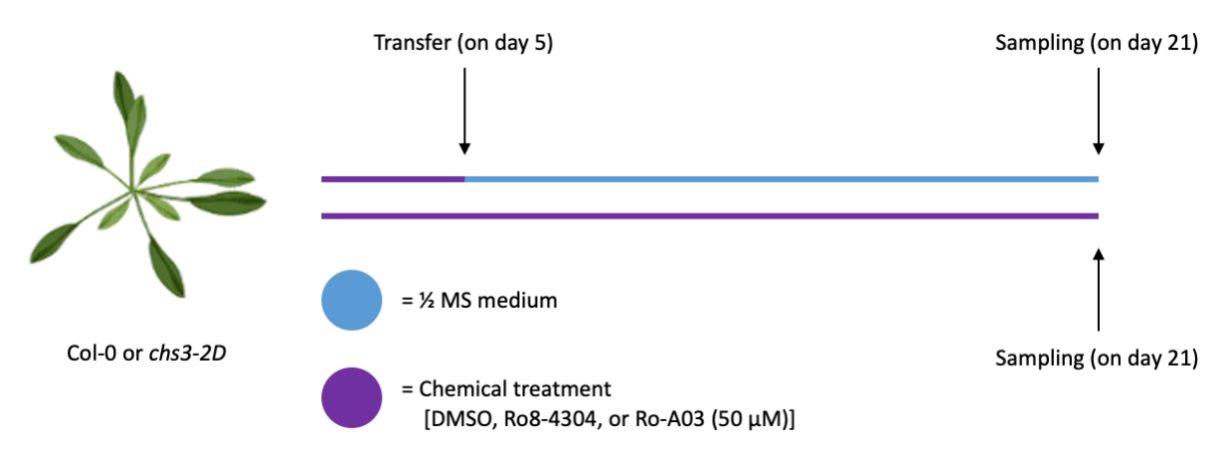


Figure 11. Arabidopsis thaliana Col-0 or *chs3-2D* were chemically treated with 50 μ M DMSO, Ro8-4304 or Ro-A03 for 4 days or 20 days. Plant material was harvested on day 21.

3.3.5.1 Determination of free SA and SAG

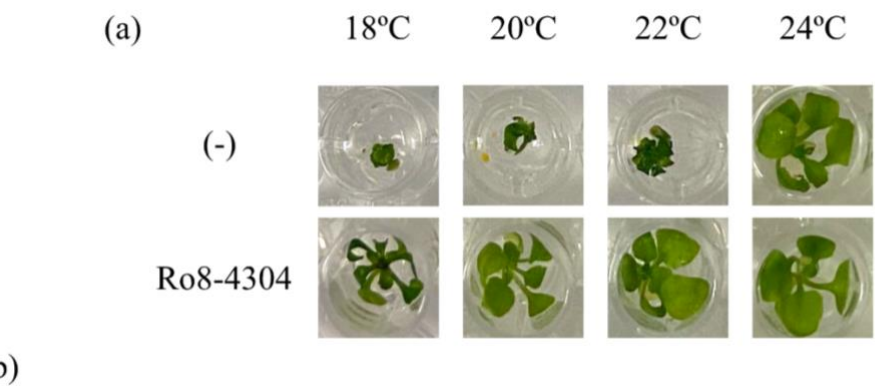
For each genotype x treatment combination, 12 seedlings were weighed and harvested by shock-freezing in liquid nitrogen at the indicated time points. Free SA and SAG were extracted as described previously 102 . HPLC separation of SA and the internal standard o-anisic acid was performed with a binary gradient on an Agilent 1260 Infinity II system [Agilent Technologies, Inc.] equipped with a SecurityGuard Ultra guard Column [3 mm; Phenomenex] followed by an Agilent Poroshell 120 EC-C18, 150x3mm, 2.7µm [Agilent Technologies, Inc.] at 40°C. SAG samples were diluted 1:10 in the starting mobile phase prior to analysis. Elution began with 10% eluent A (25 mM KH2PO4, pH 2.6) and 90% eluent B (99:1 Acetonitrile: H_2O) at a flow rate of 1 ml·min-1, and the following gradient was applied: 0-1 min - 10% eluent B; 1-6 min - 10-25% B; 6-9 min - 25-50% B; 9-9.5 min - 50-80% B; 9.5-11.5 min - 80% B; 11.5-12 min - 80-10 % B; 12-15 min - 10% B. The fluorescence detector was programmed appropriately to measure o-anisic acid (excitation 305 nm, emission 365 nm, retention time: 5.3 min) and SA (excitation 305 nm, emission 407 nm, retention time 6.4 min). Peak identification and quantification were performed by comparison to authentic standards in the range of 1.25 ng to 125 ng.

4 Results

Plants have evolved a plethora of mechanisms to successfully defend against pathogen attack ^{56–58}. Often, high resistance to pathogens results in reduced growth of plants. This growth-defence trade-off is a genetically determined process that can be regulated by molecular events ^{96,97,104}. In consequence, the balance between resistance and growth has been a target for the identification of regulatory molecules ¹⁵⁹.

4.1 Characterization of the chemical activity of Ro8-4304

Chemical genetic screening led to the identification of the chemical Ro8-4304, which could rescue the deficient growth phenotype of Arabidopsis *chs3-2D* autoimmune mutants ¹⁶⁶. However, even though the effect of this chemical was described, its properties were not investigated in detail. Since the rescuing effect of Ro8-4304 was only studied at 16°C ¹⁶⁶, we examined the temperature dependence of the fresh weight of *chs3-2D*. Ro8-4304 was able to rescue the growth of *chs3-2D* in a range of temperatures (Figure 12). Plants were generally growing larger at higher temperatures in line with the temperature regulation of autoimmunity ^{79,80,84,85,185,186}. The *chs3-2D* mutant did not show an autoimmune phenotype at 24°C, and Ro8-4304 did not additionally stimulate the growth of the *chs3-2D* mutant at this temperature, thus indicating that Ro8-4304 is not a general growth regulator. At 18°C, 20°C and 22°C, the addition of Ro8-4304 rescued growth of *chs3-2D* seedings (Figure 12a). The temperature dependence of the Ro8-4304 effect on *chs3-2D* growth was confirmed by quantification of the fresh weight (Figure 12b). A temperature of 18°C was chosen for further experiments.



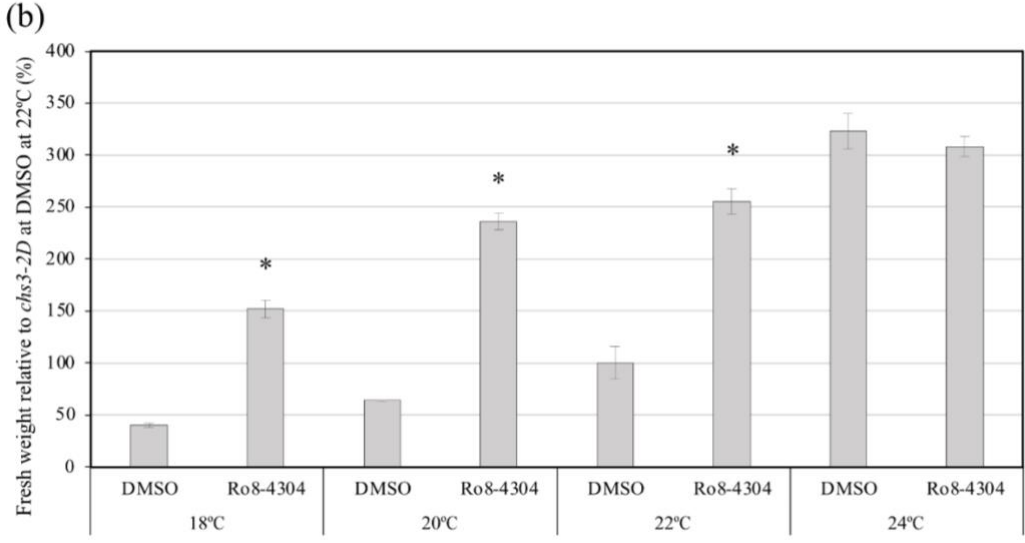


Figure 12. The effect of Ro8-4304 on *chs3-2D* rescue at different temperatures. (a) Morphology of *chs3-2D* grown for 20 days on MS media containing 15 μ M Ro8-4304 or DMSO, at the indicated temperatures. (b) The measured fresh weight of *chs3-2D* was normalized against the mean value of *chs3-2D* grown on DMSO at 22°C. The data are represented as mean \pm SE of three biological replicates (n=3, with 10 \pm 2 plants each). Error bars represent the standard error. An asterisk indicates a significant difference to the relevant negative control (Student's t-test, p < 0.05).

The action of a chemical is also dependent on the concentration. Huang et al. (2016) discovered the chemical in the screening at a concentration of 15 μ M 166 . Additionally, they made a concentration curve from 0.1 μ M up to 30 μ M. At 30 μ M the effect of Ro8-4304 decreased slightly, but not significantly. Therefore, Huang et al. (2016) kept using a concentration of 15 μM ¹⁶⁶. Throughout this thesis 15 μM was pre-dominantly used for further experiments, while this allows for an easier comparison to the original work. Nonetheless, it is important to know, whether Ro8-4304 has a toxic effect at higher concentrations. Chs3-2D was grown on 5, 15, 30, 50, 100 and 200 μM Ro8-4304, respectively (Figure 13). Since the chemical Ro8-4304 was dissolved in DMSO, the dissolvent was used as the negative control. George Osgood Estes already demonstrated in 1969 that DMSO aids the uptake of various chemicals in plants ¹⁸⁷. DMSO levels higher than 0.1% were toxic to *Phaseolus vulgaris* and *Solanum tuberosum* ¹⁸⁷. A more recent study reported on a toxicity in rice at a concentration of 10 mM DMSO ¹⁸⁸. Therefore, the toxicity of DMSO was also tested (Figure 13a). DMSO did neither show a positive nor a negative effect on the fresh weight of chs3-2D. The concentration used in the experiments were lower than the previously reported toxicity inducing concentrations ^{187,188}. The chemical Ro8-4304 showed a growth rescuing effect in the range of 15 to 100 μM (Figure 13b), as previously reported

 $^{166}.$ At 200 μM the chemical was still not toxic, although the rescue on the phenotype was significantly diminished. This may also be due to a minimal toxic effect of 1.3% DMSO. For further experiments, a concentration of 15 to 50 μM was selected.

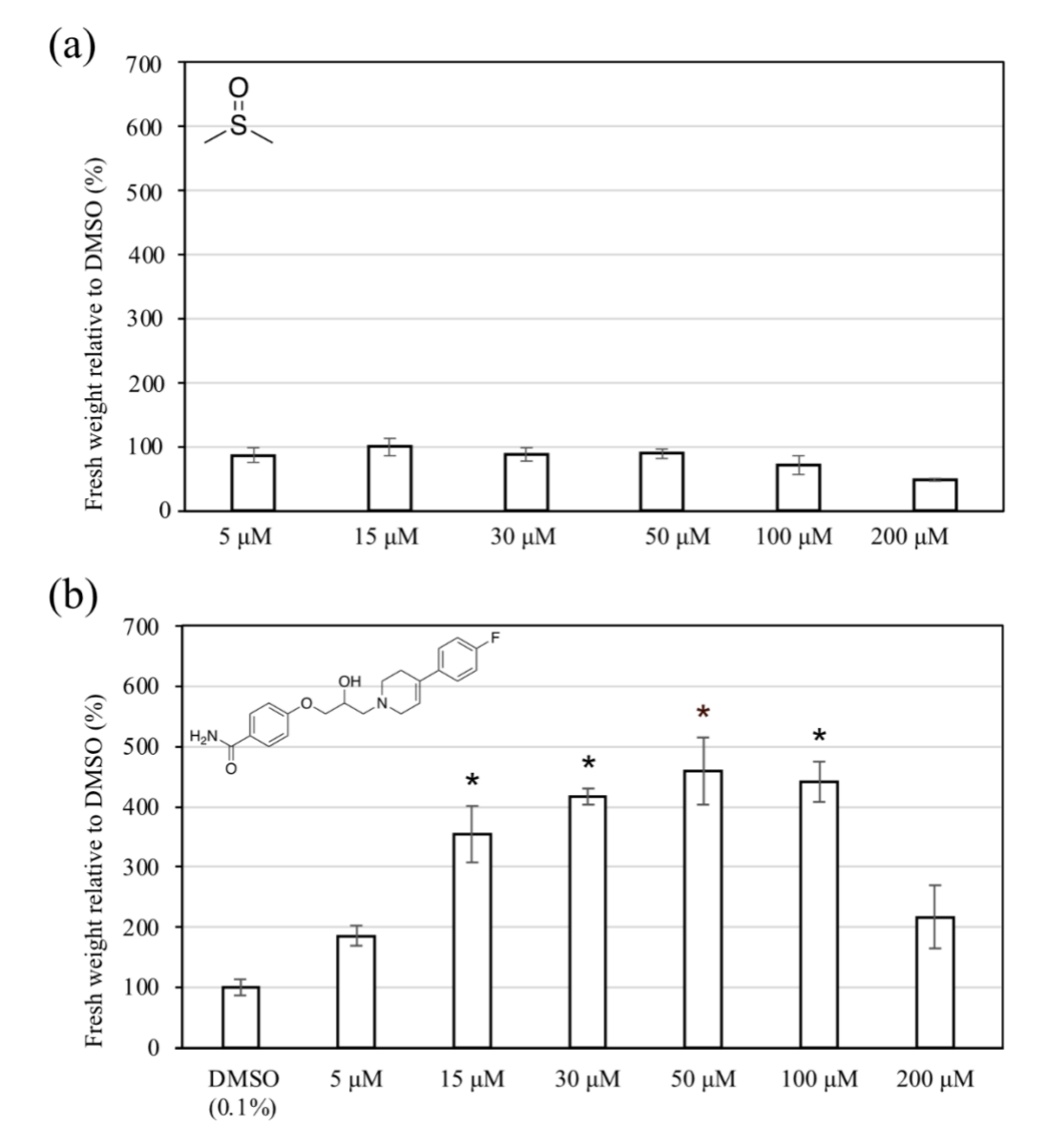
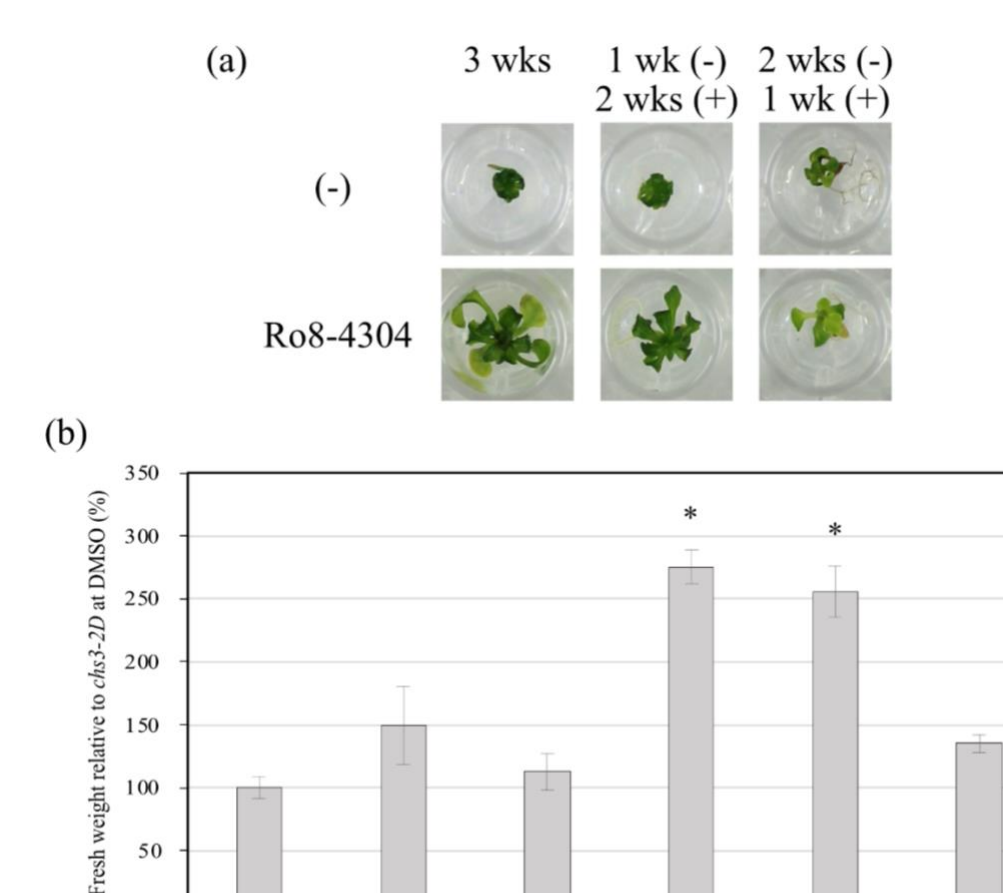


Figure 13. The effect of Ro8-4304 on *chs3-2D* rescue at different concentrations. (a) Fresh weight of *chs3-2D* grown for 20 days at 18°C on different concentrations of DMSO. (b) Fresh weight of *chs3-2D* grown for 20 days at 18°C on different concentrations of Ro8-4304 dissolved in DMSO. (a and b) The data was normalized against the mean value of *chs3-2D* grown on 0.1% DMSO. The data represent the mean \pm SE of three biological replicates (n=3, with 10 \pm 2 plants each). An asterisk indicates a significant difference to DMSO (0.1%) (Student's t-test, p < 0.05).

In addition to dependence on temperature and concentration, it is important to know at which stage in the plant's life cycle a chemical is capable to execute its function. Verly et al. (2020) discussed that the developmental stage of a plant is important for the defence establishment in the presence of pathogens or plant defence stimulators ¹⁸⁹. We therefore investigated at which developmental stage Ro8-4304 needs to be applied. For that purpose, *chs3-2D* seedlings were grown for three weeks in the presence of the chemical, or grown for

1 week and 2 weeks, respectively, in the absence of the chemical on MS medium before transferring the seedlings to media containing Ro8-4304. The transfer may result in an additional stress, but Huang et al. (2016) already determined that spraying plants with Ro8-4304 did not yield any visible effects ¹⁶⁶, thus indicating that uptake via the root system was required. The treatments demonstrated that Ro8-4304 needs to be applied via the root system in the first weeks of development, whereas chs3-2D was not susceptible to the chemical after 2 weeks of growing on MS (Figure 14).



50

3wks DMSO

1 wk MS:

2wks DMSO

Figure 14. The effect of Ro8-4304 on chs3-2D rescue at later stages of development. (a) Morphology of chs3-2D seedlings grown for 20 days at 18° C on MS media with different treatments of 15 μ M Ro8-4304 or DMSO. (b) Fresh weight of chs3-2D seedlings normalized against the mean value of chs3-2D grown on DMSO for 3 weeks. The data shows the mean \pm SE of three biological replicates (n=3, with 10 \pm 2 plants each). An asterisk indicates a significant difference to the relevant negative control (Student's t-test, p < 0.05).

3 weeks

Ro8-4304

1 wk MS:

2 wks

Ro8-4304

2wks MS:

1 wk

Ro8-4304

2wks MS:

1wk DMSO

Finally, we applied pulse-chase experiments to determine how long the chemical needs to be applied for a significant increase in fresh weight. Chs3-2D seedlings were grown on 15 μM Ro8-4304 for different amounts of time before being transferred to MS media (Figure 15). Ro8-4304 already mediated a significant rescue of chs3-2D autoimmunity when applied for 2 days only. However, a more pronounced effect was visible after 7 or more days of chemical incubation (Figure 15a). Quantification of chs3-2D fresh weight indicated that a duration of 1 day was not sufficient for rescue, whereas 2 or more days of treatment resulted in a significant rescue of growth (Figure 15b).

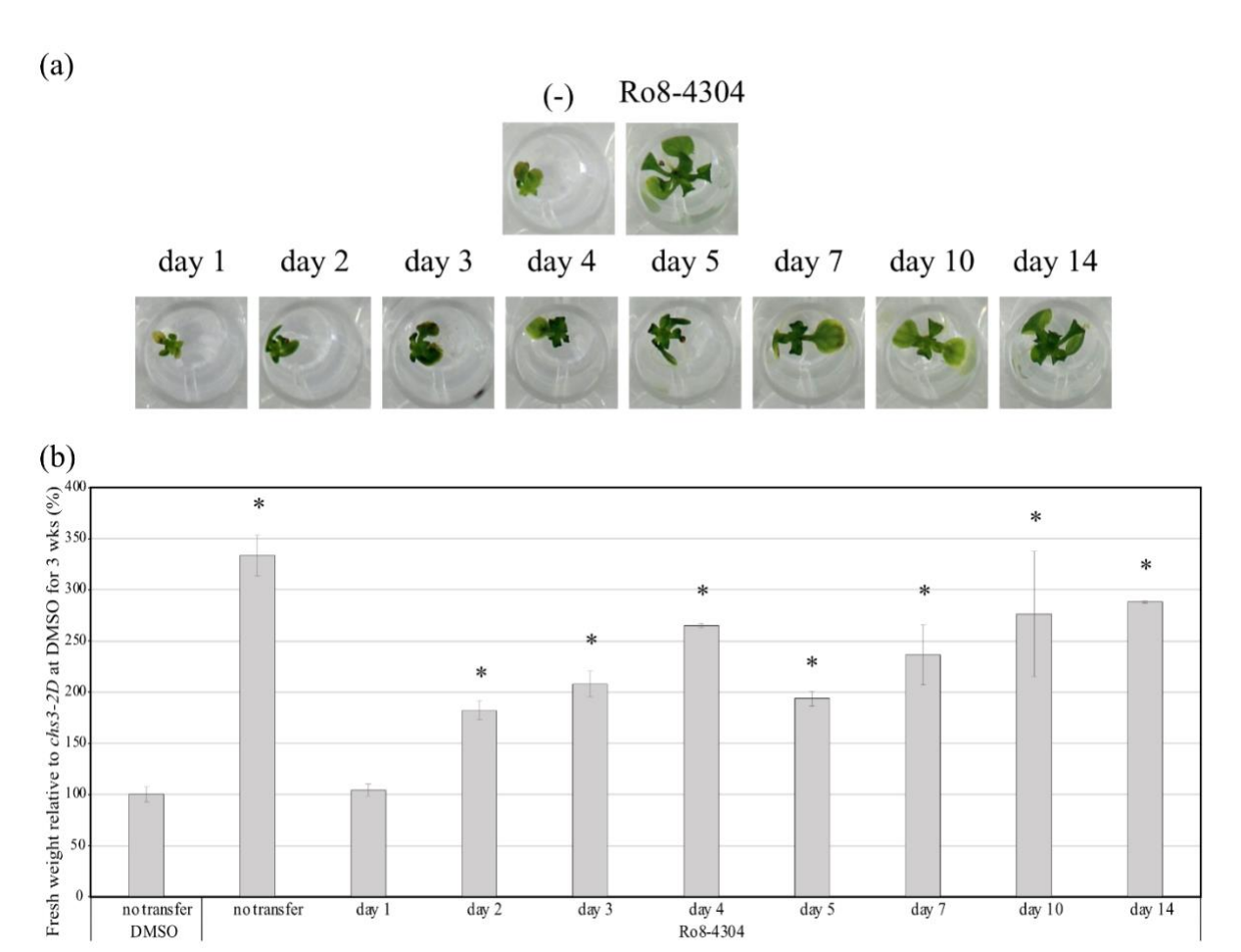
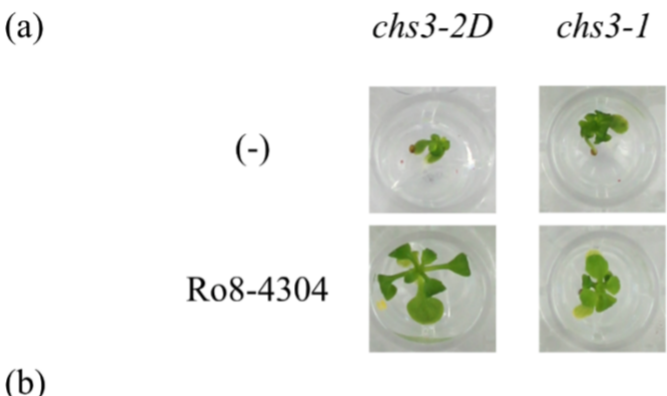


Figure 15. The effect of Ro8-4304 on *chs3-2D* rescue early in development. (a) Morphology of *chs3-2D* plants grown for 20 days at 18°C on MS media with DMSO or with 15 μ M Ro8-4304 applied for the indicated durations. (b) Fresh weight of *chs3-2D* seedlings normalized against the mean value of *chs3-2D* grown on DMSO for 3 weeks. The data shows the mean \pm SE of three biological replicates (n=3, with 10 \pm 2 plants each). An asterisk indicates a significant difference to the relevant negative control (Student's t-test, p < 0.05).

In addition to *chs3-2D* a couple of autoimmune mutants were already tested for their responsiveness to Ro8-4304 in the original paper, including *snc1*, *snc4*, and *bir1* pad4 ^{80,166}. These mutants were unresponsive to the chemical. The autoimmune mutant *saul1-1* ⁷³ was also unresponsive [data not shown] ¹⁹⁰. We tested additional chilling mutants, namely *chs1* ^{79,185}, *chs2* ¹⁸⁶, and *chs3* ⁸⁵. *Chs1-1* and *chs2-1* seedlings did not show an autoimmune phenotype when grown on plates [data not shown] and were therefore not included. *Chs3-1* showed an autoimmune phenotype less severe than *chs3-2D* (Figure 16). The Ro8-4304 chemical appeared to increase the fresh weight of *chs3-1* (Figure 16a), however, fresh weight quantification indicated that the increase was not significant (Figure 16b).



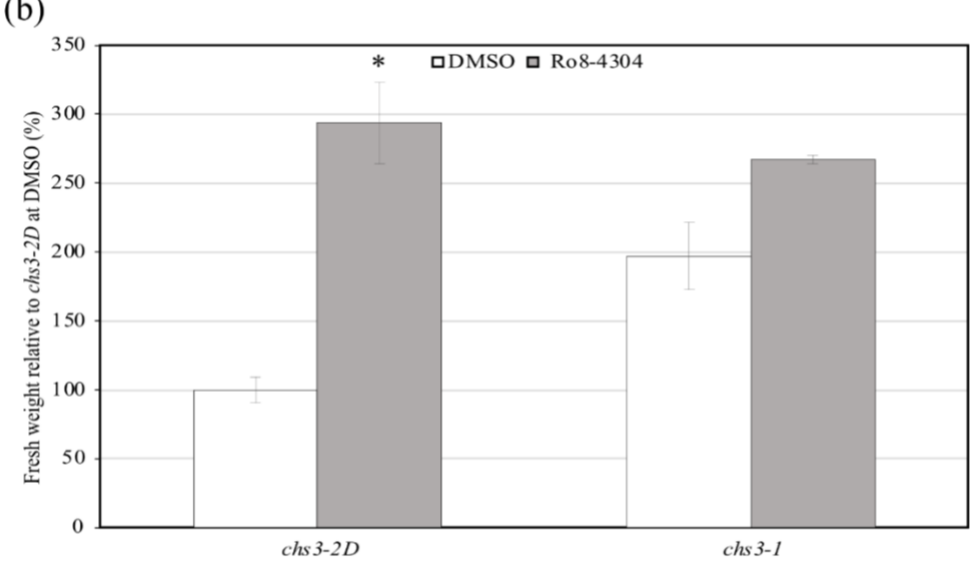


Figure 16. The effect of Ro8-4304 on the autoimmune phenotype of *chs3-1* mutants. (a) Morphology of *chs3-2D* and *chs3-1* grown for 20 days at 18°C on MS media with 15 μ M Ro8-4304 or DMSO. (b) Fresh weight normalized against the mean value of *chs3-2D* grown on DMSO. The data show the mean \pm SE of three biological replicates (n=3, with 10 \pm 2 plants each). An asterisk indicates a significant difference to the relevant negative control (Student's t-test, p < 0.05).

Huang et al. (2016) reported that Ro8-4304 could rescue the growth defect of the *chs3-2D* autoimmune mutant ¹⁶⁶, but negatively affects the immunity, which was shown by a reduction of immune marker genes (*PR1* and *PR2*) ¹⁶⁶. Additionally, the direct target is still unknown. To solve these problems, we planned to bind Ro8-4304 to a matrix and execute an affinity purification experiment. If we know the direct target, we may understand the mechanism of action and we might be able to rescue both growth and immunity. For affinity purification, a lot of solid support matrixes are commercially available ¹⁹¹. However, none of these can bind Ro8-4304 in its current form. Therefore, we aimed to synthesize an analogue with a different active group that can bind to a matrix in collaboration with the organic chemistry department. By chemically modifying Ro8-4304, we aimed to improve on the action of the chemical. Secondly, modifying and testing of analogues will give us insights about the important parts of the molecule, so in theory it will allow us to do a small structure activity relationship study. And lastly, it may give us a compound which can be bound to activated agarose, so we can pull down the unknown protein. Therefore, we proceeded with the chemical optimization.

4.2 Organic chemical modification of Ro8-4304

4.2.1 The synthesis of Ro8-4304

Initially, we planned to synthesize Ro8-4304. Fortuitously, the synthesis of Ro8-4304 was already described in the United States Patent no. 3674799A of Edenhofer et al. (1972) (Scheme 1) ¹⁶⁹. Firstly, 4-oxiranylmethoxy benzamide (BB01) needs to be synthesized. This is achieved by combining 4-hydroxybenzamide and epichlorohydrin in a solution of NaOH for 18 hours (hrs) at room temperature (RT). The white precipitate is washed with water and recrystallized from methanol. The synthesized compound is then combined with 4-(4-fluorophenyl)-1,2,3,6-tetrahydropyridine (PTP-F) in EtOH and stirred at reflux for 1 h. The synthesized Ro8-4304 should separate out upon cooling. However, no precipitate was detected in the first try. This was probably due to PTP-F; I used the hydrochloride (HCI) version of this compound, which is not mentioned in the patent. So, to improve the reaction 1 equivalent (Eq) of triethylamine (TEA) was added. In addition, the reaction was stirred for a longer time (4 hrs). Using these improvements, pure Ro8-4304 was synthesized. Thus, the reported synthesis is suitable for producing Ro8-4304. Additionally, by adjusting the starting compounds of this synthesis, analogues could be synthesized.

Scheme 1. The synthesis of Ro8-4304, as described by Edenhofer et al. (1972) ¹⁶⁹. Reagents and conditions: (a) 4-hydroxybenzamide and epichlorohydrin are reacted O/N at RT in a solution of NaOH. (b) The synthesized, 4-oxiranylmethoxy benzamide and 4-(4-fluorophenyl)-1,2,3,6-tetrahydropyridine • HCl are combined in EtOH, pre-treated with TEA. The mixture is heated to reflux for 4 hrs. (c) Ro8-4304 separates out upon cooling, and is treated with 1M ethanolic HCl, to create the HCl salt version of Ro8-4304.

In the following, synthesis of 18 Ro8-4304 derivatives will be described. The main goal in these synthesis reactions was to create a molecule which could be bound to a matrix.

Thus, we aimed to synthesize a variant which could be bound to DADPA activated agarose (Section 4.2.2). For this an acid group needed to be incorporated on the fluorine site of the structure. During this endeavour multiple analogues were synthesized (Ro-A01 to Ro-A06) and these analogues were also tested and included in a structure activity relationship study. Since we didn't have any information on the active site, we also chose to synthesize a version which binds to a matrix on the benzamide site of the molecule. Thus, we synthesized a version which could be bound to NHS activated agarose (Section 4.2.3) (Ro-A07 and Ro-A08). Therefore, if the active site of the protein is on the left the DADPA matrix would yield results and if the active site of the protein is on the right the NHS matrix would yield the necessary data. The venture of the NHS activated agarose was easier than the DADPA activated agarose, therefore we decided to make some additional analogues with changes on the benzamide side (Ro-A09 to Ro-A012). With this we had two sets of analogues with changes on the left and right side of the structure. Next, we synthesized some analogues with changes in the middle (Ro-A13 to Ro-A18), to be able to include all the

aspects of the structure in the conclusion and discussion of the structure activity relationship study.

4.2.2 A Ro analogue that binds to DADPA activated agarose

Originally, we intended a collaboration with the chemistry department to make an analogue which can be bound to a matrix. The structure of Ro8-4304 is quite a linear, without a lot of active groups. The unreactive fluorine atom of Ro8-4304 (Figure 7) could possibly be changed for a more reactive group, which then binds to a matrix. One possibility would be to change the fluorine atom for an acid group. This group is less nucleophilic than an amine, and will therefore not alter the reactions, as described in Scheme 1. Furthermore, an acid group is able to bind to certain matrixes e.g., DADPA activated agarose in the presence of EDC ¹⁹¹. The second synthesis step of Ro8-4304 requires two building blocks: BB01, and PTP-F (Scheme 1). Developing a reaction which can transform PTP-F, to PTP-COOH, should lead to a Ro8-4304 analogue with an acid group. For the purpose of this goal, different synthesis routes were tried.

4.2.2.1 The synthesis of Ro-A01

A method to incorporate acid groups is by creating a Grignard reagent, and to combine the resulting reactive species with dry ice. Furthermore, the Grignard reaction has already been used successfully for the creation of pyridine analogues previously ^{192,193}. In a first step, 4-(4-bromophenyl)-4-piperidinol was dehydrated using an acid to prevent that the alcohol would react with the Grignard reagent (BB02). This molecule was protected (E5), and the Grignard reaction was tried but no product could be identified. The dehydration reaction may not have been completely successful, and some water could still have been present in the synthesized product BB02, affecting the Grignard reaction, which only functions in a completely dry environment. Anyway, we used BB02 to synthesize the first analogue (Ro-A01) by adding BB01, as described in Scheme 1.

4.2.2.2 The synthesis of Ro-A02

Since the Grignard reaction did not yield satisfactory results, other methods were tried. One of these was what we called the Gessner reaction. Gessner et al. (1985) combined phenol and 4-piperidone monohydrate in the presence of gaseous HCl, to synthesize 4-(4'-hydroxyphenyl)-1,2,3,6-tetrahydropyridine (BB03) (Scheme 2) ¹⁷².

Scheme 2. The synthesis of PTP-OH was imitated from Gessner et al. (1985) ¹⁷². (a) Phenol and 4-piperidone monohydrate were joined in glacial acetic acid. Gaseous HCl was passed through this solution for 3 min, the reaction was heated to reflux for 10 min, and gaseous HCl was passed through the solution, again, for

another 2 min. Or (a) Phenol and 4-piperidone monohydrate were dissolved in 1M ethanolic HCl, this was heated to reflux for 24 hrs.

The Gessner reaction was imitated and resulted in BB03. However, the production of gaseous HCl was quite troublesome. Thus, the reaction was tried with 1M ethanolic HCl. This alteration also yielded BB03, however a longer reaction time was necessary to yield enough of the product. Lastly, 37% aqueous HCl was tried, but this did not produce any product. Probably, the acid catalysed reaction only works water free.

The synthesized BB03 was combined with BB01, as described in Scheme 1, to yield the second analogue Ro-A02. Considering that the reaction to synthesize BB03 was quite successful, phenol was changed for benzoic acid. However, stirring this mixture for 3 days at reflux in 1M ethanolic acid did not yield any PTP-COOH. This was probably due to the mesomeric effect. An alcohol group is an electron donating group, in contrast to an acid group, which is electron withdrawing moiety. Due to the mesomeric effect, the electron density is increased in the phenol version. Hereby, improving the reaction conditions, so that the Gessner reaction can take place. However, in benzoic acid the benzene ring is destabilised, and therefore this molecule is probably unreactive to the Gessner reagent.

The Gessner reaction is an acid catalysed reaction to combine piperidone with another fragment. This reaction of 3,5-dimethoxy-phenol and N-methyl-piperidone has been reported previously ^{194,195}. To avoid the mesomeric effect, starting compounds containing oxygen groups were used. Similarly, we synthesized 2-phenoxyacetic acid (E2) (Scheme 3) and 2-phenoxy ethanol (E3) (Scheme 4), according to literature ^{178–180}. Both were used as a substrate in the Gessner reaction. However, the desired products were not synthesized while ¹HNMR only showed the peaks of the starting products. It may have been that the linker, with the acid or ethanol group, slightly reduced the stability of the ring. Therefore, the benzene ring may have been more stable than with the acid moiety, but this stability was not sufficient for the reaction to take place. Another option may be that the ethanolic HCl can only be used when the stability of the starting compounds is optimal. And less suitable conditions may need a completely dry environment for the reaction to function. Therefore, it would have been useful if this Gessner reaction was tried on E2 and E3 using HCl gas, instead of ethanolic HCl. However, due to time restraints this was not done, and this may be interesting to confirm in the future.

Scheme 3. The synthesis of 2-phenoxyacetic acid according to He et al. (2015) and Yan et al. (2015) 178,179 . (a) Phenol was dissolved in a mixture of NaOH in H₂O and stirred for 20 min. (b) Chloroacetic acid was dissolved in H₂O, at 0°C, and a 25% NaOH solution was added dropwise until the pH reached 9-10, to create a solution of sodium chloroacetate. This was added dropwise to the phenol solution. The mixture was heated to 105°C, and refluxed O/N. (c) The solution was allowed to cool down, and a 5M HCl solution was added until the pH reached 1, and a precipitate formed.

Scheme 4. The synthesis of 2-phenoxyethanol according to Hu et al. 180 . (a) Phenol was dissolved in a mixture of NaOH in H_2O and stirred for 20 min. (b) 2-bromoethanol was added dropwise to the phenol solution. The mixture was heated to $90^{\circ}C$, and heated O/N.

There were two remaining possibilities to finally synthesize Ro-COOH, by using the Gessner reaction. In the first synthesis plan phenol would be reacted with 4-piperidone according to the Gessner reaction (Scheme 2). Hereafter, the amine would be protected and the 2-phenoxyacetic acid reaction executed (Scheme 3). Lastly, the amine needs to be deprotected and reacted with BBO1 to produce the desired analogue. However, currently the yield of the Gessner reaction was too small for multiple follow-up reactions and scaling-up was quite hard due to the use of HCl gas. Another option would be to use a compound with multiple groups on the ring, according to previous reports ^{194,195}. Nonetheless, the excess side groups may decrease the binding in the protein pocket.

4.2.2.3 The synthesis of Ro-A03 & Ro-A04

For the planned structure activity relationship study, various analogues needed to be synthesized. One thing that might be interesting is to determine the effect of a smaller group. Therefore, we synthesized an analogue with an even smaller atom (Ro-A03). In this analogue, the fluorine atom was changed for a hydrogen atom. This was achieved by dehydrating 4-phenyl-4-piperidinol (BB04) and combining the product with BB01, to synthesize Ro-A03. Additionally, an even more drastic change was made in Ro-A04. Using 1,2,3,6-tetrahydropyridine • HCl and BB01, an analogue was synthesized, in which the benzene ring with the fluorine atom was lacking.

Furthermore, the synthesized BB04 was used for another interesting reaction, which is described in the European Patent no. EP0604800A1 of Himmelsbach et al. (1994). In this publication, they used oxalyl chloride in combination with 1-acetyl-4-phenyl-piperidine to synthesise 4-(4-carboxy-phenyl)-piperidine • HCl ¹⁹⁶. In the last step of this reaction, a precipitate should have formed. However, this was not the case, and cleaning up by standard methods did not yield the pure product.

4.2.2.4 The synthesis of Ro-A05 & Ro-A06

In addition to analogues with a smaller group (Ro-A03 and Ro-A04), we were also aiming to synthesize an analogue with an even bigger and more electronegative side chain. Therefore, an analogue with a 4-trifluoromethyl side group was synthesized. In this case, both the hydrated 4-(4-trifluoromethyl-phenyl) piperidin-4-ol and the non-hydrated version were used for the synthesis. This resulted in Ro-A05 and Ro-A06, respectively.

Due to time limitations, we were unable to complete the goal of synthesizing a Ro8-4304 analogue with an acid group, which could be bound to DADPA activated agarose. However, early testing of the analogues in *chs3-2D* showed that larger groups on the fluorine site reduced the activity, and Ro-A05 and Ro-A06 have no remaining activity at all (see Section 4.3). Thus, it seems that the fluorine site of the molecule is quite important for the activity of Ro8-4304. A matrix on that side of the molecule will most likely not yield any outcome, because this seems to be the binding site of the protein. Therefore, we did not continue with the synthesis of a Ro8-4304 analogue with an acid group, though some reactions could have been performed such as the Kumada coupling ^{197,198}, a carboxylation of bromides ^{199,200}, a heck reaction followed by a hydrolysis ²⁰¹, or a cyanation followed by a hydrolysis ²⁰².

Since the synthesizes of the Ro8-4304 analogue with an acid group was unsuccessful, we continued the effort to synthesize an analogue that could bind to NHS activated agarose.

4.2.3 A Ro analogue that binds to NHS activated agarose (Ro-A07 and Ro-A08)

DADPA activated agarose is not the only matrix applicable. There are other matrixes commercially available like NHS activated agarose ²⁰³. The NHS activated agarose matrix contains a succinimide group at the end of its linker, which can react with amines. Ro8-4304 has an amino group at the left side of the molecule (Figure 7). However, this is next to an oxygen atom, hereby not being an official amino group, but a benzamide group ((-C=O)-NH₂), and this oxygen alters the reactivity of the nitrogen significantly. The oxygen atom is a strongly electron withdrawing group, which decreases the electron density on the neighbouring nitrogen atom, and hereby reduces the nucleophilicity of the amine. Additionally, the amine is stabilized by the oxygen due to resonance, which results in an increased stability, but in a decreased reactivity, in comparison to a vacant amine. Notably, Yang et al. (2007) modified their compound, quinostatin, for affinity chromatography, to determine its target, even though it already had a benzamide group ²⁰⁴. Therefore, it was presumable that Ro8-4304 may also need an adaption before it can bind to NHS activated agarose. To test if Ro8-4304 could react with NHS activated agarose, a small succinimide molecule was synthesized, according to literature ^{176,177}. This molecule, Nhydroxy succinimide propanoate (E1, Scheme 5), was used as a substituent for the NHS activated agarose.

Scheme 5. The synthesis of N-hydroxy succinimide propanoate, as describe by Keller et al. (2008) and Bonnitcha et al. (2010) ^{176,177}. (a) Propionic acid, n-hydroxy succinimide, and dicyclohexylcarbodiimid (DCC) were combined in tetrahydrofuran (THF) at 0°C, and this mixture was stirred for 2 hrs. After this, the mixture was warmed up to RT and stirred for another 12 hrs.

Compound E1 was combined with benzamide, or benzylamine in H_2O/ACN (Scheme 6). The mixtures were left at RT for 4 hrs, whereafter they were sent in for MS (Figures 17 and 18). For the 1H -NMR experiment, both compounds were combined with E1, in DMSO- d_6 , and a spectrum was taken every 10 min for 2 hrs (Figures 19 and 20). Both experiments were done without any purification steps.

Scheme 6. N-hydroxy succinimide propanoate was combined with benzamide (upper row), or benzylamine (lower row), to yield either N-(1-oxopropyl)-benzamide, or N-(phenylmethyl)-propanamide. Mass to charge ratios of all the compounds are indicated.

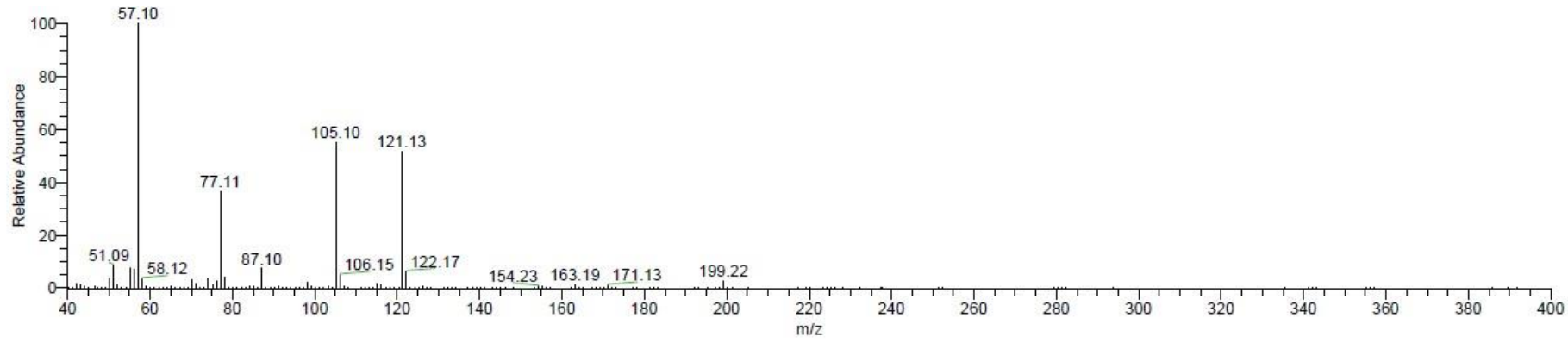


Figure 17. The EI MS of the reaction mixture consisting of N-hydroxy succinimide propanoate and benzamide, taken after 4 hrs, at RT. The *m/z* at 171.13 corresponds to the [M]⁻⁺ of N-hydroxy succinimide propanoate, and the *m/z* at 121.13 corresponds to the [M]⁻⁺ of benzamide.

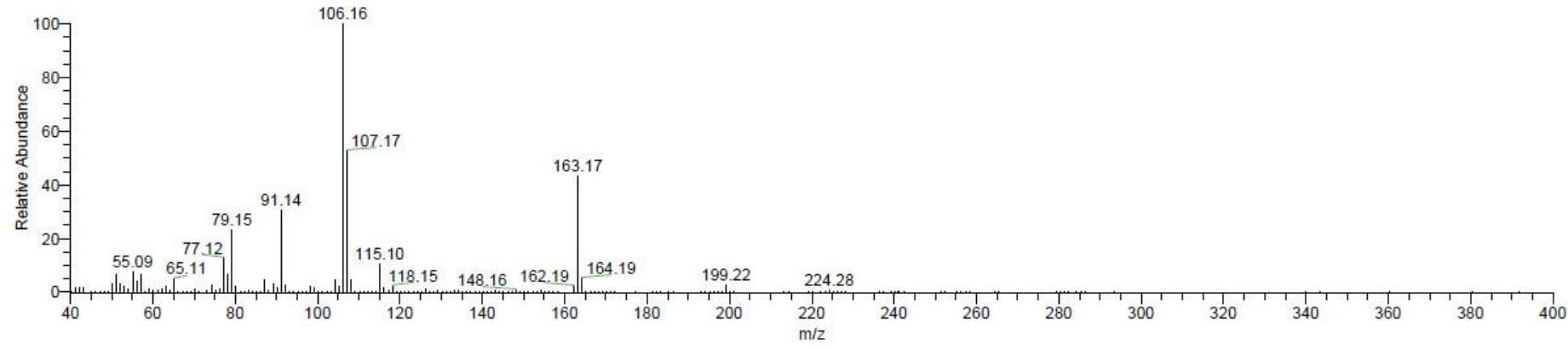


Figure 18. The EI MS of the reaction mixture consisting of N-hydroxy succinimide propanoate and benzylamine, taken after 4 hrs, at RT. The *m/z* at 107.17 corresponds to the [M]⁻⁺ of benzylamine. Also, the [M]⁻⁺ of the synthesis product, N-(phenylmethyl)-propanamide, could be detected at a *m/z* of 163.17. The [M]⁻⁺ of N-hydroxy succinimide propanoate was absent.

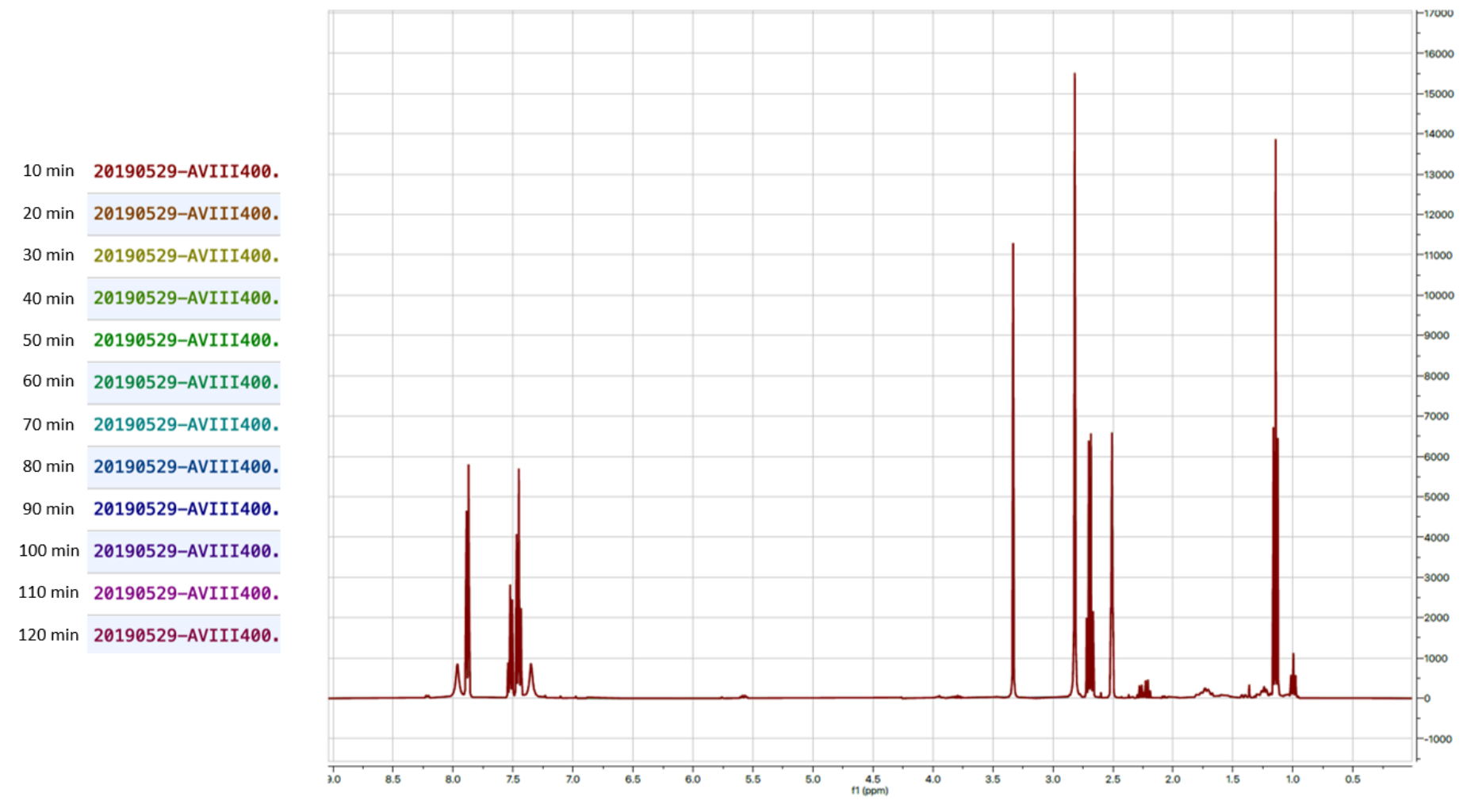


Figure 19. H-NMR stack spectrum of the reaction mixture consisting of N-hydroxy succinimide propanoate and benzamide, in DMSO-d₆, 300 K, 400 MHz. Every 10 min a new spectrum was taken, for 2 hrs, and these spectra were stacked together. The Colours of the different time points can be seen in the legend.

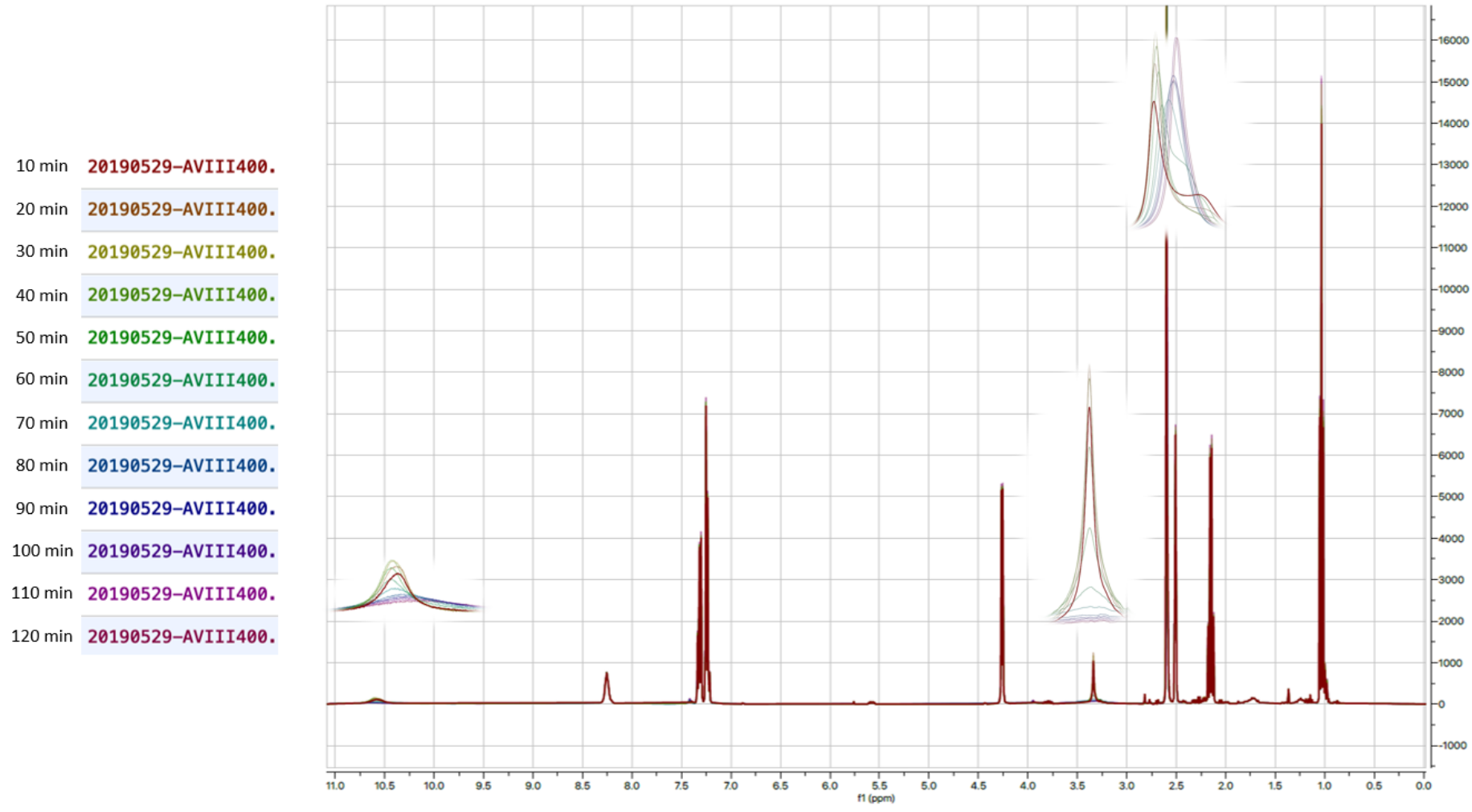


Figure 20. 'H-NMR stack spectrum of the reaction mixture consisting of N-hydroxy succinimide propanoate and benzylamine, in DMSO- d_6 , 300 K, 400 MHz. Every 10 min a new spectrum was taken, for 2 hrs, and these spectra were stacked together. The Colours of the different time points can be seen in the legend. The peaks at 10.5, 3.3, and 2.6 ppm were enlarged.

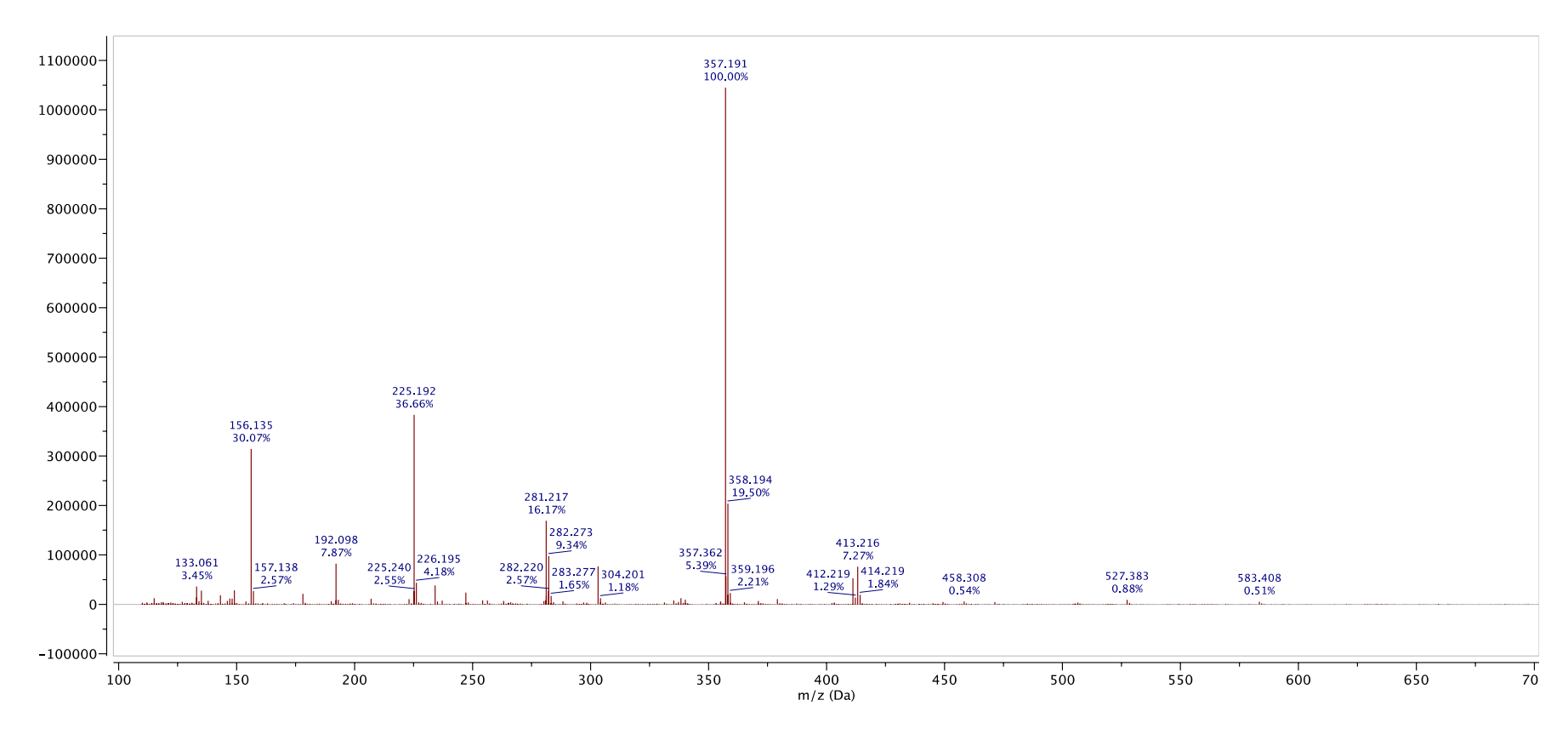


Figure 21. The ESI MS of the reaction mixture consisting of N-hydroxy succinimide propanoate and Ro-A07, taken after 4 hrs, at RT. The *m/z* at 357.191 corresponds to the [M+H] ⁺ of Ro-A07. Also, the [M+H] ⁺ of the synthesis product can be detected at a *m/z* of 413.216. The [M+H] ⁺ of N-hydroxy succinimide propanoate is absent.

The reaction of N-hydroxy succinimide propanoate and benzamide should yield, in theory, N-(1-oxopropyl)-benzamide. The m/z of this product is 177.0790 (Scheme 6). However, the EI-MS spectrum of this combination (Figure 17) did not show this m/z, although the m/z of the starting products could correctly be detected at 121.13, and 171.13. These preliminary results suggested that benzamide was quite unreactive. This result was confirmed by a time-course experiment in the ¹H-NMR (Figure 19). In the stacked spectra, no clear difference was visible in any of the peaks, indicating that no change occurred in the two-hour reaction time. To confirm that this result was due to the reactivity of the amine group, and not due to the reactivity of the N-hydroxy succinimide propanoate, both experiments were repeated with a positive control. N-hydroxy succinimide propanoate and benzylamine were combined to yield N-(phenylmethyl)-propanamide (m/z 163.0997), in the same conditions as with benzamide. The EI-MS spectrum of this combination (Figure 18) showed distinct peaks at m/z 107.17 and 163.17, which corresponded to the starting compound benzylamine and the product N-(phenylmethyl)-propanamide, respectively. The m/z of N-hydroxy succinimide propanoate (171.0532) was not visible. This may indicate that benzylamine could react with N-hydroxy succinimide propanoate. This was supported in the time-course ¹H-NMR of this reaction (Figure 20). No significant change could be detected when N-hydroxy succinimide propanoate and benzamide were measured (Figure 19), but with benzylamine there were three peaks that showed recognizable changes when the different time spectra were stacked (Figure 20). The peak at 2.6 showed a slight shift to a lower ppm. The peak at 3.4 was possibly due to the loss of the -NH2 group, while the peak had a visible decrease. The peak at 10.5 was a bit unusual, because this high shift pointed to an acid group, however, no acid group was present in benzylamine or N-hydroxy succinimide propanoate. Nonetheless, the N-hydroxy succinimide propanoate was successfully synthesized by combining propionic acid, N-hydroxy succinimide and DCC (Scheme 5). It is possible that some propionic acid was still present and reacted with benzylamine. Nevertheless, none of these changes could be seen when using benzamide as reagent. Confirming that benzamide was probably too unreactive to be used in the affinity purification experiment, and therefore Ro8-4304 required adaption. Hence, we decided to synthesize a Ro8-4304 derivative, in which the benzamide group was replaced by an amine group.

For this reason, 4-hydroxybenzylamine was used as starting compound, instead of 4-hydroxybenzamide. Since both the alcohol- and amino-group of 4-hydroxybenzylamine are reactive to epichlorohydrin, a protection step was necessary. Likewise, indicating that an amino group is more reactive than a benzamide group. The amino group of 4-hydroxybenzylamine was first protected with di-tert-butyldicarbonaat (Boc₂O). This group was chosen, because it preferably protects amino groups, and because it is efficiently removed by a weak acid. The intermediate protected version was also included in structure activity relationship study (Ro-A08). The last step of the synthesis of Ro8-4304 is an acidification using 1M ethanolic HCl. Thus, the removal of Boc₂O could be effortlessly integrated in this acidification step and would yield the final product Ro-A07. The rest of the synthesis was done as previously described and the complete synthesis is shown in Scheme 7.

Scheme 7. The synthesis of Ro-A07. (a) 4-hydroxybenzylamine and Boc₂O were combined in DCM, in the presence of TEA. And this mixture was stirred for 16 hrs at RT. (b) 4-[(tert-butoxy-carbonyl)-amino]-methyl]-phenol and epichlorohydrin were combined in a solution of NaOH in methanol (MeOH), this was stirred at RT O/N. (c) Carbamic acid, N-[[4-(2-oxiranylmethoxy) phenyl] methyl]-, 1,1-dimethylethyl ester and PTP-F were combined in EtOH, pre-treated with TEA. This was heated to reflux for 4 hrs. (d) the Boc-protected Ro-NH₂ (Ro-A08) was treated with ethanolic HCl (1M) and stirred for 2 hrs.

The synthesis of Ro-A07 yielded an analogue, which could be bound to matrixes that are able to react with amines. To confirm this, Ro-A07 was combined with N-hydroxy succinimide propanoate, and this resulting mixture was measured with ESI-MS (Figure 21). Both the m/z of the [M+H]⁺ of Ro-A07 (357.191) and of the synthesis product (413.216) can be seen. The [M+H]⁺ of N-hydroxy succinimide propanoate was not visible, however this could also be due to a lesser affinity of N-hydroxy succinimide propanoate for electrospray ionisation. Ro-A07 could react with N-hydroxy succinimide propanoate, and this analogue seems applicable for the affinity Column chromatography.

4.2.4 The synthesis of the analogues Ro-A09 to Ro-A12

During the synthesis of Ro-A07, a change was made on the benzamide site. The synthesis of this analogue was quite straightforward, because 4-oxiranylmethoxy benzamide could be efficiently substituted. Therefore, we chose to synthesize other analogues with changes on this site of the molecule. 4-oxiranylmethoxy benzamide was repeatedly substituted with different phenols. Using the original reaction (Scheme 1), a modest range of analogues was obtained (Ro-A09, Ro-A10, Ro-A11, and Ro-A12). Ro-A09 was synthesized using 4-fluorophenol, Ro-A10 was synthesized using phenol, Ro-A11 was synthesized using 4-hydroxyacetophenon, and lastly Ro-A12 was synthesized using 4-ethyl phenol. All these analogues have different properties than the original Ro8-4304 molecule and are prone to give insights into the structure activity relationship study. The first one is more electrophilic, while the benzamide group was changed for a fluorine atom (Ro-A09). The second analogue has a more basic charge, while the benzamide group was removed (Ro-A10). This is also the case for the third and fourth version in which the amine was removed (Ro-A11), and the benzamide group was changed for an ethyl moiety (Ro-A12).

4.2.5 The synthesis of the analogues Ro-A13 to Ro-A18

In previous reactions alterations on the Ro8-4304 structure were made on the outermost parts of the molecule. Accordingly, we aimed to synthesize some analogues with changes in the middle linker structure. For this purpose, a different approach was used. The first step of the respective reaction was adapted from Kubota et al. (2003) and Ray et al. (2008) ^{174,175}, attaching 4-hydroxybenzamide to e.g., 1,3-dibromopropane. The obtained bromobenzamide was reacted with PTP-F, as in the original Ro8-4304 reaction, Scheme 1. Using this reaction four more analogues were synthesized, with different linker lengths (Ro-A13, Ro-A14, Ro-A15, and Ro-A16). Although this synthesis reaction resulted in a shorter or longer Ro8-4304 version, the alcohol in the middle of the structure was missing, which might be important for binding in the active site. Hence, we also aimed to synthesize a longer Ro8-4304 variant with the original alcohol group. We used the original synthesis (Scheme 1), but with another epichlorohydrin. 2-(chloroethyl) oxirane and 2-(chloromethyl)-2-methyloxirane were used to create the final analogues Ro-A17 and Ro-A18.

Scheme 8. The synthesis of Ro-A13 to Ro-A16, adapted from Kubota et al. (2003) and Ray et al. (2008) ^{174,175}. Reagents and conditions: (a) 4-hydroxybenzamide and e.g., 1,3-dibromopropane were reacted O/N at reflux, in the presence of K₂CO₃, in ACN. (b) The product, 4-(4-bromopropoxy) benzamide, and 4-(4-fluorophenyl)-1,2,3,6- tetrahydropyridine • HCl were combined in EtOH, pre-treated with ethylamine. The mixture was heated to reflux O/N, and the analogue separated out upon cooling. (c) the analogue was treated with 1M ethanolic HCl, to create the hydrochloride salt version.

Obviously, compared to the number of analogues that companies may produce for structure activity relationships studies, the 18 analogues synthesized during this the appear to be very few. However, theses analogues modify various important parts of Ro8-4304 and would in future also enable the synthesis of additional analogues. For example, a primary nitroalkane could have been incorporated, by using Ro-A01 ²⁰⁵. Another option may be to use isoguvacine • HCl. This would create an analogue like Ro-A04, along with an acid group.

In this dissertation, we chose to focus on the biological activity of 18 analogues (Figure 22).

The synthesized analogues were taken back to the biology department for testing in *Arabidopsis thaliana chs3-2D* seedlings to carry out the structure activity relationship study.

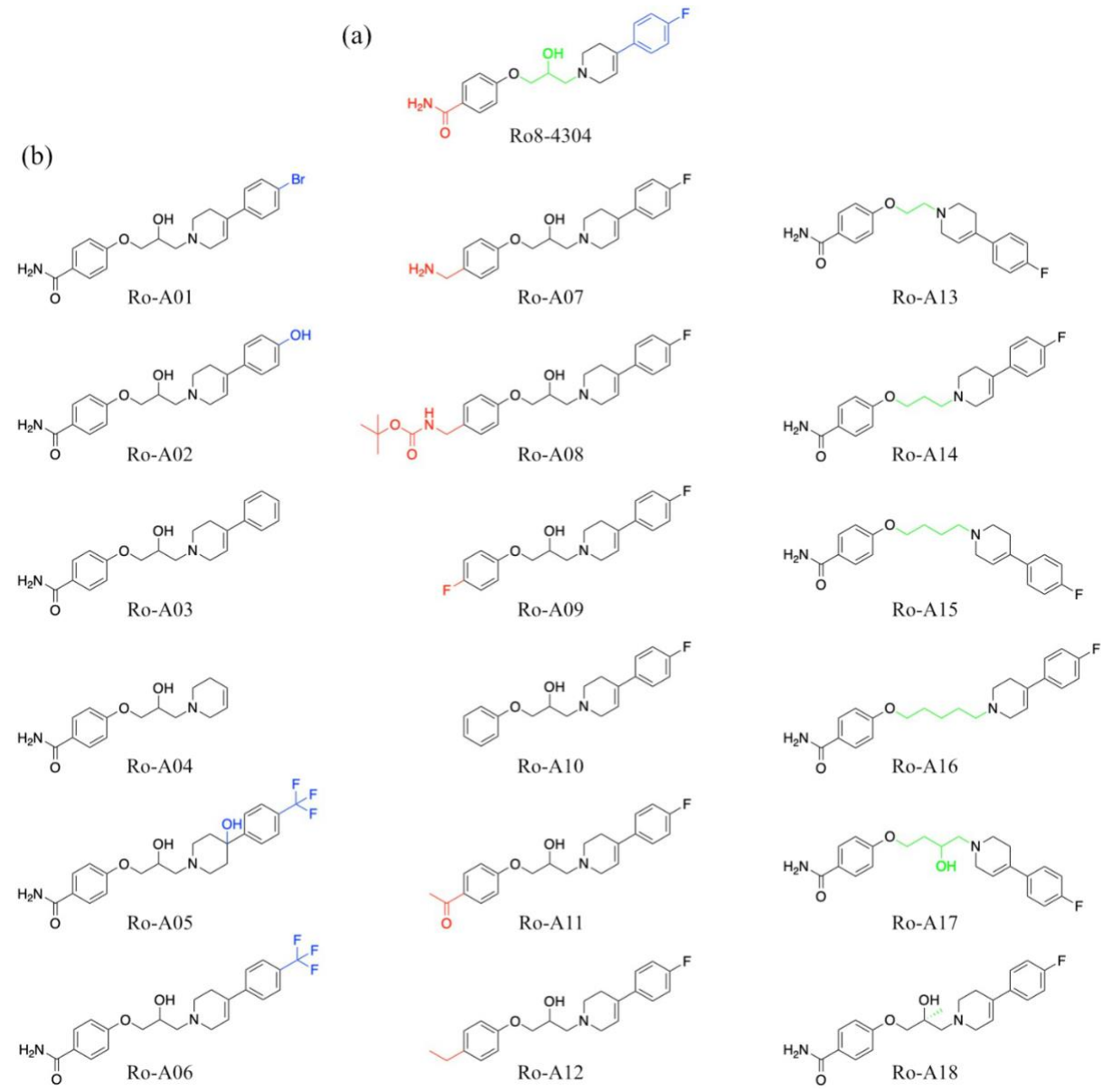


Figure 22. (a) The original chemical structure of Ro8-4304. Modifications were made on three sides of the molecule: on the right side (blue), on the left side (red), or in the middle (green). (b) The structure of all the synthesized analogues is shown.

4.3 Biological activity of the Ro8-4304 analogues

4.3.1 The effect of the analogues on the fresh weight of chs3-2D

The chemical Ro8-4304 influences both growth and immunity. Therefore, we tested the activity of the analogues synthesized in Section 4.2 on both these conditions. First, the effect of the 18 analogues on the fresh weight of *chs3-2D* was investigated (Figures 23-26). Figure 23 shows the growth curves of *chs3-2D* on the negative control DMSO (a), the positive control Ro8-4304 (b), and the two compounds used for synthesis of Ro8-4304 (c and d). These two starting compounds, 4-oxiranylmethoxy benzamide and PTP-F, did not show any effect on the fresh weight. The combination of both their structures in Ro8-4304 was necessary to yield an effect in *chs3-2D*. In contrast to the negative control DMSO that did not affect growth of *chs3-2D*, the presence of Ro8-4304 was sufficient to rescue growth of *chs3-2D*.

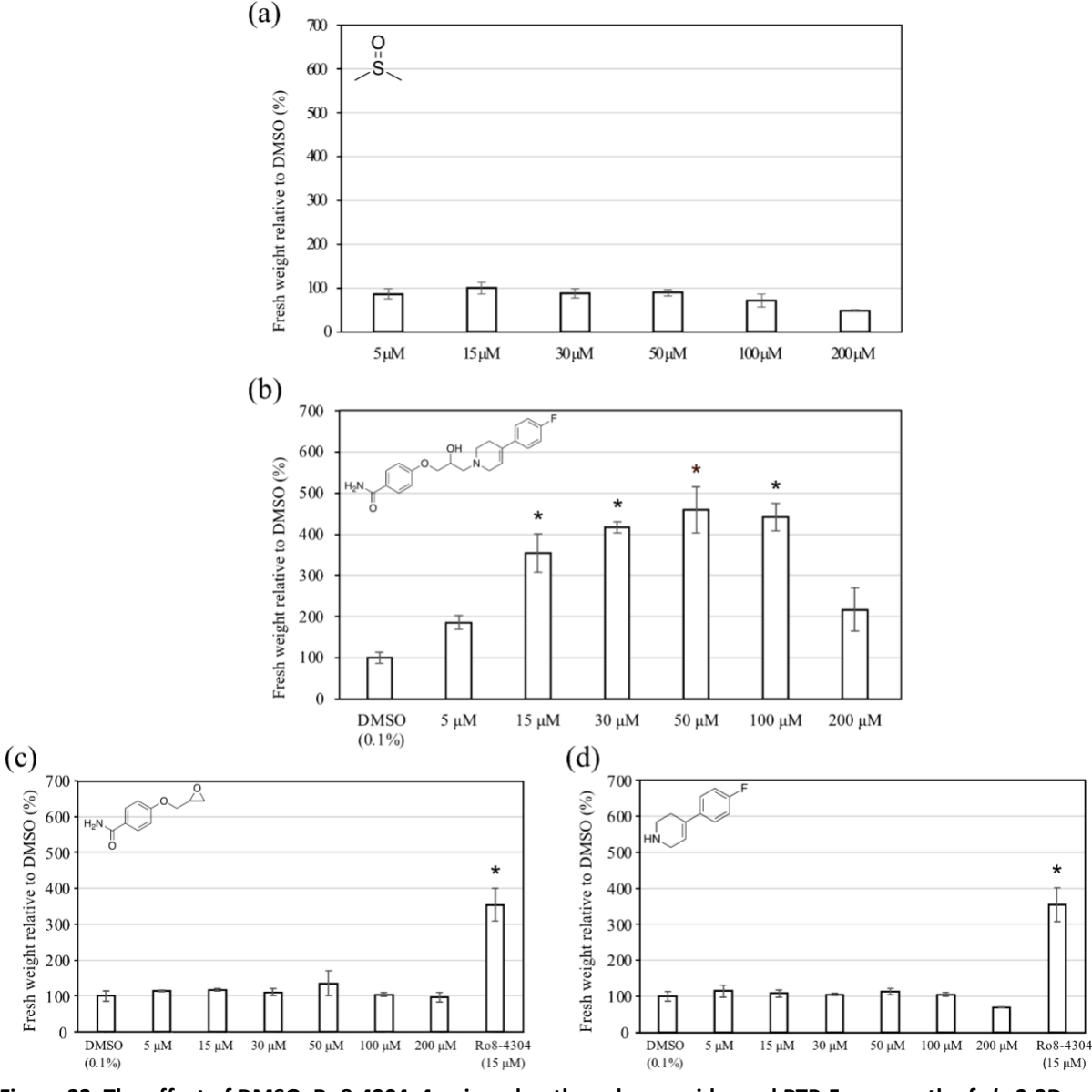


Figure 23. The effect of DMSO, Ro8-4304, 4-oxiranylmethoxy benzamide, and PTP-F on growth of *chs3-2D*. (a) Fresh weight of *chs3-2D* grown on different concentrations of DMSO. (b) Fresh weight of *chs3-2D* grown

on different concentrations of Ro8-4304. (c) Fresh weight of *chs3-2D* grown on different concentrations of 4-oxiranylmethoxy benzamide. (d) Fresh weight of *chs3-2D* grown on different concentrations of PTP-F. (a, b, c, and d) Seedlings were grown for 20 days at 18°C and LD conditions. The data was normalized against the mean value of *chs3-2D* grown on 0.1% DMSO and the bar shows the mean \pm SE of three biological replicates (n=3, with 10 \pm 2 plants each). An asterisk indicates a significant difference to DMSO (0.1%) (Student's t-test, p < 0.05).

The fluorine atom in the Ro8-4304 structure was altered in the analogues Ro-A01 to Ro-A06 (Figure 24). Changing the fluorine for an atom with a different reactivity in Ro-A01 and Ro-A02 negatively affected the fresh weight of *chs3-2D* (Figures 24a and b). Removing the fluorine didn't affect the growth inducing activity of Ro8-4304 in case of Ro-A04, but even slightly improved the effect in Ro-A03 (Figures 24c and d). Changing the fluorine for the bigger and bulkier tri-fluorine group in Ro-A05 and Ro-A06 also negatively affected the fresh weight (Figures 24e and f). This negative effect was more pronounced for Ro-A05, which has an additional alcohol group.

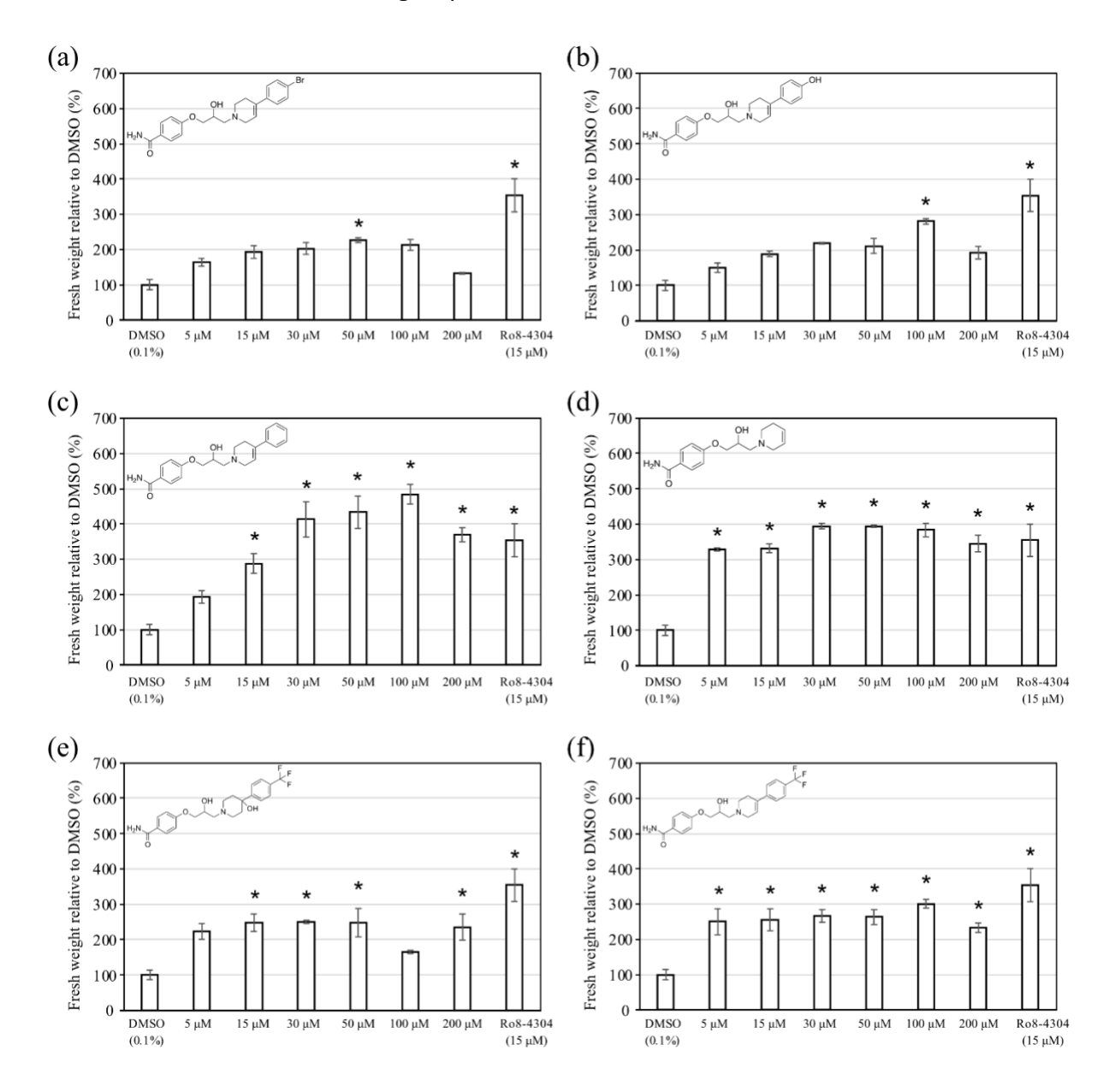


Figure 24. The effect of Ro-A01 till Ro-A06 on *chs3-2D*. (a) Fresh weight of *chs3-2D* grown on different concentrations of Ro-A01. (b) Fresh weight of *chs3-2D* grown on different concentrations of Ro-A02. (c) Fresh weight of *chs3-2D* grown on different concentrations of Ro-A03. (d) Fresh weight of *chs3-2D* grown on different concentrations of Ro-A04. (e) Fresh weight of *chs3-2D* grown on different concentrations of Ro-A05. (f) Fresh weight of *chs3-2D* grown on different concentrations of Ro-A06. (a, b, c, d, e, and f) Seedlings were grown for 20 days at 18°C, LD. The data was normalized against the mean value of *chs3-2D* grown on 0.1% DMSO and the bars shows the mean \pm SE of three biological replicates (n=3, with \pm 10 \pm 2 plants each). An asterisk indicates a significant difference to DMSO (0.1%) (Student's t-test, p < 0.05).

The benzamide on the original structure was adapted in analogues Ro-A07 to Ro-A12. The fresh weight of chs3-2D seedlings grown in the presence of these analogues was on average higher than the fresh weight of chs3-2D seedlings grown in the presence of Ro-A01 to Ro-A06 (Figure 25). This may suggest that the binding site of Ro8-4304 is on the fluorine side of the molecule. The effect of Ro-A07 was less pronounced than the one of Ro8-4304, but still significant (Figure 25a). Therefore Ro-A07 seemed to be suitable for use in the planned affinity purification experiment. A protection group on that side (Ro-A08, Figure 25b) was detrimental for its effect. Ro-A09 to Ro-A11 still had an effect but only at higher concentration (Figures 25c-e). Therefore, we propose that the benzamide group is necessary for stabilizing the structure or for a reaction. Interestingly, Ro-A12 was toxic at a concentration of 100 μ M or higher (Figure 25f).

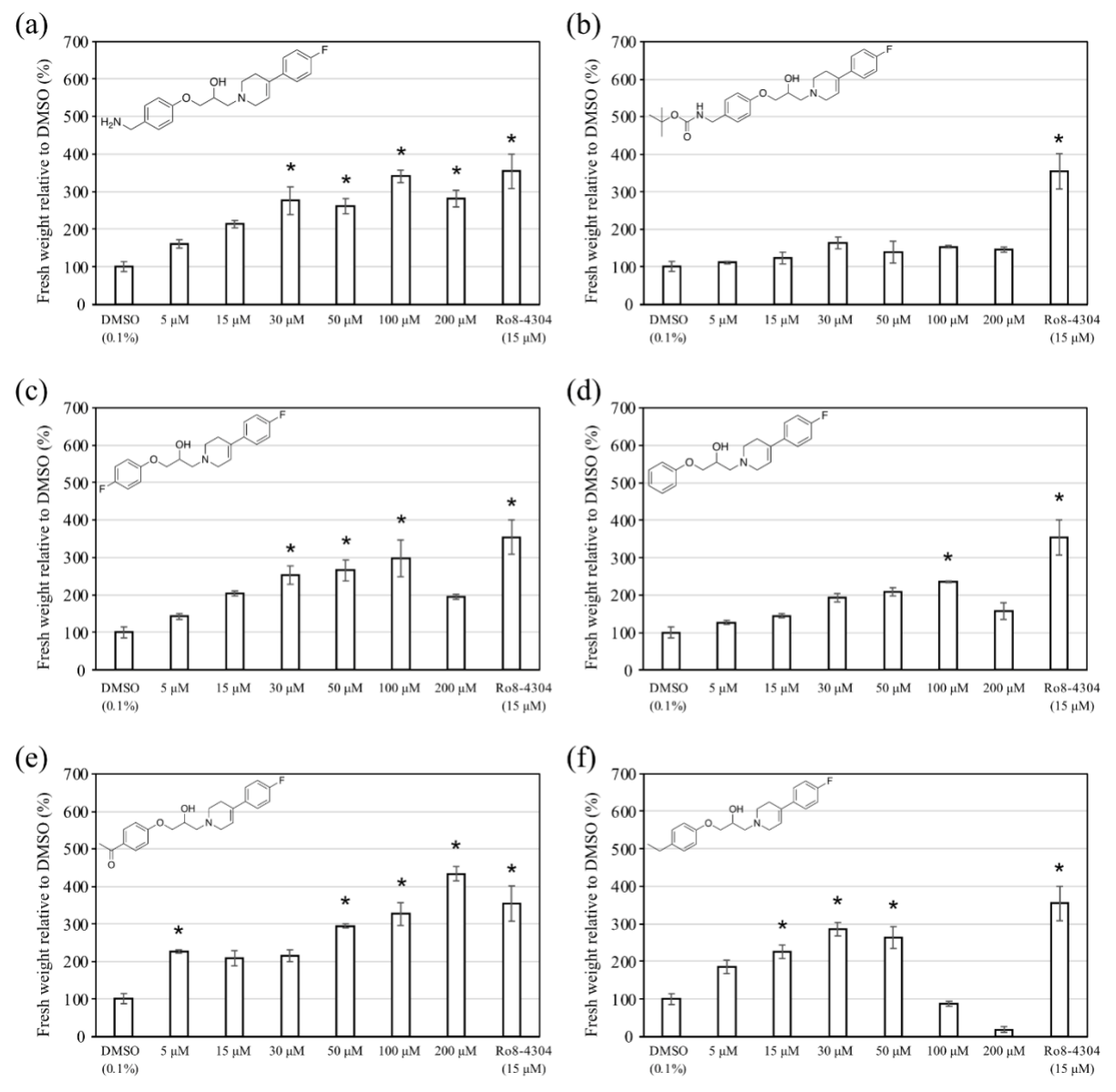


Figure 25. The effect of Ro-A07 to Ro-A12 on growth of *chs3-2D*. (a) Fresh weight of *chs3-2D* grown on different concentrations of Ro-A07. (b) Fresh weight of *chs3-2D* grown on different concentrations of Ro-A08. (c) Fresh weight of *chs3-2D* grown on different concentrations of Ro-A09. (d) Fresh weight of *chs3-2D* grown on different concentrations of Ro-A09. (e) Fresh weight of *chs3-2D* grown on different concentrations of Ro-A11. (f) Fresh weight of *chs3-2D* grown on different concentrations of Ro-A12. (a, b, c, d, e, and f) Seedlings were grown for 20 days at 18° C, LD. The data was normalized against the mean value of *chs3-2D* grown on 0.1% DMSO and the bars shows the mean \pm SE of three biological replicates (n=3, with 10 ± 2 plants each). An asterisk indicates a significant difference to DMSO (0.1%) (Student's t-test, p < 0.05).

Lastly, analogues Ro-A13 to Ro-A18 had an adaption in the middle part of the Ro8-4304 structure. Ro-A13 to Ro-A18 were shorter or longer and missed the alcohol group in the middle. Without this alcohol group the chemicals did not have any effect on the fresh weight of *chs3-2D* (Figures 26a-d). In conclusion, this alcohol may be important for an interaction with a putative binding protein and may thus be vital for the activity of Ro8-4304. Adapting the length of the structure in analogue Ro-A17 (Figure 26e) slightly decreased the activity, therefore we believe that the size of Ro8-4304 is probably the

optimal size to fit into the binding pocket. Adding another methyl group (Ro-A18, Figure 26f) shifted the concentration curve slightly, but had no major effects.

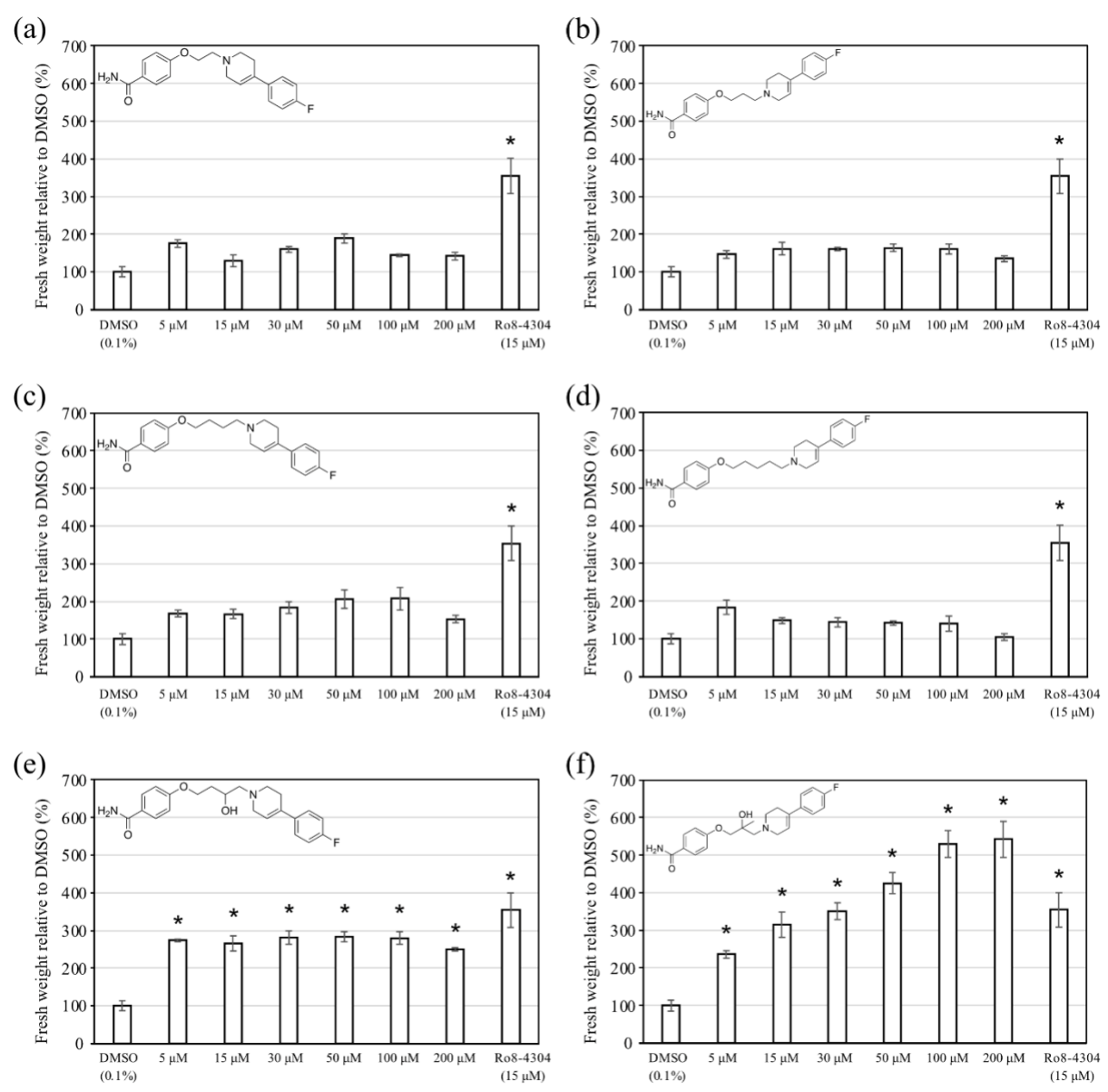


Figure 26. The effect of Ro-A13 to Ro-A18 on growth of *chs3-2D*. (a) Fresh weight of *chs3-2D* grown on different concentrations of Ro-A13. (b) Fresh weight of *chs3-2D* grown on different concentrations of Ro-A14. (c) Fresh weight of *chs3-2D* grown on different concentrations of Ro-A15. (d) Fresh weight of *chs3-2D* grown on different concentrations of Ro-A15. (e) Fresh weight of *chs3-2D* grown on different concentrations of Ro-A17. (f) Fresh weight of *chs3-2D* grown on different concentrations of Ro-A18. (a, b, c, d, e, and f) Seedlings were grown for 20 days at 18°C, LD. The data was normalized against the mean value of *chs3-2D* grown on 0.1% DMSO and the bars shows the mean \pm SE of three biological replicates (n=3, with 10 ± 2 plants each). An asterisk indicates a significant difference to DMSO (0.1%) (Student's t-test, p < 0.05).

The morphology of *chs3-2D* seedlings grown in the presence of the different analogues reflected the measured fresh weight (Figure 27a). For better comparison, all fresh weight data were combined in Figure 27b. While none of the analogues increased the effect of Ro8-4304, the analogues Ro-A03, Ro-A11, and Ro-A18 were as effective as Ro8-4304.

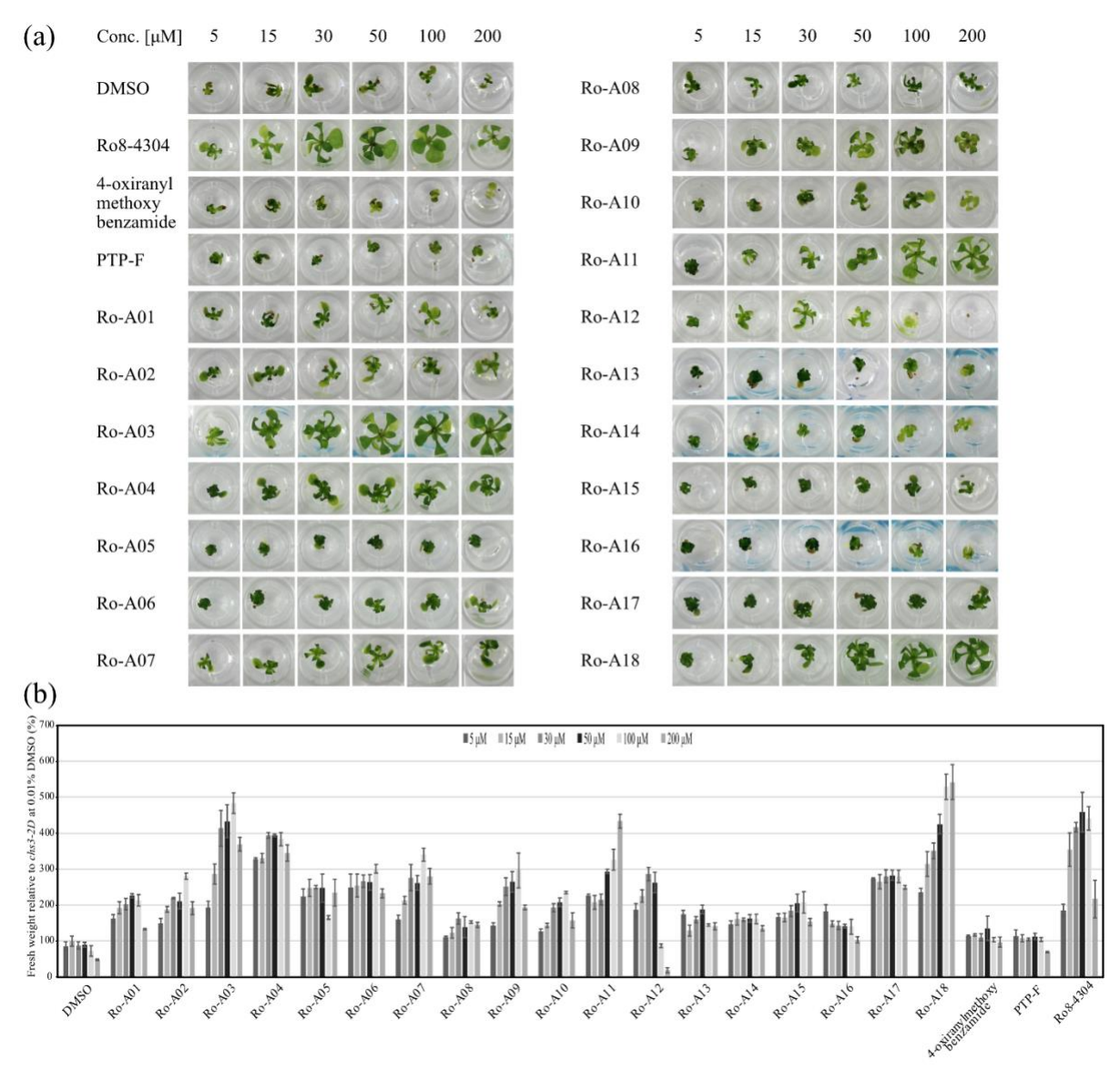


Figure 27. The effect of the analogues on growth of *chs3-2D*. (a) Morphology of *chs3-2D* seedlings grown for 20 days at 18°C on MS media with different concentrations of the different analogues. (b) The data was normalized against the mean value of *chs3-2D* grown on 0.1% DMSO and represent the mean \pm SE of three biological replicates (n=3, with 10 ± 2 plants each).

4.3.2 The effect of Ro8-4304 analogues on the expression of immunity genes in *chs3-2D*

Ro8-4304 not only rescued the reduced growth phenotype of *chs3-2D* seedlings, but also diminished its increased immunity back to normal levels 166 . We therefore tested for the effect of all analogues on the immunity in *chs3-2D* seedlings by analysing the expression of the immune marker genes *PR1* and *NIMIN1* 206 . For this purpose, *chs3-2D* seedlings were grown for 3 weeks on 15 μ M of the respective analogue. The expression levels of the immune marker genes *PR1* and *NIMIN1* are shown in Figures 28a and b, respectively. As expected, no significant expression of *PR1* or *NIMIN1* was detected in Col-0 seedlings grown in the presence of DMSO, Ro8-4304, or the randomly chosen analogue Ro-A09. The immune marker gene expression for *chs3-2D* grown on the control DMSO was high, indicating the *chs3-2D* autoimmune response, whereas Ro8-4304 resulted in a decreased expression as

previously shown ¹⁶⁶. The immune marker gene expression in the presence of the analogues ranged mostly in between the values. Most analogues had the same reducing effect on the immune marker gene expression as Ro8-4304. However, in the presence of the analogue Ro-A07, the decrease was even more pronounced. The best candidate analogue to uncouple growth and defence response was Ro-A03. While the reduced growth phenotype of *chs3-2D* was rescued by Ro-A03 (Figures 24 and 27), the expression of both immune marker genes, *PR1* and *NIMIN1*, stayed on a high level (Figure 28).

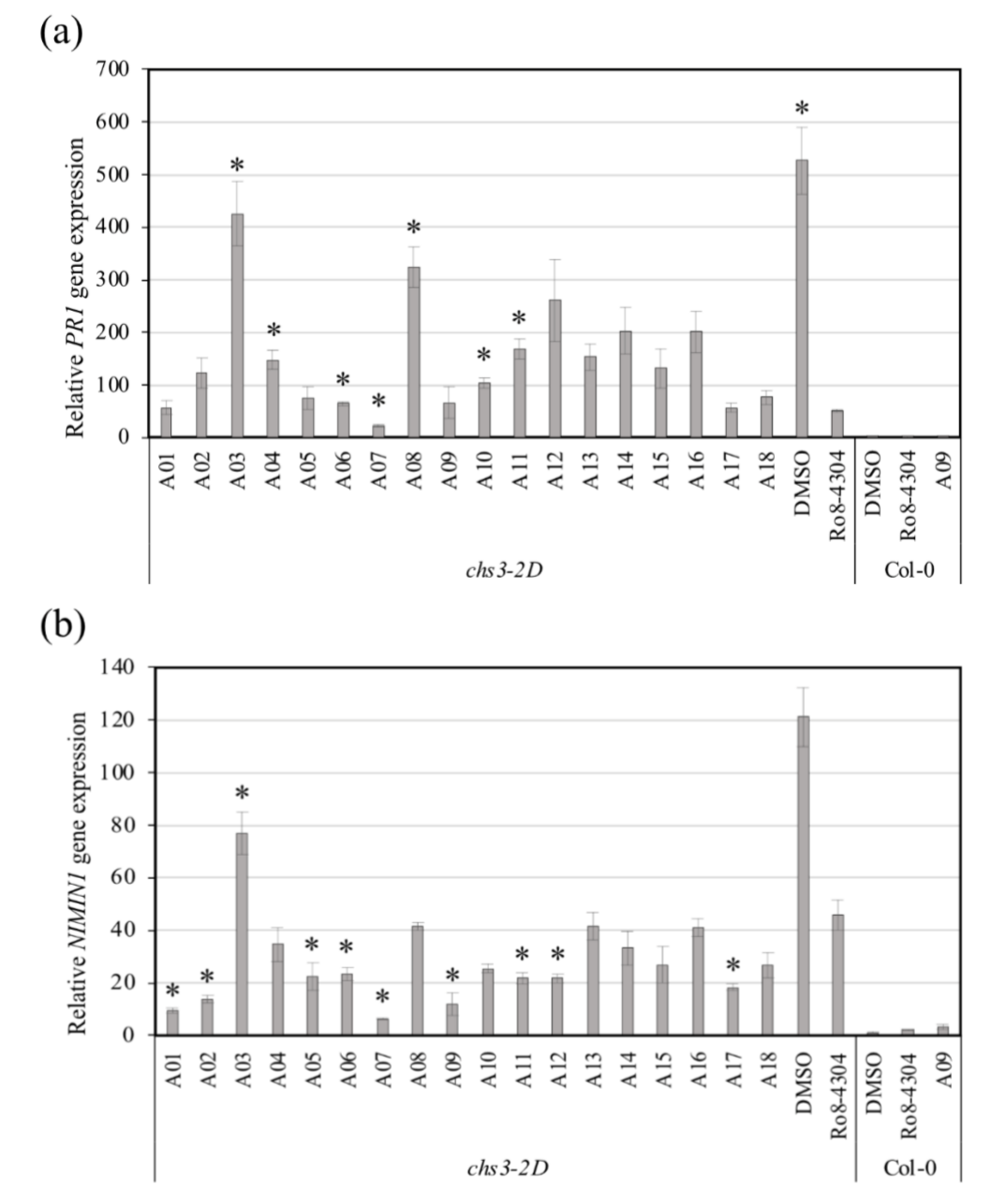


Figure 28. The effect of the analogues on immunity in *chs3-2D*. (a) Relative expression of the *PR1* gene in *chs3-2D* seedlings grown for 20 days at 18°C on MS media with 15 μ M of the respective analogue. (b) Relative expression of the *NIMIN1* gene in *chs3-2D* seedlings grown for 20 days at 18°C on MS media with 15 μ M of the respective analogue. (a and b) The data is normalized against the mean value of Col-0 grown on 0.01% DMSO. The data show the mean \pm SE of three biological replicates (n=3). An asterisk indicates a significant difference to the expression in *chs3-2D* seedlings grown on Ro8-4304 (Student's t-test, p < 0.05).

4.3.3 The effect of Ro-A03 on immunity in chs3-2D mutants

Ro-A03 was able to recover growth (Figure 29) and to retain a high expression of immune marker genes (Figure 30) in *chs3-2D* mutants. Hence, this analogue had an improved activity in comparison to the original chemical Ro8-4304. We analysed the expression of additional immune marker genes, *PR2*, *EDS1*, *PAD4*, and *SID2* to support the hypothesis that Ro-A03 may have the effect on growth without affecting immunity. *Chs3-2D* grown on Ro-A03 showed high immune marker gene expression for all defence genes tested in a range comparable to the expression in the DMSO control (Figures 29a to f).

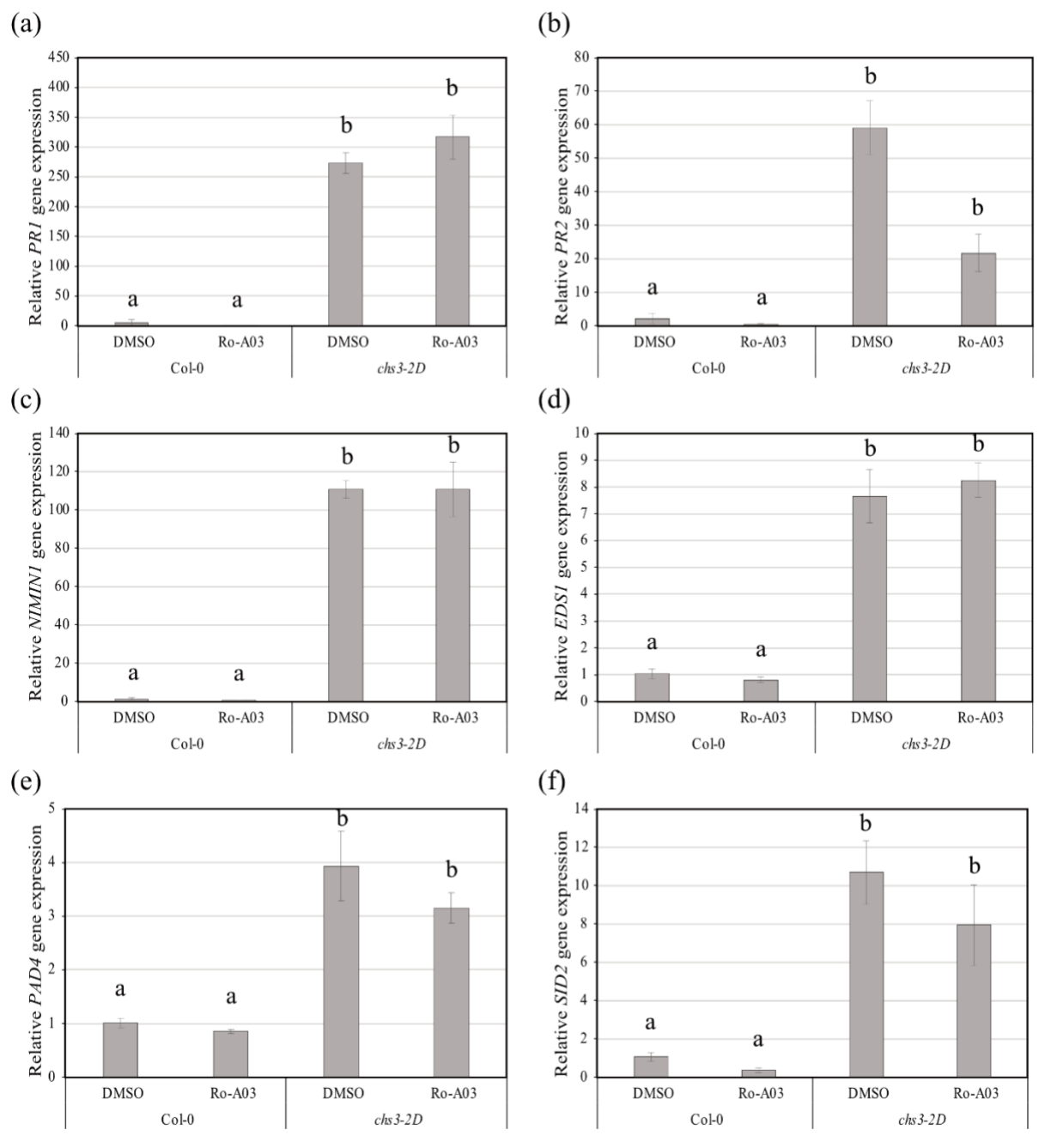


Figure 29. The expression of different defence genes in the presence or absence of 50 μ M Ro-A03 in *chs3-2D* seedlings. Plants were grown for 20 days at 18°C. The relative expression is shown for *PR1* (a), *PR2* (b), *NIMIN1* (c), *EDS1* (d), *PAD4* (e), and *SID2* (f). The data is normalized against the mean value of the expression

in Col-0 grown on 0.01% DMSO. The data shows the mean \pm SE of three biological replicates (n=3). Different letters indicate significant differences between groups, whereas identical letters denote no significant differences (Student's t-test, p < 0.05).

The high immune marker gene expression prompted us to investigate the effect of Ro-A03 on the response of *chs3-2D* to pathogen infection. To perform pathogen infection assays, Col-0 and *chs3-2D* plants were grown for 2 weeks on DMSO, Ro8-4304, and Ro-A03, respectively, and infected with *Pseudomonas syringae pv Tomato strain P.s.t. DC3000-GFP* ¹⁸⁴. Colony forming units were determined after 3 days of infection. In Col-0, the defence response was independent of the chemical composition of the medium, and the bacteria could successfully infect the plants (Figure 30). As expected from the autoimmune phenotype, *chs3-2D* plants grown on DMSO were less affected by *P. syringae* than Col-0 plants. Whereas bacterial growth was not affected by the presence of Ro8-4304 ¹⁶⁶, *chs3-2D* seedlings grown on Ro-A03 were less affected by *P. syringae* infection. Hence, *chs3-2D* grown on DMSO and Ro-A03 had a sufficient immunity to respond quickly to the pathogen and mount a strong defence response resulting in restricted bacterial growth.

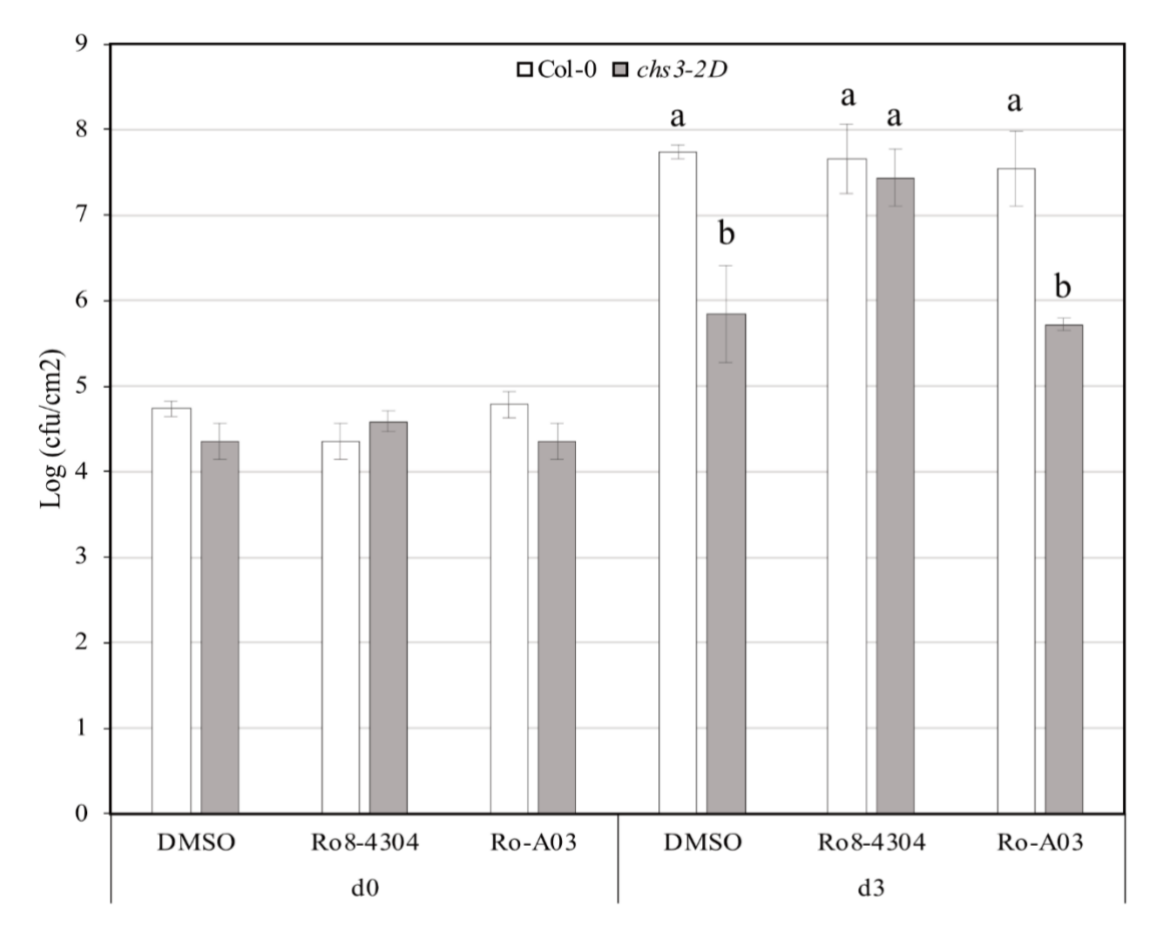
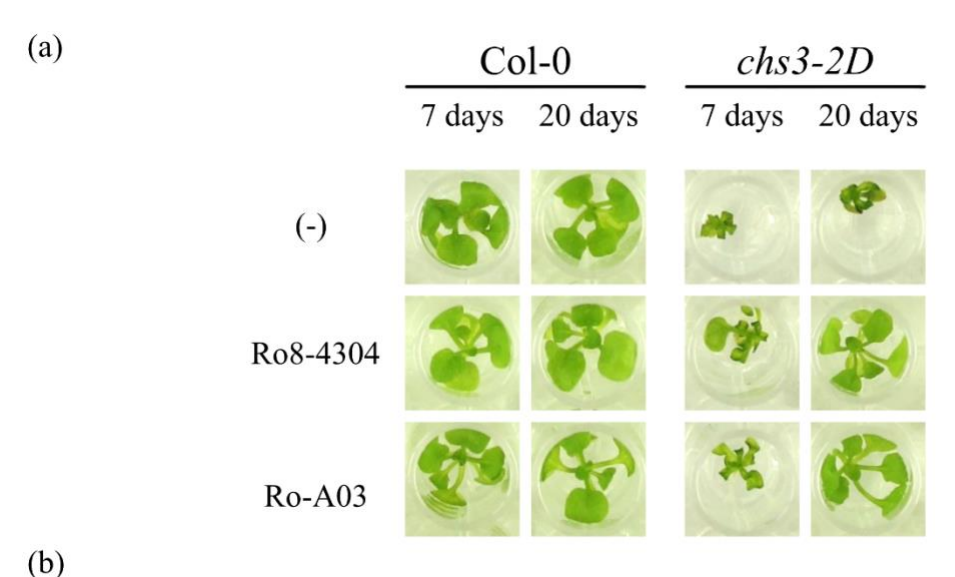
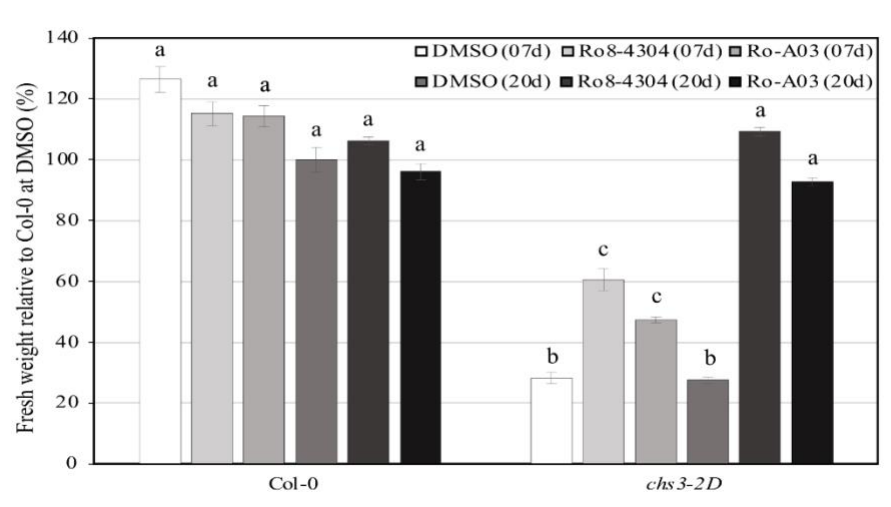


Figure 30. The effect of Ro-A03 on resistance to bacterial pathogens in Arabidopsis *chs3-2D*. Col-0 and *chs3-2D* plants were infected with the *Pseudomonas syringae pv tomato strain P.s.t. DC3000-GFP* in the presence of DMSO, 50 μ M Ro 8-4304, or 50 μ M Ro-A03. Plants were grown for 2 weeks at 20°C prior to vacuum infiltration with *P.s.t. DC3000-GFP*. Quantification of Colony-forming units (CFU) was performed at 0- and 3-days post inoculation. Data represent the mean \pm SE of three replicates with four plant discs per replicate. Different letters indicate significant differences between groups, whereas identical letters denote no significant differences (Student's t-test, p < 0.05).

Another way to investigate the immune response is by determining the amount of salicylic acid (SA) in the plants. SA is a plant hormone that is vital during an immune response 42. Col-0 and chs3-2D were grown for 7 days or 20 days on DMSO, Ro8-4304, and Ro-A03. Leaf material was harvested on day 21, and SA levels were determined in collaboration with Julia Seufer and Lars Voll from the Philipps-Universität Marburg (Figure 31). Growth for 7 days on chemical was not enough to rescue the growth levels of chs3-2D, and also the SA levels where unaffected by this short treatment and stayed on a high level. Chs3-2D grown on DMSO for 20 days showed the highest levels of SA, responsible for the reduced growth phenotype. The presence of Ro-84304 reduced the SA levels to background levels, corresponding to low immune marker gene expression (Figure 30). Chs3-2D seedlings grown for 20 days on Ro-A03 had lower levels of SA in comparison to the levels on DMSO, but higher levels in comparison to the levels on Ro8-4304. This remaining amount of SA, in Ro-A03 treated chs3-2D seedlings, was probably enough to mount a defence response, because it has been shown previously that only 10 mg fw⁻¹ of SA is necessary for an effective immune response 44,207. The lower levels of SA may also explain why Ro8-4304 and Ro-A03 could both rescue the growth phenotype, since growth and immunity are coupled via SA (see Introduction). The experiment for the determination of SA levels was repeated, but instead of 7 days or 20 days plants were grown for 3 days or 20 days on the respective chemical (Figure 32). The obtained SA levels confirmed the results from the previous experiment.





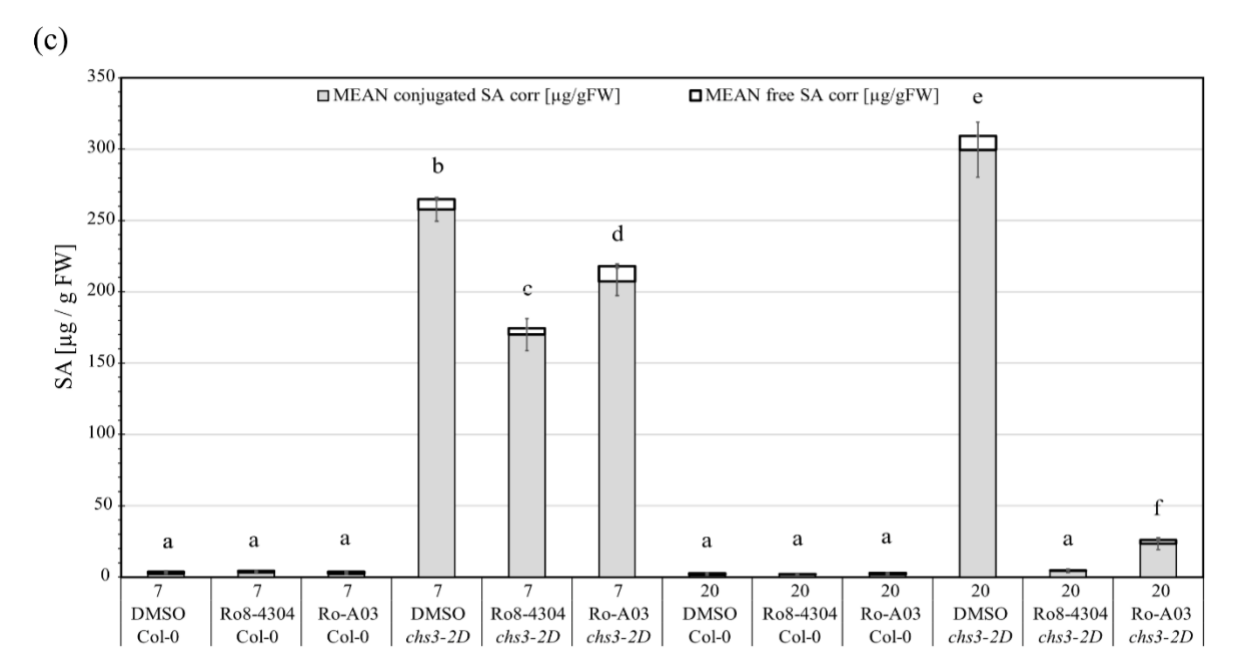
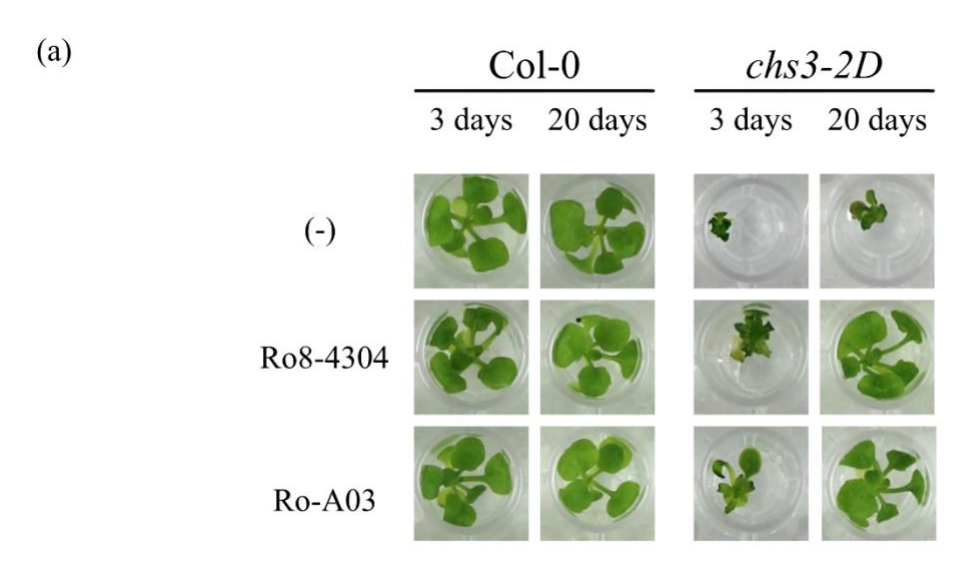


Figure 31. The effect of Ro-A03 at 7 days and 20 days on the salicylic acid composition in the leaves of Col-0 and chs3-2D. Plants were grown at 18°C for 7 days or 20 days on DMSO, 50 μ M Ro8-4304, or 50 μ M Ro-A03. Harvesting of the leaf material was done on day 21. (a) Morphology of Col-0 and chs3-2D grown for 7 or 20 days on the different conditions. (B) Fresh weight of chs3-2D seedlings relative to the mean value of Col-0 grown on DMSO. The data shows the means \pm SE of five biological replicates (n=5, with 12 plants each). Different letters indicate significant differences between groups, whereas identical letters denote no significant differences (Two tailed Anova, Tukey test, p < 0.05). (c) Free SA and SAG of Col-0 and chs3-2D grown for 7 or 20 days on different conditions normalized against the mean value of Col-0 grown on DMSO. The data shows the mean \pm SE of five biological replicates (n=5, with 12 plants each). Different letters indicate significant differences between groups, whereas identical letters denote no significant differences (Two tailed Anova, LSD test, p < 0.05).



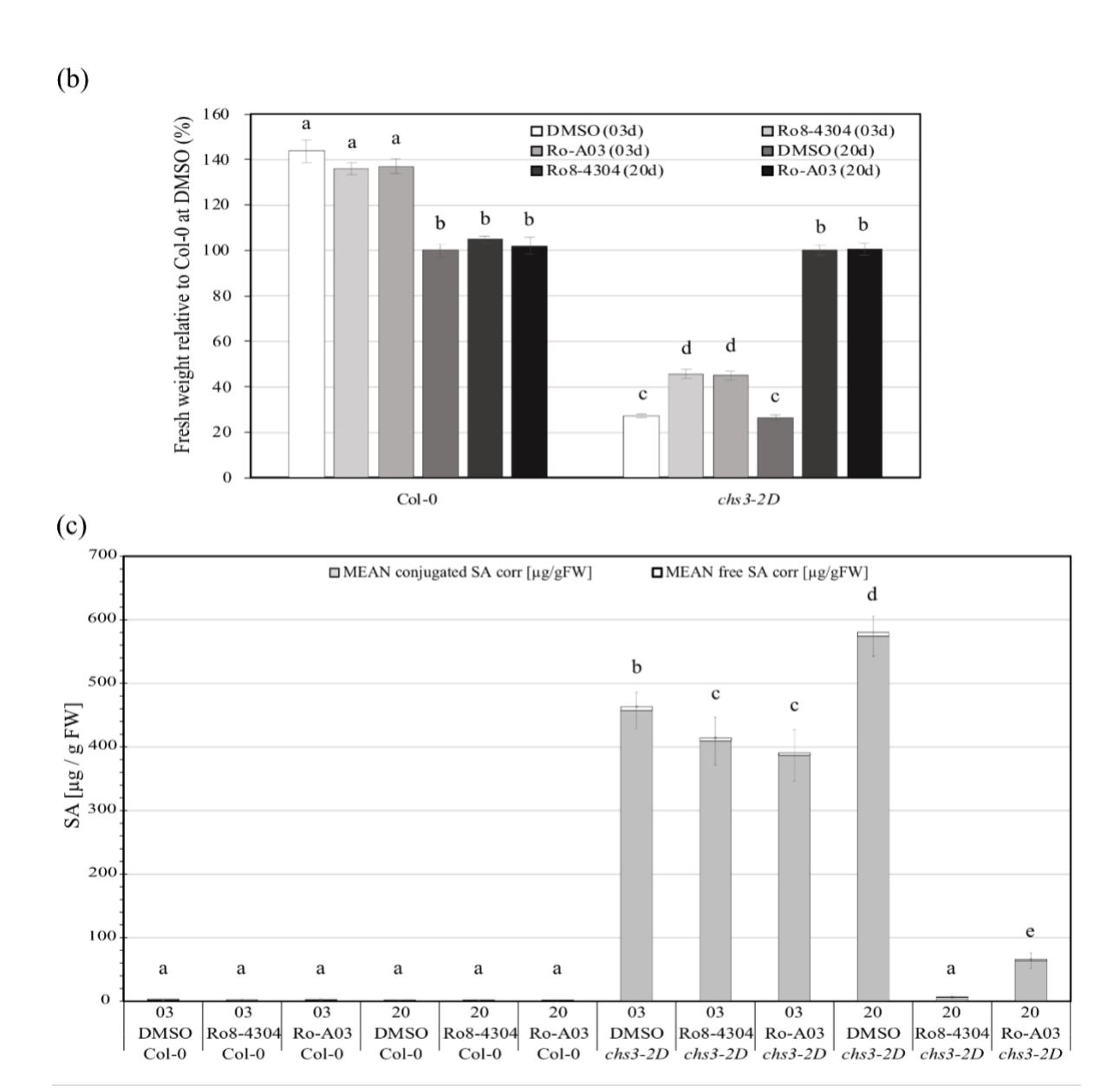


Figure 32. The effect of Ro-A03 at 3 days and 20 days on the salicylic acid composition in the leaves of Col-0 and chs3-2D. Plants were grown at 18°C for 3 days or 20 days on DMSO, 50 μ M Ro8-4304, or 50 μ M Ro-A03. Harvesting of the leaf material was done on day 21. (a) Morphology of Col-0 and chs3-2D grown for 3 or 20 days on different conditions. (b) Fresh weight of chs3-2D relative to the mean value of Col-0 grown on 0.01% DMSO. The data shows the means \pm SE of five biological replicates (n=5, with 12 plants each). Different letters indicate significant differences between groups, whereas identical letters denote no significant differences (Two tailed Anova, Tukey test, p < 0.05). (c) Free SA and SAG of Col-0 and chs3-2D grown for 3 or 20 days on different conditions normalized against the mean value of Col-0 grown on 0.01% DMSO. The data shows the mean \pm SE of five biological replicates (n=5, with 12 plants each). Different letters indicate significant differences between groups, whereas identical letters denote no significant differences (Two tailed Anova, LSD test, p < 0.05).

4.3.4 The effect of Ro-A03 on the methylosome in chs3-2D icln2 double mutants

It has previously been reported that the effect of Ro8-4304 was diminished in the double mutant *chs3-2D icln2*, in which the gene encoding the methylosome component ICLN2 was mutated in the *chs3-2D* background ¹⁶⁶. For that reason, we wanted to test whether this is also true for Ro-A03 (Figure 33). However, the reported effect was not detectable. Ro8-4304 and Ro-A03 were both able to rescue the deficient growth phenotype of *chs3-2D icln2*.

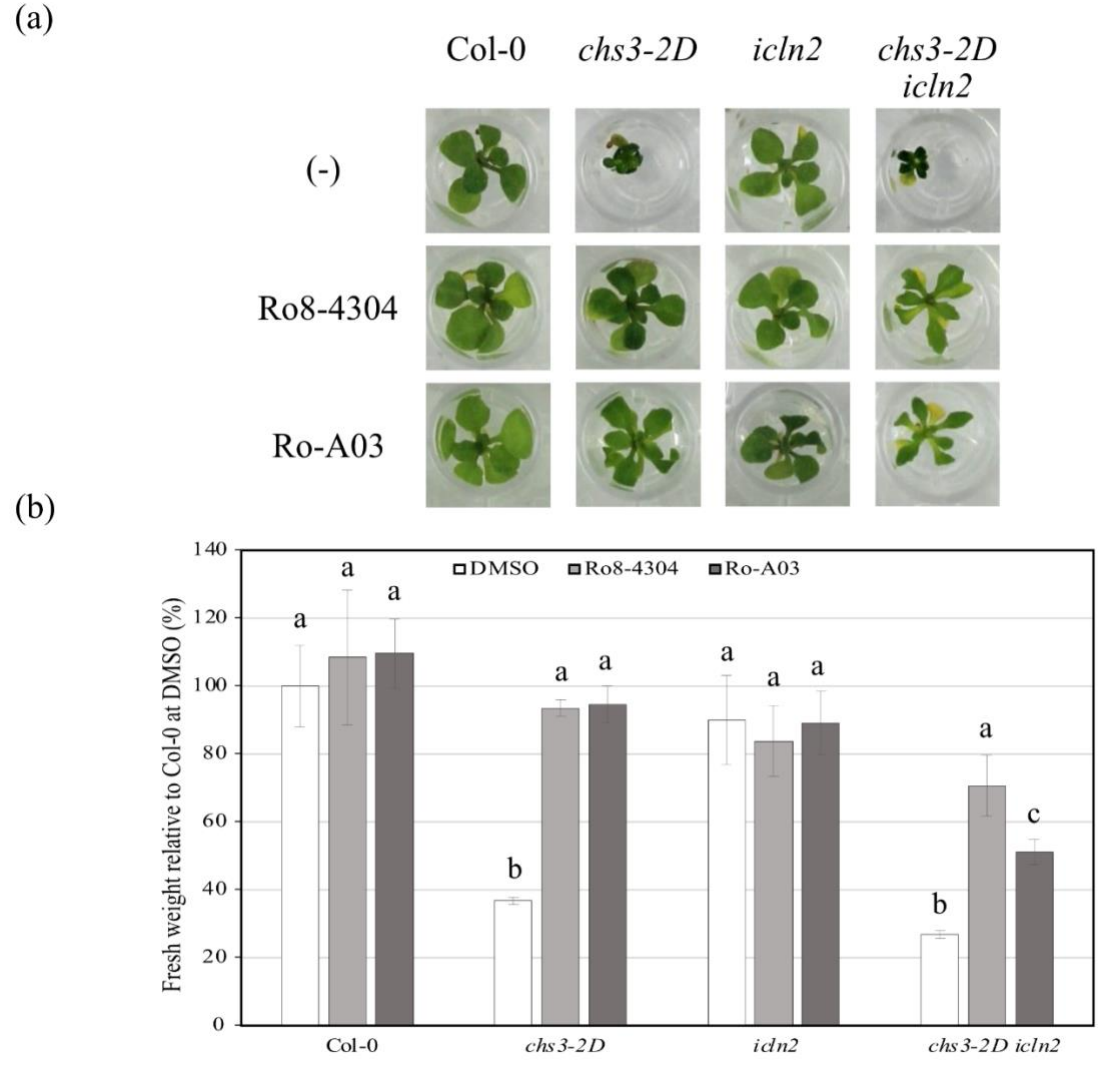


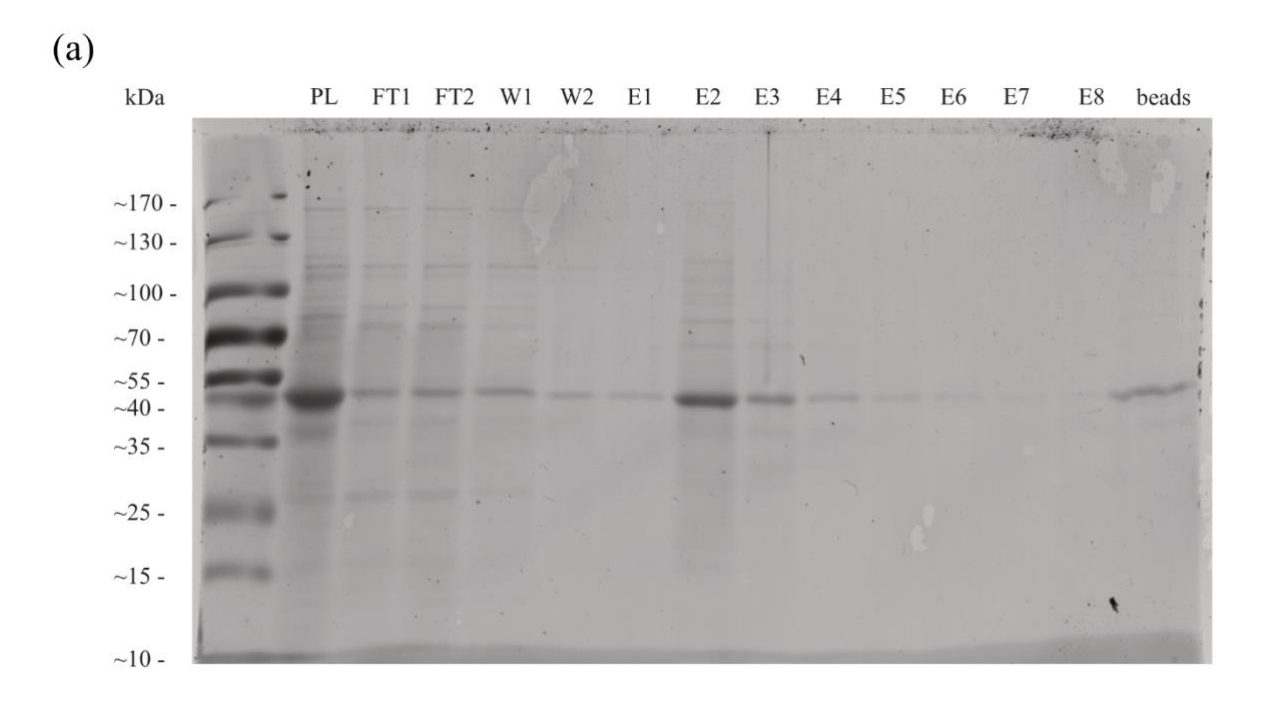
Figure 33. The effect of Ro-A03 on the *chs3-2D icln-2* methylosome mutants from Huang et al. (2016) 166 . (a) Morphology of Col-0, *chs3-2D*, *icln-2* and *chs3-2D icln-2* grown on 50 μ M DMSO, Ro8-4304 or Ro-A03 for 20 days at 18°C. (b) Fresh weight normalized against the mean value of Col-0 grown on 0.01% DMSO. The data shows the mean \pm SE of three biological replicates (n=3, with 10 ± 2 plants each). Different letters indicate significant differences between groups, whereas identical letters denote no significant differences (Two tailed Anova, Tukey test, p < 0.05).

After chemical characterization of the analogues, we noted that analogue Ro-A07 had an activity in the *chs3-2D* seedlings. Both growth (Figure 27) and immunity (Figure 28) were affected by Ro-A07 in the *chs3-2D* mutant. This led us to suspect that Ro-A07 is suitable for binding to a matrix, while chemical changes did not affect the activity. Therefore, we continued with affinity purification, by using Ro-A07, to determine the binding protein of Ro8-4304 in *Arabidopsis thaliana chs3-2D*.

4.4 The determination of Ro8-4304 binding proteins

4.4.1 Identification of putative binding proteins using matrix-bound Ro8-4304

To search for putative Ro8-4304 binding proteins, the analogue Ro-A07 was successfully bound to a matrix, namely NHS activated agarose. Protein lysate from chs3-2D grown at 20°C was purified and applied on a column loaded with the Ro-A07 bound matrix. Material from chs3-2D plants was chosen, because Ro8-4304 influenced these mutants and not on Col-0. Thus, the binding protein may not be present in sufficient amounts in Col-0. Moreover, a temperature of 20°C was chosen, while the plants were large enough to produce a significant amount of lysate, but still showed an immune phenotype. Following the incubation of the purified proteins on the column, the flow through as well as the wash and elution fractions were concentrated, boiled in SDS blue staining and separated on a 10% SDS-page gel (Figure 34a). Moreover, a lot of protein remained stuck on the beads, and were unremovable during the washing steps. Interestingly, these proteins had about the same size as the proteins released during elution step 2 and 3. Since many proteins remained on the beads, a small amount was withdrawn from the column, and the beads were included in the protein separation on SDS-page gel. When using non-activated beads, as a negative control, no protein bands could be detected neither in wash nor in elution fractions [result not shown]. In contrast, the use of the activated beads resulted in the detection of several clearly visible distinct bands following a concentrating step. The band with the highest intensity at 40-55 kDa resembled the molecular weight of Rubisco and was not taken into consideration. The other protein bands that were marked with arrows in Figure 34b were extracted and analysed by mass spectrometry in collaboration with Steffen Ostendorp and Julia Kehr (Molekulare Genetik, Universität Hamburg). Multiple bands corresponding to putative Ro8-4304 binding proteins were identified (Table 28), including CELL DIVISION CYCLE 48 (CDC48), HEAT SHOCK PROTEIN 81-2 (HSP81-2), and GLUTATHIONE-S-TRANSFERASE 2 & 7 (GSTF2&7).



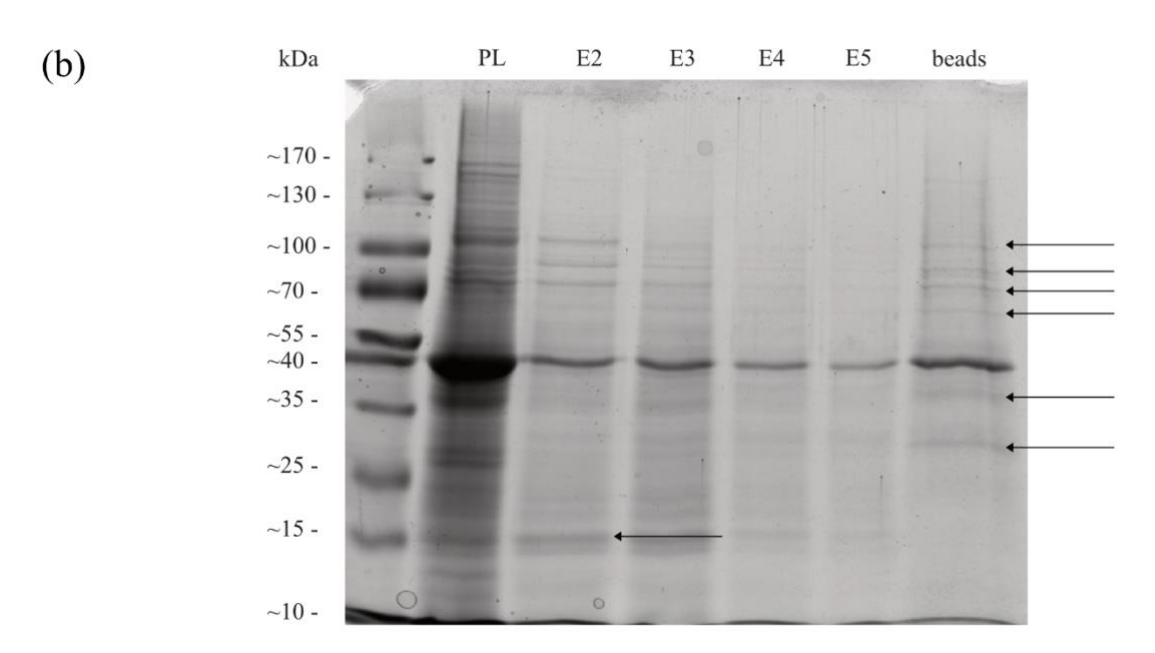


Figure 34. The determination of the direct binding protein of Ro8-4304 using affinity purification. (a) SDS-page gel of the blue stained protein flow throughs: plant lysate (PL), flow through (FT1 & 2), washing (W1 & 2), elution (E1-E8) and the boiled beads (beads). (b) SDS-page gel of the concentrated flow throughs of (a). Arrows indicate the proteins send to MS (Table 28). Affinity purification was repeated at least 3 times successfully. Non-activated beads did not give any distinct bands [results not shown].

Table 28. Table of the identified protein using the affinity purification approach, shown in Figures 10 and 34. The corresponding molecular weight (MW), score, and coverage (%) are indicated.

Sample ID	Identified Protein	Acc. No.	MW obs	Score	Coverage	Significant
S1	CELL DIVISION CYCLE 48	AT3G09840	100	89,3	23%	Υ
S2	HEAT SHOCK PROTEIN 81-2	AT5G56030	80	80	30%	Υ
S3	TRANSKETOLASE	AT3G60750	70	79,9	34%	Υ
S4	TRANSKETOLASE-1 (F4JBY2) HSC70.2 (P22953)	AT3G60750 AT5G02500	65	79,9 71,3	34% 27%	Y Y
\$5	AT3G04650 (Q9SR09) [FAD/NAD(P)-BINDING OXIDOREDUCTASE FAMILY PROTEIN]	AT3G04650	50	52	33%	Y
S6	GADPH (P25858) [GAPC-1?]	AT3G04120	40	36,8	47%	Υ
S7	GLUTATHIONE S- TRANSFERASE F2 GLUTATHIONE S- TRANSFERASE F7	AT4G02520 AT1G02920	25	24,1 23,5	58% 34%	Y Y

4.4.2 Identification of putative binding proteins by literature search

Besides affinity purification, we also did literature research, and we came upon some old publication. These publications demonstrated that the chemical Ro8-4304 has an activity in humans. It has been reported previously that Ro8-4304 selectively binds the N2B subunit of N-methyl-D-aspartate (NMDA) receptors 208,209 . This receptor belongs to the class of the glutamate-gated ion channels in humans. NMDA receptors transduce postsynaptic signals together with α -amino-3-hydroxy-5-methyl-4-isoxazolepropionic acid (AMPA), kainate, and delta receptors 210 . The plant GLUTAMATE-LIKE RECEPTORS (GLRs) are homologs of mammalian ionotropic glutamate receptors (iGluRs) including NMDA 211 . The human and plant glutamate-like receptors share a high degree of similarity (~50-60%) in most of the functional domains $^{212-214}$. Therefore, we hypothesized that Ro8-4304 might bind to plant glutamate-like receptors.

4.5 A pharmacological analysis of Ro8-4304 activity

Through the experimental and the literature-based approaches we were able to identify putative Ro8-4304 binding proteins. For these proteins several agonist and antagonists are known. Thus, we were interested to investigate whether any of these respective chemicals may affect the action of Ro8-4304 in the *chs3-2D* seedlings. Therefore, we did a pharmacological analysis of Ro8-4304 in the *chs3-2D* background in combination with agonist and antagonists of the putative binding proteins.

4.5.1 Does the chemical bikinin alter the brassinosteroid signalling in the Ro8-4304 treated *chs3-2D* seedlings?

The first compound tested in combination with Ro8-4304 was bikinin (Figure 35). Bikinin was discovered in a phenotype-based compounds screen ¹⁵¹. This compound directly binds and inhibits GSK3 BIN2, hereby activating downstream BR signalling ¹⁵¹. This signalling has been demonstrated to be an important node in the immunity growth trade off, and the brassinosteroid signalling pathway regulates many developmental responses ^{103,206}. To determine if the BR signalling pathway is important for Ro8-4304, *chs3-2D* was treated with both Ro8-4304 and bikinin. Previous literature indicated that addition of activating BR responses may result in a decrease of fresh weight ^{113,215}. This could also be seen in the phenotype of Col-0, namely long and bending petioles and blade-shaped pale green leaves (Figure 35a). A similar but less pronounced result in the presence of bikinin was observed in *chs3-2D*. Interestingly, the effect of Ro8-4304 on *chs3-2D* was abolished when adding bikinin (Figure 35a).

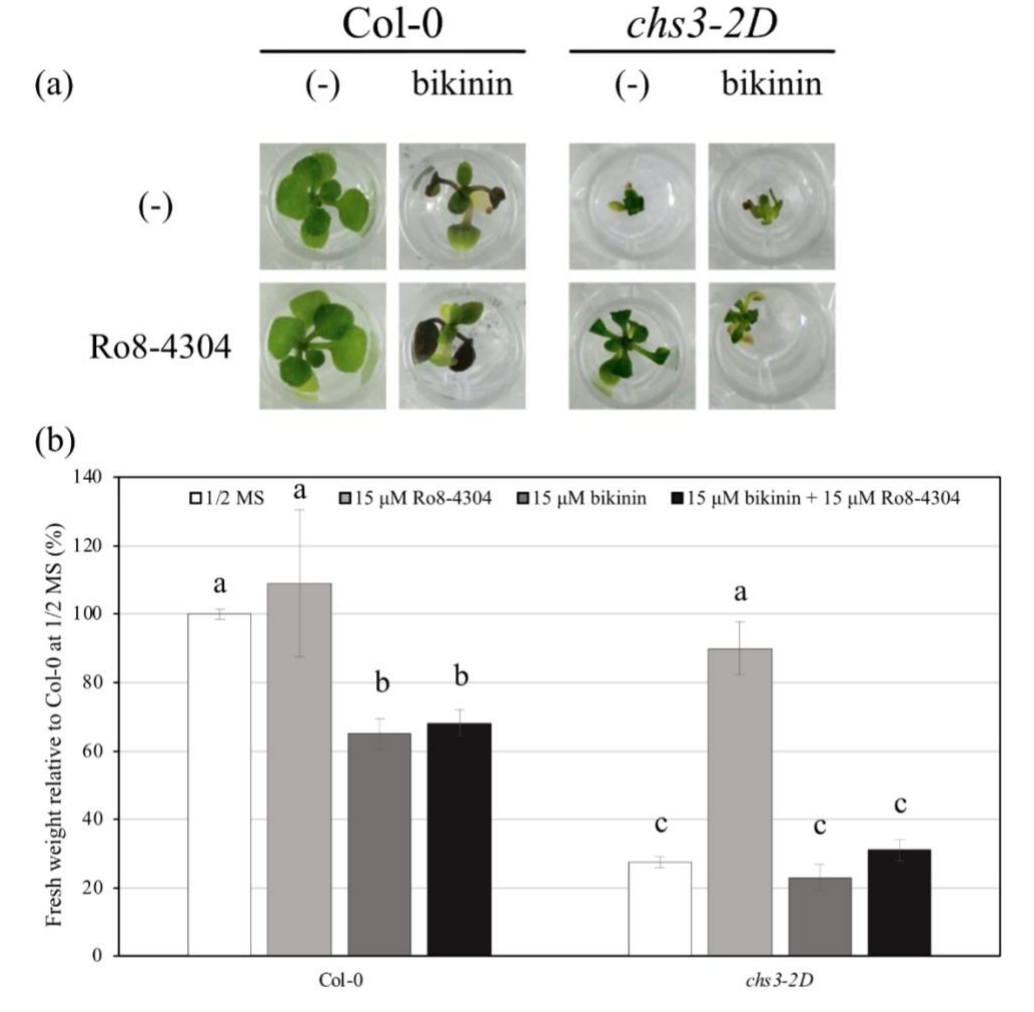


Figure 35. The effect of bikinin on the activity of Ro8-4304 in *chs3-2D* seedlings. (a) Morphology of Col-0 and *chs3-2D* grown on 15 μ M DMSO, 15 μ M Ro8-4304, 15 μ M bikinin, or 15 μ M Ro8-4304 in combination with 15 μ M bikinin for 20 days at 18°C. (b) Fresh weight normalized against the mean value of Col-0 grown on 0.01% DMSO. The data shows the mean \pm SE of three biological replicates (n=3, with 10 \pm 2 plants each). Different letters indicate significant differences between groups, whereas identical letters denote no significant differences (Two tailed Anova, Tukey test, p < 0.05).

4.5.2 Does the NMDA antagonist ifenprodil influence the effect of Ro8-4304 in the *chs3-2D* seedlings?

The second compound tested was ifenprodil. This compound has a structure similar to Ro8-4304 (Figure 36). Additionally, ifenprodil has a similar effect as Ro8-4304 on the NMDA receptors in humans ^{208,209}. Both are atypical antagonists that selectively bind and inhibit the GluN2B subunit ²⁰⁸. Therefore, we were interested to see if ifenprodil has a similar effect as Ro8-4304 in *chs3-2D* seedlings.

Figure 36. The chemical structure of Ro8-4304 and Ifenprodil respectively.

Ifenprodil was added to the growth media to a final concentration of 500 μ M, because lower concentrations of 100 and 200 μ M did not yield any visible effects [results not shown]. According to previous literature, plants are only able to respond to typical NMDA antagonist and agonist at higher concentrations 25 . The addition of ifenprodil to Col-0 resulted in reduced growth and decreased fresh weight (Figure 37). No effect of ifenprodil on the fresh weight of *chs3-2D* was detected, though in humans Ro8-4304 and ifenprodil share the same activity. On the contrary, ifenprodil prevented the growth rescue by Ro8-4304 in *chs3-2D* seedlings, thus demonstrating that the two compounds may have antagonistic effects in plants.

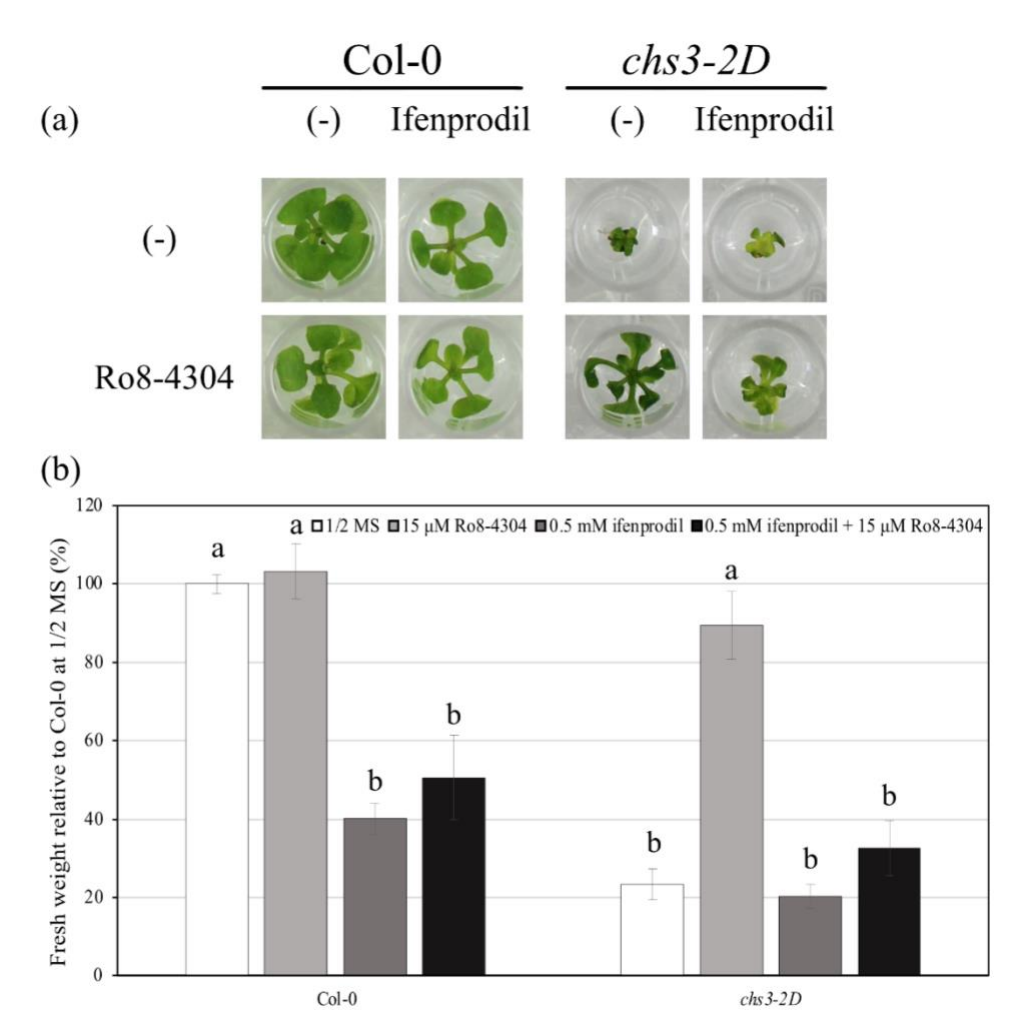


Figure 37. The effect of ifenprodil on the activity of Ro8-4304 in *chs3-2D* seedlings. (a) Morphology of Col-0, and *chs3-2D* grown on 15 μ M DMSO, 15 μ M Ro8-4304, 500 μ M ifenprodil, or 15 μ M Ro8-4304 and 500 μ M ifenprodil for 20 days at 18°C. (b) Fresh weight normalized against the mean value of Col-0 grown on 0.01% DMSO. The data shows the mean \pm SE of three biological replicates (n=3, with 10 \pm 2 plants each). Different letters indicate significant differences between groups, whereas identical letters denote no significant differences (Two tailed Anova, Tukey test, p < 0.05).

4.5.3 Do calcium levels influence the effect of Ro8-4304 in the chs3-2D seedlings?

Ca²⁺ is required as signalling molecule for a lot of processes in plants, including immune responses ^{21,216}. It has been suggested that GLRs may transport Ca²⁺-ions ^{217,218}, and a link between GLRs, Ca²⁺, and plant immune responses has been postulated ²¹⁹. Hence, we wanted to determine if calcium would alter the effect of Ro8-4304 due to its activity in immunity. Hence, calcium chloride (CaCl₂) was added to the growth medium to test whether Ca²⁺ would enhance or reduce the effect of Ro8-4304 on growth of *chs3-2D* seedlings. However, the addition of CaCl₂ did not alter the phenotype neither of Col-0 nor of *chs3-2D* in the presence and or absence of Ro8-4304 (Figure 38).

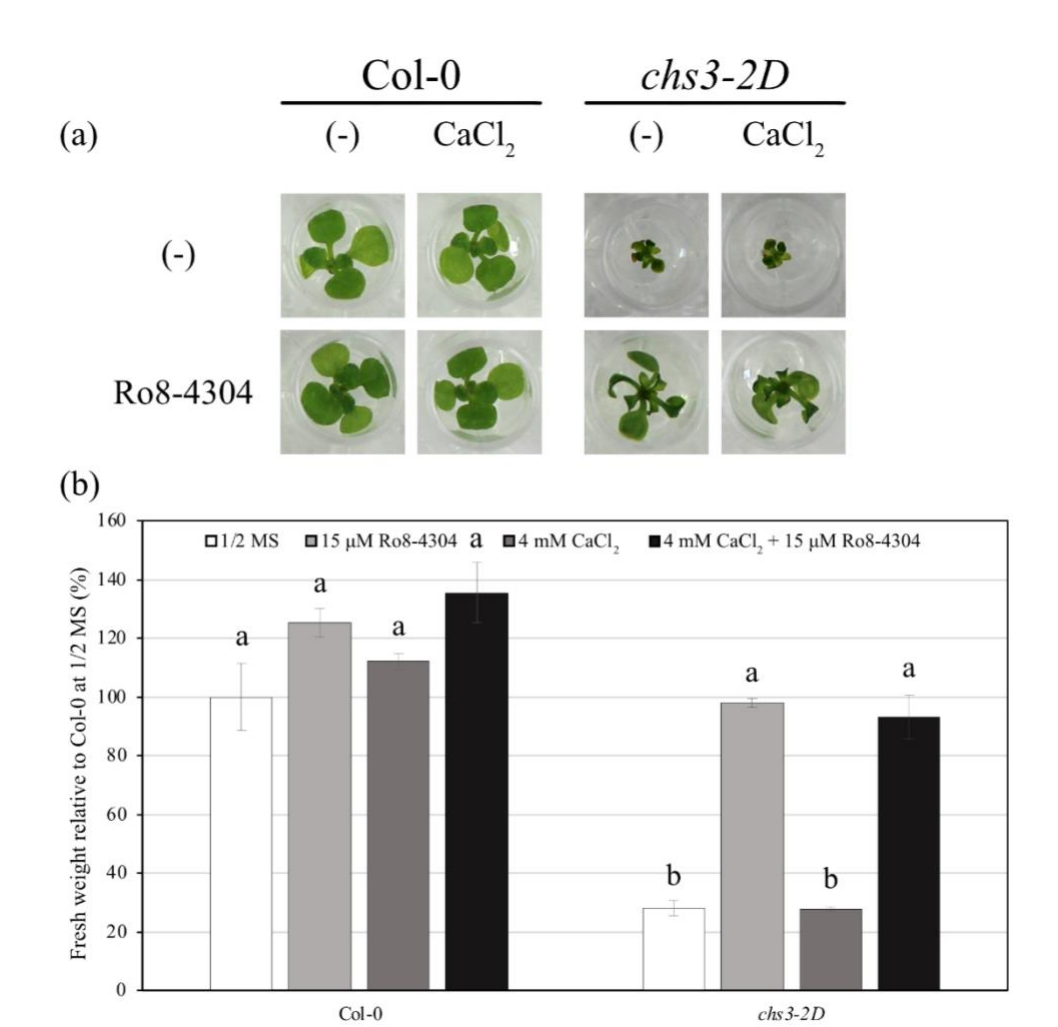


Figure 38. The effect of $CaCl_2$ on the activity of Ro8-4304 in *chs3-2D* seedlings. (a) Morphology of Col-0, and *chs3-2D* grown on 15 μ M DMSO, 15 μ M Ro8-4304, 4 mM $CaCl_2$, or 15 μ M Ro8-4304 and 4 mM $CaCl_2$ for 20 days at 18°C. (b) Fresh weight normalized against the mean value of Col-0 grown on 0.01% DMSO. The data shows the mean \pm SE of three biological replicates (n=3, with 10 \pm 2 plants each). Different letters indicate significant differences between groups, whereas identical letters denote no significant differences (Two tailed Anova, Tukey test, p < 0.05).

Since the addition of calcium did not influence the fresh weight data of Col-0 and chs3-2D, we were interested to see if lower internal calcium changes the effect of Ro8-4304. So, a lower internal CaCl₂ content was generated by addition of ethylene glycol-bis (β -aminoethyl ether)-N,N,N',N'-tetraacetic acid (EGTA), a Ca²⁺-chelator ²²⁰, to the medium (Figure 39). Adding 4 mM EGTA to the medium was harmful for the plants, Col-0 and chs3-2D alike. This was expected while Ca²⁺ is necessary for a lot of signalling processes ^{21,216}. The combination of Ro8-4304 and EGTA in the chs3-2D background was even more damaging. The plants were small and had dark leaves. This corresponds to a calcium deficient phenotype ²²¹. Ro8-4304 was unable to rescue the chs3-2D phenotype in the presence of EGTA.

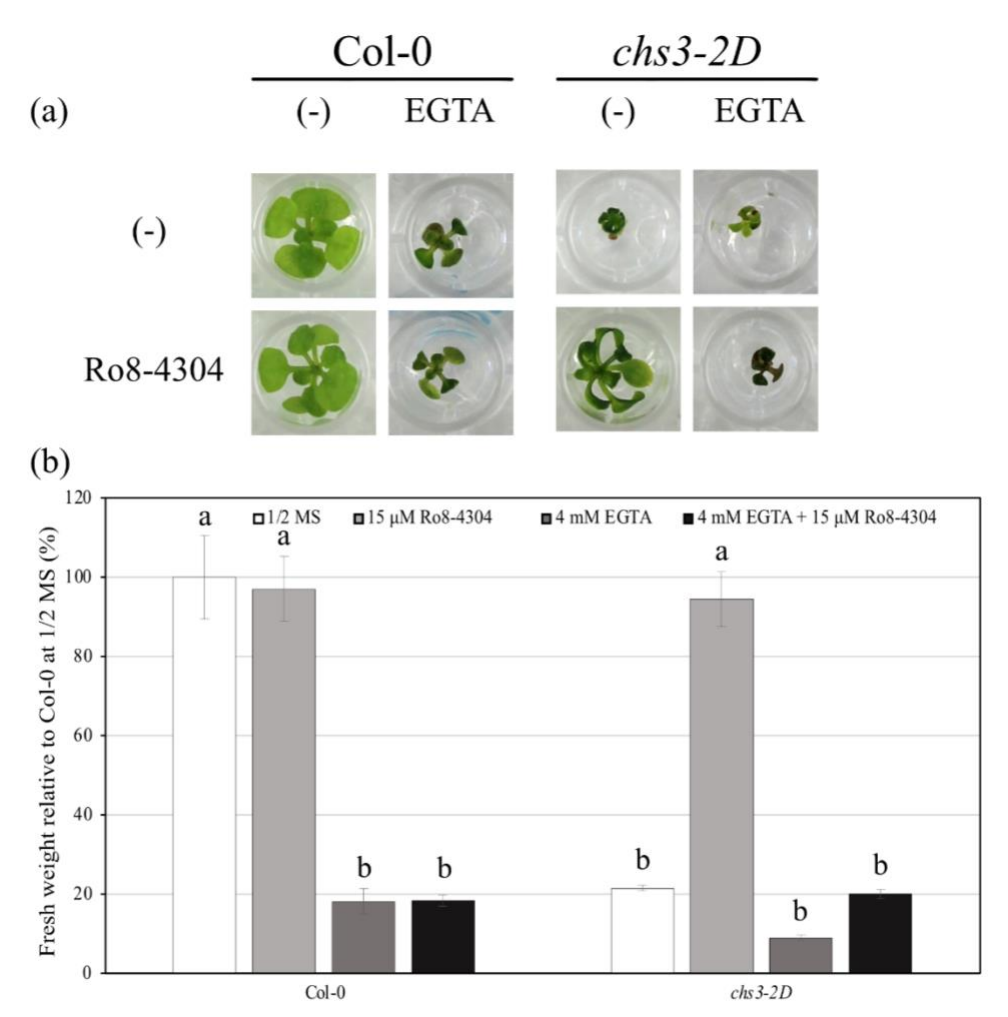


Figure 39. The effect of EGTA on the activity of Ro8-4304 in *Arabidopsis chs3-2D* seedlings. (a) Morphology of Col-0, and *chs3-2D* grown on 15 μ M DMSO, 15 μ M Ro8-4304, 4 mM EGTA, or 15 μ M Ro8-4304 and 4 mM EGTA for 20 days at 18°C. (b) Fresh weight normalized against the mean value of Col-0 grown on 0.01% DMSO. The data shows the mean \pm SE of three biological replicates (n=3, with 10 \pm 2 plants each). Different letters indicate significant differences between groups, whereas identical letters denote no significant differences (Two tailed Anova, Tukey test, p < 0.05).

4.5.4 Does the NMDA antagonist DNQX influence the effect of Ro8-4304 in the *chs3-2D* seedlings?

6,7-dinitroquinoxaline-2,3-dione (DNQX) is a potent competitive non-NMDA glutamate receptor antagonist ²²². Besides human research, this compound has been used as a marker chemical in plant research. Lam et al. demonstrated in 1988 that DNQX treated seedlings exhibited an increase in hypocotyl elongation and had a reduced chlorophyll synthesis ²²³. Additionally, multiple reports showed that DNQX influences the Ca²⁺ signalling currents and immune response of *Arabidopsis thaliana* ^{25,224,225}, and *Solanum lycopersicum L.* ²²⁶. Since, this NMDA antagonist has been demonstrated to have an activity in plants corresponding to GLRs, we believed it to be interesting to check its effect in combination with Ro8-4304. DNQX was added to the growth media (Figure 40). DNQX slightly lowered the fresh weight of Col-0, but not as significantly as ifenprodil or EGTA. This may be because DNQX is a competitive antagonist in comparison to ifenprodil. It was demonstrated that DNQX

significantly reduces the root development, and primary root apical meristem ²²⁷. Therefore, it is not surprising that the fresh weight of Col-0 and *chs3-2D* were both affected by DNQX. The combination of Ro8-4304 and DNQX resulted in small plants with toothed leaves.

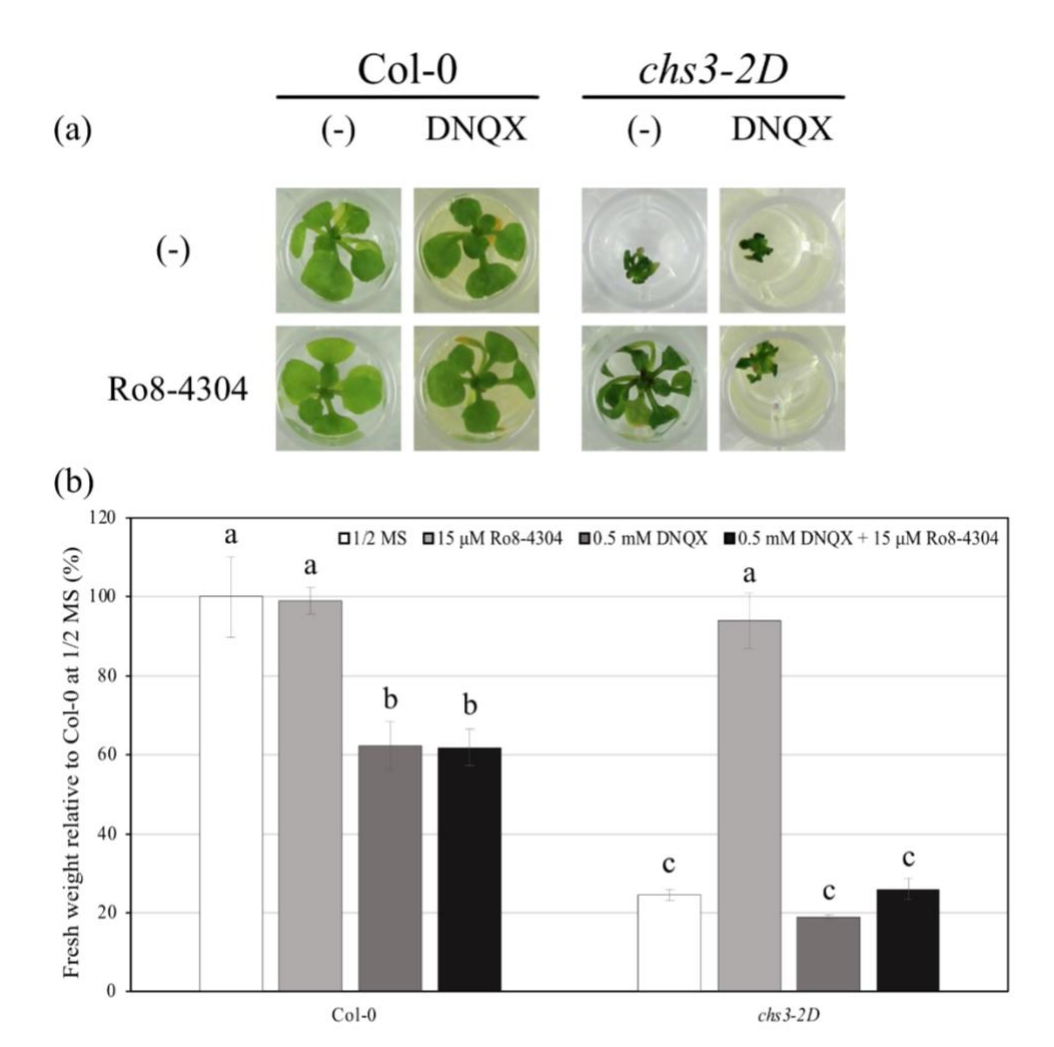


Figure 40. The effect of DNQX on the activity of Ro8-4304 in *Arabidopsis chs3-2D* seedlings. (a) Morphology of Col-0, and *chs3-2D* grown on 15 μ M DMSO, 15 μ M Ro8-4304, 500 μ M DNQX, or 15 μ M Ro8-4304 and 500 μ M DNQX for 20 days at 18°C. (b) Fresh weight normalized against the mean value of Col-0 grown on 0.01% DMSO. The data shows the mean \pm SE of three biological replicates (n=3, with 10 \pm 2 plants each). Different letters indicate significant differences between groups, whereas identical letters denote no significant differences (Two tailed Anova, Tukey test, p < 0.05).

4.5.5 Does the NMDA agonist BMAA influence the effect of Ro8-4304 in the *chs3-2D* seedlings?

Since the antagonists ifenprodil and DNQX inhibits the effect of Ro8-4304 on the fresh weight, we thought it might be interesting to test an agonist and see if that compound could induce the fresh weight, in combination with Ro8-4304. Beta-methylamino-L-alanine (BMAA) (Figure 41) is an agonist of NMDA ²²⁸, and previous research indicated that this compound is also plant active by inducing hypocotyl elongation and impaired cotyledon opening ^{229,230}. Adding BMAA to Col-0 affected the phenotype of the plants. The leaves looked bigger and greener, although this cannot be seen in the fresh weight data.

Interestingly, this is the opposite reaction of DNQX (Figure 41). The same holds true for *chs3-2D*, adding a bit of agonist increased the fresh weight. The combination of Ro8-4304 and BMAA not only rescued the fresh weight of *chs3-2D*, but slightly boosted it to greater values.

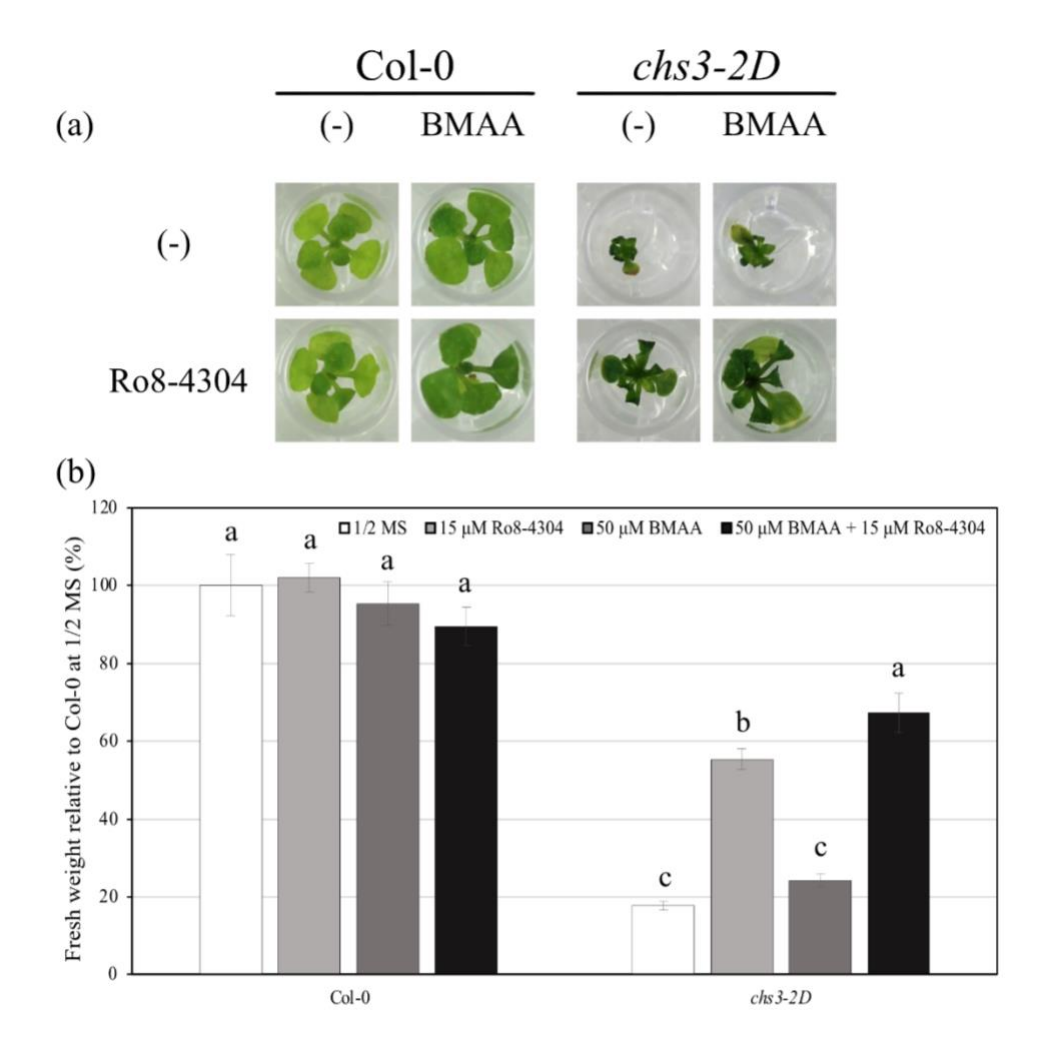


Figure 41. The effect of BMAA on the activity of Ro8-4304 in *Arabidopsis chs3-2D* seedlings. (a) Morphology of Col-0, and *chs3-2D* grown on 15 μ M DMSO, 15 μ M Ro8-4304, 50 μ M BMAA, or 15 μ M Ro8-4304 and 50 μ M DBMAA for 20 days at 18°C. (b) Fresh weight normalized against the mean value of Col-0 grown on 0.01% DMSO. The data shows the mean \pm SE of three biological replicates (n=3, with 10 \pm 2 plants each). Different letters indicate significant differences between groups, whereas identical letters denote no significant differences (Two tailed Anova, Tukey test, p < 0.05).

4.5.6 Does calcium signalling influence the effect of Ro8-4304 in the chs3-2D seedlings?

Calcium signalling is an important part of the GLRs and the immune response, and most likely for the effect of Ro8-4304. However, CaCl₂ did not affect the plants, and EGTA stressed the plants too much. Hence, we altered the calcium signalling by using the chemical trifluoperazine (TFP), which is a CaM inhibitor ²³¹. CaM proteins are Ca²⁺ sensors that control cellular functions by regulating the activity of various target protein notably proteins involved with plant immune responses like ICS1, EDS1 and NDR1 ²³². Additionally, at least nine of the 20 GLRs possess a putative CaM binding site, and treatment of CaM inhibitors

resulted in a lower Ca²⁺ signature ²³³. The results of Kwaaitaal et al. (2012) therefore indicated a CaM-dependent control of GLRs ²³³. Therefore, we hypothesized that TFP would alter the GLRs response in the *chs3-2D* background, and accordingly the action of the chemical Ro8-4304. TFP was added to the media and plants were weighed after 3 weeks (Figure 42). Col-0 on TFP looked greener and larger, but the fresh weight data showed no significant difference. *Chs3-2D* grown on TFP were slightly smaller and the effect of Ro8-4304 on the fresh weigh of *chs3-2D* seedlings was significantly less in combination with TFP.

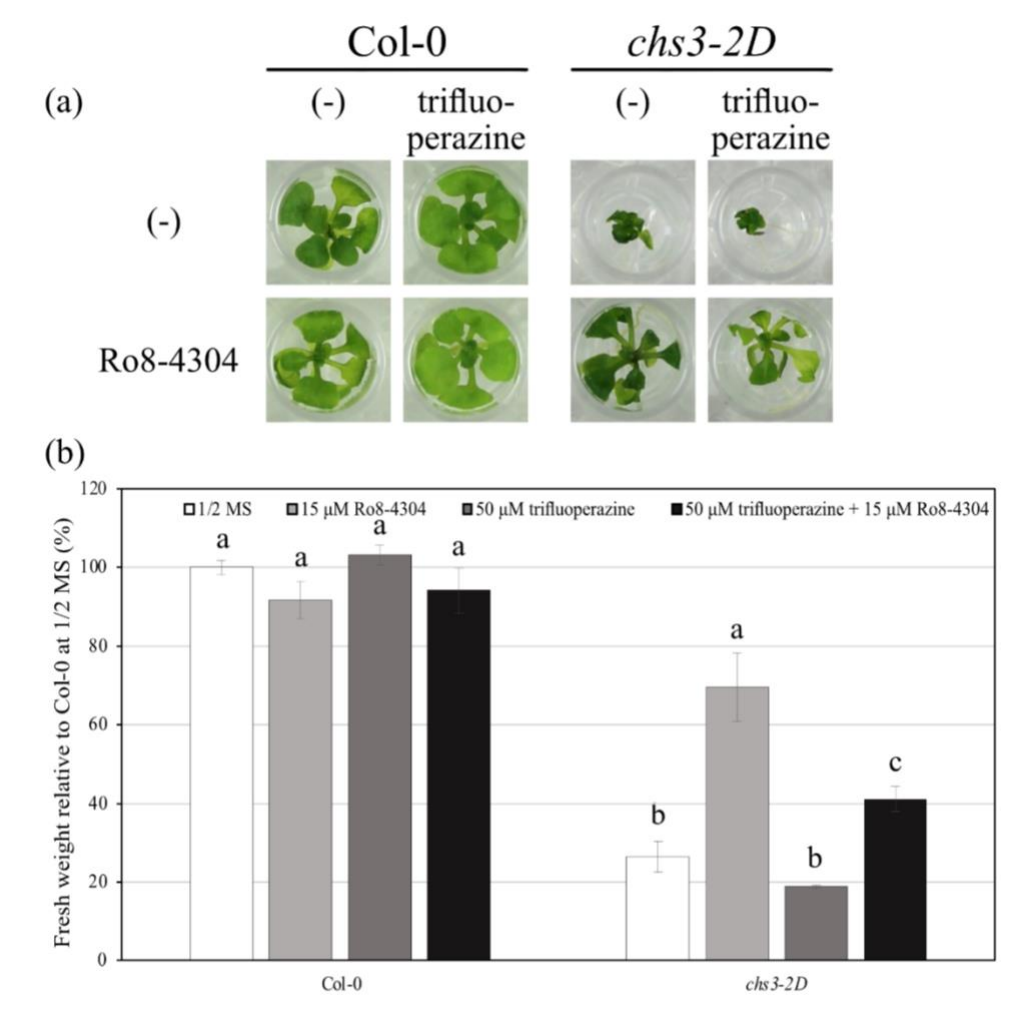


Figure 42. The effect of trifluoperazine on the activity of Ro8-4304 in Arabidopsis chs3-2D seedlings. (a) Morphology of Col-0, and chs3-2D grown on 15 μ M DMSO, 15 μ M Ro8-4304, 50 μ M trifluoperazine, or 15 μ M Ro8-4304 and 50 μ M trifluoperazine for 20 days at 18°C. (b) Fresh weight normalized against the mean value of Col-0 grown on 0.01% DMSO. The data shows the mean \pm SE of three biological replicates (n=3, with 10 \pm 2 plants each). Different letters indicate significant differences between groups, whereas identical letters denote no significant differences (Two tailed Anova, Tukey test, p < 0.05).

4.5.7 Do the substrates of NMDA (spermine and spermidine) influence the effect of Ro8-4304 in the *chs3-2D* seedlings?

Previously, we demonstrated that antagonists of GLRs negatively impact the effect of Ro8-4304 (Figures 37 and 40) and that an agonist positively impacts the effect of Ro8-4304 (Figure 41). The next step was to examine if a substrate of GLRs would also positively affect

the effect of Ro8-4304. Dubos et al. (2005) demonstrated that kanamycin could rescue the phenotype of the *de-etiolated 3 (det3)* mutant, and that this due to GLRs ²³⁴. Using a molecular modelling approach, they showed that kanamycin and polyamines like spermine bind GLRs. Additionally, in vivo experiments demonstrated that spermine can also rescue the *det3* mutant ²³⁴. Moreover, Williams et al. (1995) reported that the combined effect of glycine and a polyamine, enhances the effect of the polyamine on NMDA receptors ²³⁵. Therefore, the substrates of GLRs the polyamine spermine and spermidine were tested in combination with Ro8-4304. The chemicals spermine (Figure 43) and spermidine (Figure 44) had no effect on Col-0 or *chs3-2D* when applied solely. Adding spermine (Figure 43) or spermidine (Figure 44) in combination with Ro8-4304 slightly improved the fresh weight of *chs3-2D* in comparison to the Ro8-4304 treatment. Similar to previous reports, we demonstrated an improved effect when polyamines are applied in a combinational treatment ²³⁵.

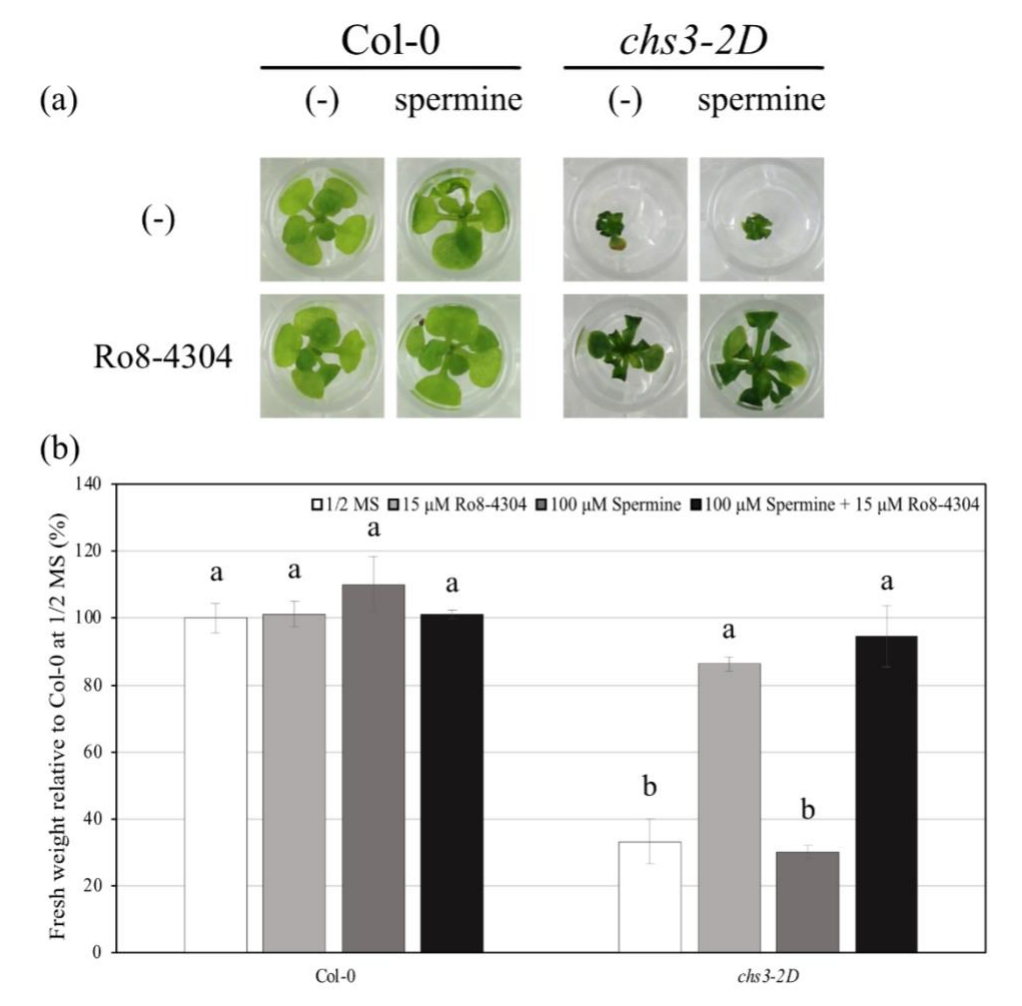


Figure 43. The effect of spermine on the activity of Ro8-4304 in *Arabidopsis chs3-2D* seedlings. (a) Morphology of CoI-0, and *chs3-2D* grown on 15 μ M DMSO, 15 μ M Ro8-4304, 100 μ M spermine, or 15 μ M Ro8-4304 and 100 μ M spermine for 20 days at 18°C. (b) Fresh weight normalized against the mean value of CoI-0 grown on 0.01% DMSO. The data shows the mean \pm SE of three biological replicates (n=3, with 10 \pm 2 plants each). Different letters indicate significant differences between groups, whereas identical letters denote no significant differences (Two tailed Anova, Tukey test, p < 0.05).

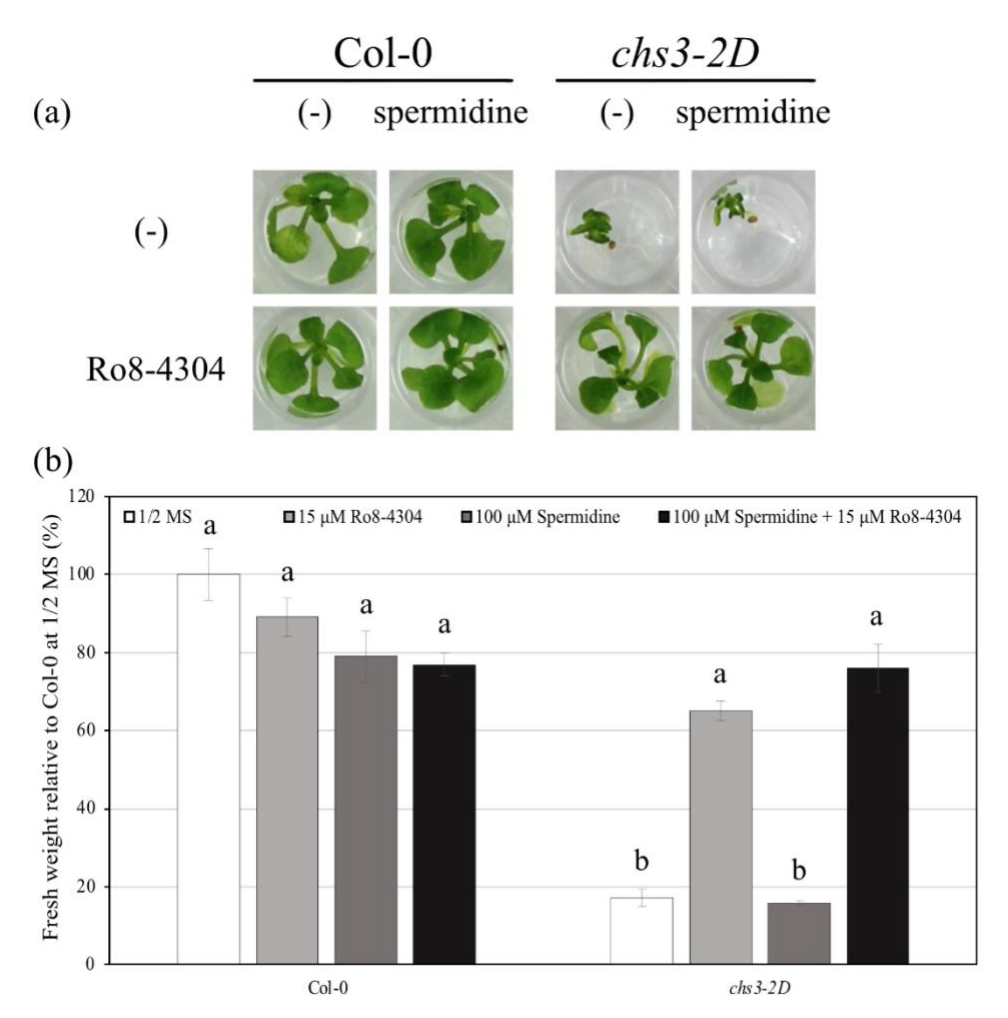


Figure 44. The effect of spermidine on the activity of Ro8-4304 in *Arabidopsis chs3-2D* seedlings. (a) Morphology of Col-0, and *chs3-2D* grown on 15 μ M DMSO, 15 μ M Ro8-4304, 100 μ M spermidine, or 15 μ M Ro8-4304 and 100 μ M spermidine for 20 days at 18°C. (b) Fresh weight normalized against the mean value of Col-0 grown on 0.01% DMSO. The data shows the mean \pm SE of three biological replicates (n=3, with 10 \pm 2 plants each). Different letters indicate significant differences between groups, whereas identical letters denote no significant differences (Two tailed Anova, Tukey test, p < 0.05).

4.5.8 Does ABA influence the effect of Ro8-4304 in the chs3-2D seedlings?

The GLR1.1 has been demonstrated to regulate abscisic acid (ABA) biosynthesis and signalling to control development via carbon and nitrogen metabolism ^{236,237}. But ABA also inhibits the germination of seeds ²³⁸, and this process has been linked to GLR3.4 and GLR3.5 ^{239–241}. Since ABA was associated with GLRs and we previously demonstrated that other agonist and antagonist of GLRs alter the effect of Ro8-4304, we thought it might be interesting to test ABA as well. *Arabidopsis thaliana* was germinated on MS media, and seedlings were transferred to media containing chemical after 1 week. Both Col-0 and *chs3-2D* were affected by ABA (Figure 45). This is not surprising, while ABA activates leaf senescence resulting in yellowing of the leaves ²⁴². The *chs3-2D* mutant was severely affected by ABA. The senescence induced by both the immune phenotype and ABA may be

too much. Interestingly, Col-0 grown on both ABA and Ro8-4304 does not show the yellowing phenotype, so Ro8-4304 seems to be able to revert or block the ABA induced senescence in Col-0. Additionally, this is the first time that we see an effect of Ro8-4304 on Col-0. *Chs3-2D* grown on both ABA and Ro8-4304 had a reduced yield in comparison to *chs3-2D* grown on Ro8-4304, nevertheless the disastrous effect of the ABA was marginally counteracted.

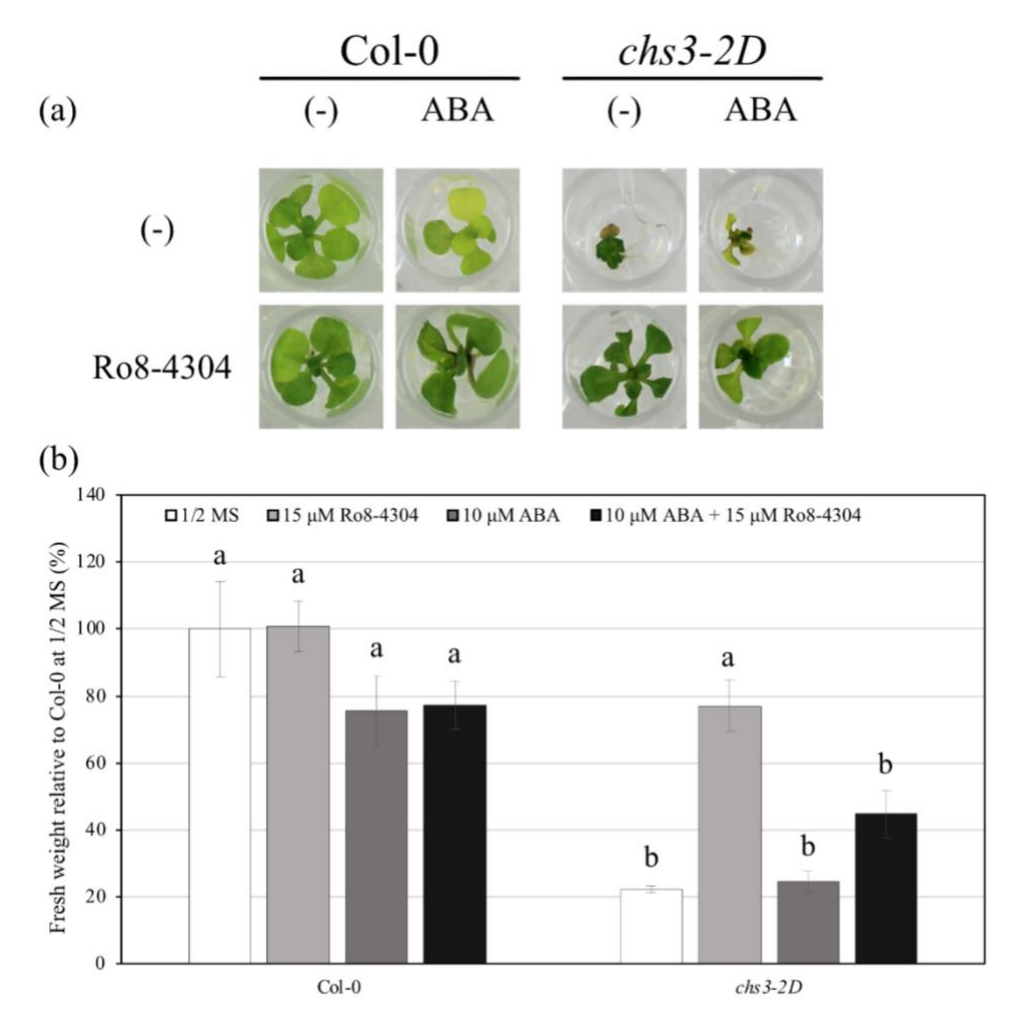


Figure 45. The effect of ABA on the activity of Ro8-4304 in *Arabidopsis chs3-2D* seedlings. (a) Morphology of Col-0, and *chs3-2D* grown on 15 μ M DMSO, 15 μ M Ro8-4304, 10 μ M ABA, or 15 μ M Ro8-4304 and 10 μ M ABA. The plants were grown for 1 week on MS before being transferred to chemical where they were grown for another 14 days at 18°C. (b) Fresh weight normalized against the mean value of Col-0 grown on 0.01% DMSO. The data shows the mean \pm SE of three biological replicates (n=3, with 10 \pm 2 plants each). Different letters indicate significant differences between groups, whereas identical letters denote no significant differences (Two tailed Anova, Tukey test, p < 0.05).

4.5.9 Does GSH influence the effect of Ro8-4304 in the *chs3-2D* seedlings?

Previously we determined that the substrates spermine and spermidine slightly boosted the effect of Ro8-4304 (Figures 43 and 44). Glutathione (GSH) is another substrate for GLRs and additionally it is a substrate for one of the other identified putative Ro8-4304 binding proteins: GLUTATHIONE S-TRANSFERASE F2 and F7 (Table 28) ^{214,243}. Previous publications

reported that exogenous GSH triggers rises in cytosolic calcium, and this rise was abolished in the loss of function mutant *glr3.3* ^{24,26}. Therefore, we wanted to determine the effect of GSH in combination with Ro8-4304 (Figure 46) and test if GSH can also boost the effect of Ro8-4304 in the *chs3-2D* seedlings. GSH had no visible effect in Col-0 and *chs3-2D*. The combinational treatment of Ro8-4304 and GSH yielded small *chs3-2D* seedlings. This was surprising, while GSH is an agonist of *GLRs* ^{24,214}, and previously tested agonists (BMAA, spermine and spermidine) showed a slight increase of the fresh weight in combination with Ro8-4304.

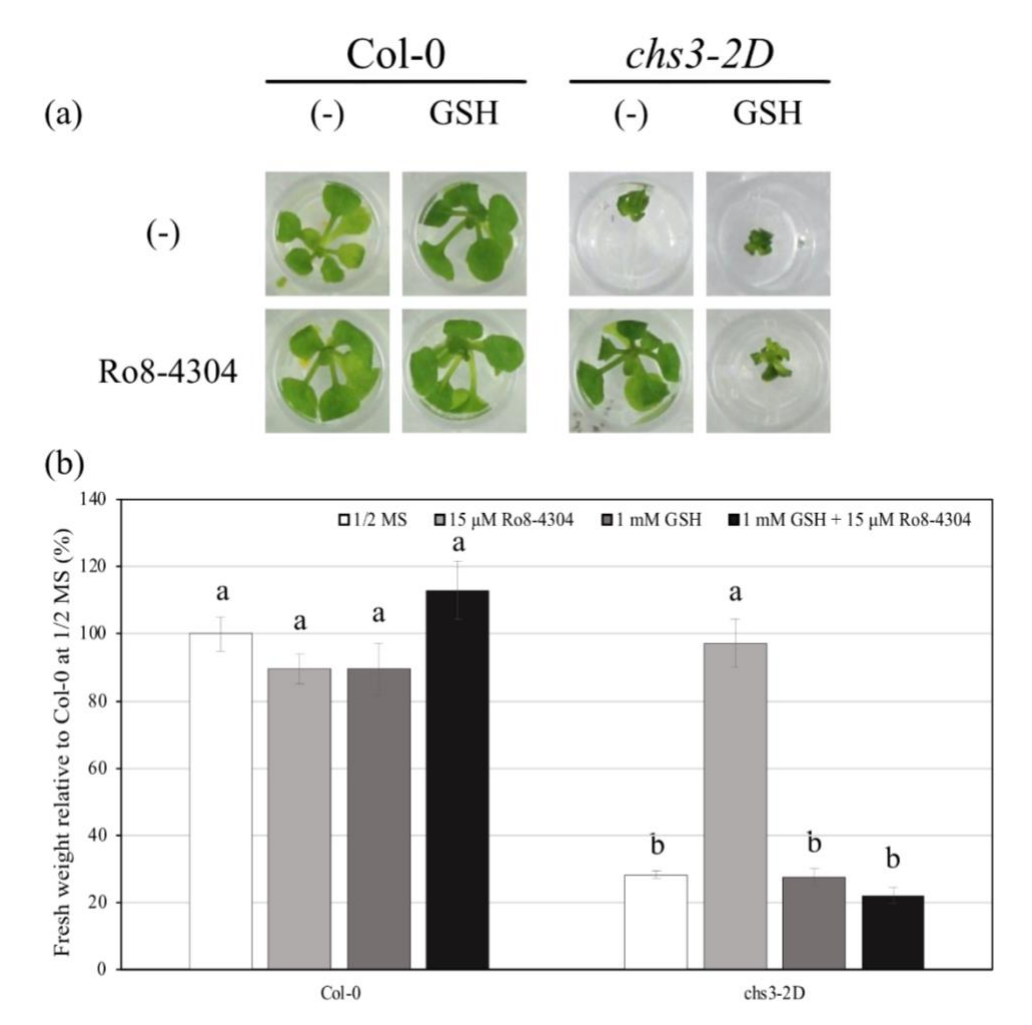


Figure 46. The effect of GSH on the activity of Ro8-4304 in *Arabidopsis chs3-2D* seedlings. (a) Morphology of Col-0, and *chs3-2D* grown on 15 μ M DMSO, 15 μ M Ro8-4304, 1 mM GSH, or 15 μ M Ro8-4304 and 1 mM GSH for 20 days at 18°C. (b) Fresh weight normalized against the mean value of Col-0 grown on 0.01% DMSO. The data shows the mean \pm SE of three biological replicates (n=3, with 10 \pm 2 plants each). Different letters indicate significant differences between groups, whereas identical letters denote no significant differences (Two tailed Anova, Tukey test, p < 0.05).

However, GSH also has a redox activity ²⁴⁴. To be certain that the reducing effect in Figure 46 is by cause of GSH and not by its redox activity, we tested another redox active compound (dithiothreitol (DTT)) in combination with Ro8-4304 (Figure 47). Adding DTT to the media resulted in a decrease of the fresh weight in Col-0. This is not surprising, while DTT is known to induce an endoplasmic reticulum (ER) stress resulting in smaller plants ²⁴⁵. Interestingly, *chs3-2D* seemed unaffected by DTT. Additionally, *chs3-2D* grown on Ro8-4304

and DTT is slightly smaller than *chs3-2D* grown on Ro8-4304, but this is not significant. The reduction of the fresh weight of *chs3-2D* seedlings grown on DTT and Ro8-4304 (Figure 47) is clearly less than *chs3-2D* seedlings grown on GSH and Ro8-4304 (Figure 46). Therefore, it seems that GSH itself is detrimental for the effect of Ro8-4304, and not its redox activity.

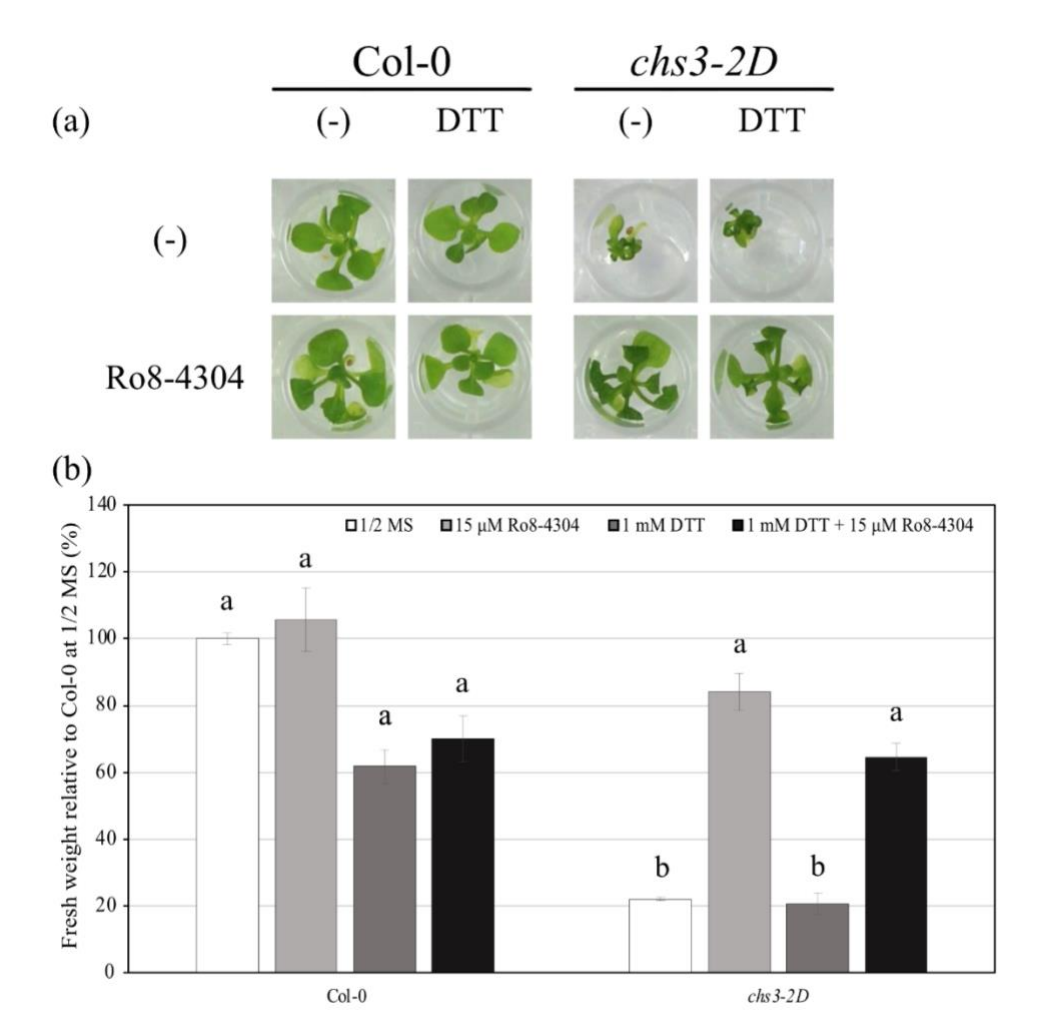


Figure 47. The effect of DTT on the activity of Ro8-4304 in *Arabidopsis chs3-2D* seedlings. (a) Morphology of Col-0, and *chs3-2D* grown on 15 μ M DMSO, 15 μ M Ro8-4304, 1 mM DTT, or 15 μ M Ro8-4304 and 1 mM DTT for 20 days at 18°C. (b) Fresh weight normalized against the mean value of Col-0 grown on 0.01% DMSO. The data shows the mean \pm SE of three biological replicates (n=3, with 10 \pm 2 plants each). Different letters indicate significant differences between groups, whereas identical letters denote no significant differences (Two tailed Anova, Tukey test, p < 0.05).

We hypothesized that Ro8-4304 may bind GLRs (Section 4.2.2). The lesser activity of Ro8-4304 on the fresh weight in the presence of GSH might be due to a competition in binding. Green et al. (2021) reported that GSH binds in the middle of the ATD clamshell 214 . The ATD in plants is similar to the N2B subunit in humans, and it was previously reported to be the site where allosteric modules like ifenprodil bind 246 . So, Ro8-4304 has been reported to bind on the same place as ifenprodil, in humans 208,209 . Therefore, the literature indicates possible competitive binding between GSH and Ro8-4304. An experiment was designed to demonstrate the competitive binding, accordingly chs3-2D was grown on different concentrations of GSH on media containing 15 μ M Ro8-4304 (Figure 48). GSH alone did not significantly affect chs3-2D at any of the concentration tested. But a concentration of GSH

higher than 0.1 M significantly altered the effect of Ro8-4304 on the fresh weight of *chs3-2D* seedlings. The fresh weight of this data was visualized (Figure 48b) and shows a clear competitive binding curve. Indicating that GSH and Ro8-4304 may bind at the same location.

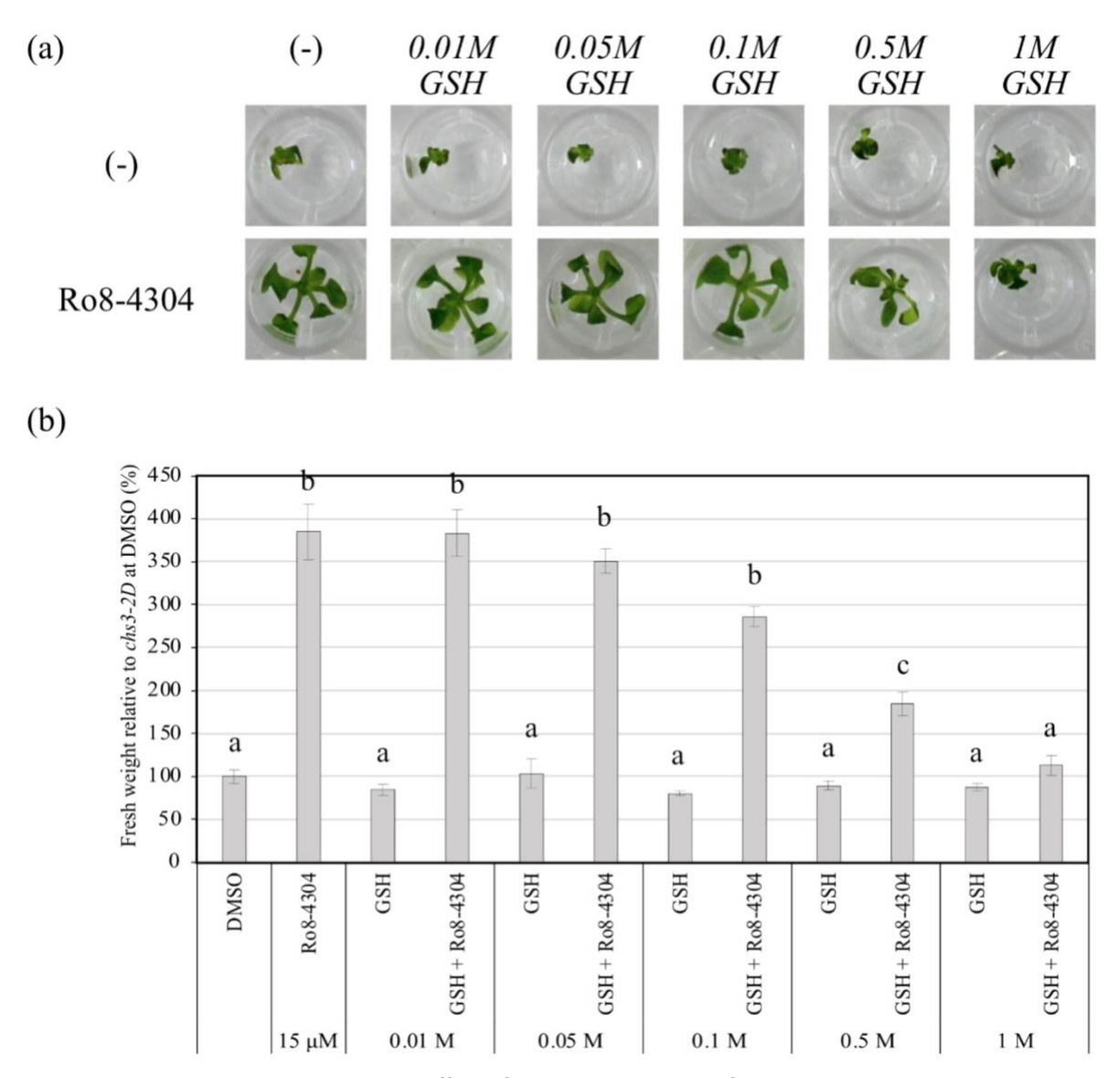


Figure 48. The concentration dependent effect of GSH on the activity of Ro8-4304 in *Arabidopsis chs3-2D* seedlings. (a) Morphology of Col-0, and *chs3-2D* grown on 15 μ M DMSO, or 15 μ M Ro8-4304 and 0.01, 0.05, 0.1, 0.5, or 1M GSH for 20 days at 18°C. (b) Fresh weight normalized against the mean value of *chs3-2D* grown on 0.01% DMSO. The data shows the mean \pm SE of three biological replicates (n=3, with 10 \pm 2 plants each). Different letters indicate significant differences between groups, whereas identical letters denote no significant differences (Two tailed Anova, Tukey test, p < 0.05).

Since GSH reduced the effect of Ro8-4304 in *chs3-2D* seedlings, we wanted to reduce the internal levels of GSH to hopefully improve the effect of Ro8-4304. Buthionine sulfoximine (BSO) is a sulfoximine derivative which reduces levels of GSH by inhibiting the first enzyme in GSH biosynthesis ²⁴⁷. The application of BSO to Col-0 and *chs3-2D* resulted in smaller and more damaged plants (Figure 49). This is not unexpected, while depletion of GSH lead to inhibition of root growth and growth reduction ^{248–251}. Thus, a lower amount of internal GSH did not improve the effect of Ro8-4304 on *chs3-2D*. It is possible that the

amount of applied BSO is too high, and the resulting internal GSH content too low. Resulting that the damage is too severe for Ro8-4304 to rescue the *chs3-2D* phenotype in the presence of BSO.

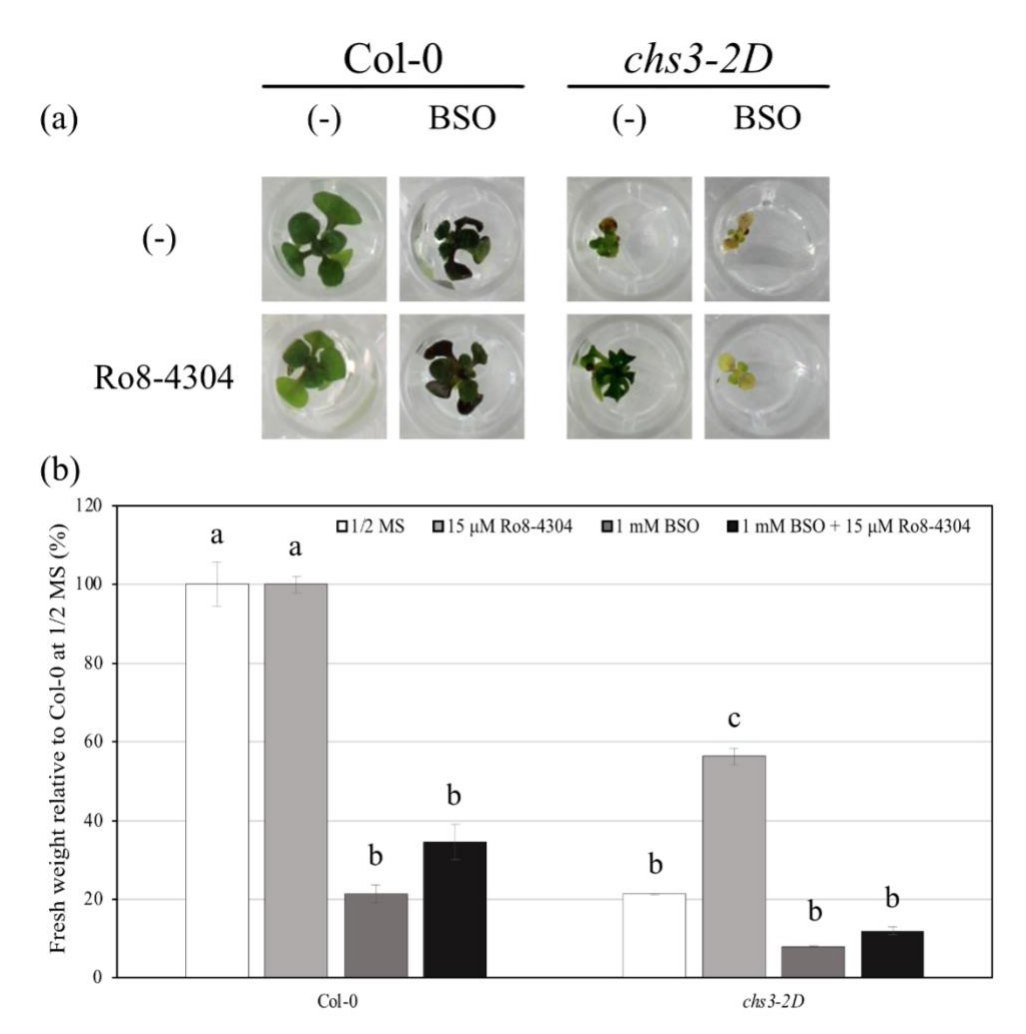


Figure 49. The effect of BSO on the activity of Ro8-4304 in *Arabidopsis chs3-2D* seedlings. (a) Morphology of Col-0, and *chs3-2D* grown on 15 μ M DMSO, 15 μ M Ro8-4304, 1 mM BSO, or 15 μ M Ro8-4304 and 1 mM BSO for 20 days at 18°C. (b) Fresh weight normalized against the mean value of Col-0 grown on 0.01% DMSO. The data shows the means of three replicates, and error bars represents the mean \pm SE (n=3, with 8 \pm 2 plants each). Different letters indicate significant differences between groups, whereas identical letters denote no significant differences (Two tailed Anova, Tukey test, p < 0.05).

4.5.10 Does GDA, an inhibitor of HSP90 protein, influence the effect of Ro8-4304 in the *chs3-2D* seedlings?

Another one of the binding proteins identified was HSP81-2 (Figure 34 and Table 28), and this is a member of the *HEAT SHOCH PROTEIN 90* gene family (*HSP90.2*). Geldanamycin (GDA) is a chemical that universally inhibits the function of HSP90 ²⁵². Takahashi et al. (2003) demonstrated that GDA could inhibit HR cell death and resistance mediated by RIBOSOMAL PROTEIN S2 (RPS2) through inhibition of HSP90 ²⁵³. Thus, if HSP81-2 is the binding protein from Ro8-4304, inhibiting the function of HSP should also reduce the effect of Ro8-4304 on the fresh weight of *chs3-2D*. The treatment of GDA did not alter the phenotype of Col-0 and

chs3-2D (Figure 50). In the presence of Ro8-4304, no significant effect could be seen either. So, GDA does not influence *Arabidopsis thaliana chs3-2D*, which is curious, while Lu et al. (2022) demonstrated that the *chs3-2D* phenotype is dependent on HSP90 ⁸⁸, and Sangster et al. (2007) demonstrated that seedlings with reduced HSP90 function have an altered phenotype ¹¹². They also mentioned that GDA is light sensitive, and the phenotype on GDA can therefore only be analysed at the seedling stage ¹¹². We grew the plants in the light for a longer period, and the light sensitivity of GDA may have altered the results. So, testing the activity of HSP90 in the *chs3-2D* background using GDA was unsuccessful at the time of writing, and hence this pharmacological analysis was unconclusive.

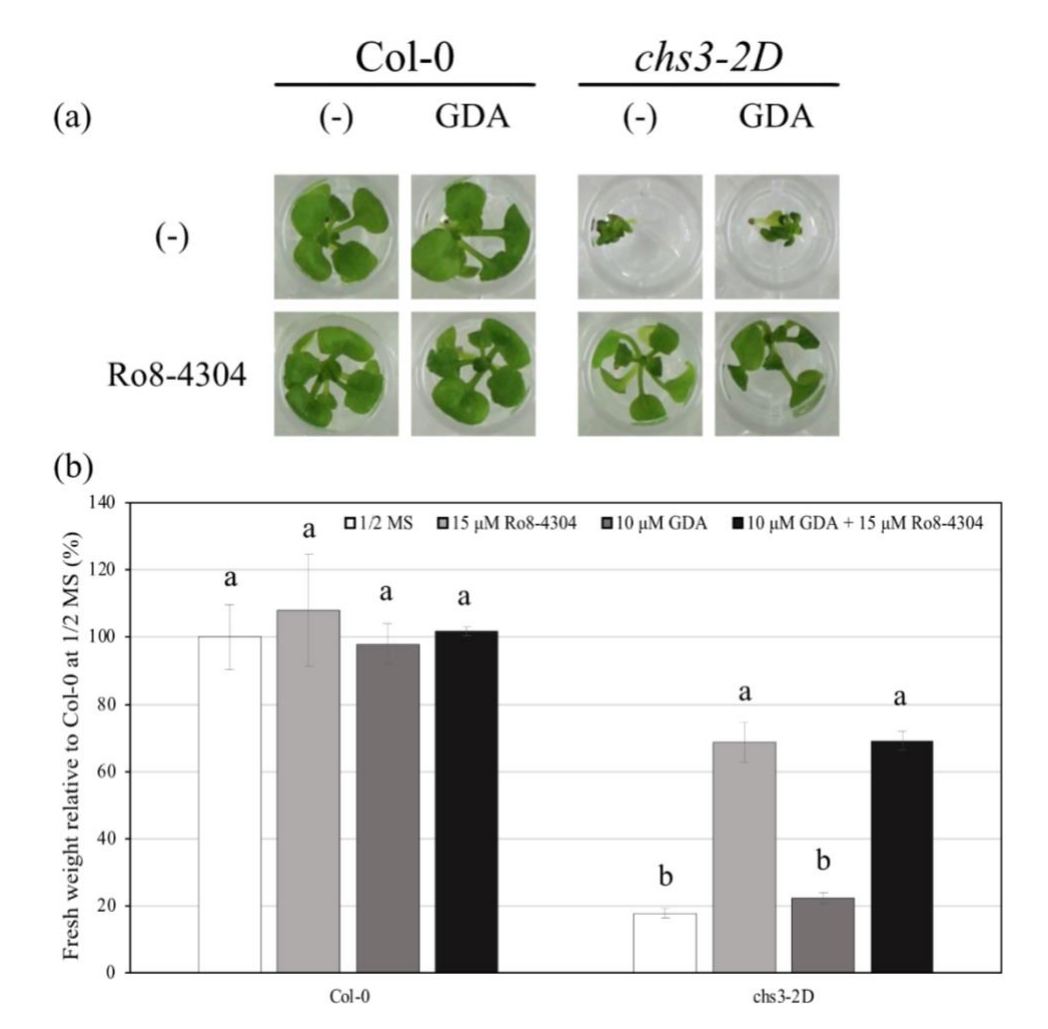


Figure 50. The effect of GDA on the activity of Ro8-4304 in *chs3-2D* seedlings. (a) morphology of Col-0, and *chs3-2D* grown on 15 μ M DMSO, 15 μ M Ro8-4304, 10 μ M GDA, or 15 μ M Ro8-4304 and 10 μ M GDA for 20 days at 18°C. (b) the measured fresh weight normalized against the mean value of Col-0 grown on DMSO. The data shows the mean \pm SE of three biological replicates (n=3, with 10 \pm 2 plants each). Different letters indicate significant differences between groups, whereas identical letters denote no significant differences (Two tailed Anova, Tukey test, p < 0.05).

4.5.11 Does UPC, an inhibitor of CDC48 protein, influence the effect of Ro8-4304 in the *chs3-2D* seedlings?

During the binding protein assay, CDC48A was also detected (Table 28). CDC48A has a high homology to the human protein p97 ²⁵⁴. UPCDC30245 (UPC) is a chemical that inhibits p97 function ²⁵⁵ and possibly CDC48A function. The binding of Ro8-4304 may be disrupted by UPC if CDC48A is the legitimate target, so UPC was applied to the plants (Figure 51). This chemical did not alter the phenotype of Col-0 nor *chs3-2D*. Which was unexpected, since CDC48 plays a critical role in the development of the plant ²⁵⁶. Nevertheless, the effect of Ro8-4304 is slightly diminished in the presence of UPC in *chs3-2D* seedlings. The effect of Ro8-4304 may be altered due to a competition of the binding site, or due to a change in the related pathways in development ²⁵⁶, or immunity ²⁵⁷.

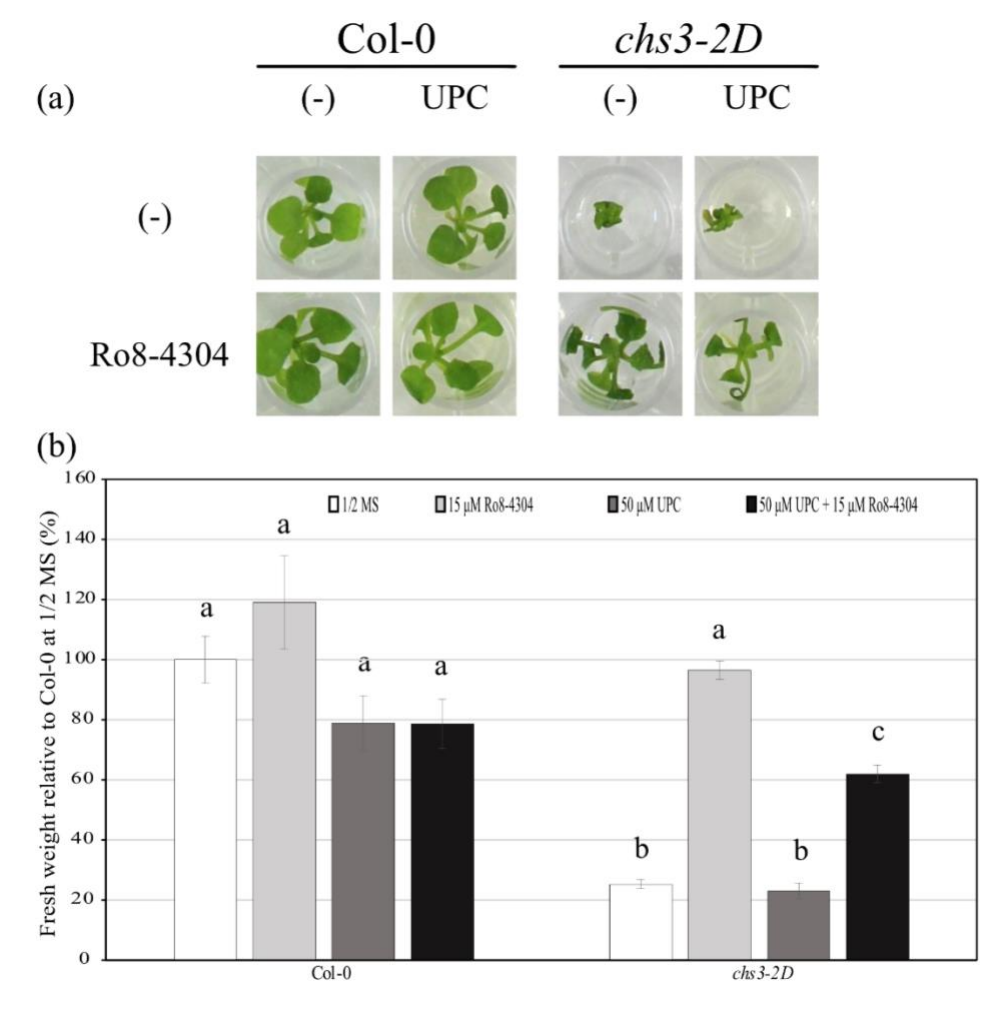
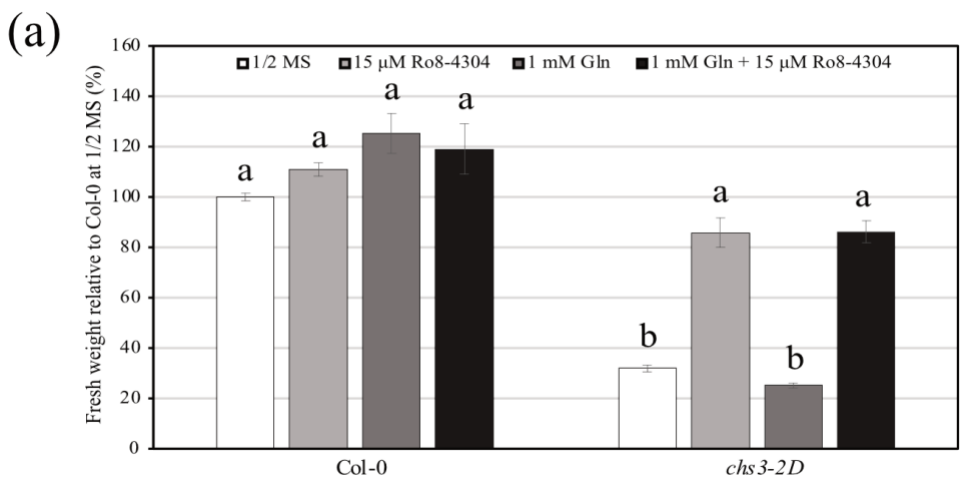
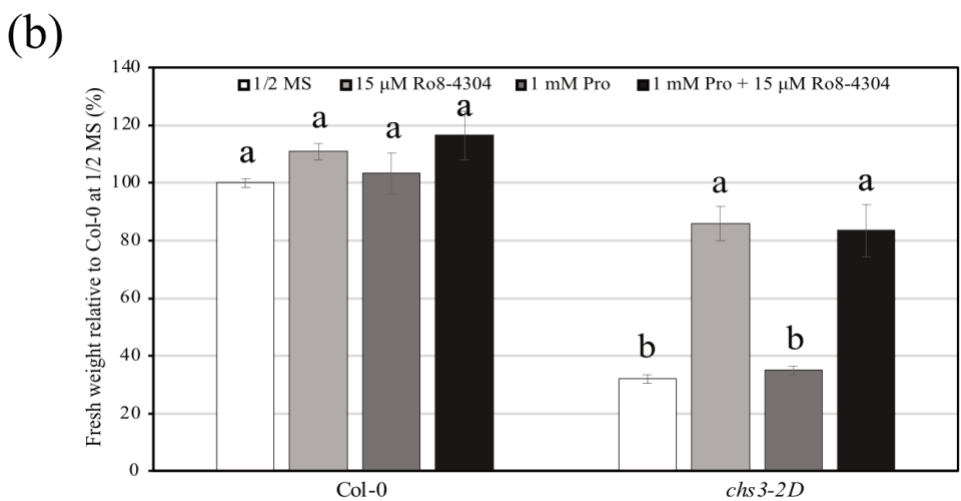


Figure 51. The effect of UPC on the activity of Ro8-4304 in *Arabidopsis chs3-2D* seedlings. (a) Morphology of Col-0, and *chs3-2D* grown on 15 μ M DMSO, 15 μ M Ro8-4304, 50 μ M UPC, or 15 μ M Ro8-4304 and 50 μ M UPC for 20 days at 18°C. (b) Fresh weight normalized against the mean value of Col-0 grown on 0.01% DMSO. The data shows the mean \pm SE of three biological replicates (n=3, with 10 \pm 2 plants each). Different letters indicate significant differences between groups, whereas identical letters denote no significant differences (Two tailed Anova, Tukey test, p < 0.05).

4.5.12 Do the natural substrates of NMDA receptors influence the effect of Ro8-4304 in the *chs3-2D* seedlings?

The natural substrate for NMDA receptors, and GLRs are amino acids. In plants different GLRs clades have different affinities for different amino acids ²⁵⁸. Additionally, the amino acid glutamate has been demonstrated to activate plant defence signalling ^{225,259–262}. Previously, we already demonstrated that the substrates spermine (Figure 43), spermidine (Figure 44), and GSH (Figures 46 and 48) alter the influence of Ro8-4304 on the fresh weight of *chs3-2D* seedlings. Therefore, we also tested the effect of the amino acids glutamine (Gln), proline (Pro), glycine (Gly), glutamate (Glu) and methionine (Met) (Figure 52). The amino acids Glu, Pro and Gly yielded no modified response on the fresh weight of *chs3-2D* seedlings (Figures 52a, b, c). *Chs3-2D* grown on Glu and Ro8-4304 was slightly smaller than *chs3-2D* grown on only Ro8-4304 (Figure 52d). The consequence of Met was more pronounced. *Chs3-2D* grown on Met and Ro8-4304 was significantly smaller than *chs3-2D* grown on Ro8-4304 (Figure 52e).





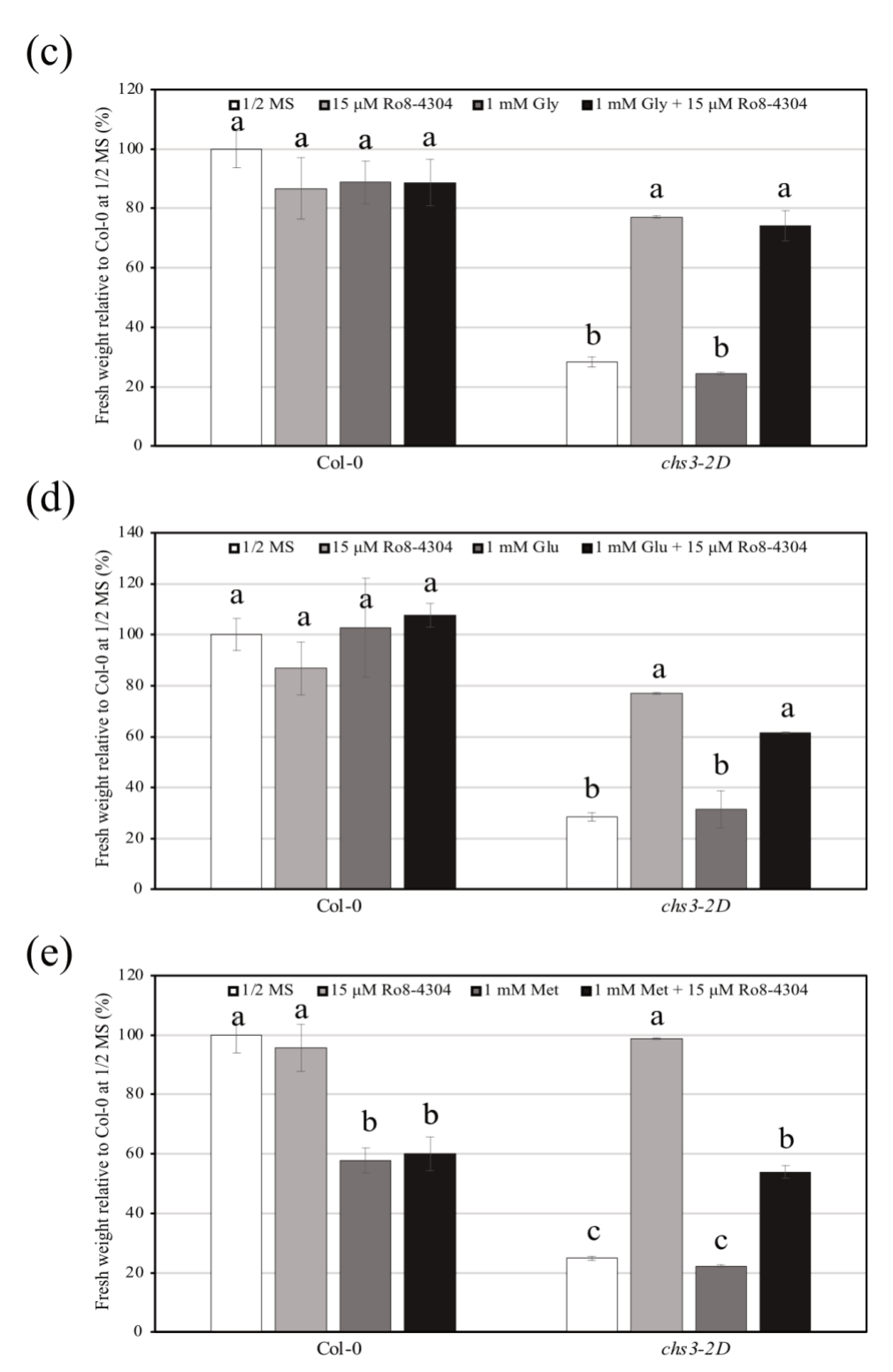


Figure 52. The effect of different amino acids on the activity of Ro8-4304 in *Arabidopsis chs3-2D* seedlings. (a) Fresh weight of Col-0, and *chs3-2D* grown on 15 μ M DMSO, 15 μ M Ro8-4304, 1 mM Gln, or 15 μ M Ro8-4304 and 1 mM Gln for 20 days at 18°C. (b) Fresh weight of Col-0, and *chs3-2D* grown on 15 μ M DMSO, 15 μ M Ro8-4304, 1 mM Pro, or 15 μ M Ro8-4304 and 1 mM Pro for 20 days at 18°C. (c) Fresh weight of Col-0, and *chs3-2D* grown on 15 μ M DMSO, 15 μ M Ro8-4304, 1 mM Gly, or 15 μ M Ro8-4304 and 1 mM Gly for 20 days at 18°C. (d) Fresh weight of Col-0, and *chs3-2D* grown on 15 μ M Ro8-4304 and 1 mM Glu for 20 days at 18°C. (e) Fresh weight of Col-0, and *chs3-2D* grown on 15 μ M DMSO, 15 μ M Ro8-4304, 1 mM Met, or 15 μ M Ro8-4304 and 1 mM Met for 20 days at 18°C. (a, b, c, d, and e) The fresh weight was normalized against the mean value of Col-0 grown on 0.01% DMSO. The data shows

the mean \pm SE of three biological replicates (n=3, with 10 \pm 2 plants each). Different letters indicate significant differences between groups, whereas identical letters denote no significant differences (Two tailed Anova, Tukey test, p < 0.05).

Pharmacological analysis indicated an importance for GLRs in the action of Ro8-4304 in *Arabidopsis thaliana chs3-2D*. For more conclusive results, we continued the research by generating double mutant lines, and testing of the chemical Ro8-4304 in this background.

4.6 Generation and characterization of double mutants between *chs3-2D* and mutants lacking the respective gene encoding putative Ro8-4304 binding proteins

Using the pharmacological analysis, we discovered that antagonist of GLRs diminished the effect of Ro8-4304 (Figures 37 and 41). While agonist and substrates slightly boosted the effect of the chemical Ro8-4304, except GSH and methionine (Figures 41, 43, 44, 46, 48 and 52). These results indicated that GLRs may be important for the action of Ro8-4304 in the chs3-2D background. The next step was to generate double mutant lines. Atglr3.3 was chosen, while this particular GLRs has already been shown to be necessary for immune responses ^{24,26}. Col-0, chs3-2D, glr3.3-1 (SALK_040458) ²⁴⁻²⁶, and glr3.3-1 chs3-2D were grown on DMSO, Ro8-4304, and Ro-A03. The fresh weight and SA content was measured (Figure 53). The chemicals had no effect on the single qlr3.3-1 mutant. The qlr3.3-1 chs3-2D double mutant was even smaller than chs3-2D, under DMSO control conditions. This was unexpected, since GLRs are involved in immunity, and therefore we hypothesized that knocking out GLR3.3 would reduce the immune response and the corresponding immune phenotype. Instead GLR3.3 seemed to repress something in the chs3-2D background. Strikingly, the effect of the chemicals Ro8-4304 and Ro-A03 (Figure 53b) was significantly less than in the chs3-2D single mutant. Although, the response of Ro8-4304 and Ro-A03 was significantly less in chs3-2D glr3.3-1 seedlings, a small influence was still detectable. This could be due to redundancy of the GLRs or a concentration dependency. The SA content in the double mutant qlr3.3-1 chs3-2D was less than the single mutant, even though the fresh weight is lower. GLR3.3 is necessary for the immune response in plants and knocking out this gene probably diminished the defence response in the chs3-2D background. Interestingly, adding Ro8-4304 and Ro-A03 to chs3-2D glr3.3-1 increased the SA content, in contrast to the single mutant line.

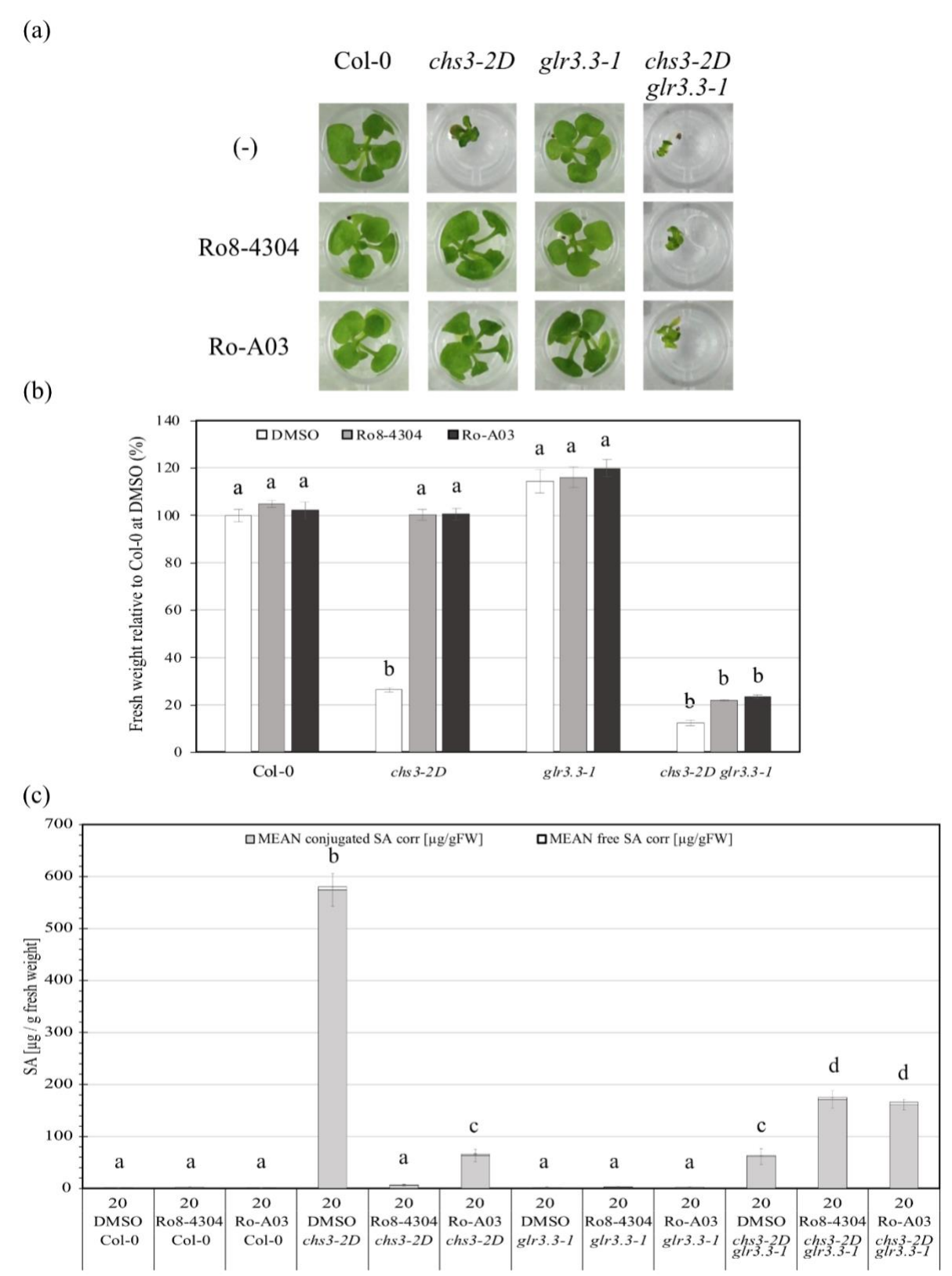
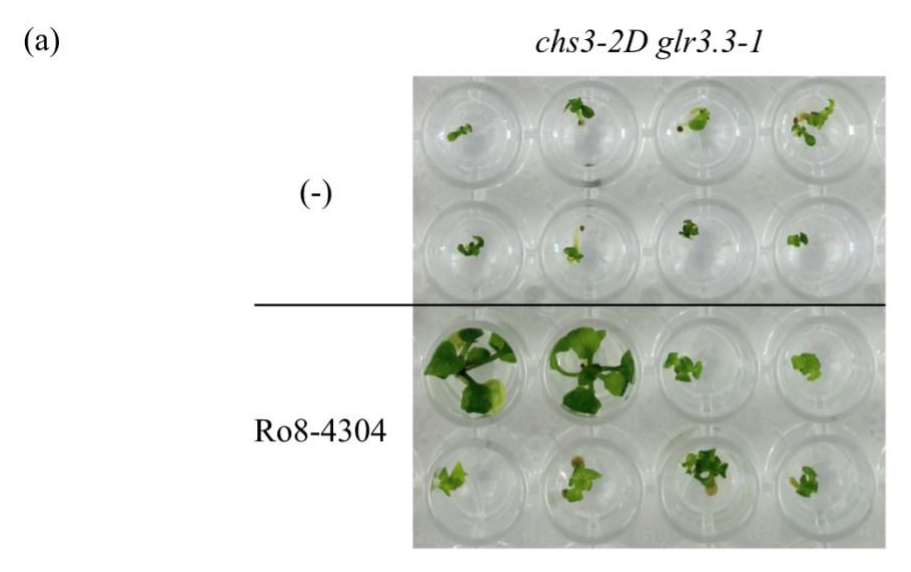


Figure 53. The effect of Ro8-4304 and Ro-A03 on *Arabidopsis glr3.3-1* and *chs3-2D glr3.3-1*. (a) Morphology of Col-0, *chs3-2D*, *glr3.3-1* and *chs3-2D glr3.3-1* grown on 50 μ M DMSO, Ro8-4304 or Ro-A03 for 20 days at 18°C. (b) Fresh weight normalized against the mean value of Col-0 grown on 0.01% DMSO. The data shows the mean \pm SE of five biological replicates (n=5, with 12 plants each). Different letters indicate significant differences between groups, whereas identical letters denote no significant differences (Two tailed Anova,

Tukey test, p < 0.05). (c) Free SA and SAG of Col-0, chs3-2D, glr3.3-1 and chs3-2D glr3.3-1 normalized against the mean value of Col-0 grown on 0.01% DMSO The data shows the mean \pm SE of five biological replicates (n=5, with 12 plants each). Different letters indicate significant differences between groups, whereas identical letters denote no significant differences (Two tailed Anova, LSD test, p < 0.05).

However, the data shown in Figure 53 is not flawless. To create double mutants, multiple crosses were made, and multiple lines were analysed. Regrettably, not all lines were completely unresponsive (Figure 54). 3 of the lines were completely insensitive to the chemical. But 4 lines showed the growth rescuing phenotype in about 25% of the cases. This is not only true for the chs3-2D qlr3.3-1 mutant. Crosses were made to generate Arabidopsis chs3-2D glr1.1 and chs3-2D glr3.4-2 [data not shown], and these had the same deficiency. Additionally, mutants for the discovered binding proteins were crossed in the chs3-2D background, and some of these lines demonstrated the same effect (Figure 56). In the defective lines, Ro8-4304 has a growth rescuing effect with a percentage of 25%. Therefore, we suspect that there is another gene present in the chs3-2D background which is necessary for the action of Ro8-4304. The percentage of 25% seemed to correlate with Mendel's Laws of Inheritance. Additionally, this may explain why the chemical is so selective for the Arabidopsis thaliana chs3-2D mutant. The chs3-2D mutants was created by EMSmutagenesis 84, therefore other mutations are not completely unexpected. Still, if this holds true, it is unusual that Ro8-4304 has a slight effect in chs3-1 (Figure 16), while this is another EMS-mutagenized line 85. The chance that both lines have the same secondary mutation is quite low. Furthermore, Huang et al. (2016) 166 didn't mention this uncertainty in their publication. Although, variation of the effect of Ro8-4304 can also be seen in their published pictures. Nonetheless, they may have selected the most stable line for their experiments. To be sure of this hypothesis, a couple of mutant lines were sent in for complete genome sequencing. But, at the time of writing this data was not yet applicable.



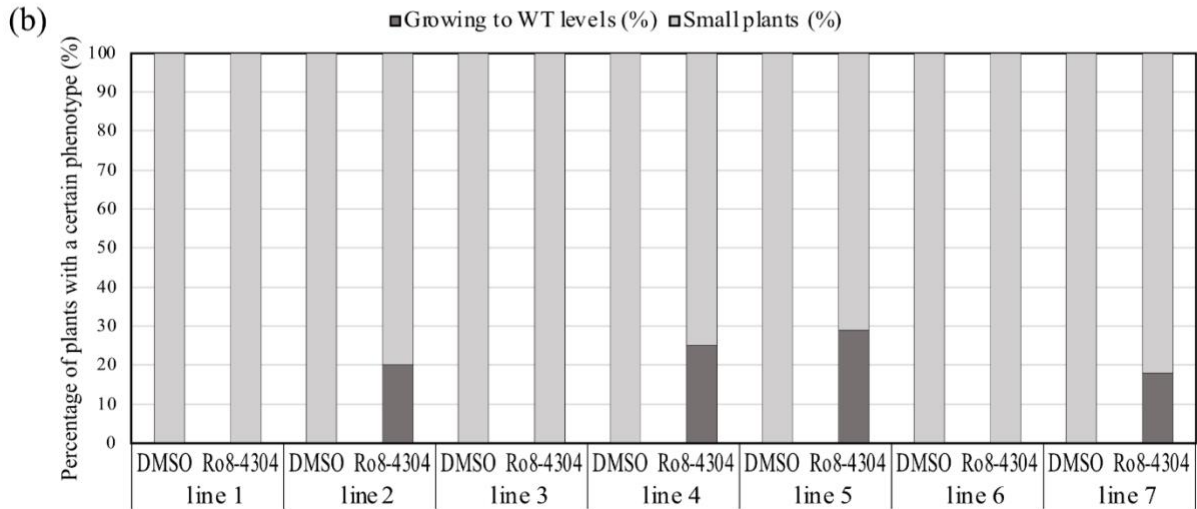


Figure 54. The complication with the double mutant lines. (a) Morphology of *chs3-2D glr3.3-1* line 5 grown on 50 μM DMSO or Ro8-4304 for 20 days at 18°C. (b) Percentage of plants with a certain phenotype.

Since some of the lines *chs3-2D glr3.3-1* lines were stable in their reaction to Ro8-4304, we chose to continue with the characterization of these lines. *Arabidopsis chs3-2D glr3.3-1* line 3 was grown on DMSO, Ro8-4304, or Ro-A03 and the expression of the defence genes was measured (Figure 55). The expression of *GLR3.3* was reduced in the double mutant. The expression of the defence gene in the *chs3-2D glr3.3-1* background is a bit variable, but in most cases remains high, similar to *chs3-2D* grown on DMSO. This is quite surprising, since the SA content was lower than in the *chs3-2D* mutant. Demonstrating that the lower SA content in *chs3-2D glr3.3-1* was still enough to induce defence gene expression.

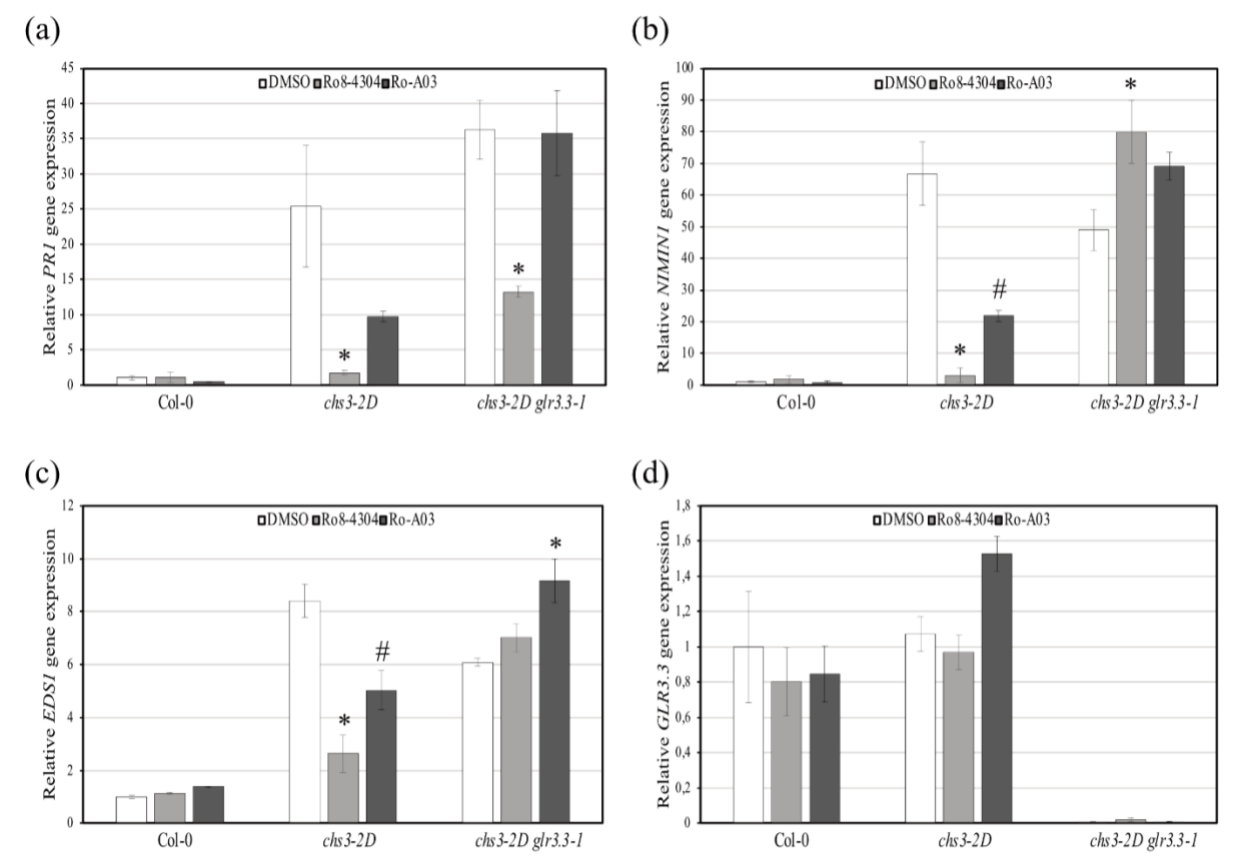


Figure 55. The expression of the defence gene in *Arabidopsis chs3-2D glr3.3-1*. Plants were grown for 20 days at 18°C in the presence of DMSO, 50 μ M Ro8-4304, or 50 μ M Ro-A03. The relative expression is shown for *PR1* (a), *NIMIN1* (b), *EDS1* (c), and *GLR3.3* (d). The data were normalized against the mean value of Col-0 grown on DMSO (0.1%). The data shows the mean \pm SE of three biological replicates (n=3). An asterisk indicates a significant difference to relevant mutant grown on DMSO (Two tailed Anova, Tukey test, p < 0.05). A hash indicates a significant difference to relevant mutant grown on DMSO and Ro8-4304 (Two tailed Anova, Tukey test, p < 0.05).

Not only the *glr3.3-1* mutant was crossed into the *chs3-2D* background. For the other putative binding proteins, mutants were established to test the effect of Ro8-4304 in these lines. The *Arabidopsis thaliana* mutant lines SALK_030186 (*gstf2-1K*), GK-261D05 (*gstf7-1K*), N69995 (*cdc48a4*), SALK_038646 (hsp81-2K or *hsp90-2K*), and N68671 (hsp81-2.7 or *hps90-2.7*) were obtained from NASC ²⁶³(Figure 9). After confirmation of the genotype the lines were crossed into the *chs3-2D* background. The combination *chs3-2D tkl1* was not viable. The other generated double mutants were treated with DMSO, Ro8-4304 and Ro-A03, and after three weeks the fresh weight (Figure 56), the expression of defence genes (Figure 57), and the expression of genes encoding the binding protein (Figure 58) was determined.

Chs3-2D gstf2-1K did not have a different effect to the chemical in comparison to chs3-2D (Figure 56). This could be due to redundancy, while GSTF2 and GSTF3 have a similarity of 95% ²⁶⁴. Moreover, GSTF7 and GSTF6 have a redundancy of 96% ²⁶⁴, and GSTF2 and GSTF7 share an identity of 72% ²⁶⁴. Therefore, it is quite unexpected that Ro8-4304 shows a slight effect on the fresh weight in Arabidopsis chs3-2D gstf7-1K (Figure 56), and no significant differences in defence gene expression (Figure 57). However, testing the expression of the binding proteins indicate that GSTF2 levels were reduced in chs3-2D gstf2-1K (Figure 58a). In contrast to GSTF7 levels in the chs3-2D gstf7-1K seedlings, these were increased (Figures 58c and d). GSTFs have been shown to bind and transport small organic ligands like pesticides ²⁶⁵⁻²⁶⁸. Knocking-out this gene may result in more bio-active Ro8-4304, while over-expression may result in faster removal of the chemical.

The expression of the binding protein *CDC48* was not distinguishable using RT-qPCR (Figure 58b) in *Arabidopsis chs3-2D cdc48a4*. The expression of *CDC48* may be too inadequate to be detected. The same holds true for the *chs3-2D hsp90-2* mutants (Figure 58e). No significant changes can be seen in the RT-qPCR data.

The fresh weight and defence gene expression of *chs3-2D cdc48a4* was not altered by Ro8-4304 and Ro-A03 (Figures 56 and 57). This mutant seems to be completely unresponsive to chemical treatment of Ro8-4304 or Ro-A03. The fresh weight of the *chs3-2D hsp90-2K* and the *chs3-2D hsp90-2.7* were significantly less affected by the chemicals Ro8-4304 or Ro-A03, but a slight increase in fresh weight was still visible (Figure 56). Furthermore, Ro8-4304 and Ro-A03 did not affect the defence gene expression in the *Arabidopsis chs3-2D hsp90-2* double mutants (Figure 57). Nonetheless, also for HSP90 redundancy has been demonstrated ^{183,269}, and this may have influenced the results.

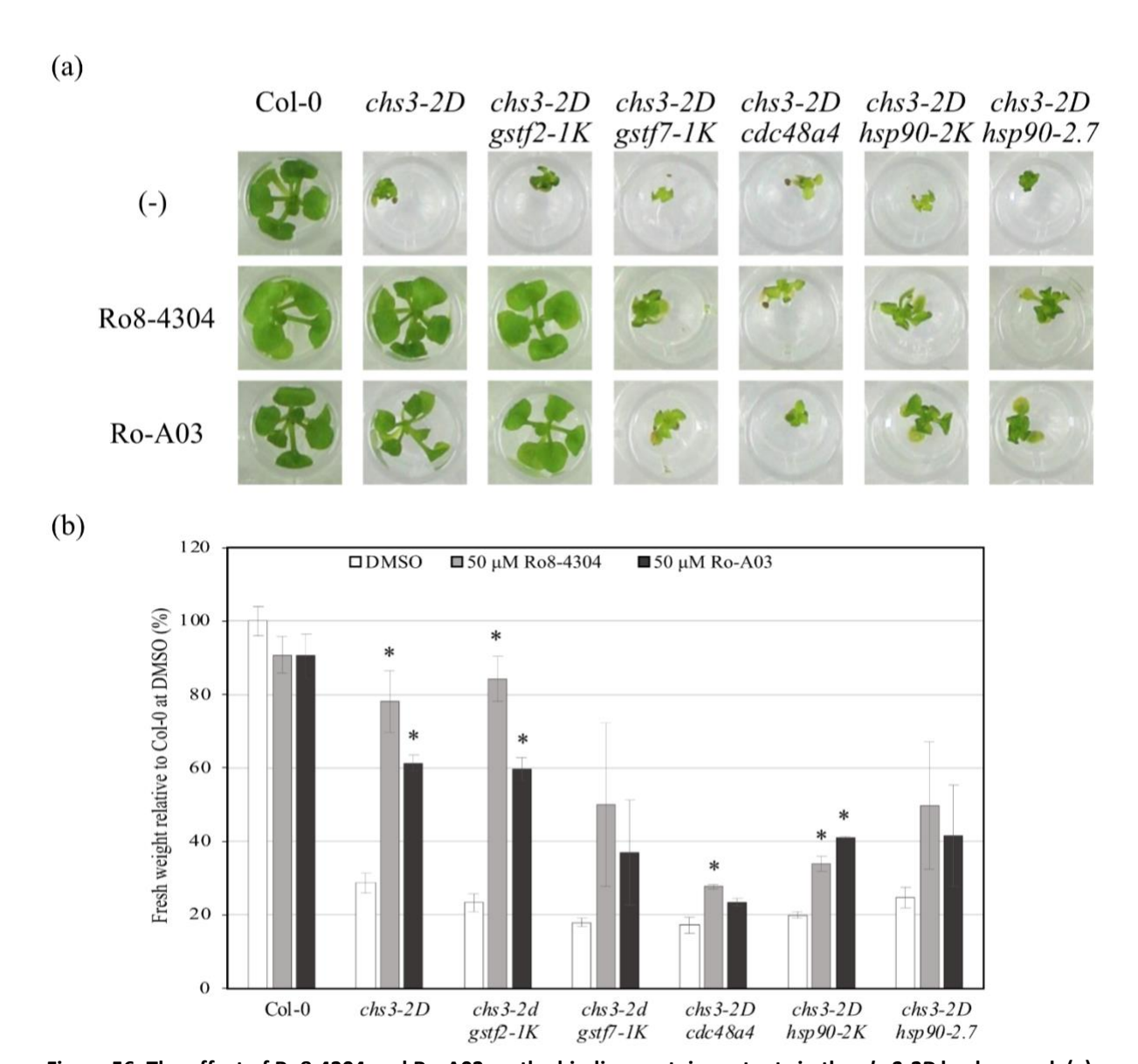
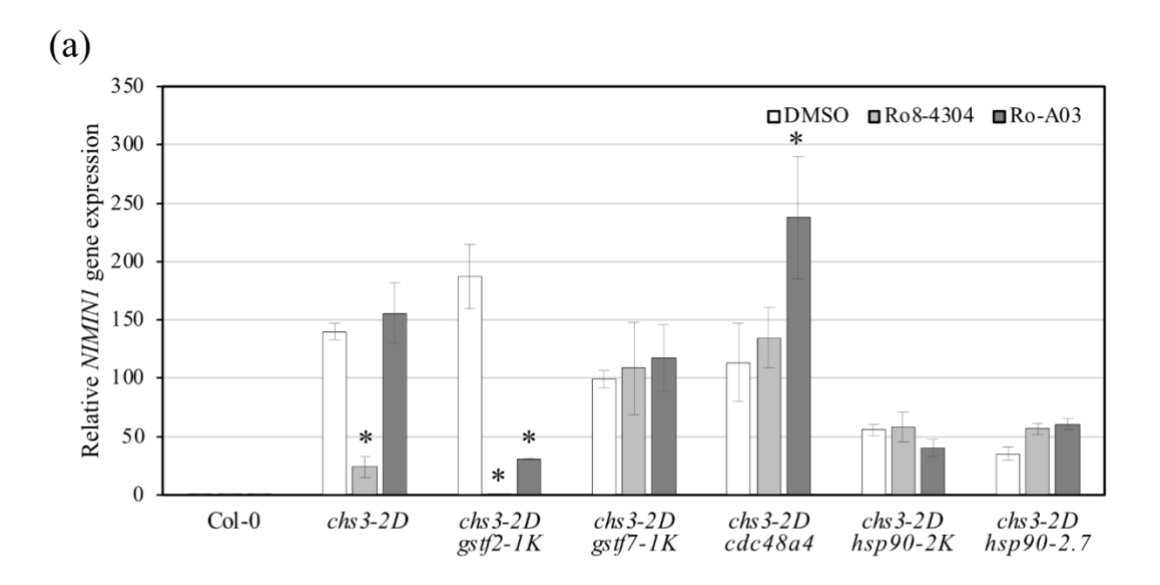
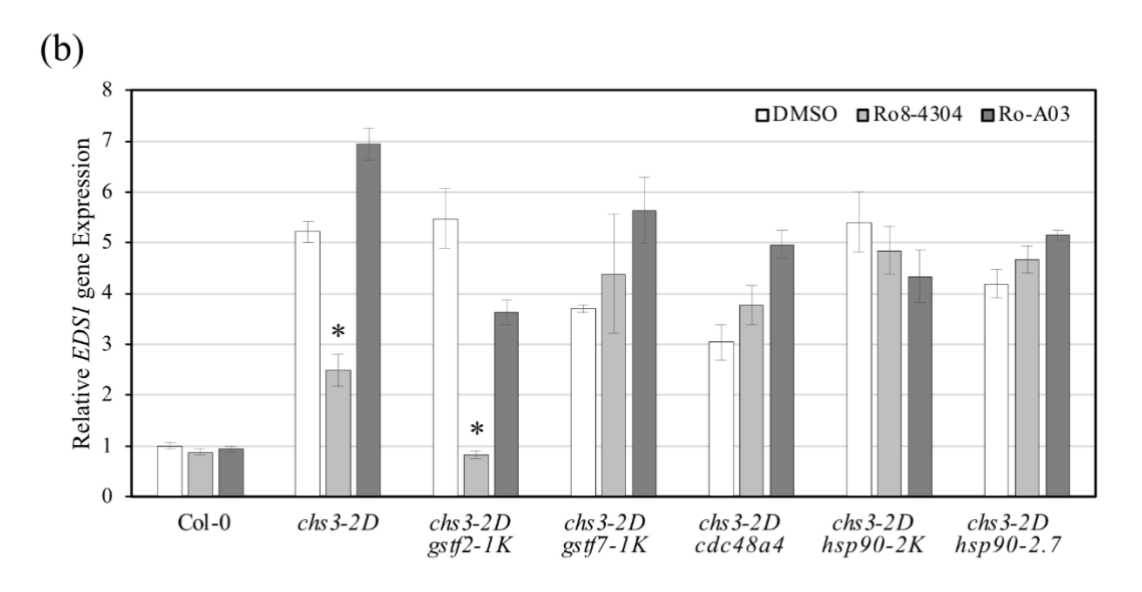


Figure 56. The effect of Ro8-4304 and Ro-A03 on the binding protein mutants in the *chs3-2D* background. (a) Morphology of CoI-0, *chs3-2D*, *chs3-2D gstf2-1K*, *chs3-2D GSTF7-1K*, *chs3-2D CDC48a4*, *chs3-2D hsp90-2K*, and *chs3-2D hsp90-2*.7 grown on DMSO, 50 μ M Ro8-4304 or 50 μ M Ro-A03 for 20 days at 18°C. (b) Fresh weight normalized against the mean value of CoI-0 grown on 0.01% DMSO. The data shows the mean \pm SE of three biological replicates (n=3, with 10 \pm 2 plants each). An asterisk indicates a significant difference to the relevant negative control (Student's t-test, p < 0.05).





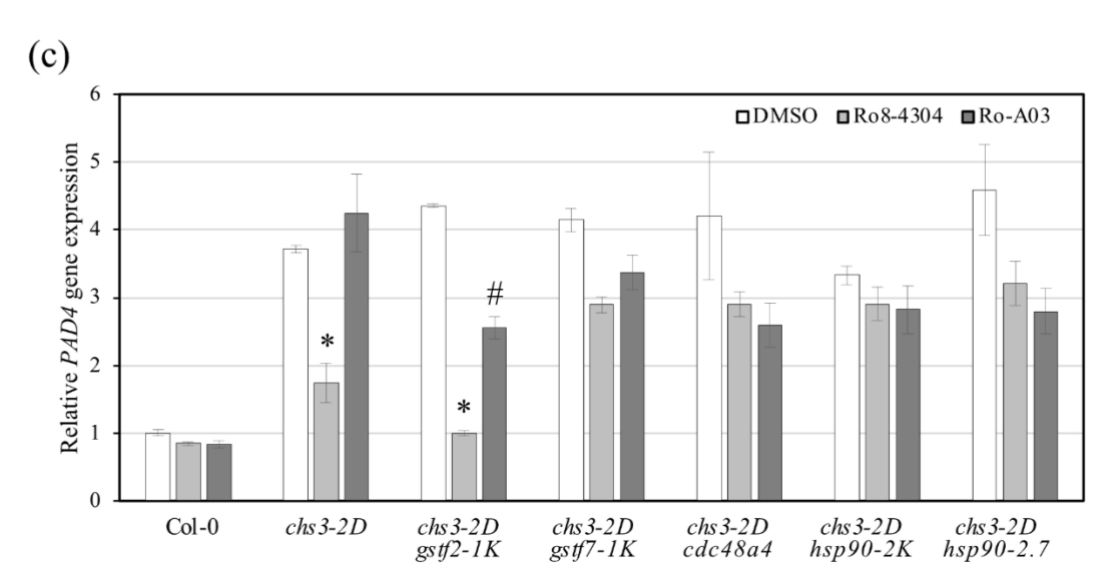


Figure 57. The expression of the defence gene in the binding protein mutants in the *chs3-2D* background. Plants were grown for 20 days at 18° C in the presence of DMSO, 50 μ M Ro8-4304, or 50 μ M Ro-A03. The

relative expression is shown for NIMIN1 (a), EDS1 (b), and PAD4 (c). The data is normalized against the mean value of Col-0 grown on DMSO (0.1%). The data shows the mean \pm SE of three biological replicates (n=3). An asterisk indicates a significant difference to relevant mutant grown on DMSO (Two tailed Anova, Tukey test, p < 0.05). A hash indicates a significant difference to corresponding mutant grown on DMSO and Ro8-4304 (Two tailed Anova, Tukey test, p < 0.05).

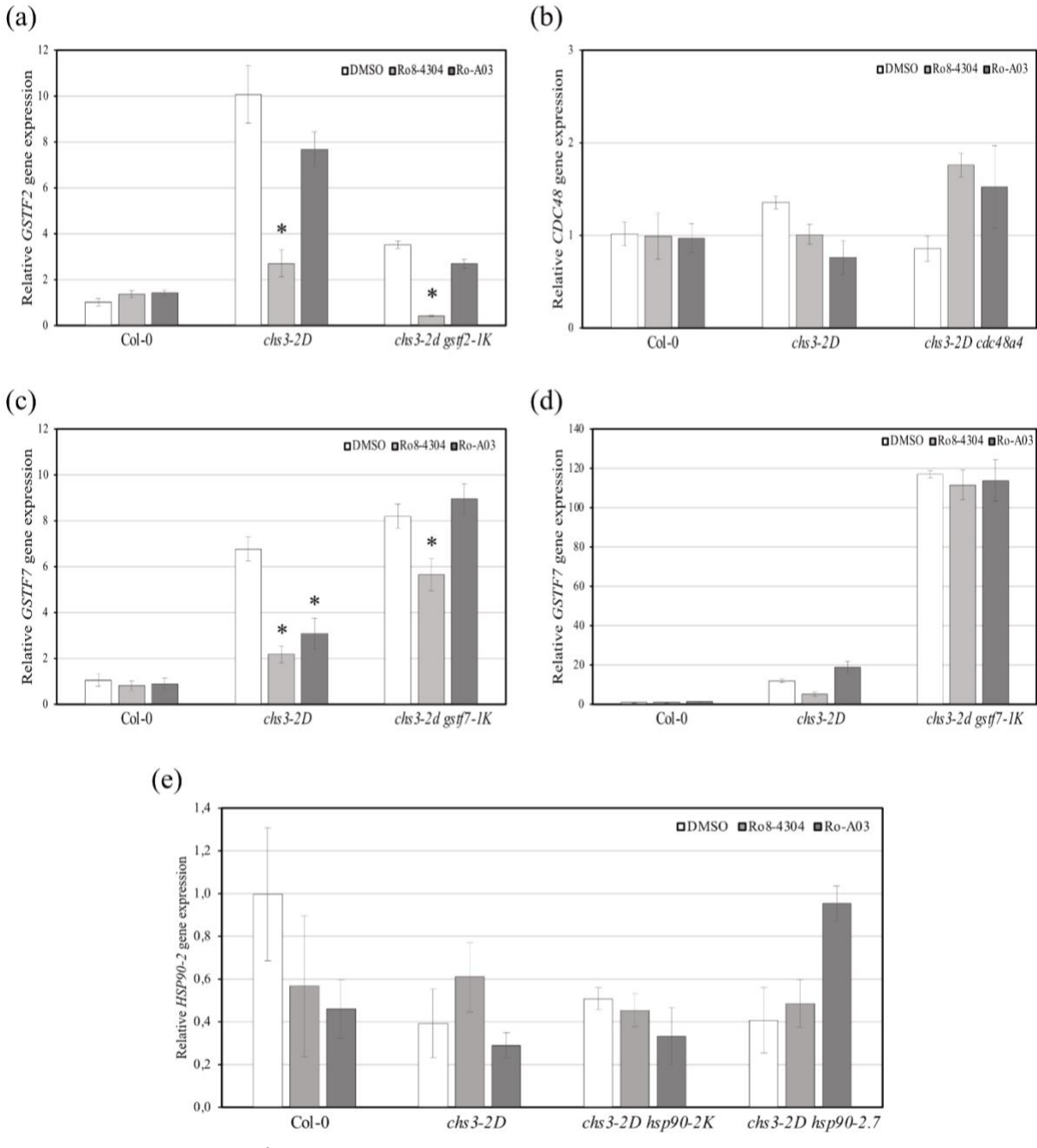


Figure 58. The expression of the binding proteins in the relevant mutants in the *chs3-2D* background. Plants were grown for 20 days at 18°C in the presence of DMSO, 50 μ M Ro8-4304, or 50 μ M Ro-A03. The relative expression is shown for *GSTF2* (a), *CDC48* (b), *GSTF7* primer pair 1 (c), *GSTF7* primer pair 2 (d), and *HSP90-2* (e). The data is normalized against the mean value of Col-0 grown on DMSO (0.1%). The data shows the mean \pm SE of three biological replicates (n=3). An asterisk indicates a significant difference to relevant mutant grown on DMSO (Two tailed Anova, Tukey test, p < 0.05).

5 Discussion and conclusion

Growth and immunity are important traits of a plant. While the farmer would opt for a crop with a respectable size, which is not harmed by pathogens. These two characteristics, growth and immunity, are regulated by small organic molecules like SA, JA, auxin, and many more [see Introduction]. A lot of the pathways that regulate the balance between growth and immunity are still unknown. Chemical genetics is a powerful tool for dissecting pathways, although for additional progress new marker compounds need to be identified, too. The chemical genetics technique had its breakthrough when Park et al. (2009) identified the ABA receptor PYR1 using the agonist pyrabactin4 ¹⁴⁹. After their success many more groups successfully identified small molecules that could alter the respective *Arabidopsis thaliana* phenotype ^{150–158}. High throughput screening also led to the identification of the chemical Ro8-4304 that was able to rescue reduced growth of the autoimmune mutant *chs3-2D* ¹⁶⁶. Nonetheless, many properties of this chemical were not studied. Hence, we used chemical and genetic tools to uncover its characteristics and determine its putative binding protein.

5.1 Characterization of properties and chemical optimization of Ro8-4304

5.1.1 Important properties of Ro8-4304 affecting growth and immunity of chs3-2D seedlings

Firstly, we demonstrated the important properties of Ro8-4304 in the *chs3-2D* background with respect to temperature, concentration and time of treatment.

At 18°C, 20°C and 22°C, the addition of Ro8-4304 rescued growth of *chs3-2D* seedlings (Figure 12). The *chs3-2D* mutant did not show an auto-immune phenotype at 24°C, according to previous publications ¹⁶⁶. The chemical Ro8-4304 did not additionally stimulate the growth of the *chs3-2D* mutant at this temperature or Col-0 at any temperature, thus indicating that Ro8-4304 is not a general growth regulator. This was confirmed by the immunity marker gene expression (Figure 28), which was significantly down-regulated when Ro8-4304 was applied to the *chs3-2D* seedlings. Therefore, it is more likely that Ro8-4304 is a regulator of immunity. The downregulation of immunity may result in an increase in growth, because immunity and growth are coupled ^{8,80}. However, testing this compound on various auto-immune mutants, incl. *chs3-1* (Figure 16) did not yield any significant increase in fresh weight, thus suggesting that Ro8-4304 is not a general immunity-regulating compound either, but has a particular chemical activity in the *chs3-2D* background. The only effect that Ro8-4304 had on Col-0 wildtype plants was in combination with ABA (Figure 45). In this case, Ro8-4304 rescued the yellowing phenotype of the ABA treatment.

The investigation of the concentration dependency of Ro8-4304 activity demonstrated that the chemical Ro8-4304 rescued growth of *chs3-2D* seedlings in the concentration range of 15 to 100 μ M (Figure 13). For the Ro8-4304 effect a treatment of only 1 day was not sufficient for rescue, whereas 2 or more days of treatment resulted in a significant rescue of growth in *chs3-2D* seedlings (Figure 15). Application of Ro8-4304 via the root system was required to happen in the first weeks of development, whereas *chs3-2D* was not susceptible to the chemical after 2 weeks of growth on MS medium (Figure 14).

Boyes et al. (2001) described four major stages in Arabidopsis development ²⁷⁰, and it seems that Ro8-4304 has an effect at the principal growth stage 0, and early principal growth stage 1. This indicated that Ro8-4304 may be able to prime *chs3-2D* for a certain developmental fate. Huang et al. (2016) sprayed *chs3-2D* with Ro8-4304 at a later stage ¹⁶⁶, and did not report any significant effect on growth or immunity. This was likely due to the late treatment, and that the seedlings cannot take up the chemical via the leaf system. Whereas the root system of a plant is more accessible for chemical uptake. It has been demonstrated that organic pollutants with low-molecular mass and volatility can be absorbed via leaves, in contrast to high-molecular mass compounds (<1000), which are more easily absorbed via roots ²⁷¹. The molecular weight of Ro8-4304 is 406.88 g/mol and it is therefore more likely that Ro8-4304 must be taken-up via the root system.

5.1.2 Ro8-4304 derivatives with novel properties have distinct effects on the performance of *chs3-2D* seedlings

The characterization of Ro8-4304 properties showed that it could be used at different temperatures and concentrations to rescue growth of *chs3-2D* seedlings (Figures 12 and 13). However, in line with the data published by Huang et al. (2016) the immunity of *chs3-2D* was reduced after treatment with Ro8-4304 (Figure 28) ¹⁶⁶, thus indicating that growth and immunity were still coupled. We therefore synthesized 18 derivatives to change and improve the properties of Ro8-4304, and eventually uncouple growth and defence (Figure 22). The synthesized analogues were tested for their potential to affect growth and immunity of *chs3-2D* seedlings. Several alterations diminished the growth rescuing effect (Figure 27), pointing to the importance of distinct functional groups for Ro8-4304 activity. While none of the analogues increased the effect of Ro8-4304, the three analogues Ro-A03, Ro-A11, and Ro-A18 were as effective as Ro8-4304 considering the rescue of growth in *chs3-2D* seedlings. It would be interesting to investigate whether an analogue containing all three modifications of Ro-A03, Ro-A11, and Ro-A18 simultaneously may even increase the fresh weight of *chs3-2D* seedlings (Figure 59).

Figure 59. The chemical structure of the perfect Ro8-4304 derivative?

With respect to the immunity response, treatment with most analogues resulted in reduced expression of the defence marker genes in *chs3-2D* when compared to control conditions (Figure 28). Though the expression was still higher when compared to the positive control condition: treatment with Ro8-4304. Changes on the fluorine site of the molecule were more harmful than changes on the benzamide site on the molecule, suggesting that the fluorine site may be the binding site of Ro8-4304. Except for Ro-A03 and Ro-A04, these analogues had a similar effect on fresh weight as Ro8-4304 and were able to have a significant immune response in comparison to Ro8-4304 treated *chs3-2D*. Indicating that removal of parts at the fluorine site of the structure is tolerable, but changes that replaces the fluorine reduces the fresh weight and immunity.

Changes on the benzamide site of the structure resulted in compounds that had a defence gene expression compared to Ro8-4304, but their growth was a bit lower compared to Ro8-4304 treatment (Ro-A08, Ro-A10 to Ro-A12). Alterations in the middle part of the structure did not improve the action of Ro8-4304 either. The analogues Ro-A13 to Ro-A18 had a higher or similar expression of defence genes in comparison to Ro8-4304, but this correlated with a lesser effect on growth. This data demonstrated that the oxygen in the middle of the Ro8-4304 structure is vital for the activity of the chemical.

The only analogue that improved growth of *chs3-2D* seedlings while keeping a reasonable amount of defence marker gene expression was Ro-A03. Previous research already indicated that incorporation of a fluorine substituent into drugs blocks biodegradation or bioactivation of the compound ^{272,273}. Removing the fluorine from Ro8-4304 may thus induce bioactivation, and therefore we assume that the fluorine atom in the original Ro8-4304 structure is probably redundant.

The data suggested that the derivative Ro-A03 may uncouple growth and defence. Treatment with this analogue rescued growth of chs3-2D seedlings while immune marker gene expression was still high (Figure 29). Infection assays with Pseudomonas syringae on Col-0 and chs3-2D plants in the presence or absence of Ro8-4304 or Ro-A03 demonstrated that *chs3-2D* indeed maintained a higher resistance in the presence of Ro-A03 (Figure 30). Bacterial growth was lower in chs3-2D grown on DMSO and Ro-A03 than in chs3-2D grown on Ro8-4304 (or Col-0 grown on any condition). Apparently, the increased defence marker gene expression of chs3-2D grown on Ro-A03 was sufficient to mount a significant pathogen defence. This was also reflected by levels of free SA and SAG in chs3-2D plants grown on those conditions (Figures 31 and 32). The amount of SA and SAG in chs3-2D grown on Ro8-4304 was as small in Col-0, and this explained why an immune response was absent. The SA levels of chs3-2D grown on Ro-A03 were also reduced, but still present, and previous literature mentioned that an amount of 10 g⁻¹ FW is sufficient for a defence response ^{44,207}. The high SA levels in the auto-immune mutant *chs3-2D* may affect its growth phenotype. This has already been observed for the snc1 mutant, in which the stunted morphological trait is recessive and dependent on SA, while the constitutive PR gene expression trait is semi dominant ²⁷⁴. Moreover, dose dependent application of benzothiadiazole (BTH), a chemical analogue of SA, reduced plant biomass and this was correlated with the induction of SA-mediated defence responses ²⁷⁵. A similar dosage effect may be present in *chs3-2D*, and the rescue of the growth by Ro8-4304 and Ro-A03 is probably due to the lower amounts of SA. The measured effect of Ro-A03 may yield intermediate SA levels, which in turn results in chs3-2D seedlings with decent growth levels and a significant strong immunity response.

5.1.3 The effect of Ro8-4304 and Ro-A03 on the methylosome mutant *chs3-2D icln2*

It has been speculated previously that Ro8-4304 may manipulate methylosome complexes and thus affect splicing ¹⁶⁶. The effect of chemical treatment with Ro8-4304 and Ro-A03 was less pronounced in the *chs3-2D icln2* double mutant originating from a cross between *chs3-2D* and the methylosome mutant *icln2* (Figure 33), but there was still a significant effect. These data were slightly in conflict with the data reported ¹⁶⁶. In any case, the methylosome is necessary for the correct splicing of transcripts and proteins ²⁷⁶. Jordan

et al. (2002) demonstrated that alternative splicing is crucial for defence responses mediated by TIR domain-containing R proteins ²⁷⁷. Moreover, Zhang and Gassman (2003) demonstrated that a truncated version of RPS4, due to alternative splicing, was not sufficient to confer resistance ²⁷⁸. So, alternative splicing of the *CHS3* gene or another gene connected to immunity may alter the *chs3-2D* phenotype considerably. Therefore, the methylosome is unlikely the direct target of Ro8-4304. However, the splicing of genes encoding the putative binding protein or an important protein necessary for the immune response might be altered in the *chs3-2D icln2* mutant. Subsequentially, changing the phenotype unintentionally, and ensuing a different chemical response to Ro8-4304.

Most of the genes of the putative binding proteins discovered in the affinity purification experiment (Figure 34 and Table 28) have been shown to be affected by alternative splicing. Thus, alternative splicing of any of these genes may have changed the phenotype and chemical activity of Ro8-4304. For example, alternative splicing of *GLRs* has not been extensively studied, but several splicing variants occur in respective genetic regions of *AtGLRs* resulting in different channel activities and specificity e.g., the splicing variant of *GLR2.4* completely lacks the gate motif ²⁴⁶. Alternative splicing of *HSP90* altered the heat response of grape and wheat ^{279,280}, and interestingly the spliceosome complex is maintained by HSP90 ²⁸¹. Additionally, it was reported that a splicing error in the SGT1b protein of TIR1-1 AUXIN RESISTANCE3 (ETA3) reduces HSC70 interaction ¹⁰⁹. So, mutation in the spliceosome already alter components necessary for the *chs3-2D* background by itself, and therefore it is not surprising that also the effect of Ro8-4304 is reduced in the *chs3-2D icln2* mutant.

5.2 May the identified putative binding proteins play a role in Ro8-4304 activity?

By coupling Ro8-4304 to a matrix we identified several putative Ro8-4304 binding proteins (Figure 34 and Table 28). The coupling was achieved via the benzamide side of the molecule leaving the fluorine side of the molecule intact. Since the removal of the fluorine drastically affected the activity of Ro8-4304, we suspected that the fluorine environment may be most important for binding. All the identified proteins have some relationship to immunity and/or growth, and by double mutant analyses we could show that some of these putative binding proteins may be important for the *chs3-2D* phenotype (Figures 56-58). In addition, we identified GLRs as putative targets of Ro8-4304 by literature search. For all candidate binding proteins, the putative role in Ro8-4304 activity will be discussed based on pharmacological analyses and the data from characterization of the generated double mutants between *chs3-2D* and mutant lines lacking expression of the respective genes encoding candidate binding proteins.

5.2.1 The possible role of GLRs in Ro8-4304 activity

The literature research indicated that Ro8-4304 in analogy to the mammalian system may bind GLRs ^{208,209}. The study of Vincent et al. (2017) provided direct evidence for the involvement of BAK1 in inducing PTI via GLR3.3 and GLR3.6 by the release of Ca²⁺²⁰, thus supporting why GLRs have been shown to be involved in immunity ^{25,26,233,261,282,283}. Therefore, we hypothesized that Ro8-4304 binds one or more GLR(s), hereby potentially blocking Ca²⁺ signalling and the corresponding immune response in the *chs3-2D* seedlings.

According to human literature, ifenprodil and Ro8-4304 share the same target and have a similar structure ^{208,209}. However, adding ifenprodil to *chs3-2D* seedlings, in combination with Ro8-4304 only resulted in lower fresh weights when compared to adding Ro8-4304 only (Figure 37). This was unexpected since normally we would have expected that an inhibitor would yield a higher fresh weight. Previous literature indicated that GLRs have evolved divergently in humans and plants ^{211,212,246}. Thus, NMDA analogues may still be able to bind with unique properties or only bind to certain GLRs, which may explain the different effect of these two similar chemicals, namely ifenprodil and Ro8-4304. It can also be that the respective binding of both chemicals to a target protein requires the same binding site, and adding both chemicals at the same time, in this case ifenprodil and Ro8-4304, results in an unfavourable competition.

In addition to ifenprodil, the plant NMDA antagonistic DNQX, which is active in plants, was used for treatment of chs3-2D seedlings in the presence of Ro8-4304. This treatment resulted in a diminished effect of Ro8-4304 on growth rescue in chs3-2D seedlings, similar to ifenprodil (Figure 40). This was somehow contradictory to previous reports indicating that DNQX inhibits the Ca²⁺ signalling via GLRs, normally resulting in a compromised resistance ^{25,217,225,226,240,261}. Therefore, we treated the *chs3-2D* seedlings with the plant active NMDA agonist L-BMAA (Figure 41). Activating the GLRs with the agonist BMAA resulted in a small increase in the fresh weight of chs3-2D, and in combination with Ro8-4304 this chemical could even boost the fresh weight response. Furthermore, the substrates spermine and spermidine showed the same effect (Figures 43 and 44). Additionally, we tested some of the amino acids known to activate GLRs (Figure 52), but only the amino acid L-Met affected the chemical response of Ro8-4304 in the chs3-2D seedlings. It has been published that the most effective agonist for GLR1.4 and GLR3.2 is Lmethionine ^{224,284}. Additionally, the effect of L-Met on ROS production and stomatal movement has been demonstrated ²⁸³. Hence, L-Met may be the only amino acid able to alter GLR function and the effect of Ro8-4304 in the chs3-2D background.

Since Ca²⁺ signalling is important for the GLRs response, plants were also stressed with an excess of Ca²⁺, low Ca²⁺, and disturbed Ca²⁺ signalling. Adding CaCl₂ to the medium did not affect the growth of *chs3-2D* seedlings (Figure 38). Adding the Ca²⁺ chelator EGTA to the media was generally too detrimental (Figure 39). However, at this stage it is unclear if this is due to the detrimental effect of the Ca²⁺ deficiency on a developmental pathway, or if Ca²⁺ is necessary for the effect of Ro8-4304, or if both hypotheses are valid. Inhibiting Ca²⁺ signalling using TFP resulted in smaller plants (Figure 42). In line with that, it was published that the expression of defence genes can be negatively regulated by CaM-binding transcription factors ²⁸⁵.

Finally, we tested one more substrate, GSH that has been shown to bind to GLRs ²¹⁴ (Figure 46). Adding GSH to *chs3-2D* seedlings reduced the effect of Ro8-4304. This reduction was not due to its redox activity, because DTT did not affect *chs3-2D* seedlings (Figure 47). Adding GSH in a concentration dependent manner showed a clear competitive effect (Figure 48), indicating that GSH and Ro8-4304 may bind at the same site. Lowering the internal GSH content with BSO was generally too damaging to the seedlings for conclusive results.

Generally, all results following treatments, with the different chemicals connected to GLRs, turned out to be opposite to the effect of these chemicals in mammalian cells. Blocking GLRs with inhibitors reduced the effect of Ro8-4304 and increased the immune response, while agonists and substrates increased both processes, except for GSH and L-Met.

To possibly unravel the underlying mechanism, in a next step *chs3-2D glr3.3* double mutants were generated by crossing the respective single mutants. In comparison to *chs3-2D* single mutants, growth reduction of *chs3-2D glr3.3* double mutants was even more pronounced (Figures 53, 54, and 55), and these mutants were significantly less responsive to the Ro8-4304 (Figure 53). Moreover, their immunity remained high with and without chemical treatment (Figure 55). Considering all this data, we hypothesize that *GLRs* suppress an unknown response in the *chs3-2D* background, and somehow Ro8-4304 can antagonize this effect.

One more chemical tested in combination with Ro8-4304 was ABA. This chemical severely affected the *Arabidopsis thaliana chs3-2D* mutant. The senescence induced by both the immune phenotype and ABA may be too much for the plants to handle. Interestingly, Col-0 grown on ABA has a yellowing phenotype but in the presence of Ro8-4304 this is not detectable. So, Ro8-4304 seems to be able to revert or block the ABA induced senescence in Col-0. Strikingly, this is the only time in this experimental work that we see an effect of Ro8-4304 on Col-0. *Chs3-2D* grown on both ABA and Ro8-4304 had a reduced yield in comparison to *chs3-2D* grown on Ro8-4304, nevertheless the disastrous effect of ABA was counteracted. Kang et al. (2004) ²³⁷ demonstrated the effect of inhibitory or stimulatory chemicals on AtGLR1.1, which in turn induced or inhibited ABA biosynthesis. So, in a similar way, Ro8-4304 may activate GLR1.1, induce a calcium flux and via this route inhibit ABA synthesis, hereby rescuing the phenotype of Col-0 and *chs3-2D*. The effect of this rescue is less successful in *chs3-2D* in comparison to Ro8-4304, but the concentration of ABA may be too high in the *chs3-2D* background for a complete rescue.

Another option may be that Ro8-4304 does not bind GLRs but is transported through the receptor pocket. Inhibiting GLRs using DNQX, ifenprodil, or GSH would block entry of Ro8-4304 and therefore the chemical is unable to bind and affect its intracellular target proteins. On the other hand, activating the receptor by using BMAA or spermine, opens the transporter, so that Ro8-4304 can enter more easily. However, such transport of small molecules through GLRs has not yet been demonstrated to our knowledge.

Taken together, the data did not explain the action of Ro8-4304 on growth of *chs3-2D* seedlings by direct binding to GLRs. Therefore, we continued with an affinity purification via matrix-bound Ro8-4304 to pull down putative target binding proteins. This approach did not result in the pull down of any GLR protein (Figure 34 and Table 28), suggesting that GLR is not a direct target of Ro8-4304 or that the chosen condition did not allow for pull down of membrane receptor proteins, which are generally harder to pull down than cytosolic proteins.

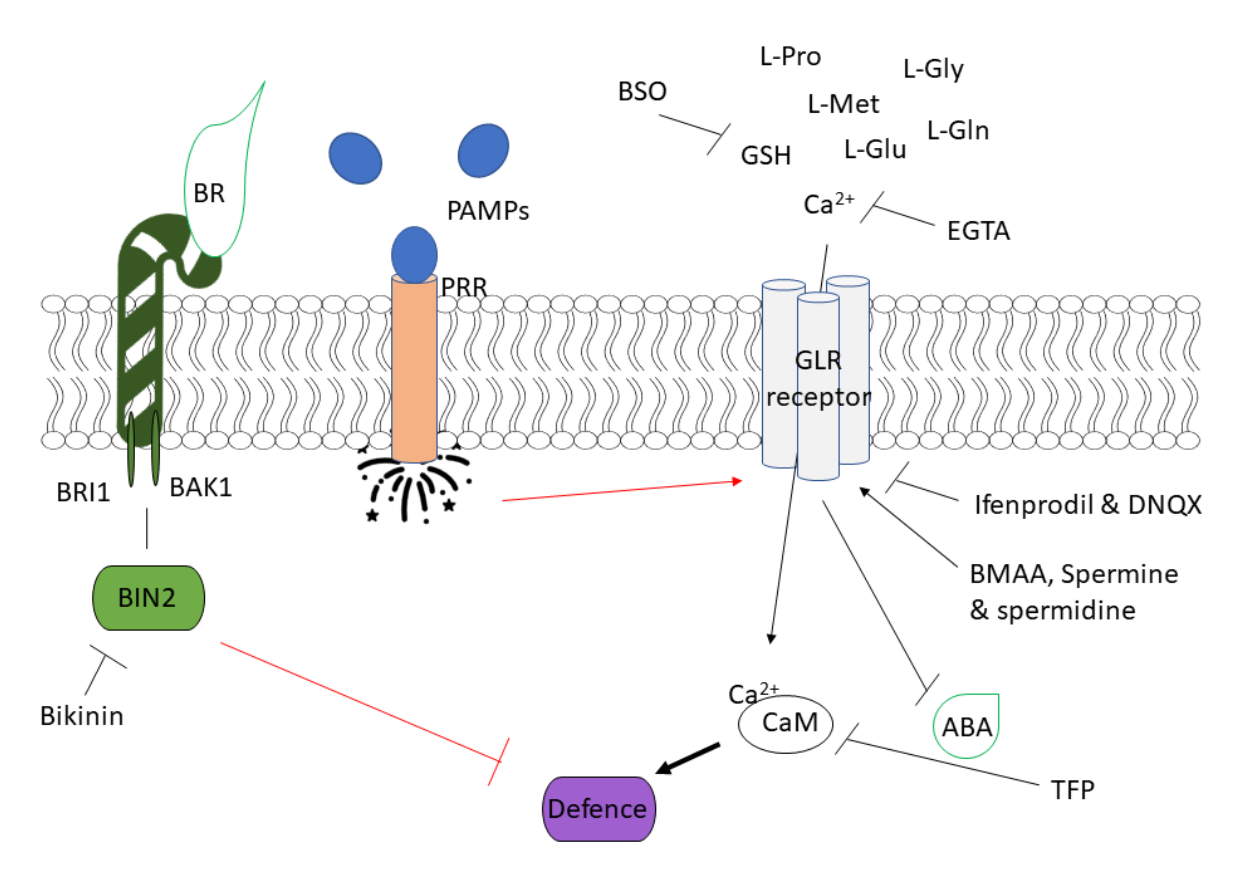


Figure 60. Schematic representation of a few interactions of GLRs, as discussed in Section 5.2.1. The agonist and antagonists used in the pharmaceutical analysis and the respective molecular targets are indicated. Arrows and blunted lines represent positive and negative regulations. The black lines indicate known connections, whereas red lines indicate unknown connections or missing steps between components of the pathway. Grey lines indicate protein-protein interactions.

5.2.2 The role of the putative binding protein CDC48A in Ro8-4304 activity

One of the binding proteins found was CYCLIC DIVISION CYLCE 48 (AtCDC48A). CDC48A was demonstrated to be a negative regulator of NLR mediated immunity in Arabidopsis ¹⁸². Mutant *cdc48a* plants with a loss-of-function allele of *CDC48A* showed dwarf morphology and enhanced disease resistance ¹⁸². It seemed that CDC48A also regulated immunity in the *chs3-2D* background, while plants carrying both mutations were smaller than *chs3-2D* plants (Figure 56). Moreover, the chemical UPC, which acts on the human CDC48 analogue ^{254,255}, demonstrated the same inhibiting effect on *chs3-2D* seedlings (Figure 51). In addition, the effect of Ro8-4304 was reduced in both the double mutant and plants treated with UPC (Figure 51). This at least seems to indicate a synergy between CDC48 and Ro8-4304, however it is unlikely that this is due to a direct interaction. If Ro8-4304 would directly bind CDC48, a more severe immune phenotype would be expected in the *chs3-2D* background. While inhibition of CDC48A would theoretically lead to a stronger immune phenotype.

The reduced effect of Ro8-4304 in the *chs3-2D cdc48* mutant may also be due to additional reasons. It was previously demonstrated that CDC48 interacts with cytosolic ascorbate peroxidase (cAPX), and that overexpression of *CDC48* resulted in a reduced cAPX activity and as consequently lower levels of GSH ²⁸⁶. Thus, higher levels of GSH may be

present in the *chs3-2D cdc48a* mutant, and we demonstrated that higher amount of GSH negatively impacts the effect of Ro8-4304 in the *chs3-2D* seedlings (Figure 47).

The *chs3-2D cdc48* mutant may also have a different phenotype due to its effect on GLRs. Previous publications demonstrated that CDC48 regulates NLR turnover by ubiquitination ^{182,287,288}. E.g., the human analogue of CDC48/p97 interacts and promotes the formation of the glutamate receptor AMPA ²⁸⁹, and interestingly in yeast the chaperone HSP70 is necessary for this action ²⁹⁰. Bègue et al. (2019) discovered that CDC48 and PROTEASOMAL REGULATORY PARTICLE AAA-ATPase-3 (RPT3) form a complex ²⁹¹, and that a mutation in the *Arabidopsis thaliana RPT3* resulted in a BMAA insensitive morphology dependent on GLRs ²³⁰. It may therefore well be that the *cdc48a* mutation exhibits a BMAA insensitive morphology due to its effect on GLR turnover. And if the action of Ro8-4304 is dependent on GLRs, the reduced turnover of GLRs in *chs3-2D cdc48a* may affect the chemical activity of Ro8-4304 in the *chs3-2D cdc48a* mutant.

In conclusion, the effect of Ro8-4304 in the *chs3-2D cdc48a4* mutant might be altered due to the influence of CDC48 on GLRs and/ or GSH. Aryal et al. (2017) pulled down the CDC48 protein in one of the largest known protein complexes ²⁹², and interaction with three other binding proteins has been demonstrated (HSP90-2, GAPC1, HSP70) ^{290–293}. So, binding of Ro8-4304 to E.g., HSP90-2 may have resulted in the additional pull-down of CDC48 due to complex interactions.

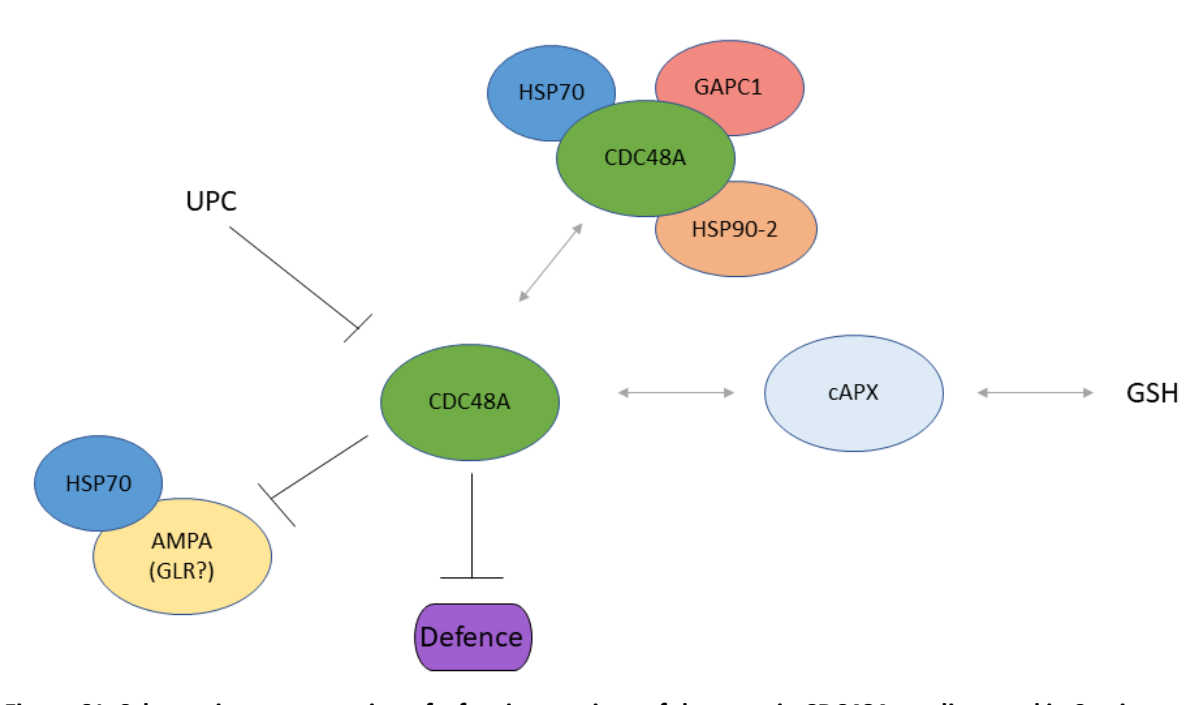


Figure 61. Schematic representation of a few interactions of the protein CDC48A, as discussed in Section 5.2.2. The antagonists used in the pharmaceutical analysis and the respective molecular target is indicated. Arrows and blunted lines represent positive and negative regulations. The black lines indicate known connections. Grey lines indicate protein-protein interactions.

5.2.3 The role of the putative binding protein TKL1 in Ro8-4304 activity

TRANSKETOLASE 1 (TKL1) was another identified protein with potential binding to Ro8-4304. This protein is important in the Calvin cycle and oxidative pentose phosphate pathway

(OPPP). It catalyses the synthesis of erythrose-4-phosphate (E4P), which is a precursor for the shikimate pathway and for secondary metabolites involved in plant defence ^{294,295}. Due to its importance in the Calvin cycle, knock out mutants have been shown to be lethal at the embryo stage ²⁹⁶, thus prohibiting the generation of double mutants with *chs3-2D*. Rocha et al. (2014) determined that TKL is an important regulator of carbon allocation controlled by calcium-dependent phosphorylation ²⁹⁷. The EGTA treatment resulted in severely damaged plants (Figure 39). Correspondingly, a small decrease in TKL content due to low Ca²⁺ levels resulted in reduced levels of E4P, leading to photosynthesis inhibition and a significant decrease in aromatic amino acids and soluble phenylpropanoids ^{294,297}. Thus, the amount of calcium present inside the plant determines whether TKL supports growth or immunity. Additionally, GLRs have been shown to transport Ca²⁺²⁴, so the action of GLRs and TKL1 might be linked. Disrupting GLRs with by Ro8-4304 treatment may alter the TKL1 pathway as well, while lower amounts of free calcium may induce a different phosphorylation state of TKL.

In theory, Ro8-4304 could bind TKL1, because TKL1 is a positive regulator of immunity. Tobacco plants overexpressing *TKL* exhibited a smaller and chlorotic phenotype comparable to other auto-immune mutants ²⁹⁸. But we do not consider it to be highly likely. The action of TKL1 is quite universal, and if Ro8-4304 would act on TKL1 we would hypothesize that Ro8-4304 treatment affects significantly more (auto-immune) mutants.

Zhao et al. (2018) tried to identify the proteins that were affected by a treatment of the herbicide α -terthienyl, and interestingly they discovered some of the same binding proteins as we did e.g., TKL1, HSC70-1, and GST DHAR2 ²⁹⁹. Binding of Ro8-4304 to any of these proteins may have resulted in a pull-down of a complex including TKL1. Furthermore, these three proteins have all been shown to be subjected to glutaredoxins reactions ³⁰⁰. Indicating that pull down of TKL1 may be due to GSH, while this compound is important for glutaredoxins reactions but also an important substrate of GSTF, and GLRs, and an interesting modulator of the effect of Ro8-4304 in *chs3-2D* seedlings (Figure 46).

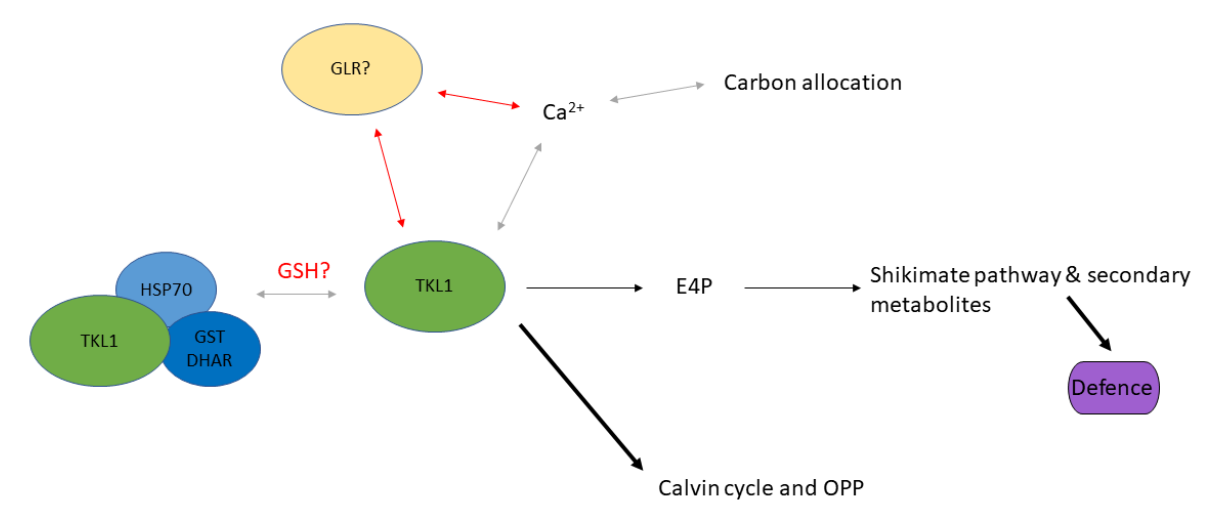


Figure 62. Schematic representation of a few interactions of the protein TKL1, as discussed in Section 5.2.3. Arrows and blunted lines represent positive and negative regulations. The black lines indicate known connections, whereas red lines or text indicates unknown connections or missing steps between components of the pathway. Grey lines indicate protein-protein interactions.

5.2.4 The role of the putative binding protein GAPC in Ro8-4304 activity

TKL has the same localization as one of the other identified proteins, namely GLYCERALDEHYDE-3-PHOSPHATE DEHYDROGENASE C SUBUNIT (GAPC) ²⁹⁴. Although, this is not surprising since GAPC, a subclass of glyceraldehyde-3-phosphate dehydrogenase (GADPH), is also involved in the Calvin cycle and oxidative pentose phosphate pathway (OPPP) ³⁰¹. Knocking out GAPC resulted in dwarfism, sterility, and drastic changes in the amino acid balance, especially in serine homeostasis ^{301,302}. Which has been shown to be one of the most important amino acids for activation of GLRs ^{24,217,284}.

It was reported that GADPH is a negative regulator of immunity ^{303,304}. Therefore, if Ro8-4304 would bind GAPC, the active site would be blocked, and the protein activity would be reduced leading to an increased immunity. This is the opposite of what we see with the regular Ro8-4304 treatment (Figure 28), and therefore it is highly unlikely that GAPC is the direct binding target of Ro8-4304.

It is more likely that the action of GAPC is altered via GSH. It was reported that catalytic cysteine residues in GAPC are altered after a stress response $^{305-307}$. Oxidation of GAPC1 by $\rm H_2O_2$ in the presence of GSH leads to aggregation and inactivation of GAPC1 306,308,309 , resulting in an immune response 303 . We could hypothesize that Ro8-4304 is able to affect the redox state of cells. On the other hand, it may be that not GSH, but HSP is predominant for the action of GAPC in the *chs3-2D* background, while molecular chaperones affect protein aggregation $^{309-311}$. Additionally, Vescovi et al. (2013) reported that the treatment with cadmium led to enhanced nuclear accumulation of Arabidopsis GAPC1 in root tip cells 307 . And HSP chaperones have been demonstrated to translocate proteins 312,313 . Furthermore, Zemanovic et al. (2018) demonstrated that HSP70 directly participate in reactive oxygen metabolism and altering of redox balance, which is important for the action of GAPC 314 .

Therefore, it is possible that GAPC has been pulled down in combination with HSP90, or due to its vulnerability to GSH.

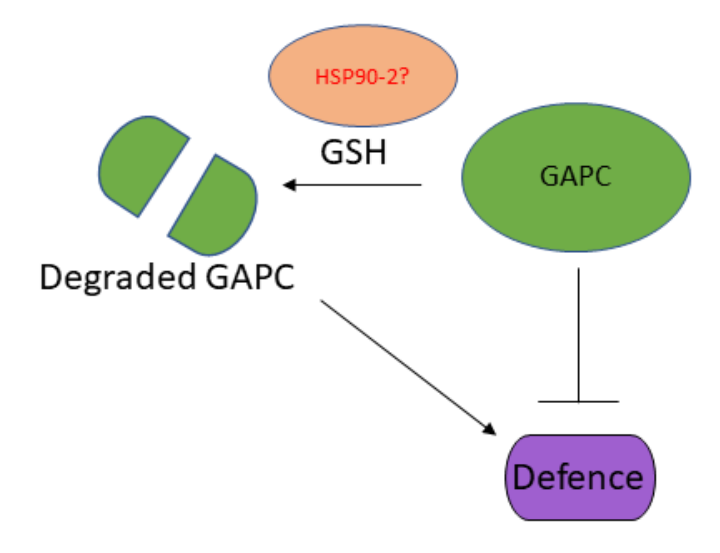


Figure 63. Schematic representation of an interaction of the protein GAPC, as discussed in Section 5.2.4. Arrows and blunted lines represent positive and negative regulations. The black lines indicate known connections, whereas red lines or text indicates unknown connections or missing steps between components of the pathway.

5.2.5 The role of the putative binding protein HSC in Ro8-4304 activity

HEAT SHOCK COGNATE 70 (HSC70), the constitutively expressed version of HSP70-1, has been reported to be involved in immunity $^{315-317}$. Interestingly, HSC70 chaperones interact with SGT1a in the nucleus and cytosol 315,316,318 , and both the HSC70 and SGT1 protein have been reported to associate with HSP90 $^{317-319}$. This association is regulated in a Ca²⁺-dependent manner 318 . So, HSC70 can interact with the other pulled down HEAT SHOCK PROTEIN (HSP81-2/HSP90.2). Moreover, we demonstrated that ABA treatment altered the chemical response of Ro8-4304 (Figure 45) and it has previously been reported that plants overexpressing HSC70-1 or with a reduced HSP90.2 activity were hypersensitive to ABA 317 .

The binding of Ro8-4304 to HSC70 is quite likely but will be discussed more thoroughly in the following section.

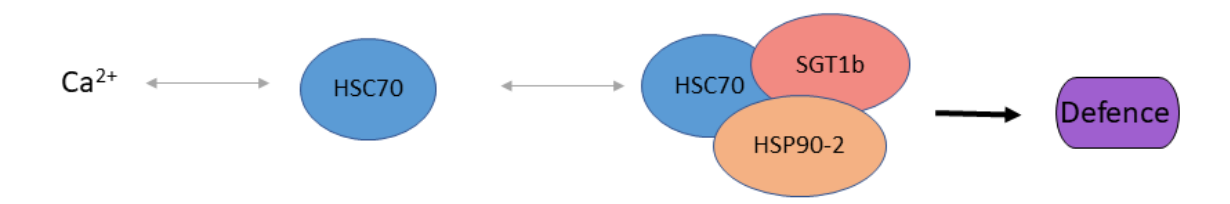


Figure 64. Schematic representation of an interaction of the protein HSC70, as discussed in Section 5.2.5. Arrows and blunted lines represent positive and negative regulations. The black lines indicate known connections. Grey lines indicate protein-protein interactions.

5.2.6 The role of the putative binding protein HSP90 in Ro8-4304 activity

Interestingly, all four proteins discussed in the previous sections, have been demonstrated to interact with HEAT SHOCK PROTEIN 90.2 (HSP90.2), also known as HSP81-2, and this HSP90.2 protein was described to be a positive regulator of immunity ⁷². Therefore, we think that there is a high probability that Ro8-4304 directly binds to HSP90. Besides, previous publications already demonstrated that many small molecules could disrupt HSP90 action ³²⁰. Additionally, *HSC70*, *HSP90*, and *SGT1b* have been shown to be essential for the *chs3-2D* phenotype ^{88,89}, because knock outs of these proteins partially suppress the *chs3-2D* phenotype. So, a direct or indirect action of Ro8-4304 on HSC70 and/or HSP90 may alter the chaperone function and hereby the phenotype of *chs3-2D*.

It has been demonstrated that plants without functional HSP90s or their co-chaperone RAR1 exhibit reduced R protein-mediated immunity ³²¹, and they also accumulate fewer immune receptors including RPM1 ¹⁸³ and RPS5 ³²². This suggests that HSP90 chaperones are critical for the stability of NLRs and the formation of the immune receptor complex ³²³. Modification to this system, using Ro8-4304 treatment, may alter the *chs3-2D* phenotype.

However, chs3-2D is not the only immune genotype dependent on SGT1b and HSP90. Other mutants that dependent on this pathway include chs1-1, chs2-1, chs3-1, ssi4 and snc1. However, testing chs1-1 and chs2-1 did not yield any conclusive results [data not shown]. The chs3-1 mutant showed a slight response to Ro8-4304 (Figure 16), but this was insignificant. One reason could be that the phenotype of chs3-1 is less severe, and therefore

the rescue with Ro8-4304 is less distinct. Therefore, it would be helpful if the treatment of the chemical is improved, so Ro8-4304 can also be tested auspiciously on other autoimmune mutants, which are dependent on *HSP90*.

The exclusive action of Ro8-4304 in *chs3-2D* seedlings can also be explained otherwise. E.g., *SNC1* has been shown to be repressed by three modes of regulation ³²⁴. Different modes of regulation between auto-immune mutants may halt the effect of Ro8-4304 in divergent auto-immune mutants. Next to that, previous publications showed that the co-chaperones RAR1 and SGT1b act additively or antagonistically on HSP90 function for different R proteins ^{322,325,326}. This rationalizes why only CHS3 seems affected by Ro8-4304. Thus, an exact balance between RAR1, SGT1b and HSP90 may be critical for the activity of Ro8-4304. Moreover, Prince et al. (2015) demonstrated that their chemical treatment only influenced certain HSP90 protein isoforms ³²⁷. So, various auto-immune mutants may have different HSP90 proteins isoforms, with different chemical sensitivity. And this distinction may also explain why Ro8-4304 doesn't have any significant effect in any other auto-immune mutants.

The *chs3-2D* mutant is dependent on *HSP90* ⁸⁸, but the *chs3-2D* mutant does not demonstrate a similar phenotype compared to other auto-immune mutants, possibly due to a semi-dominant nature ⁸⁴. As mentioned in Section 5.2.1 knocking out the *GLR* genes would normally result in a decreased immunity and an increase of the fresh weight. But introducing the *glr3.3* mutation in the *chs3-2D* background, resulted in a decrease of the fresh weight in contrast to other mutants. The *chs3-2D* mutant was created by ethyl methane sulfonate mutagenesis ⁸⁴, and it is unlikely but still possible that there is an additional mutation, which is necessary for Ro8-4304 to have an effect. This would also explain the uncertainty with the crossings (Figure 54). To be certain that the effect is only due to a mutation in *CHS3* and not any other gene, sequencing results needs to be confirmed.

As mentioned above, most of the putative proteins pulled down by the affinity purification have a direct link with HSP90. CDC48a is an important regulator of the NLR turnover stability ^{182,287,288}, being necessary to deploy the ubiquitin ligase complex. This regulation is dependent on SGT1, HSP90, SKP1 and SCF ²⁸⁸ and is important in the removal of unfolded NLRs ^{182,293}. The *chs3-2D cdc48a4* mutant did not demonstrate an effect of Ro8-4304 (Figure 56), even though we hypothesized that Ro8-4304 binds HSP90 and not CDC48. But the rate of ubiquitination is probably reduced in the *chs3-2D cdc48a4* mutant and therefore CHS3 is not ubiquitinated nor degraded. Even though Ro8-4304 may bind HSP90 in this mutant, the degradation and the removal of CHS3 cannot take place, and therefore there is no effect of Ro8-4304 in *chs3-2D cdc48a* (Figure 56).

Previously, we also hypothesized that the *GLRs* suppress something in the *chs3-2D* mutant (Section 5.2.1). It has been demonstrated that Ca²⁺ and CaM3 are necessary for the expression of certain HSPs ^{328–330}. But interestingly, in sugar beet, not all HSPs were regulated by Ca^{2+ 330}. Treatment of EGTA and TFP may induce a smaller phenotype in the *chs3-2D* seedlings (Figures 39 and 42) due to the lower expression of HSP proteins which are also important in developmental pathways. The double mutant *hsp90.1^{KO} hsp90.2* was demonstrated to be lethal ⁷², due to the reduced HSP chaperone activity in development. Treatment of the antagonists DNQX or ifenprodil (Figures 37 and 40) could reduce internal

Ca²⁺ levels, and hereby also inhibit the expression of certain HSPs, while both treatments reduce the fresh weight of Col-0 and *chs3-2D*, albeit insignificantly.

Intriguingly, Hop/Sti1 is a co-chaperone that binds to both HSP90 and HSP70 to fold proteins into complexes such as the glucocorticoid receptor ^{331,332}, a special NMDA receptor. It has been reported that HSP90 must be bound to the ligand-binding domain (LBD) of the glucocorticoid receptor (GR) to induce a high steroid binding affinity ³³². Additionally, it was demonstrated that HSP70, Ssa1P and two HSP40s are required for the efficient degradation of NBD2, in complex with CDC48p ²⁹⁰. So, HSP90 and HSP70 might be able to interact with GLRs and induce the right conformation for Ro8-4304 to function or enter.

An optional explanation might be that as soon as a substrate binds to a GLR, the conformation of the GLR changes. After this conformational change, HSP90 might be tightly bound to the GLR and be unable to execute its other functions. It was already demonstrated that the dynamic HSP90-mediated cycling of ligand-bound steroid receptors is necessary for receptor trafficking to the nucleus ^{333,334}.

Moreover, Clément et al. (2011) reported that HSC70 and HSP90 can modulate ABA dependent physiological response ³¹⁷, and these ABA responses can either act positively or negatively on immunity depending on the situation ³³⁵. The data showed that Ro8-4304 can rescue the effect of ABA in WT (Figure 45). In the *chs3-2D* mutant the simultaneous treatment with Ro8-4304 and ABA resulted in a lower fresh weight, possibly indicating an effect of Ro8-4304 on HSP90 and ABA.

Furthermore, the bikinin treatment (Figure 35) may indicate the importance of HSP90 for the action of Ro8-4304. Bikinin directly binds and inhibits GSK3 BIN2, hereby activating downstream BR signalling ¹⁵¹. The *BRI1* receptor normally associates with *BAK1* to regulate the gene expression of plant growth and development via the *BES1* and *BZR1* transcription factors ¹¹³. But the BAK1 receptor also has been demonstrated to associate with FLS2 and EFR in the presence of PAMPs to induce immune signalling ¹¹⁴. Belkhadir et al. (2012) demonstrated that BR biosynthesis and signalling can be rate-limiting modulators for the *BAK1*-immune mediated responses due to a limited amount of the receptor ¹¹⁵, and we already demonstrated that the immune phenotype is necessary for the action of Ro8-4304 (Figure 12). Moreover, the immune chaperone HSP90 is necessary for the trafficking of BIN2–HSP90 complexes into the cytoplasm and the corresponding brassinosteroid signalling ¹¹⁷. Therefore, activating the brassinosteroid developmental pathway via HSP90 may reduce the immunity pathway and by this the effect of Ro8-4304 might be altered.

Lu et al. (2022) demonstrated that the *chs3-2D* phenotype is dependent on HSP90 ⁸⁸. A mutant allele in the *chs3-2D* background resulted in a partial rescue of the phenotype ⁸⁸. Interestingly, in the crossings *chs3-2D hsp90-2K* and *chs3-2D hsp90-2.7*, this effect was not visible (Figure 56). The pharmaceutical analysis with GDA was also unsuccessful (Figure 50). *Chs3-2D* grown on GDA was a bit larger, however this effect was not significant, also in combination with Ro8-4304 no significant difference could be detected. The concentration of GDA might have been too low, however GDA is known to be light sensitive ¹¹², and this may have affected the results. Moreover, Hubert et al. (2009) already demonstrated that certain alleles and mutations of *HSP90.2* e.g., *hsp90.2-5* (SALK_058553), *hsp90.2-7* and *hsp90.2-8* do not display pronounced phenotypes ⁷², due to redundancy. Furthermore, the *HSP* mutations realized in the mutants are quite upstream of the gene (Figure 9) and are probably not substantial enough to alter the active form of HSP90, while RT-qPCR indicated that expression of *HSP90* was still present in the mutants (Figure 58). Moreover, an earlier

publication demonstrated that one of the other three cytosolic HSP90s can compensate for the loss of one HSP90 ^{183,269}. Therefore, it is quite hard to create a suitable *HSP90* mutant. And this might also explain why the growth was not rescued in the *chs3-2D hsp90-2K* and *chs3-2D hsp90-2.7* mutants.

Despite this, we could demonstrate that the *HSP90* mutation altered the action of the chemical (Figures 56 and 57). Ro8-4304 and Ro-A03 were able to increase the fresh weight of *chs3-2D hsp90-2K* and *chs3-2D hsp90-2.7*, but this was significantly less compared to the original activity of Ro8-4304 in *chs3-2D* seedlings (Figure 56). Albeit the developmental activity of the HSP90 immune response was not altered, the binding of Ro8-4304 to HSP90 might be different in the double mutants compared to the single mutant.

Prince et al. (2015) demonstrated that small molecule inhibitors have a binding preference for certain isoforms of HSP90 ³²⁷, and this is likely important for Ro8-4304 as well. The other HSP90s might be able to rescue the auto-immune phenotype of *chs3-2D* and keep the fresh weight low in *chs3-2D hsp90-2K* and *chs3-2D hsp90-2.7*. However, the binding of Ro8-4304 might be specific for HSP90-2 and since the binding is specific to a certain isoform, the chemical effect of Ro8-4304 is significantly reduced in the *chs3-2D hsp90-2K* and *chs3-2D hsp90.2-7* mutants (Figures 56 and 57). Thus, the redundant nature of HSP90 rescues the fresh weight, but not the chemical activity to Ro8-4304.

If Ro8-4304 and Ro-A03 bind HSP90, we could hypothesize that these chemicals have an effect in wild-type after infection. However, bacterial growth in Col-0 grown on Ro-A03 was not lower than control conditions (Figure 30). However, previous work researched the expression of genes in *Arabidopsis thaliana* after infection with *Pst* ^{336,337}, and *HSP81-2* (or *HSP90*) was not significantly differentially expressed in comparison to untreated Col-0. So, if Ro8-4304 and Ro-A03 only act on a certain isoform of HSP90, it is not surprising that Ro-A03 is unable to rescue Col-0 infected with *Pst*. It might be interesting to challenge Arabidopsis with other pathogens, which activate an immune response relying on *HSP90*, to see if Ro8-4304 has an effect in these conditions.

Lastly, if Ro8-4304 binds HSP90 we could possibly explain the results of the pulse chase experiments. The developmental stage of a plant is important for the defence establishment in the presence of a pathogen or defence stimulator ¹⁸⁹. In the *chs3-2D* mutant the defence response is always on. When Ro8-4304 is applied in the first weeks of growth, HSP90 is bound, and the immune phenotype is immediately reversed (Figure 14). However, after two weeks the immune phenotype is too severe or in other words, too many active NLR receptors are already available for a constitutive immune response. Treatment of Ro8-4304 at this stage is counterproductive, while the immunity phenotype cannot be reversed to the original order. To summarize, binding of Ro8-4304 to HSP90, in week 3, cannot nullify the amount of NLRs and overrule the immunity repones. Additionally, a significant rescue was only visible after 2 days (Figure 15), because at that time sufficient HSP90 was captured to change the amounts of NLR and to induce rescue.

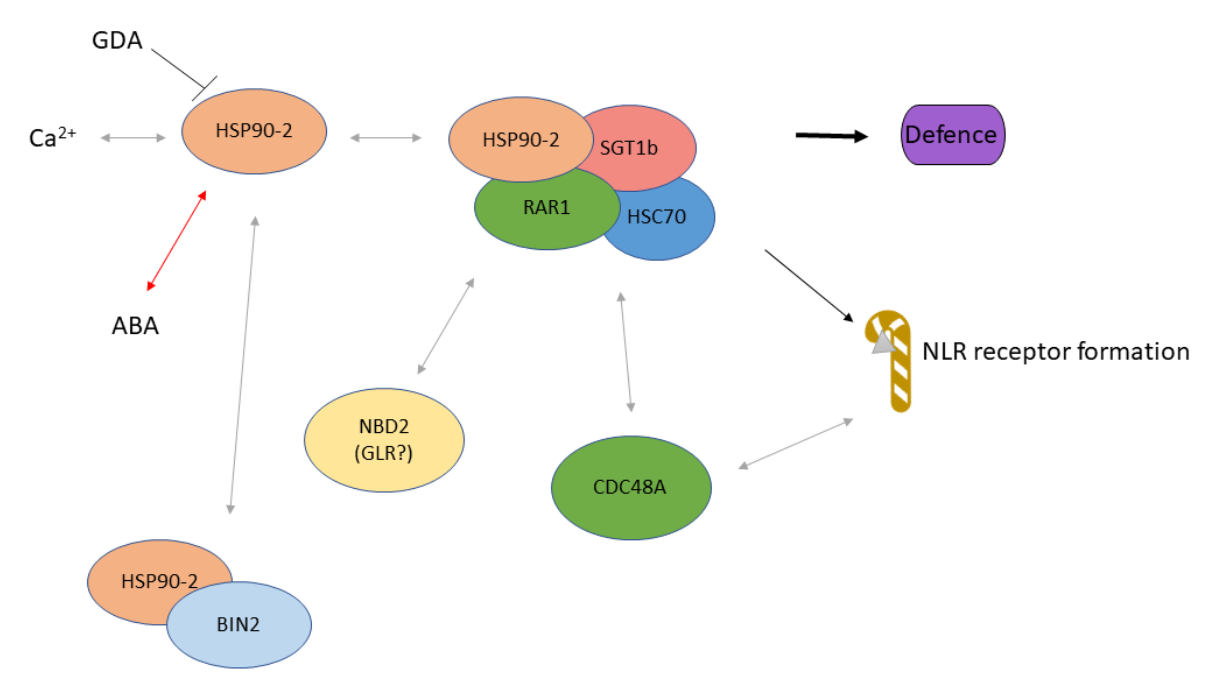


Figure 65. Schematic representation of a few interactions of the protein HSP90-2, also known as HSP81-2, as discussed in Section 5.2.6. Arrows and blunted lines represent positive and negative regulations. The black lines indicate known connections, whereas red lines or text indicates unknown connections or missing steps between components of the pathway. Grey lines indicate protein-protein interactions.

5.2.7 The role of the putative binding proteins GSTF2 and/ or GSTF7 in Ro8-4304 activity

Another protein pulled down was Glutathione-S-transferase 2 & 7 (GSTF2/ GSTF7).

Interestingly, the expression of HSP70 and HSP90.1 is induced by GSH, and this induction also increases the chaperone effect of HSP70 on GSTF2 ³³⁸. This hypothesis would be in line with the GSH treatment (Figures 46 and 48). Addition of GSH would increase the expression of HSP90, and higher amounts of HSP90 would lead to the correct folding of the NLR protein and a diminished effect of Ro8-4304 (Figures 46 and 48). DTT does not enhance the expression of HSP ³³⁸, and treatment of DTT does therefore not affect the Ro8-4304 treatment (Figure 47).

Samakovli et al. (2014) demonstrated that a decrease in the amount of nuclear HSP90.1 or HSP90.3 shifts the equilibrium of the HSP90.3-BIN2 complex, resulting in more freely available BIN2 and an altered BR signalling cascade ¹¹⁷. Altering the BR pathway with bikinin resulted in plants that were unable to respond to the Ro8-4304 treatment (Figure 35), thus indicating that BR responses linked to HSP90 trafficking are probably important. Additionally, Zhu et al. (2010) demonstrated that the dwarfed *snc1* phenotype is correlated with the localization of the protein to the nucleus ³³⁹. And Shih et al. (2022) demonstrated that S-gluthionylation of HSP90 enhances its degradation ³⁴⁰. All these data indicates that HSP90 is necessary for the nuclear localization of proteins and that this is tightly regulated by means of GSH. The double mutant *hsp90.1^{KO} hsp90.2* was lethal ⁷², so GSH may induce a smaller phenotype due to the importance of HSP90 in developmental pathways.

Previous reports indicated that GSTFs are induced upon salicylic acid, xenobiotic treatment and pathogen attack 341,342 , and their importance in immunity has been demonstrated $^{343-346}$. The expression of GSTFs is significantly activated after a fungal or

bacterial infection ³³⁷. Moreover, GSTFs are also able to detoxify herbicides ^{265,266,347}, and to transfer small organic ligands ^{267,268}. So, binding of Ro8-4304 to GSTF2/7, next to HSP90, is not completely ruled out. Therefore, we used SeamDock ³⁴⁸ to bind Ro8-4304 and Ro-A03 in the structure of GSTF2 (Figure 66) ²⁶⁶. According to SeamDock, RoA-03 binds at position 118-120, 65-67, and 10-12. Reinemer et al. (1996) formulated two important binding sites in the GSTF structure ²⁶⁵. Whereas the G site (glutathione binding site) contains the ligands His40, Lys41, Glu53, Val54, Glu66, Ser67, and Arg68, the electrophilic substrate binding site (H-site, which can bind two inhibitor molecules) is coated with His8, Ala10, Ser11, Leu35, Phe119, Phe123, Tyr127 and Tyr178. Interestingly, the same binding sites were identified in the docking of Ro8-4304. So technically, it may be possible that Ro8-4304 binds to GSTFs. Thus, we propose that GSTF may have a ligand function, and binding of GSTFs might be necessary to translocate Ro8-4304 across the cell. This transport activity of GSTFs has been demonstrated with auxin and anthocyanins ^{349–352}.

Another action might be the detoxifying reaction of GSTFs ³⁵³. The mutant analysis may indicate a function of GSTF in the detoxification of Ro8-4304. The mutant *chs3-2D gstf2-1K* had a lower expression of *GSTF2* (Figure 58) and did not show an altered phenotype after Ro8-4304 treatment (Figures 56 and 57). However, RT-qPCR of *chs3-2D gstf7-1K* demonstrated a higher expression of *GSTF7* (Figure 52), and this higher expression resulted in a lower effect of the chemical (Figures 56 and 57). This seems to indicate that GSTFs detoxify Ro8-4304, while lower amounts of GSTFs do not influence the action of Ro8-4304. Therefore, Ro8-4304 is still able to act on HSP90 and induce a high fresh weight. Hon the other hand, higher amounts of GSTFs results in lower amounts of bioactive Ro8-4304, and a reduced effect of the chemical. This hypothesis could also explain the results of the GSH treatment. Higher amounts of GSH induces GSTF2 expression (Figures 46 and 48) ³⁵², and the higher amounts of GSTFs detoxify Ro8-4304. Resulting that the fresh weight of *chs3-2D* treated with GSH and Ro8-4304 is less compared to Ro8-4304 treated *chs3-2D* seedlings. However, this is highly speculative and needs to be confirmed by using triple or quadruple mutant lines, because other research already reported the redundancy of GSTFs ³⁴⁴.

Moreover, it would be interesting to prove the direct binding of Ro8-4304 to the purified protein of GSTF2/7. Interestingly, the substrate of GSTF2 and GLRs is shared; both proteins can bind GSH 214,265 . So, if GSTFs can bind Ro8-4304, this might also be the case for GLRs, thus Indicating that non-specific binding of Ro8-4304 is probable.

We conclude that inhibitor treatment and mutant analyses revealed the involvement of GSH, GSTFs and GLRs in the action of Ro8-4304. However, more research is necessary to determine the exact mechanisms and complete pathway.

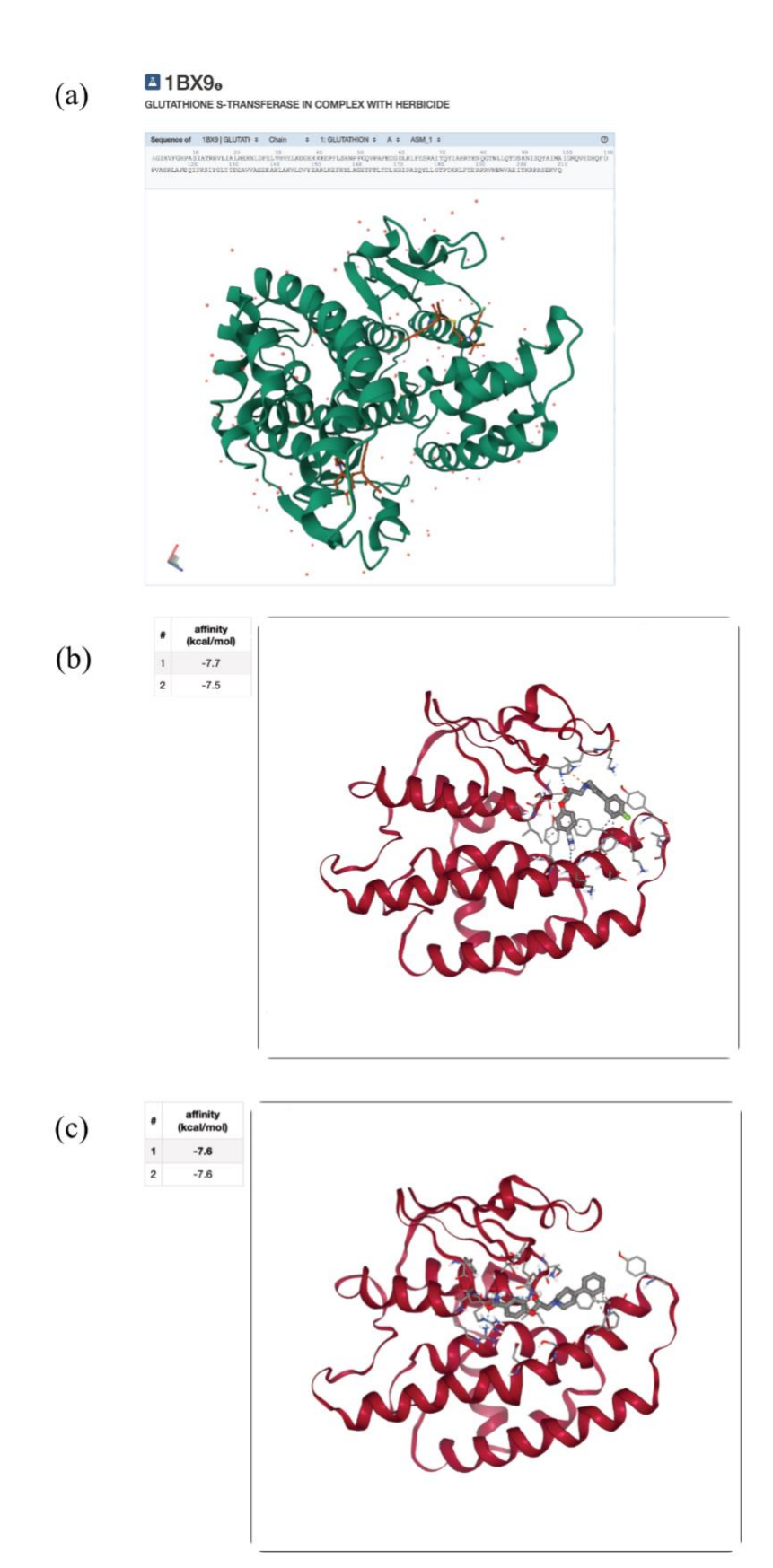


Figure 66. The docking of Ro8-4304 and Ro-A03 in the GSTF2 protein. (a) Structure of the complex formed between GSTF2 (green) and an herbicide (PDB: 1BX9) ²⁶⁶. (b) The structure of GSTF2 in complex with Ro8-4304, according to SeamDock ³⁴⁸. (c) The structure of GSTF2 in complex with Ro-A03, according to SeamDock ³⁴⁸.

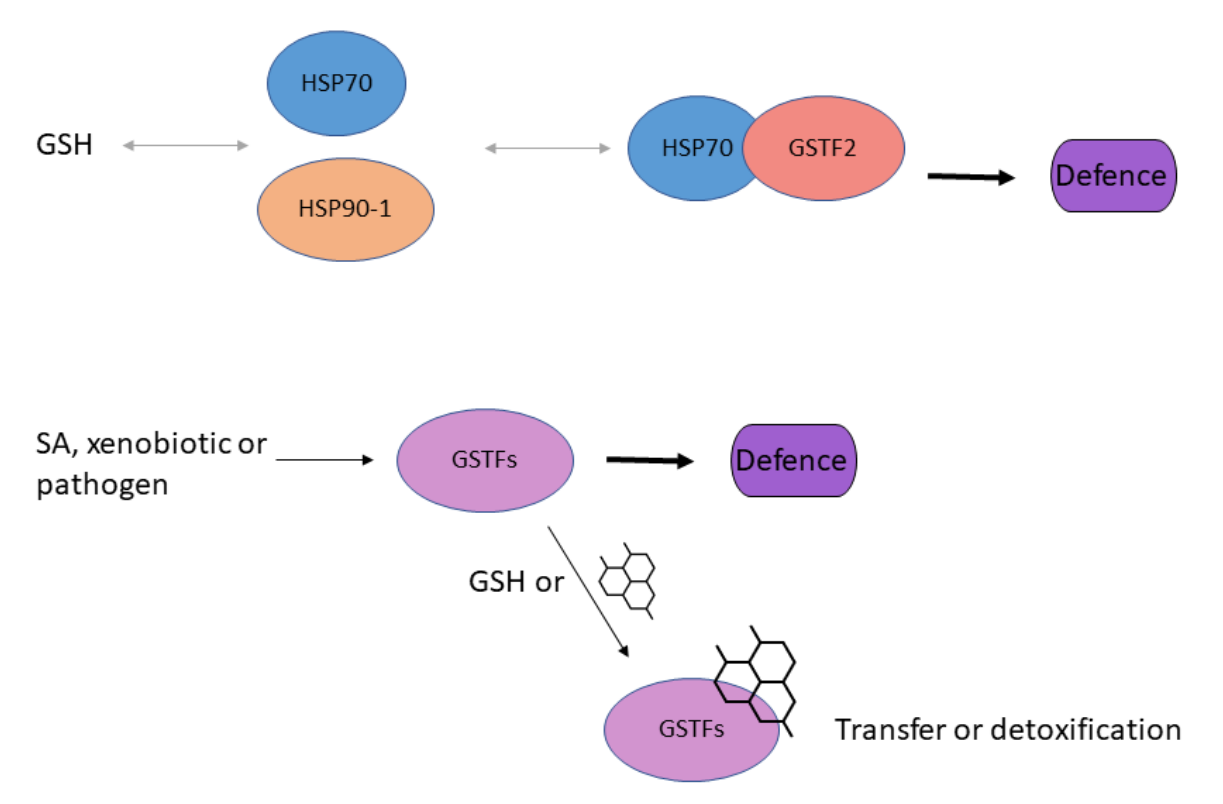


Figure 67. Schematic representation of a few interactions of the protein GSTFs, as discussed in Section 5.2.7. Arrows and blunted lines represent positive and negative regulations. The black lines indicate known connections, whereas red lines or text indicates unknown connections or missing steps between components of the pathway. Grey lines indicate protein-protein interactions.

5.3 A model for the action of Ro8-4304

As discussed above, all the proteins pulled down in the affinity purification (Figure 34 and Table 28), have been reported to be in complex with HSP90. Additionally, the GLRs which was a possible target according to literature, has been demonstrated to be in complex with HSP90. Furthermore, HSP90 is required for the formation of NLR receptors. Therefore, it seems like the most probable putative binding protein target for the chemical Ro8-4304. Although binding to GSTFs and GLRs might still be a possibility (see Discussion), it can't explain the complete phenotype of *chs3-2D*.

Consequently, we used SeamDock ³⁴⁸ to insert Ro8-4304 and Ro-A03 into the active site of HSP90 (Figure 68) ³⁵⁴. According to the docking results, Ro8-4304 and Ro-A03 bind at the same position as adenosine-5'-diphophate (ADP), although the docking is not 100% accurate. Moreover, we hypothesized that the fluorine site of Ro8-4304 would be buried in the active pocket, since changes on this site were less successful. However, this is not clearly seen in this docking data.

Stebbins et al. (1997) demonstrated the binding of geldanamycin to HSP90 ³⁵⁵, and this seems to be the same for Ro8-4304. However, the amino acids important for binding In the HSP90 protein are not completely shared between the different binding partners (GDA and Ro8-4304). Nonetheless, this docking still demonstrates that Ro8-4304 and Ro-A03 fit into the binding pocket of HSP90, and that Ro8-4304 and Ro-A03 may possibly alter HSP90 function.

The determined docking affinity of Ro-A03 was lower than Ro8-4304 (Figures 68b and c). The difference in docking may explain why Ro8-4304 and Ro-A03 have different effects on *chs3-2D* seedlings (Figures 27 and 28). The docking of Ro8-4304 may be too strong and HSP90 is rendered completely unavailable for stabilizing the NLR protein. In contrast to the weaker binding of Ro-A03, which results in inactive HSP90, but also a small amount of active HSP90 putatively sufficient to fold *chs3-2D* into its immune active state.

Considering all data, we propose a model, in which Ro8-4304 and Ro-A03 bind HSP90 (Figure 69). The binding of chemical to HSP90 results in lower amounts of active HSP90. Because of the chemical treatment the amount of stabilized *chs3-2D* is reduced, and the auto-immunity phenotype is reversed.

The different binding activities between Ro8-4304 and Ro-A03 may result in variable effects on immunity. The medium amounts of bioactive HSP90, in the presence of Ro-A03, yields an auto-immune mutant with a decent growth, and a high immunity.

To confirm this hypothesis, direct binding needs to be demonstrated. So, the next step would be to isolate HSP90 from *chs3-2D* and determine the direct binding and dissociation constant (KD) of Ro8-4304 and Ro-A03. Since Ro8-4304 only has an action in *chs3-2D*, we assume that it is important to isolate the *chs3-2D* isoform of HSP90, although docking also indicated binding in *Hordeum vulgare* (Figure 68). Moreover, the double mutants (*chs3-2D hsp90-2K* and *chs3-2D hsp90-2.7*) did not show the phenotype that was previously reported (Figure 56) ⁸⁸. Possibly because the mutations in the double mutants are quite up-stream of the gene and therefore not sufficient to change expression. Therefore, we would suggest testing Ro8-4304 on the double mutant created by Lu et al. (2022) and some additional *chs3-2D hsp* mutants with mutations in different domains of HSP90.2 ⁸⁸. Likewise, the inhibitor geldanamycin did not yield any distinctive results (Figure 50). It would be beneficial to re-test the chemical at higher concentrations, and with fresh aliquots in the absence and presence of Ro8-4304. However, since the chemical is light sensitive ¹¹², another inhibitor might be more reliable ³²⁰.

All these results would strengthen the hypothesis, that Ro8-4304 binds HSP90 (Also known as HSP81-2) in the *chs3-2D* background, and these experiments are therefore prerequisite for further research.

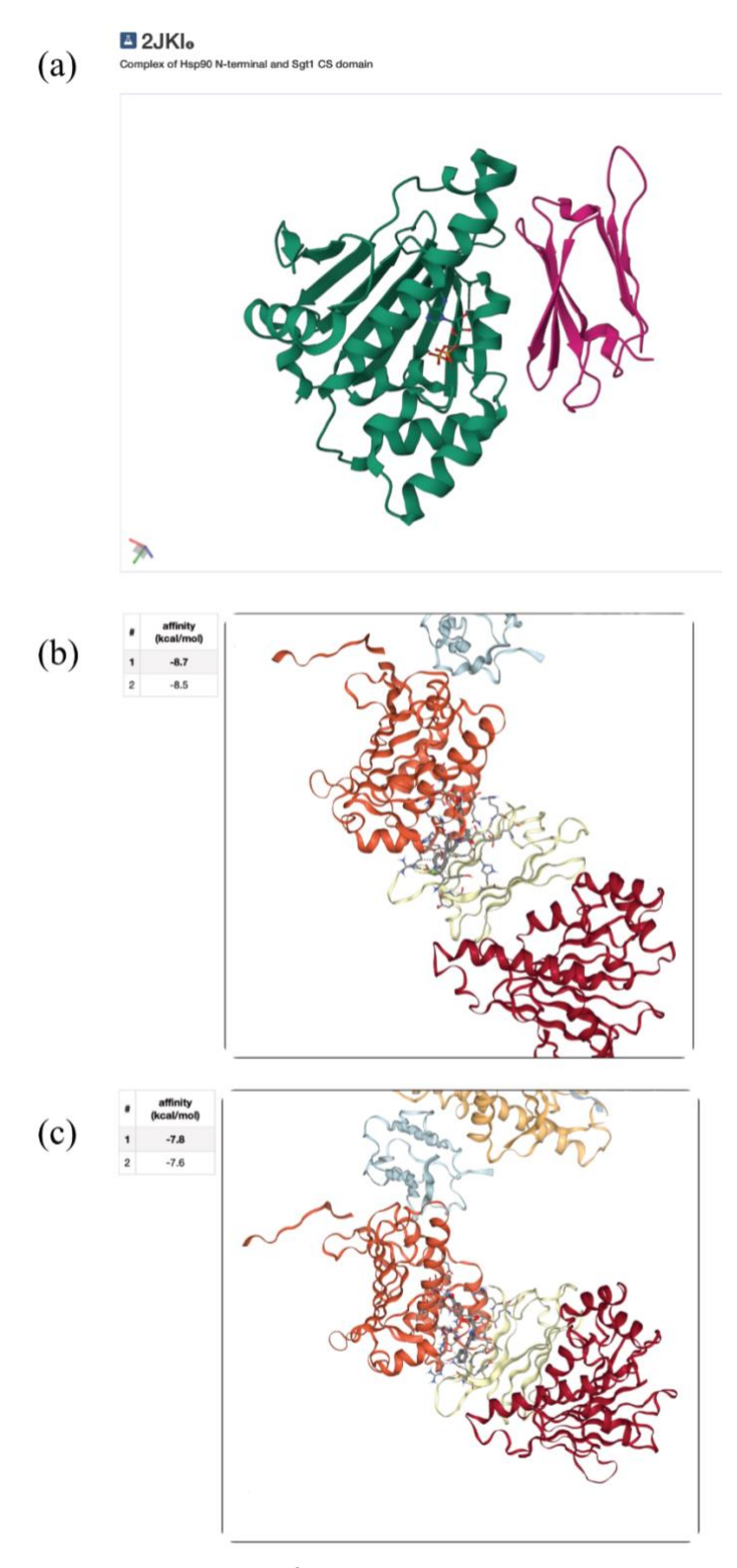


Figure 68. The docking of Ro8-4304 and Ro-A03 in the HSP81-2 protein. (a) Structure of the complex formed between SGT1-CS (pink) and HSP90-ND (green) (PDB: 2JKI) ³⁵⁴. (b) The structure of HSP90 in complex with Ro8-4304, according to SeamDock ³⁴⁸. (c) The structure of HSP90 in complex with Ro-A03, according to SeamDock ³⁴⁸.

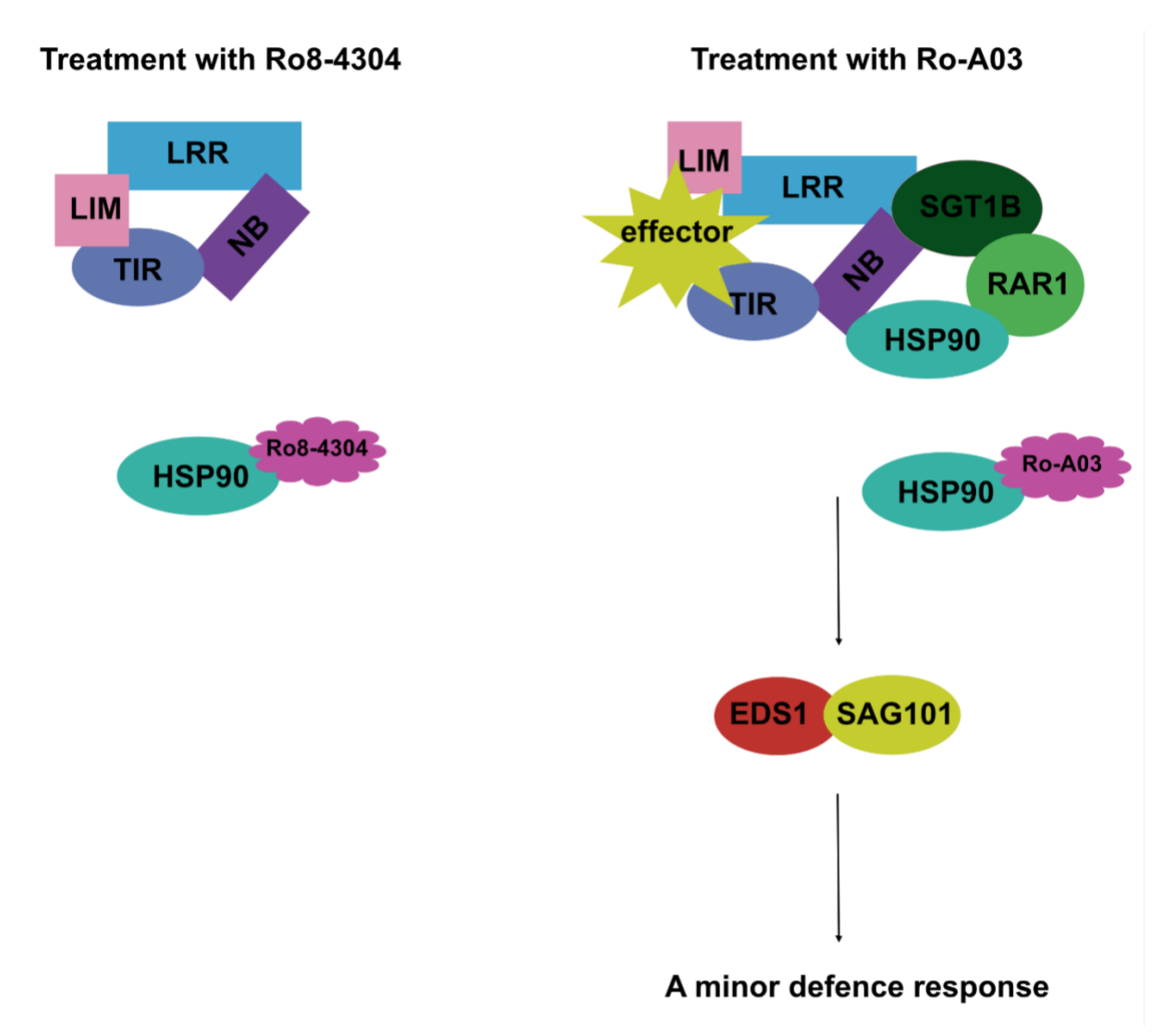


Figure 69. Proposed working model for the disruption of the CHS3-mediated defence pathway by Ro8-4304 and Ro-A03. Ro8-4304 binds HSP90 and renders its inactive. Due to the absence of HSP90 the chaperone complex of CHS3 is not able to properly fold the receptor. Hence, Ro8-4304 inactivates the immune signalling pathway. The binding of Ro-A03 to HSP90 is not so strong, and due to this HSP90 is still able to assemble some CHS3. Resulting in plants with a decent yield and a high immunity. Figure was adapted from Kadota et al. (2009), Bao et al. (2014), and Xu et al. (2015) 34,89,90.

5.4 Conclusive summary

In this work, the important aspects of the chemical rescue of Ro8-4304 were demonstrated. It was shown that Ro8-4304 needs a temperature of 22°C or lower for its activity. Additionally, it was discovered that Ro8-4304 needs to be applied early in the stages of *chs3-2D* seedling growth, otherwise the chemical activity of Ro8-4304 would be reduced.

Using chemical optimization 18 analogues were synthesized. By doing a structure activity relationship study, we could show that changes on the fluorine site, or the alcohol group in the middle of the molecule were more destructive for the fresh weight rescue in *chs3-2D* seedlings than changes on the benzamide site. One analogue had an improved activity in comparison to the original Ro8-4304 molecule. Ro-A03 was able to rescue the fresh weight of *chs3-2D* to similar levels as Ro8-4304. Additionally, defence marker gene expression, an infection assay and salicylic acid quantification showed that *chs3-2D* treated with this analogue still had a decent immunity. So, Ro-A03 was able to un-couple growth and immunity in the *chs3-2D* mutant and Ro-A03 is thus an improved version of Ro8-4304. It would be interesting to synthesize more analogues and see if these could improve the chemical activity even further.

One of the analogues (Ro-A07) was bound to NHS activated agarose and using this matrix and literature research some putative direct binding proteins were identified. Pharmaceutical, genetic mutant data and literature suggests that HSP90 is the most likely binding target of Ro8-4304. Binding of the chemical to HSP90 in the *chs3-2D* mutant reduces the amount of activated CHS3, because the correct folding of this immune activating NLR receptor cannot take place without the active form of HSP90. The un-coupling effect of Ro-A03 is probably due to a less strong binding affinity and therefore only a medium amount of HSP90 is rendered inactive. However, this hypothesis needs to be validated. One option would be that the chemical could be tested even further in additional *chs3-2D hsp90* lines with better mutation than the previously tested *chs3-2D hsp90-2K*. Additionally, it would be interesting to purify HSP90 and determine the binding of Ro8-4304 in this protein.

It was also demonstrated that by pharmaceutical and literature data that GTSFs and GLRs are vital for the action of Ro8-4304. However, currently it is unclear if this is due to direct binding, a transporter function or due to a general effect of these proteins on immunity. More plant physiology research in this area would be necessary for a conclusive answer. Also in this case, it would be interesting to determine the binding of Ro8-4304 in the corresponding purified proteins.

Thus, important aspects of the chemical activity of Ro8-4304 in the *chs3-2D* background have been discovered. This gave us insight into the *chs3-2D* genotype and may be useful for the characterization of other auto-immune mutants. However, more research is necessary if we want to use Ro-AO3 as a marker compound or global modulator for the growth-immunity trade-off.

7 Literature

- 1. Savary, S. *et al.* The global burden of pathogens and pests on major food crops. *Nat Ecol Evol* **3**, 430–439 (2019).
- 2. Strange, R. N. & Scott, P. R. Plant disease: a threat to global food security. *Annu Rev Phytopathol* **43**, 83–116 (2005).
- 3. Darvill, A. G. & Albersheim, P. Phytoalexins and their Elicitors-A Defense Against Microbial Infection in Plants. *Annu Rev Plant Physiol* **35**, 243–275 (1984).
- 4. Wu, Y. & Zhou, J.-M. Receptor-like kinases in plant innate immunity. *J Integr Plant Biol* **55**, 1271–1286 (2013).
- 5. Felix, G., Duran, J. D., Volko, S. & Boller, T. Plants have a sensitive perception system for the most conserved domain of bacterial flagellin. *The Plant Journal* **18**, 265–276 (1999).
- 6. Boller, T. Chemoperception of Microbial Signals in Plant Cells. *Annu Rev Plant Physiol Plant Mol Biol* **46**, 189–214 (1995).
- 7. Gómez-Gómez, L. & Boller, T. FLS2: An LRR Receptor–like Kinase Involved in the Perception of the Bacterial Elicitor Flagellin in Arabidopsis. *Mol Cell* **5**, 1003–1011 (2000).
- 8. Zipfel, C. *et al.* Perception of the bacterial PAMP EF-Tu by the receptor EFR restricts Agrobacterium-mediated transformation. *Cell* **125**, 749–760 (2006).
- 9. Gómez-Gómez, L. & Boller, T. Flagellin perception: a paradigm for innate immunity. *Trends Plant Sci* **7**, 251–256 (2002).
- 10. Heese, A. *et al.* The receptor-like kinase SERK3/BAK1 is a central regulator of innate immunity in plants. *Proc Natl Acad Sci U S A* **104**, 12217–12222 (2007).
- 11. Chinchilla, D. *et al.* A flagellin-induced complex of the receptor FLS2 and BAK1 initiates plant defence. *Nature* **448**, 497–500 (2007).
- 12. Lu, D. *et al.* A receptor-like cytoplasmic kinase, BIK1, associates with a flagellin receptor complex to initiate plant innate immunity. *Proc Natl Acad Sci U S A* **107**, 496–501 (2010).
- 13. Lin, W. *et al.* Tyrosine phosphorylation of protein kinase complex BAK1/BIK1 mediates Arabidopsis innate immunity. *Proc Natl Acad Sci U S A* **111**, 3632–3637 (2014).
- 14. Boller, T. & Felix, G. A Renaissance of Elicitors: Perception of Microbe-Associated Molecular Patterns and Danger Signals by Pattern-Recognition Receptors. *Annu Rev Plant Biol* **60**, 379–406 (2009).
- 15. Dodds, P. N. & Rathjen, J. P. Plant immunity: towards an integrated view of plant–pathogen interactions. *Nat Rev Genet* **11**, 539–548 (2010).
- 16. Jeworutzki, E. *et al.* Early signaling through the Arabidopsis pattern recognition receptors FLS2 and EFR involves Ca2+-associated opening of plasma membrane anion channels. *The Plant Journal* **62**, 367–378 (2010).
- 17. Keinath, N. F. *et al.* Live cell imaging with R-GECO1 sheds light on flg22- and chitin-induced transient [Ca2+]cyt patterns in Arabidopsis. *Mol Plant* **8**, 1188–1200 (2015).
- 18. Miya, A. *et al.* CERK1, a LysM receptor kinase, is essential for chitin elicitor signaling in Arabidopsis. *Proceedings of the National Academy of Sciences* **104**, 19613–19618 (2007).
- 19. Ma, Y., Walker, R. K., Zhao, Y. & Berkowitz, G. A. Linking ligand perception by PEPR pattern recognition receptors to cytosolic Ca2+ elevation and downstream immune

- signaling in plants. *Proceedings of the National Academy of Sciences* **109**, 19852–19857 (2012).
- 20. Vincent, T. R. *et al.* Interplay of plasma membrane and vacuolar ion channels, together with BAK1, elicits rapid cytosolic calcium elevations in Arabidopsis during aphid feeding. *Plant Cell* **29**, 1460–1479 (2017).
- 21. Dodd, A. N., Kudla, J. & Sanders, D. The language of calcium signaling. *Annu Rev Plant Biol* **61**, 593–620 (2010).
- 22. Yu, I., Parker, J. & Bent, A. F. Gene-for-gene disease resistance without the hypersensitive response in Arabidopsis dnd1 mutant. *Proceedings of the National Academy of Sciences* **95**, 7819–7824 (1998).
- 23. Clough, S. J. *et al.* The Arabidopsis dnd1 "defense, no death" gene encodes a mutated cyclic nucleotide-gated ion channel. *Proceedings of the National Academy of Sciences* **97**, 9323–9328 (2000).
- 24. Qi, Z., Stephens, N. R. & Spalding, E. P. Calcium entry mediated by GLR3.3, an Arabidopsis glutamate receptor with a broad agonist profile. *Plant Physiol* **142**, 963–971 (2006).
- 25. Manzoor, H. *et al.* Involvement of the glutamate receptor AtGLR3.3 in plant defense signaling and resistance to Hyaloperonospora arabidopsidis. *The Plant Journal* **76**, 466–480 (2013).
- 26. Li, F. *et al.* Glutamate receptor-like channel3.3 is involved in mediating glutathione-triggered cytosolic calcium transients, transcriptional changes, and innate immunity responses in Arabidopsis. *Plant Physiol* **162**, 1497–1509 (2013).
- 27. Asai, T. *et al.* MAP kinase signalling cascade in Arabidopsis innate immunity. *Nature* **415**, 977–983 (2002).
- 28. Boudsocq, M. *et al.* Differential innate immune signalling via Ca2+ sensor protein kinases. *Nature* **464**, 418–422 (2010).
- 29. Meng, X. & Zhang, S. MAPK Cascades in Plant Disease Resistance Signaling. *Annu Rev Phytopathol* **51**, 245–266 (2013).
- 30. Dubiella, U. *et al.* Calcium-dependent protein kinase/NADPH oxidase activation circuit is required for rapid defense signal propagation. *Proceedings of the National Academy of Sciences* **110**, 8744–8749 (2013).
- 31. Asai, T. *et al.* MAP kinase signalling cascade in Arabidopsis innate immunity. *Nature* **415**, 977–983 (2002).
- 32. Eulgem, T., Rushton, P. J., Robatzek, S. & Somssich, I. E. The WRKY superfamily of plant transcription factors. *Trends Plant Sci* **5**, 199–206 (2000).
- 33. Lamb, C. & Dixon, R. A. The Oxidative Burst in Plant Disease Resistance. *Annu Rev Plant Physiol Plant Mol Biol* **48**, 251–275 (1997).
- 34. Kadota, Y. *et al.* Direct Regulation of the NADPH Oxidase RBOHD by the PRR-Associated Kinase BIK1 during Plant Immunity. *Mol Cell* **54**, 43–55 (2014).
- 35. Bolwell, G. P. & P., W. Mechanisms for the generation of reactive oxygen species in plant defence a broad perspective. *Physiol Mol Plant Pathol* **51**, 347–366 (1997).
- 36. Bolwell, G. P. Role of active oxygen species and NO in plant defence responses. *Curr Opin Plant Biol* **2**, 287–294 (1999).
- 37. Munné-Bosch, S., Queval, G. & Foyer, C. H. The impact of global change factors on redox signaling underpinning stress tolerance . *Plant Physiol* **161**, 5–19 (2013).
- 38. Mittler, R., Vanderauwera, S., Gollery, M. & Van Breusegem, F. Reactive oxygen gene network of plants. *Trends Plant Sci* **9**, 490–498 (2004).

- 39. Luna, E. *et al.* Callose Deposition: A Multifaceted Plant Defense Response. *Molecular Plant-Microbe Interactions* **24**, 183–193 (2011).
- 40. Ellinger, D. *et al.* Elevated Early Callose Deposition Results in Complete Penetration Resistance to Powdery Mildew in Arabidopsis. *Plant Physiol* **161**, 1433–1444 (2013).
- 41. Clay, N. K., Adio, A. M., Denoux, C., Jander, G. & Ausubel, F. M. Glucosinolate metabolites required for an Arabidopsis innate immune response. *Science* (1979) **323**, 95–101 (2009).
- 42. Uknes, S. et al. Acquired resistance in Arabidopsis. Plant Cell 4, 645–656 (1992).
- 43. Grant, M. *et al.* The RPM1 plant disease resistance gene facilitates a rapid and sustained increase in cytosolic calcium that is necessary for the oxidative burst and hypersensitive cell death. *The Plant Journal* **23**, 441–450 (2000).
- 44. Wildermuth, M. C., Dewdney, J., Wu, G. & Ausubel, F. M. Isochorismate synthase is required to synthesize salicylic acid for plant defence. *Nature* **414**, 562–565 (2001).
- 45. Wang, L. *et al.* Arabidopsis CaM binding protein CBP60g contributes to MAMP-induced SA accumulation and is involved in disease resistance against Pseudomonas syringae. *PLoS Pathog* **5**, e1000301 (2009).
- 46. Wu, Y. *et al.* The Arabidopsis NPR1 protein is a receptor for the plant defense hormone salicylic acid. *Cell Rep* **1**, 639–647 (2012).
- 47. Spoel, S. H. & Dong, X. How do plants achieve immunity? Defence without specialized immune cells. *Nat Rev Immunol* **12**, 89–100 (2012).
- 48. Rochon, A., Boyle, P., Wignes, T., Fobert, P. R. & Després, C. The coactivator function of Arabidopsis NPR1 requires the core of its BTB/POZ domain and the oxidation of Cterminal cysteines. *Plant Cell* **18**, 3670–3685 (2006).
- 49. Boyle, P. *et al.* The BTB/POZ domain of the Arabidopsis disease resistance protein NPR1 interacts with the repression domain of TGA2 to negate its function. *Plant Cell* **21**, 3700–3713 (2009).
- 50. Zhu, Q., Dröge-Laser, W., Dixon, R. A. & Lamb, C. Transcriptional activation of plant defense genes. *Curr Opin Genet Dev* **6**, 624–630 (1996).
- 51. Tang, X. *et al.* Overexpression of Pto Activates Defense Responses and Confers Broad Resistance. *Plant Cell* **11**, 15–29 (1999).
- 52. Spoel, S. H. *et al.* Proteasome-mediated turnover of the transcription coactivator NPR1 plays dual roles in regulating plant immunity. *Cell* **137**, 860–872 (2009).
- 53. Fu, Z. Q. *et al.* NPR3 and NPR4 are receptors for the immune signal salicylic acid in plants. *Nature* **486**, 228–232 (2012).
- 54. Zhou, P., Zavaliev, R., Xiang, Y. & Dong, X. Seeing is believing: understanding functions of NPR1 and its paralogs in plant immunity through cellular and structural analyses. *Curr Opin Plant Biol* **73**, 1–7 (2023).
- 55. Bray Speth, E., Lee, Y. N. & He, S. Y. Pathogen virulence factors as molecular probes of basic plant cellular functions. *Curr Opin Plant Biol* **10**, 580–586 (2007).
- 56. Chisholm, S. T., Coaker, G., Day, B. & Staskawicz, B. J. Host-Microbe Interactions: Shaping the Evolution of the Plant Immune Response. *Cell* **124**, 803–814 (2006).
- 57. Jones, J. D. G. & Dangl, J. L. The plant immune system. *Nature* **444**, 323–329 (2006).
- 58. Grant, S. R., Fisher, E. J., Chang, J. H., Mole, B. M. & Dangl, J. L. Subterfuge and Manipulation: Type III Effector Proteins of Phytopathogenic Bacteria. *Annu Rev Microbiol* **60**, 425–429 (2006).
- 59. Lopez, V. A. *et al.* A bacterial effector mimics a host HSP90 client to undermine immunity. *Cell* **179**, 205-218.e21 (2019).

- 60. Dangl, J. L. & Jones, J. D. G. Plant pathogens and integrated defence responses to infection. *Nature* **411**, 826–833 (2001).
- 61. Wang, G.-F. & Balint-Kurti, P. J. Cytoplasmic and nuclear localizations are important for the hypersensitive response conferred by maize autoactive RP1-D21 protein. *Molecular Plant-Microbe Interactions®* **28**, 1023–1031 (2015).
- 62. Wang, G.-F. *et al.* Molecular and functional analyses of a maize autoactive NB-LRR protein identify precise structural requirements for activity. *PLoS Pathog* **11**, e1004830 (2015).
- 63. Kourelis, J. & van der Hoorn, R. A. L. Defended to the nines: 25 years of resistance gene cloning identifies nine mechanisms for R protein function. *Plant Cell* **30**, 285–299 (2018).
- 64. Aarts, N. et al. Different requirements for EDS1 and NDR1 by disease resistance genes define at least two R-gene-mediated signaling pathways in Arabidopsis. *Proceedings of the National Academy of Sciences* **95**, 10306–10311 (1998).
- 65. Feys, B. J. *et al.* Arabidopsis SENESCENCE-ASSOCIATED GENE101 stabilizes and signals within an ENHANCED DISEASE SUSCEPTIBILITY1 complex in plant innate immunity. *Plant Cell* **17**, 2601–2613 (2005).
- 66. Lindgren, P. B., Peet, R. C. & Panopoulos, N. J. Gene cluster of Pseudomonas syringae pv. 'phaseolicola' controls pathogenicity of bean plants and hypersensitivity of nonhost plants. *J Bacteriol* **168**, 512–522 (1986).
- 67. Richberg, M. H., Aviv, D. H. & Dangl, J. L. Dead cells do tell tales. *Curr Opin Plant Biol* **1**, 480–485 (1998).
- 68. Lam, E., Kato, N. & Lawton, M. Programmed cell death, mitochondria and the plant hypersensitive response. *Nature* **411**, 848–853 (2001).
- 69. Mur, L. A. J., Kenton, P., Lloyd, A. J., Ougham, H. & Prats, E. The hypersensitive response; the centenary is upon us but how much do we know? *J Exp Bot* **59**, 501–520 (2008).
- 70. Balint-Kurti, P. The plant hypersensitive response: concepts, control and consequences. *Mol Plant Pathol* **20**, 1163–1178 (2019).
- 71. Delledonne, M., Zeier, J., Marocco, A. & Lamb, C. Signal interactions between nitric oxide and reactive oxygen intermediates in the plant hypersensitive disease resistance response. *Proceedings of the National Academy of Sciences* **98**, 13454–13459 (2011).
- 72. Hubert, D. A., He, Y., McNulty, B. C., Tornero, P. & Dangl, J. L. Specific Arabidopsis HSP90.2 alleles recapitulate RAR1 cochaperone function in plant NB-LRR disease resistance protein regulation. *Proceedings of the National Academy of Sciences* **106**, 9556–9563 (2009).
- 73. Azevedo, C. *et al.* The RAR1 interactor SGT1, an essential component of R genetriggered disease resistance. *Science* (1979) **295**, 2073–2076 (2002).
- 74. Vierstra, R. The ubiquitin/26S proteasome pathway, the complex last chapter in the life of many plant proteins. *Trends Plant Sci* **8**, 135–142 (2003).
- 75. Hatsugai, N. *et al.* A plant vacuolar protease, VPE, mediates virus-induced hypersensitive cell death. *Science* (1979) **305**, 855–858 (2004).
- 76. Rojo, E. *et al.* VPEγ exhibits a caspase-like activity that contributes to defense against pathogens. *Current Biology* **14**, 1897–1906 (2004).
- 77. Yamada, K., Shimada, T., Nishimura, M. & Hara-Nishimura, I. A VPE family supporting various vacuolar functions in plants. *Physiol Plant* **123**, 369–375 (2005).

- 78. Schneider, J. C., Suzanne, H. & Somerville, C. R. Chilling-sensitive mutants of arabidopsis. *Plant Mol Biol Report* **13**, 11–17 (1995).
- 79. Hugly, S., McCourt, P., Browse, J., Patterson, G. W. & Somerville, C. A chilling sensitive mutant of Arabidopsis with altered steryl-ester metabolism. *Plant Physiol* **93**, 1053–1062 (1990).
- 80. Wersch, R. van, Li, X. & Zhang, Y. Mighty dwarfs: Arabidopsis autoimmune mutants and their usages in genetic dissection of plant immunity. *Front Plant Sci* **7**, 1–8 (2016).
- 81. Schneider, J. C., Nielsen, E. & Somerville, C. A chilling-sensitive mutant of Arabidopsis is deficient in chloroplast protein accumulation at low temperature. *Plant Cell Environ* **18**, 23–32 (1995).
- 82. Seo, Y.-S. *et al.* The HSP90-SGT1-RAR1 molecular chaperone complex: a core modulator in plant immunity. *Journal of Plant Biology* **51**, 1–10 (2008).
- 83. Kadota, Y., Shirasu, K. & Guerois, R. NLR sensors meet at the SGT1–HSP90 crossroad. *Trends Biochem Sci* **35**, 199–207 (2010).
- 84. Bi, D. *et al.* Mutations in an Atypical TIR-NB-LRR-LIM Resistance Protein Confer Autoimmunity. *Front Plant Sci* **2**, 1–10 (2011).
- 85. Yang, H. *et al.* A mutant CHS3 protein with TIR-NB-LRR-LIM domains modulates growth, cell death and freezing tolerance in a temperature-dependent manner in Arabidopsis. *The Plant Journal* **63**, 283–296 (2010).
- 86. Srivastava, V. & Verma, P. K. The plant LIM proteins: unlocking the hidden attractions. *Planta* **246**, 365–375 (2017).
- 87. Xu, F. *et al.* Autoimmunity conferred by chs3-2D relies on CSA1, its adjacent TNL-encoding neighbour. *Sci Rep* **5**, 1–7 (2015).
- 88. Lu, J., Liang, W., Zhang, N., van Wersch, S. & Li, X. HSP90 contributes to chs3-2D-mediated autoimmunity. *Front Plant Sci* **13**, 1–8 (2022).
- 89. Xu, F. *et al.* Autoimmunity conferred by chs3-2D relies on CSA1, its adjacent TNL-encoding neighbour. *Sci Rep* **5**, 1–7 (2015).
- 90. Bao, F. *et al.* Arabidopsis HSP90 protein modulates RP4-mediated temperature-dependent cell death and defense responses. *New Phytologist* **202**, 1320–1334 (2014).
- 91. Smedegaard-Petersen, V. & Stolen, O. Effect of Energy-Requiring Defense Reactions on Yield and Grain Quality in a Powdery Mildew-Resistant Barley Cultivar. *Phytopathology* **71**, 396–399 (1981).
- 92. Rosenthal, J. P. & Dirzo, R. Effects of life history, domestication and agronomic selection on plant defence against insects: Evidence from maizes and wild relatives. *Evol Ecol* **11**, 337–355 (1997).
- 93. Kurashige, N. & Agrawal, A. Phenotypic plasticity to light competition and herbivory in Chenopodium album (Chenopodiaceae). *Am J Bot* **92**, 21–26 (2005).
- 94. Donaldson, J., Kruger, E. & Lindroth, R. Competition- and resource-mediated tradeoffs between growth and defensive chemistry in trembling aspen (Populus tremuloides). *New Phytologist* **169**, 561–570 (2006).
- 95. Rodriguez-Saona, C. *et al.* Tracing the history of plant traits under domestication in cranberries: potential consequences on anti-herbivore defences. *J Exp Bot* **62**, 2633–2644 (2011).
- 96. Fan, M. et al. The bHLH Transcription Factor HBI1 Mediates the Trade-Off between Growth and Pathogen-Associated Molecular Pattern–Triggered Immunity in Arabidopsis. Plant Cell 26, 828–841 (2014).

- 97. Yuan, P., Du, L. & Poovaiah, B. W. Ca2+/Calmodulin-Dependent AtSR1/CAMTA3 Plays Critical Roles in Balancing Plant Growth and Immunity. *Int J Mol Sci* **19**, 1–18 (2018).
- 98. Herms, D. A. & Mattson, W. J. The Dilemma of Plants: To Grow or Defend. *Q Rev Biol* **67**, 283–335 (1992).
- 99. Baldwin, I. T. & Callahan, P. Autotoxicity and chemical defense: nicotine accumulation and carbon gain in Solanaceous plants. *Oecologia* **94**, 534–541 (1993).
- 100. Zangerl, A. R., Arntz, A. M. & Berenbaum, M. R. Physiological price of an induced chemical defense: photosynthesis, respiration, biosynthesis, and growth. *Oecologia* **109**, 433–441 (1997).
- 101. Heil, M., Hilpert, A., Kaiser, W. & Linsenmair, K. E. Reduced growth and seed set following chemical induction of pathogen defence: does systemic acquired resistance (SAR) incur allocation costs? *Journal of Ecology* **88**, 645–654 (2000).
- 102. Engelsdorf, T. *et al.* Reduced carbohydrate availability enhances the susceptibility of Arabidopsis toward Colletotrichum higginsianum . *Plant Physiol* **162**, 225–238 (2013).
- 103. Ullmann-Zeunert, L. *et al.* Quantification of growth-defense trade-offs in a common currency: nitrogen required for phenolamide biosynthesis is not derived from ribulose-1,5-bisphosphate carboxylase/oxygenase turnover. *The Plant Journal* **75**, 417–429 (2013).
- 104. Wang, W. & Wang, Z.-Y. At the Intersection of Plant Growth and Immunity. *Cell Host Microbe* **15**, 400–402 (2014).
- 105. Robert-Seilaniantz, A. *et al.* The microRNA miR393 re-directs secondary metabolite biosynthesis away from camalexin and towards glucosinolates. *The Plant Journal* **67**, 218–231 (2011).
- 106. Navarro, L. *et al.* A plant miRNA contributes to antibacterial resistance by repressing auxin signaling. *Science* (1979) **312**, 436–439 (2006).
- 107. Wang, D., Pajerowska-Mukhtar, K., Culler, A. H. & Dong, X. Salicylic acid inhibits pathogen growth in plants through repression of the auxin signaling pathway. *Current Biology* **17**, 1784–1790 (2007).
- 108. Gray, W. M. *et al.* Identification of an SCF ubiquitin-ligase complex required for auxin response in Arabidopsis thaliana. *Genes Dev* **13**, 1678–1691 (1999).
- 109. Gray, W. M., Muskett, P. R., Chuang, H. & Parker, J. E. Arabidopsis SGT1b is required for SCF-TIR1-mediated auxin response. *Plant Cell* **15**, 1310–1319 (2003).
- 110. Gray, W. M., Kepinski, S., Rouse, D., Leyser, O. & Estelle, M. Auxin regulates SCFTIR1-dependent degradation of AUX/IAA proteins. *Nature* **414**, 271–276 (2001).
- 111. Kepinski, S. & Leyser, O. Auxin-induced SCFTIR1—AUX/IAA interaction involves stable modification of the SCFTIR1 complex. *Proceedings of the National Academy of Sciences* 101, 12381–12386 (2004).
- 112. Sangster, T. A. *et al.* Phenotypic diversity and altered environmental plasticity in Arabidopsis thaliana with reduced HSP90 levels. *PLoS One* **2**, e648 (2007).
- 113. Clouse, S. D. Brassinosteroid signal transduction: from receptor kinase activation to transcriptional networks regulating plant development. *Plant Cell* **23**, 1219–1230 (2011).
- 114. Chinchilla, D. *et al.* A flagellin-induced complex of the receptor FLS2 and BAK1 initiates plant defence. *Nature* **448**, 497–500 (2007).

- 115. Belkhadir, Y. *et al.* Brassinosteroids modulate the efficiency of plant immune responses to microbe-associated molecular patterns. *Proceedings of the National Academy of Sciences* **109**, 297–302 (2012).
- 116. Lozano-Durán, R. *et al.* The transcriptional regulator BZR1 mediates trade-off between plant innate immunity and growth. *Elife* **2**, 1–15 (2013).
- 117. Samakovli, D., Margaritopoulou, T., Prassinos, C., Milioni, D. & Hatzopoulos, P. Brassinosteroid nuclear signaling recruits HSP90 activity. *New Phytologist* **203**, 743–757 (2014).
- 118. Gallego-Giraldo, L., Escamilla-Trevino, L., Jackson, L. A. & Dixon, R. A. Salicylic acid mediates the reduced growth of lignin down-regulated plants. *Proceedings of the National Academy of Sciences* **108**, 20814–20819 (2011).
- 119. Navarro, L. *et al.* DELLAs control plant immune responses by modulating the balance of jasmonic acid and salicylic acid signaling. *Current Biology* **18**, 650–655 (2008).
- 120. Li, Y. *et al.* DELLA and EDS1 form a feedback regulatory module to fine-tune plant growth–defense tradeoff in Arabidopsis. *Mol Plant* **12**, 1485–1498 (2019).
- 121. Murase, K., Hirano, Y., Sun, T. & Hakoshima, T. Gibberellin-induced DELLA recognition by the gibberellin receptor GID1. *Nature* **456**, 459–463 (2008).
- 122. Sun, T. The molecular mechanism and evolution of the GA–GID1–DELLA signaling module in plants. *Current Biology* **21**, R338–R345 (2011).
- 123. McGinnis, K. M. *et al.* The Arabidopsis SLEEPY1 gene encodes a putative F-box subunit of an SCF E3 ubiquitin ligase. *Plant Cell* **15**, 1120–1130 (2003).
- 124. Jaillais, Y. & Vert, G. Brassinosteroids, gibberellins and light-mediated signalling are the three-way controls of plant sprouting. *Nat Cell Biol* **14**, 788–790 (2012).
- 125. Stewart Lilley, J. L., Gan, Y., Graham, I. A. & Nemhauser, J. L. The effects of DELLAs on growth change with developmental stage and brassinosteroid levels. *The Plant Journal* **76**, 165–173 (2013).
- 126. Bai, M.-Y. *et al.* Brassinosteroid, gibberellin and phytochrome impinge on a common transcription module in Arabidopsis. *Nat Cell Biol* **14**, 810–817 (2012).
- 127. Huot, B., Yao, J., Montgomery, B. L. & He, S. Y. Growth–defense tradeoffs in plants: a balancing act to optimize fitness. *Mol Plant* **7**, 1267–1287 (2014).
- 128. Wasternack, C. Jasmonates: an update on biosynthesis, signal transduction and action in plant stress response, growth and development. *Ann Bot* **100**, 681–697 (2007).
- 129. Guo, Q. *et al.* JAZ repressors of metabolic defense promote growth and reproductive fitness in Arabidopsis. *Proceedings of the National Academy of Sciences* **115**, (2018).
- 130. Sheard, L. B. *et al.* Jasmonate perception by inositol-phosphate-potentiated COI1–JAZ co-receptor. *Nature* **468**, 400–405 (2010).
- 131. Chini, A. *et al.* The JAZ family of repressors is the missing link in jasmonate signalling. *Nature* **448**, 666–671 (2007).
- 132. Thines, B. *et al.* JAZ repressor proteins are targets of the SCFCOI1 complex during jasmonate signalling. *Nature* **448**, 661–665 (2007).
- 133. Pauwels, L. *et al.* NINJA connects the co-repressor TOPLESS to jasmonate signalling. *Nature* **464**, 788–791 (2010).
- 134. Withers, J. *et al.* Transcription factor-dependent nuclear localization of a transcriptional repressor in jasmonate hormone signaling. *Proceedings of the National Academy of Sciences* **109**, 20148–20153 (2012).

- 135. Staswick, P. E., Su, W. & Howell, S. H. Methyl jasmonate inhibition of root growth and induction of a leaf protein are decreased in an Arabidopsis thaliana mutant.

 *Proceedings of the National Academy of Sciences 89, 6837–6840 (1992).
- 136. Sun, J. *et al.* Jasmonate modulates endocytosis and plasma membrane accumulation of the Arabidopsis PIN2 protein. *New Phytologist* **191**, 360–375 (2011).
- 137. Chen, Q. *et al.* The basic helix-loop-helix transcription factor MYC2 directly represses PLETHORA expression during jasmonate-mediated modulation of the root stem cell niche in Arabidopsis . *Plant Cell* **23**, 3335–3352 (2011).
- 138. Grunewald, W. *et al.* Expression of the Arabidopsis jasmonate signalling repressor JAZ1/TIFY10A is stimulated by auxin. *EMBO Rep* **10**, 923–928 (2009).
- 139. Ren, C. *et al.* A leaky mutation in DWARF4 reveals an antagonistic role of brassinosteroid in the inhibition of root growth by jasmonate in Arabidopsis. *Plant Physiol* **151**, 1412–1420 (2009).
- 140. Campos, M. L. *et al.* Brassinosteroids interact negatively with jasmonates in the formation of anti-herbivory traits in tomato. *J Exp Bot* **60**, 4347–4361 (2009).
- 141. Heinrich, M. *et al.* High levels of jasmonic acid antagonize the biosynthesis of gibberellins and inhibit the growth of Nicotiana attenuata stems. *The Plant Journal* **73**, 591–606 (2013).
- 142. Hou, X., Lee, L. Y. C., Xia, K., Yan, Y. & Yu, H. DELLAs modulate jasmonate signaling via competitive binding to JAZs. *Dev Cell* **19**, 884–894 (2010).
- 143. Wild, M. *et al.* The Arabidopsis DELLA RGA-LIKE3 is a direct target of MYC2 and modulates jasmonate signaling responses. *Plant Cell* **24**, 3307–3319 (2012).
- 144. Yang, D.-L. *et al.* Plant hormone jasmonate prioritizes defense over growth by interfering with gibberellin signaling cascade. *Proceedings of the National Academy of Sciences* **109**, E1192–E1200 (2012).
- 145. Zhang, L., Du, L., Shen, C., Yang, Y. & Poovaiah, B. W. Regulation of plant immunity through ubiquitin-mediated modulation of Ca2+-calmodulin-AtSR1/CAMTA3 signaling. *The Plant Journal* **78**, 269–281 (2014).
- 146. Yuan, P., Tanaka, K. & Poovaiah, B. W. Calmodulin-binding transcription activator AtSR1/CAMTA3 fine-tunes plant immune response by transcriptional regulation of the salicylate receptor NPR1. *Plant Cell Environ* **44**, 3140–3154 (2021).
- 147. Yuan, P., Du, L. & Poovaiah, B. Ca2+/calmodulin-dependent AtSR1/CAMTA3 plays critical roles in balancing plant growth and immunity. *Int J Mol Sci* **19**, 1764 (2018).
- 148. Gupta, V., Willits, M. G. & Glazebrook, J. Arabidopsis thaliana EDS4 contributes to salicylic acid (SA)-dependent expression of defense responses: evidence for inhibition of jasmonic acid signaling by SA. *Molecular Plant-Microbe Interactions®* **13**, 503–511 (2000).
- 149. Park, S.-Y. *et al.* Abscisic acid inhibits type 2C protein phosphatases via the PYR/PYL family of START proteins. *Science* (1979) **324**, 1068–1071 (2009).
- 150. Armstrong, J. I., Yuan, S., Dale, J. M., Tanner, V. N. & Theologis, A. Identification of inhibitors of auxin transcriptional activation by means of chemical genetics in Arabidopsis. *Proceedings of the National Academy of Sciences* **101**, 14978–14983 (2004).
- 151. De Rybel, B. *et al.* Chemical inhibition of a subset of Arabidopsis thaliana GSK3-like kinases activates brassinosteroid signaling. *Chem Biol* **16**, 594–604 (2009).

- 152. Schreiber, K., Ckurshumova, W., Peek, J. & Desveaux, D. A high-throughput chemical screen for resistance to Pseudomonas syringae in Arabidopsis. *The Plant Journal* **54**, 522–531 (2008).
- 153. Noutoshi, Y., Okazaki, M. & Shirasu, K. Isolation and characterization of the plant immune-priming compounds Imprimatin B3 and -B4, potentiators of disease resistance in Arabidopsis thaliana. *Plant Signal Behav* **7**, 1526–1528 (2012).
- 154. Joglekar, S. *et al.* Chemical activation of EDS1/PAD4 signaling leading to pathogen resistance in Arabidopsis. *Plant Cell Physiol* **59**, 1592–1607 (2018).
- 155. O'Neill, E. M. *et al.* Phevamine A, a small molecule that suppresses plant immune responses. *Proceedings of the National Academy of Sciences* **115**, E9514–E9522 (2018).
- 156. Halder, V., Suliman, M. N. S., Kaschani, F. & Kaiser, M. Plant chemical genetics reveals colistin sulphate as a SA and NPR1-independent PR1 inducer functioning via a p38-like kinase pathway. *Sci Rep* **9**, 1–12 (2019).
- 157. Fiers, M. *et al.* A plant-based chemical genomics screen for the identification of flowering inducers. *Plant Methods* **13**, 1–9 (2017).
- 158. Shirakawa, M., Morisaki, Y., Gan, E.-S., Sato, A. & Ito, T. Identification of a devernalization inducer by chemical screening approaches in Arabidopsis thaliana. *Front Plant Sci* **12**, (2021).
- 159. Walters, D. R. & Fountaine, J. M. Practical application of induced resistance to plant diseases: an appraisal of effectiveness under field conditions. *J Agric Sci* **147**, 523–535 (2009).
- 160. Goellner, K. & Conrath, U. Priming: it's all the world to induced disease resistance. *Eur J Plant Pathol* **121**, 233–242 (2008).
- 161. van Hulten, M., Pelser, M., van Loon, L. C., Pieterse, C. M. J. & Ton, J. Costs and benefits of priming for defense in Arabidopsis. *Proceedings of the National Academy of Sciences* **103**, 5602–5607 (2006).
- 162. Walters, D. R., Ratsep, J. & Havis, N. D. Controlling crop diseases using induced resistance: challenges for the future. *J Exp Bot* **64**, 1263–1280 (2013).
- 163. Savvides, A., Ali, S., Tester, M. & Fotopoulos, V. Chemical priming of plants against multiple abiotic stresses: mission possible? *Trends Plant Sci* **21**, 329–340 (2016).
- 164. Buswell, W. *et al.* Chemical priming of immunity without costs to plant growth. *New Phytologist* **218**, 1205–1216 (2018).
- 165. Sun, T.-J. *et al.* A novel pyrimidin-like plant activator stimulates plant disease resistance and promotes growth. *PLoS One* **10**, e0123227 (2015).
- 166. Huang, S. *et al.* Identification of methylosome components as negative regulators of plant immunity using chemical genetics. *Mol Plant* **9**, 1620–1633 (2016).
- 167. Rasmann, S. *et al.* Recruitment of entomopathogenic nematodes by insect-damaged maize roots. *Nature* **434**, 732–737 (2005).
- 168. Dávila-Flores, A. M., DeWitt, T. J. & Bernal, J. S. Facilitated by nature and agriculture: performance of a specialist herbivore improves with host-plant life history evolution, domestication, and breeding. *Oecologia* **173**, 1425–1437 (2013).
- 169. Edenhofer, A. & Spiegelberg, H. [4'-(Phenyl-3,6-Dihydro-1-(2H)Pyridyl]-2-hydroxypropoxy-anilides and derivatives thereof. 10 (1972).
- 170. Conway, R. J. *et al.* Synthesis and SAR study of 4-arylpiperidines and 4-aryl-1,2,3,6-tetrahydropyridines as 5-HT2C agonists. *Bioorg Med Chem Lett* **22**, 2560–2564 (2012).

- 171. Junker, A. *et al.* Structure-Based Design of 3-(4-Aryl-1H-1,2,3-triazol-1-yl)-Biphenyl Derivatives as P2Y14 Receptor Antagonists. *Journal of Medical Chemistry* **59**, 6149–6168 (2016).
- 172. Gessner, W., Brossi, A., Shen, R. & Abell, C. W. Synthesis and dihydropteridine reductase inhibitory effects of potential metabolites of the neurotoxin 1-Methyl-4-phenyl-1,2,3,6-tetrahydropyridine. *Journal of Medical Chemistry* **28**, 311–317 (1985).
- 173. Arnáiz, F. J. A Convenient Way to Generate Hydrogen Chloride in the Freshman Lab. *J Chem Educ* **72**, 1139 (1995).
- 174. Kubota, H. *et al.* Synthesis and pharmacological evaluation of 1-oxo-2-(3-piperidyl)-1,2,3,4- tetrahydroisoquinolines and related analogues as a new class of specific bradycardic agents possessing if channel inhibitory activity. *Journal of Medical Chemistry* **46**, 4728–4740 (2003).
- 175. Ray, N. C., Bull, R. J., Finch, H., Heuvel, M. van den & Bravo, J. A. Oxazole and thiazole derivatives and their uses. 1–87 (2008).
- 176. Keller, M. *et al.* Guanidine-acylguanidine bioisosteric approach in the design of radioligands: synthesis of a tritium-labeled NG-propionylargininamide ([3H]-UR-MK114) as a highly potent and selective neuropeptide Y Y1 receptor antagonist. *Journal of Medical Chemistry* **51**, 8168–8172 (2008).
- 177. Bonnitcha, P. D. *et al.* nitroimidazole conjugates of bis(thiosemicarbazonato)64Cu(II) potential combination agents for the PET imaging of hypoxia. *J Inorg Biochem* **104**, 126–135 (2010).
- 178. Yan, D. *et al.* Synthesis, characterization and properties of novel coumarin derivatives and their europium complexes. *J Fluoresc* **25**, 849–859 (2015).
- 179. He, X. *et al.* Finding new elicitors that induce resistance in rice to the white-backed planthopper Sogatella furcifera. *Bioorg Med Chem Lett* **25**, 5601–5603 (2015).
- 180. Hu, Z., Zhang, S., Zhou, W., Maa, X. & Xiang, G. Synthesis and antibacterial activity of 3-benzylamide derivatives as FtsZ inhibitors. *Bioorg Med Chem Lett* **27**, 1854–1858 (2017).
- 181. Alekseyev, R. S., Kurkin, A. V. & Yurovskaya, M. A. The Piloty-Robinson reaction of N-substituted Piperidin-4-one azines. A novel route for the synthesis of 3,6-Diazacarbazole. *Chem Heterocycl Compd (N Y)* **47**, 706–720 (2011).
- 182. Copeland, C., Woloshen, V., Huang, Y. & Li, X. AtCDC48A is involved in the turnover of an NLR immune receptor. *The Plant Journal* **88**, 294–305 (2016).
- 183. Hubert, D. A. *et al.* Cytosolic HSP90 associates with and modulates the Arabidopsis RPM1 disease resistance protein. *EMBO J* **22**, 5679–5689 (2003).
- 184. Oh, H.-S., Park, D. H. & Collmer, A. Components of the pseudomonas syringae type III secretion system can suppress and may elicit plant innate immunity. *Molecular Plant-Microbe Interactions* **23**, 727–739 (2010).
- 185. Wang, Y., Zhang, Y., Wang, Z., Zhang, X. & Yang, S. A missense mutation in CHS1, a TIR-NB protein, induces chilling sensitivity in Arabidopsis. *The Plant Journal* **75**, 553–565 (2013).
- 186. Huang, X., Li, J., Bao, F., Zhang, X. & Yang, S. A gain-of-function mutation in the Arabidopsis disease resistance gene RPP4 confers sensitivity to low temperature. *Plant Physiol* **154**, 796–809 (2010).
- 187. Estes, G. O. The influence of dimethyl sulfoxide (DMSO) on growth and the uptake of nutritive elements. (Oregon State University, 1969).

- 188. Zhang, X.-H., Yu, X.-Z. & Yue, D.-M. Phytotoxicity of dimethyl sulfoxide (DMSO) to rice seedlings. *International Journal of Environmental Science and Technology* **13**, 607–614 (2016).
- 189. Verly, C. *et al.* Plant defense stimulator mediated defense activation is affected by nitrate fertilization and developmental stage in Arabidopsis thaliana. *Front Plant Sci* **11**, 1–15 (2020).
- 190. Raab, S. *et al.* Identification of a novel E3 ubiquitin ligase that is required for suppression of premature senescence in Arabidopsis. *The Plant Journal* **59**, 39–51 (2009).
- 191. Greg T. Hermanson. Chapter 3 The Reactions of Bioconjugation. in *Bioconjugate Techniques* (ed. Greg T. Hermanson) 229–258 (Academic Press, 2013). doi:B978-0-12-382239-0.00003-0.
- 192. Wimalasena, D. S., Perera, R. P., Heyen, B. J., Balasooriya, I. S. & Wimalasena, K. Vesicular monoamine transporter substrate/inhibitor activity of MPTP/MPP+ derivatives: a structure—activity study. *Journal of Medical Chemistry* **51**, 760–768 (2008).
- 193. Chen, G. *et al.* Synthesis and SAR study of diphenylbutylpiperidines as cell autophagy inducers. *Bioorg Med Chem Lett* **21**, 234–239 (2011).
- 194. Murthi, K. K. *et al.* Structure-activity relationship studies of flavopiridol analogues. *Bioorg Med Chem Lett* **10**, 1037–1041 (2000).
- 195. Hampson, L. J. *et al.* Bioactivity of glycogen phosphorylase inhibitors that bind to the purine nucleoside site. *Bioorg Med Chem* **14**, 7835–7845 (2006).
- 196. Himmelsbach, F. *et al.* 4-4-4-(carboxyalkyl)-phenylaminocarbonyl -phenyl-piperedines as aggregation inhibitors. 1–49 (1994).
- 197. Liu, N. & Wang, Z.-X. Kumada coupling of aryl, heteroaryl, and vinyl chlorides catalyzed by amido pincer nickel complexes. *J Org Chem* **76**, 10031–10038 (2011).
- 198. Zhang, X.-Q. & Wang, Z.-X. Amido pincer nickel catalyzed kumada cross-coupling of aryl, heteroaryl, and vinyl chlorides. *Synlett* **24**, 2081–2084 (2013).
- 199. Liu, Y., Cornella, J. & Martin, R. Ni-catalyzed carboxylation of unactivated primary alkyl bromides and sulfonates with CO2. *J Am Chem Soc* **136**, 11212–11215 (2014).
- 200. Hurst, T. E. *et al.* Sodium methyl carbonate as an effective C1 synthon. Synthesis of carboxylic acids, benzophenones, and unsymmetrical ketones. *Org Lett* **21**, 3882–3885 (2019).
- 201. Kantam, M. L., Srinivas, P., Yadav, J., Likhar, P. R. & Bhargava, S. Trifunctional N,N,O-terdentate amido/pyridyl carboxylate ligated Pd(II) complexes for heck and suzuki reactions. *J Org Chem* **74**, 4882–4885 (2009).
- 202. Cristau, H.-J., Ouali, A., Spindler, J.-F. & Taillefer, M. Mild and efficient coppercatalyzed cyanation of aryl iodides and bromides. *Chemistry: A European Journal* **11**, 2483 2492 (2005).
- 203. Hermanson, G. T. *Bioconjugate techniques*. (Elsevier Inc., 2013). doi:/10.1016/C2009-0-64240-9.
- 204. Yang, J., Shamji, A., Matchacheep, S. & Schreiber, S. L. Identification of a small-molecule inhibitor of class Ia PI3Ks with cell-based screening. *Chem Biol* **14**, 371–377 (2007).
- 205. Ballini, R., Barboni, L. & Giarlo, G. The first conversion of primary alkyl halides to nitroalkanes under aqueous medium. *J Org Chem* **69**, 6907–6908 (2004).

- 206. Yalpani, N., Silverman, P., Wilson, T. M., Kleier, D. A. & Raskin, I. Salicylic acid is a systemic signal and an inducer of pathogenesis-related proteins in virus-infected Tobacco. *Plant Cell* **3**, 809–818 (1991).
- 207. Nawrath, C. & Métraux, J.-P. Salicylic acid induction—deficient mutants of Arabidopsis express PR-2 and PR-5 and accumulate high levels of camalexin after pathogen inoculation. *Plant Cell* **11**, 1393—1404 (1999).
- 208. Kew, J. N. C. & Kemp, J. A. An allosteric interaction between the NMDA receptor polyamine and ifenprodil sites in rat cultured cortical neurones. *Journal of Physiology* **512**, 17–28 (1998).
- 209. Kew, J. N. C., Trube, G. & Kemp, J. A. State-dependent NMDA receptor antagonism by Ro 8-4304, a novel NR2B selective, non-competitive, voltage-independent antagonist. *Br J Pharmacol* **123**, 463–472 (1998).
- 210. Kemp, John. A. & McKernan, R. M. NMDA receptor pathways as drug targets. *Nat Neurosci* **5**, 1039–1042 (2002).
- 211. Price, M. B., Jelesko, J. & Okumoto, S. Glutamate receptor homologs in plants: functions and evolutionary origins. *Front Plant Sci* **3**, 1–10 (2012).
- 212. Chiu, J. C. *et al.* Phylogenetic and expression analysis of the glutamate-receptor like gene family in Arabidopsis thaliana. *Mol Biol Evol* **19**, 1066–1082 (2002).
- 213. Gangwar, S. P. *et al.* Structure of the Arabidopsis glutamate receptor-like channel GLR3.2 ligand-binding domain. *Structure* **29**, 161-169.e4 (2021).
- 214. Green, M. N. *et al.* Structure of the Arabidopsis thaliana glutamate receptor-like channel GLR3.4. *Mol Cell* **81**, 3216-3226.e8 (2021).
- 215. Mandava, N. B. Plant growth-promoting brassinosteroids. *Annu Rev Plant Physiol Plant Mol Biol* **39**, 23–52 (1988).
- 216. Kudla, J., Batistič, O. & Hashimoto, K. Calcium signals: the lead currency of plant information processing. *Plant Cell* **22**, 541–563 (2010).
- 217. Michard, E. *et al.* Glutamate receptor–like genes form Ca2+ channels in pollen tubes and are regulated by pistil D-Serine. *Science* (1979) **332**, 434–437 (2011).
- 218. Vincill, E. D., Bieck, A. M. & Spalding, E. P. Ca2+ conduction by an amino acid-gated ion channel related to glutamate receptors. *Plant Physiol* **159**, 40–46 (2012).
- 219. Forde, B. G. & Roberts, M. R. Glutamate receptor-like channels in plants: a role as amino acid sensors in plant defence? *F1000Prime Rep* **6**, (2014).
- 220. De Vriese, K., Costa, A., Beeckman, T. & Vanneste, S. Pharmacological strategies for manipulating plant Ca2+ signalling. *Int J Mol Sci* **19**, 1506 (2018).
- 221. Simon, E. W. The symptoms of calcium deficiency in plants. *New Phytologist* **80**, 1–15 (1978).
- 222. Honoré, T. *et al.* Quinoxalinediones: potent competitive non-NMDA glutamate receptor antagonists. *Science* (1979) **241**, 701–703 (1988).
- 223. Lam, H.-M. et al. Glutamate-receptor genes in plants. Nature 396, 125–126 (1998).
- 224. Tapken, D. *et al.* A plant homolog of animal glutamate receptors is an ion channel gated by multiple hydrophobic amino acids. *Sci Signal* **6**, (2013).
- 225. Vatsa, P. *et al.* Involvement of putative glutamate receptors in plant defence signaling and no production. *Biochimie* **93**, 2095–2101 (2011).
- 226. Feng, S. *et al.* The glutamate receptor plays a role in defense against Botrytis cinerea through electrical signaling in tomato. *Applied Sciences* **11**, 11217 (2021).
- 227. Singh, S. K. & Chang, I.-F. Pharmacological studies with specific agonist and antagonist of animal iGluR on root growth in Arabidopsis thaliana. in *GABA And Glutamate New*

- Developments In Neurotransmission Research (ed. Samardzic, J.) 47–63 (InTech, 2018). doi:10.5772/intechopen.72121.
- 228. Weiss, J. H., Koh, J. & Choi, D. W. Neurotoxicity of β-N-methylamino-l-alanine (BMAA) and β-N-oxalylamino-l-alamine (BOAA) on cultured cortical neurons. *Brain Res* **497**, 64–71 (1989).
- 229. Brenner, E. D. *et al.* Arabidopsis mutants resistant to S(+)- β -Methyl- α , β -Diaminopropionic Acid, a cycad-derived glutamate receptor Aaonist. *Plant Physiol* **124**, 1615–1624 (2000).
- 230. Brenner, E. D., Feinberg, P., Runko, S. & Coruzzi, G. M. A mutation in the Proteosomal Regulatory Particle AAA-ATPase-3 in Arabidopsis impairs the light-specific hypocotyl elongation response elicited by a glutamate receptor agonist, BMAA. *Plant Mol Biol* **70**, 523–533 (2009).
- 231. Zhao, Q. *et al.* Involvement of calmodulin in regulation of primary root elongation by N-3-oxo-hexanoyl homoserine lactone in Arabidopsis thaliana. *Front Plant Sci* **5**, (2015).
- 232. Cheval, C., Aldon, D., Galaud, J.-P. & Ranty, B. Calcium/calmodulin-mediated regulation of plant immunity. *Biochimica et Biophysica Acta (BBA) Molecular Cell Research* **1833**, 1766–1771 (2013).
- 233. Kwaaitaal, M., Maintz, J., Cavdar, M. & Panstruga, R. On the ligand binding profile and desensitization of plant ionotropic glutamate receptor (iGluR)-like channels functioning in MAMP-triggered Ca2+ influx. *Plant Signal Behav* **7**, 1373–1377 (2012).
- 234. Dubos, C., Willment, J., Huggins, D., Grant, G. H. & Campbell, M. M. Kanamycin reveals the role played by glutamate receptors in shaping plant resource allocation. *The Plant Journal* **43**, 348–355 (2005).
- 235. Williams, K., Kashiwagi, K., Fukuchi, J.-I. & Igarashi, K. An acidic amino acid in the N-methyl-D-aspartate receptor that is important for spermine stimulation. *Mol Pharmacol* **48**, 1087–1098 (1995).
- 236. Kang, J. & Turano, F. J. The putative glutamate receptor 1.1 (AtGLR1.1) functions as a regulator of carbon and nitrogen metabolism in Arabidopsis thaliana. *Proceedings of the National Academy of Sciences* **100**, 6872–6877 (2003).
- 237. Kang, J., Mehta, S. & Turano, F. J. The putative glutamate receptor 1.1 (AtGLR1.1) in Arabidopsis thaliana regulates abscisic acid biosynthesis and signaling to control development and water loss. *Plant Cell Physiol* **45**, 1380–1389 (2004).
- 238. Rajjou, L. et al. Seed germination and vigor. Annu Rev Plant Biol 63, 507–533 (2012).
- 239. Kong, D. *et al.* Arabidopsis glutamate receptor homolog3.5 modulates cytosolic Ca2+ level to counteract effect of abscisic acid in seed germination . *Plant Physiol* **167**, 1630–1642 (2015).
- 240. Cheng, Y., Zhang, X., Sun, T., Tian, Q. & Zhang, W.-H. Glutamate receptor homolog3.4 is involved in regulation of seed germination under salt stress in Arabidopsis. *Plant Cell Physiol* **59**, 978–988 (2018).
- 241. Ju, C., Song, Y. & Kong, D. Arabidopsis GLR3.5-modulated seed germination involves GA and ROS signaling. *Plant Signal Behav* **15**, 1729537 (2020).
- 242. Song, Y. *et al.* Abscisic acid as an internal integrator of multiple physiological processes modulates leaf senescence onset in Arabidopsis thaliana. *Front Plant Sci* **7**, (2016).
- 243. Dixon, D. P. & Edwards, R. Glutathione transferases. *Arabidopsis Book* **8**, e0131 (2010).

- 244. Noctor, G. *et al.* Glutathione in plants: an integrated overview. *Plant Cell Environ* **35**, 454–484 (2012).
- 245. Huber, M. *et al.* Disruption of the N α -Acetyltransferase NatB causes sensitivity to reductive stress in Arabidopsis thaliana. *Front Plant Sci* **12**, (2022).
- 246. Wudick, M. M., Michard, E., Oliveira Nunes, C. & Feijó, J. A. Comparing plant and animal glutamate receptors: common traits but different fates? *J Exp Bot* **69**, 4151–4163 (2018).
- 247. Meyer, A. J. & Fricker, M. D. Control of demand-driven biosynthesis of glutathione in green Arabidopsis suspension culture cells. *Plant Physiol* **130**, 1927–1937 (2002).
- 248. Vernoux, T. *et al.* The ROOT MERISTEMLESS1/CADMIUM SENSITIVE2 gene defines a glutathione-dependent pathway involved in initiation and maintenance of cell division during postembryonic root development. *Plant Cell* **12**, 97–109 (2000).
- 249. Cheng, M. *et al.* Increased glutathione contributes to stress tolerance and global translational changes in Arabidopsis. *The Plant Journal* **83**, 926–939 (2015).
- 250. Urbancsok, J., Bones, A. M. & Kissen, R. Arabidopsis mutants impaired in glutathione biosynthesis exhibit higher sensitivity towards the glucosinolate hydrolysis product allyl-isothiocyanate. *Sci Rep* **8**, 9809 (2018).
- 251. Bangash, S. A. K. *et al.* Low-glutathione mutants are impaired in growth but do not show an increased sensitivity to moderate water deficit. *PLoS One* **14**, e0220589 (2019).
- 252. Whitesell, L., Mimnaugh, E. G., De Costa, B., Myers, C. E. & Neckers, L. M. Inhibition of heat shock protein HSP90-pp60v-src heteroprotein complex formation by benzoquinone ansamycins: essential role for stress proteins in oncogenic transformation. *Proceedings of the National Academy of Sciences* **91**, 8324–8328 (1994).
- 253. Takahashi, A., Casais, C., Ichimura, K. & Shirasu, K. HSP90 interacts with RAR1 and SGT1 and is essential for RPS2-mediated disease resistance in Arabidopsis.

 *Proceedings of the National Academy of Sciences 100, 11777–11782 (2003).
- 254. Bègue, H., Jeandroz, S., Blanchard, C., Wendehenne, D. & Rosnoblet, C. Structure and functions of the chaperone-like p97/CDC48 in plants. *Biochim Biophys Acta* **1861**, 3053–3060 (2017).
- 255. Banerjee, S. *et al.* 2.3 Å resolution cryo-EM structure of human p97 and mechanism of allosteric inhibition. *Science* (1979) **351**, 871–875 (2016).
- 256. Park, S., Rancour, D. M. & Bednarek, S. Y. In planta analysis of the cell cycle-dependent localization of AtCDC48A and its critical roles in cell division, expansion, and differentiation . *Plant Physiol* **148**, 246–258 (2008).
- 257. Bègue, H., Mounier, A., Rosnoblet, C. & Wendehenne, D. Toward the understanding of the role of CDC48, a major component of the protein quality control, in plant immunity. *Plant Science* **279**, 34–44 (2019).
- 258. Weiland, M., Mancuso, S. & Baluska, F. Signalling via glutamate and GLRs in Arabidopsis thaliana. *Functional Plant Biology* **43**, 1 (2016).
- 259. Kan, C.-C., Chung, T.-Y., Wu, H.-Y., Juo, Y.-A. & Hsieh, M.-H. Exogenous glutamate rapidly induces the expression of genes involved in metabolism and defense responses in rice roots. *BMC Genomics* **18**, 1–17 (2017).
- 260. Toyota, M. *et al.* Glutamate triggers long-distance, calcium-based plant defense signaling. *Science* (1979) **361**, 1112–1115 (2018).

- 261. Li, Z.-G., Ye, X.-Y. & Qiu, X.-M. Glutamate signaling enhances the heat tolerance of maize seedlings by plant glutamate receptor-like channels-mediated calcium signaling. *Protoplasma* **256**, 1165–1169 (2019).
- 262. Goto, Y. *et al.* Exogenous treatment with glutamate induces immune responses in Arabidopsis. *Molecular Plant-Microbe Interactions*® **33**, 474–487 (2020).
- 263. Scholl, R., May, S. & Ware, D. Seed and molecular resources for Arabidopsis. *Plant Physiol* **124**, 1477–1480 (2000).
- 264. Wagner, U., Edwards, R., Dixon, D. P. & Mauch, F. Probing the diversity of the Arabidopsis glutathione S-transferase gene family. *Plant Mol Biol* **49**, 515–532 (2002).
- 265. Reinemer, P. *et al.* Three-dimensional structure of glutathione-S-transferase from Arabidopsis thaliana at 2.2 Å resolution: structural characterization of herbicide-conjugating plant glutathione S-transferases and a novel active site architecture. *J Mol Biol* **255**, 289–309 (1996).
- 266. Prade, L., Huber, R. & Bieseler, B. Structures of herbicides in complex with their detoxifying enzyme glutathione S-transferase explanations for the selectivity of the enzyme in plants. *Structure* **6**, 1445–1452 (1998).
- 267. Dixon, D. P., Sellars, J. D. & Edwards, R. The Arabidopsis phi class glutathione transferase AtGSTF2: binding and regulation by biologically active heterocyclic ligands. *Biochemical Journal* **438**, 63–70 (2011).
- 268. Ahmad, L., Rylott, E. L., Bruce, N. C., Edwards, R. & Grogan, G. Structural evidence for Arabidopsis glutathione transferase AtGSTF2 functioning as a transporter of small organic ligands. *FEBS Open Bio* **7**, 122–132 (2017).
- 269. Borkovich, K. A., Farrelly, F. W., Finkelstein, D. B., Taulien, J. & Lindquist, S. HSP82 is an essential protein that is required in higher concentrations for growth of cells at higher temperatures. *Mol Cell Biol* **9**, 3919–3930 (1989).
- 270. Boyes, D. C. *et al.* Growth stage—based phenotypic analysis of Arabidopsis. *Plant Cell* **13**, 1499—1510 (2001).
- 271. Zhang, C. *et al.* Uptake and translocation of organic pollutants in plants: a review. *J Integr Agric* **16**, 1659–1668 (2017).
- 272. Scribner, J. D., Scribner, N. K. & Koponen, G. Metabolism and nucleic acid binding of 7-fluoro-2-acetamidofluorene in rats: oxidative defluorination and apparent dissociation from hepatocarcinogenesis of 8-(N-arylamide)guanine adducts on DNA. *Chem Biol Interact* **40**, 27–43 (1982).
- 273. Oravec, C. T., Daniel, F. B. & Wong, L. K. Comparative metabolism of 7,12-dimethylbenz[a]anthracene and its non-carcinogenic 2-fluoro analogue by Syrian hamster embryo cells. *Cancer Lett* **21**, 43–55 (1983).
- 274. Li, X., Clarke, J. D., Zhang, Y. & Dong, X. Activation of an EDS1-mediated R-gene pathway in the snc1 mutant leads to constitutive, NPR1-independent pathogen resistance. *Molecular Plant-Microbe Interactions*® **14**, 1131–1139 (2001).
- 275. Canet, J. V., Dobón, A., Ibáñez, F., Perales, L. & Tornero, P. Resistance and biomass in Arabidopsis: a new model for salicylic acid perception. *Plant Biotechnol J* **8**, 126–141 (2010).
- 276. Staiger, D. & Brown, J. W. S. Alternative splicing at the intersection of biological timing, development, and stress responses. *Plant Cell* **25**, 3640–3656 (2013).
- 277. Jordan, T., Schornack, S. & Lahaye, T. Alternative splicing of transcripts encoding toll-like plant resistance proteins what's the functional relevance to innate immunity? *Trends Plant Sci* **7**, 392–398 (2002).

- 278. Zhang, X.-C. & Gassman, W. RPS4-mediated disease resistance requires the combined presence of RPS4 transcripts with full-length and truncated open reading frames. *Plant Cell* **15**, 2333–2342 (2003).
- 279. Jiang, J. *et al.* Integrating omics and alternative splicing reveals insights into grape response to high temperature. *Plant Physiol* **173**, 1502–1518 (2017).
- 280. Lu, Y. *et al.* Alternative splicing diversified the heat response and evolutionary etrategy of conserved heat shock protein 90s in hexaploid wheat (Triticum aestivum L.). *Front Genet* **11**, 1–12 (2020).
- 281. Esteve-Bruna, D. *et al.* Prefoldins contribute to maintaining the levels of the spliceosome LSM2–8 complex through HSP90 in Arabidopsis. *Nucleic Acids Res* **48**, 6280–6293 (2020).
- 282. Kwaaitaal, M., Huisman, R., Maintz, J., Reinstädler, A. & Panstruga, R. Ionotropic glutamate receptor (iGluR)-like channels mediate MAMP-induced calcium influx in Arabidopsis thaliana. *Biochemical Journal* **440**, 355–365 (2011).
- 283. Kong, D. *et al.* L-Met activates Arabidopsis GLR Ca2+ channels upstream of ROS production and regulates stomatal movement. *Cell Rep* **17**, 2553–2561 (2016).
- 284. Alfieri, A. et al. The structural bases for agonist diversity in an Arabidopsis thaliana glutamate receptor-like channel. *Proceedings of the National Academy of Sciences* **117**, 752–760 (2020).
- 285. Tian, W. *et al.* A calmodulin-gated calcium channel links pathogen patterns to plant immunity. *Nature* **572**, 131–135 (2019).
- 286. Bègue, H. *et al.* The chaperone-like protein CDC48 regulates ascorbate peroxidase in Tobacco. *J Exp Bot* **70**, 2665–2681 (2019).
- 287. Wang, T., Li, J. & Shen, Q.-H. Regulation of NLR stability in plant immunity. *Front Agric Sci Eng* **6**, 97–104 (2019).
- 288. Ao, K. *et al.* SCFSNIPER7 controls protein turnover of unfoldase CDC48A to promote plant immunity. *New Phytologist* **229**, 2795–2811 (2021).
- 289. Ge, Y. *et al.* p97 regulates GluA1 homomeric AMPA receptor formation and plasma membrane expression. *Nat Commun* **10**, 4089 (2019).
- 290. Guerriero, C. J., Weiberth, K. F. & Brodsky, J. L. HSP70 targets a cytoplasmic quality control substrate to the SAN1p ubiquitin ligase. *Journal of Biological Chemistry* **288**, 18506–18520 (2013).
- 291. Bègue, H., Mounier, A., Rosnoblet, C. & Wendehenne, D. Toward the understanding of the role of CDC48, a major component of the protein quality control, in plant immunity. *Plant Science* **279**, 34–44 (2019).
- 292. Aryal, U. K., McBride, Z., Chen, D., Xie, J. & Szymanski, D. B. Analysis of protein complexes in Arabidopsis leaves using size exclusion chromatography and label-free protein correlation profiling. *J Proteomics* **166**, 8–18 (2017).
- 293. Rosnoblet, C. *et al.* The chaperone-like protein CDC48 regulates ubiquitin-proteasome system in plants. *Plant Cell Environ* **44**, 2636–2655 (2021).
- 294. Henkes, S., Sonnewald, U., Badur, R., Flachmann, R. & Stitt, M. A small decrease of plastid transketolase activity in antisense Tobacco transformants has dramatic effects on photosynthesis and phenylpropanoid metabolism. *Plant Cell* **13**, 535–551 (2001).
- 295. Dixon, R. A. & Paiva, N. L. Stress-induced phenylpropanoid metabolism. *Plant Cell* **7**, 1085–1097 (1995).

- 296. Andriotis, V. M. E. & Smith, A. M. The plastidial pentose phosphate pathway is essential for postglobular embryo development in Arabidopsis. *Proceedings of the National Academy of Sciences* **116**, 15297–15306 (2019).
- 297. Rocha, A. G. *et al.* Phosphorylation of Arabidopsis transketolase at Ser428 provides a potential paradigm for the metabolic control of chloroplast carbon metabolism. *Biochemical Journal* **458**, 313–322 (2014).
- 298. Khozaei, M. *et al.* Overexpression of plastid transketolase in Tobacco results in a thiamine auxotrophic phenotype. *Plant Cell* **27**, 432–447 (2015).
- 299. Zhao, B., Huo, J., Liu, N., Zhang, J. & Dong, J. Transketolase is identified as a target of herbicidal substance α-Terthienyl by proteomics. *Toxins (Basel)* **10**, 41 (2018).
- 300. Rouhier, N. *et al.* Identification of plant glutaredoxin targets. *Antioxid Redox Signal* **7**, 919–929 (2005).
- 301. Muñoz-Bertomeu, J. *et al.* Plastidial glyceraldehyde-3-phosphate dehydrogenase deficiency leads to altered root development and affects the sugar and amino acid balance in Arabidopsis . *Plant Physiol* **151**, 541–558 (2009).
- 302. Rius, S. P., Casati, P., Iglesias, A. A. & Gomez-Casati, D. F. Characterization of Arabidopsis lines deficient in GAPC-1, a cytosolic NAD-dependent glyceraldehyde-3-phosphate dehydrogenase. *Plant Physiol* **148**, 1655–1667 (2008).
- 303. Henry, E., Fung, N., Liu, J., Drakakaki, G. & Coaker, G. Beyond glycolysis: GAPDHs are multi-functional enzymes involved in regulation of ROS, autophagy, and plant immune responses. *PLoS Genet* **11**, e1005199 (2015).
- 304. Han, S. *et al.* Cytoplastic glyceraldehyde-3-phosphate dehydrogenases interact with ATG3 to negatively regulate autophagy and immunity in Nicotiana benthamiana. *Plant Cell* **27**, 1316–1331 (2015).
- 305. Romero-Puertas, M. C. *et al.* Proteomic analysis of S-nitrosylated proteins in Arabidopsis thaliana undergoing hypersensitive response. *Proteomics* **8**, 1459–1469 (2008).
- 306. Guo, L. et al. Cytosolic glyceraldehyde-3-phosphate dehydrogenases interact with phospholipase D δ to transduce hydrogen peroxide signals in the Arabidopsis response to stress. Plant Cell **24**, 2200–2212 (2012).
- 307. Vescovi, M. *et al.* Nuclear accumulation of cytosolic glyceraldehyde-3-phosphate dehydrogenase in cadmium-stressed Arabidopsis roots . *Plant Physiol* **162**, 333–346 (2013).
- 308. Bedhomme, M. *et al.* Glutathionylation of cytosolic glyceraldehyde-3-phosphate dehydrogenase from the model plant Arabidopsis thaliana is reversed by both glutaredoxins and thioredoxins in vitro. *Biochemical Journal* **445**, 337–347 (2012).
- 309. Zaffagnini, M. *et al.* Glutathionylation primes soluble glyceraldehyde-3-phosphate dehydrogenase for late collapse into insoluble aggregates. *Proceedings of the National Academy of Sciences* **116**, 26057–26065 (2019).
- 310. Hartl, F. U., Bracher, A. & Hayer-Hartl, M. Molecular chaperones in protein folding and proteostasis. *Nature* **475**, 324–332 (2011).
- 311. Mannini, B. & Chiti, F. Chaperones as suppressors of protein misfolded oligomer toxicity. *Front Mol Neurosci* **10**, (2017).
- 312. Wang, W., Vinocur, B., Shoseyov, O. & Altman, A. Role of plant heat-shock proteins and molecular chaperones in the abiotic stress response. *Trends Plant Sci* **9**, 244–252 (2004).

- 313. Su, P.-H. & Li, H. Stromal HSP70 is important for protein translocation into pea and Arabidopsis chloroplasts. *Plant Cell* **22**, 1516–1531 (2010).
- 314. Zemanovic, S. *et al.* Dynamic phosphorylation of the C terminus of HSP70 regulates the mitochondrial import of SOD2 and redox balance. *Cell Rep* **25**, 2605-2616.e7 (2018).
- 315. Noël, L. D. *et al.* Interaction between SGT1 and cytosolic/nuclear HSC70 chaperones regulates Arabidopsis immune responses. *Plant Cell* **19**, 4061–4076 (2007).
- 316. Cazalé, A.-C. *et al.* Altered expression of cytosolic/nuclear HSC70-1 molecular chaperone affects development and abiotic stress tolerance in Arabidopsis thaliana. *J Exp Bot* **60**, 2653–2664 (2009).
- 317. Clément, M. *et al.* The cytosolic/nuclear HSC70 and HSP90 molecular chaperones are important for stomatal closure and modulate abscisic acid-dependent physiological responses in Arabidopsis . *Plant Physiol* **156**, 1481–1492 (2011).
- 318. Spiechowicz, M., Zylicz, A., Bieganowski, P., Kuznicki, J. & Filipek, A. Hsp70 is a new target of Sgt1—an interaction modulated by S100A6. *Biochem Biophys Res Commun* **357**, 1148–1153 (2007).
- 319. Bansal, P. K., Abdulle, R. & Kitagawa, K. SGT1 associates with HSP90: an initial step of assembly of the core kinetochore complex. *Mol Cell Biol* **24**, 8069–8079 (2004).
- 320. Hao, H. et al. HSP90 and its inhibitors (review). Oncol Rep 23, 1438–1492 (2010).
- 321. Muskett, P. R. *et al.* Arabidopsis RAR1 exerts rate-limiting control of R gene–mediated defenses against multiple pathogens. *Plant Cell* **14**, 979–992 (2002).
- 322. Holt, B. F., Belkhadir, Y. & Dangl, J. L. Antagonistic control of disease resistance protein stability in the plant immune system. *Science* (1979) **309**, 929–932 (2005).
- 323. Zhang, M., Kadota, Y., Prodromou, C., Shirasu, K. & Pearl, L. H. Structural basis for assembly of HSP90-SGT1-CHORD protein complexes: implications for chaperoning of NLR innate immunity receptors. *Mol Cell* **39**, 269–281 (2010).
- 324. Li, Y., Yang, S., Yang, H. & Hua, J. The TIR-NB-LRR Gene SNC1 is regulated at the transcript level by multiple factors. *Molecular Plant-Microbe Interactions* **20**, 1449–1456 (2007).
- 325. Austin, M. J. *et al.* Regulatory role of SGT1 in early R gene-mediated plant defenses. *Science* (1979) **295**, 2077–2080 (2002).
- 326. Huang, S. *et al.* HSP90s are required for NLR immune receptor accumulation in Arabidopsis. *The Plant Journal* **79**, 427–439 (2014).
- 327. Prince, T. L. *et al.* Client proteins and small molecule inhibitors display distinct binding preferences for constitutive and stress-induced HSP90 isoforms and their conformationally restricted mutants. *PLoS One* **10**, e0141786 (2015).
- 328. Liu, H.-T., Sun, D.-Y. & Zhou, R.-G. Ca2+ and AtCaM3 are involved in the expression of heat shock protein gene in Arabidopsis. *Plant Cell Environ* **28**, 1276–1284 (2005).
- 329. Kiang, J. G., Carr, F. E., Burns, M. R. & McClain, D. E. HSP-72 synthesis is promoted by increase in [Ca2+]i or activation of G proteins but not pHi or cAMP. *American Journal of Physiology-Cell Physiology* **267**, C104–C114 (1994).
- 330. Kuznetsov, V., Andreev, I. & Trofimova, M. The synthesis of HSPs in sugar beet suspension culture cells under hyperthermia exhibits differential sensitivity to calcium. *IUBMB Life* **45**, 269–278 (1998).
- 331. Hernández, M. P., Sullivan, W. P. & Toft, D. O. The assembly and intermolecular properties of the HSP70-HOP-HSP90 molecular chaperone complex. *Journal of Biological Chemistry* **277**, 38294–38304 (2002).

- 332. Pratt, W. B., Galigniana, M. D., Morishima, Y. & Murphy, P. J. M. Role of molecular chaperones in steroid receptor action. *Essays Biochem* **40**, 41–58 (2004).
- 333. Picard, D. Heat-shock protein 90, a chaperone for folding and regulation. *Cellular and Molecular Life Sciences* **59**, 1640–1648 (2002).
- 334. Picard, D. Chaperoning steroid hormone action. *Trends in Endocrinology & Metabolism* **17**, 229–235 (2006).
- 335. Fan, J., Hill, L., Crooks, C., Doerner, P. & Lamb, C. Abscisic acid has a key role in modulating diverse plant-pathogen interactions. *Plant Physiol* **150**, 1750–1761 (2009).
- 336. Howard, B. E. *et al.* High-throughput RNA sequencing of pseudomonas-infected Arabidopsis reveals hidden transcriptome complexity and novel splice variants. *PLoS One* **8**, e74183 (2013).
- 337. De Vos, M. *et al.* Signal signature and transcriptome changes of Arabidopsis during pathogen and insect attack. *Molecular Plant-Microbe Interactions®* **18**, 923–937 (2005).
- 338. Kumar, D. & Chattopadhyay, S. Glutathione modulates the expression of heat shock proteins via the transcription factors BZIP10 and MYB21 in Arabidopsis. *J Exp Bot* **69**, 3729–3743 (2018).
- 339. Zhu, Y., Qian, W. & Hua, J. Temperature modulates plant defense responses through NB-LRR proteins. *PLoS Pathog* **6**, e1000844 (2010).
- 340. Shih, Y.-Y. *et al.* S-glutathionylation of HSP90 enhances its degradation and correlates with favorable prognosis of breast cancer. *Redox Biol* **57**, 1–10 (2022).
- 341. Mauch, F. & Dudler, R. Differential induction of distinct glutathione-S-transferases of wheat by xenobiotics and by pathogen attack. *Plant Physiol* **102**, 1193–1201 (1993).
- 342. Sappl, P. G., Oñate-Sánchez, L., Singh, K. B. & Millar, A. H. Proteomic analysis of glutathione S-transferases of Arabidopsis thaliana reveals differential salicylic acid-induced expression of the plant-specific phi and tau classes. *Plant Mol Biol* **54**, 205–219 (2004).
- 343. Lieberherr, D., Wagner, U., Dubuis, P.-H., Métraux, J.-P. & Mauch, F. The rapid induction of glutathione S-transferases AtGSTF2 and AtGSTF6 by avirulent Pseudomonas syringae is the result of combined salicylic acid and ethylene signaling. *Plant Cell Physiol* **44**, 750–757 (2003).
- 344. Su, T. *et al.* Glutathione-indole-3-acetonitrile is required for camalexin biosynthesis in Arabidopsis thaliana. *Plant Cell* **23**, 364–380 (2011).
- 345. Gullner, G., Komives, T., Király, L. & Schröder, P. Glutathione S-transferase enzymes in plant-pathogen interactions. *Front Plant Sci* **9**, 1–19 (2018).
- 346. Stavridou, E. *et al.* Tolerance of transplastomic Tobacco plants overexpressing a theta class glutathione transferase to abiotic and oxidative stresses. *Front Plant Sci* **9**, 1–17 (2019).
- 347. Brazier-Hicks, M. *et al.* Catabolism of glutathione conjugates in Arabidopsis thaliana. *Journal of Biological Chemistry* **283**, 21102–21112 (2008).
- 348. Murail, S., de Vries, S. J., Rey, J., Moroy, G. & Tufféry, P. SeamDock: an interactive and collaborative online docking resource to assist small compound molecular docking. *Front Mol Biosci* **8**, 1–8 (2021).
- 349. Bilang, J. & Sturm, A. Cloning and characterization of a glutathione S-transferase that can be photolabeled with 5-azido-indole-3-acetic acid. *Plant Physiol* **109**, 253–260 (1995).

- 350. Droog, FNJ., Hooykaas, PJJ. & van der Zaal, B. J. 2,4-dichlorophenoxyacetic acid and related chlorinated compounds inhibit two auxin-regulated type-III Tobacco glutathione S-transferases. *Plant Physiol* **107**, 1139–1146 (1995).
- 351. Mueller, L. A., Goodman, C. D., Silady, R. A. & Walbot, V. AN9, a Petunia Glutathione S-Transferase required for anthocyanin sequestration, is a flavonoid-binding protein. *Plant Physiol* **123**, 1561–1570 (2000).
- 352. Smith, A. P. *et al.* Arabidopsis AtGSTF2 is regulated by ethylene and auxin, and encodes a glutathione S-transferase that interacts with flavonoids. *The Plant Journal* **36**, 433–442 (2003).
- 353. Coleman, J., Blake-Kalff, M. & Davies, E. Detoxification of xenobiotics by plants: chemical modification and vacuolar compartmentation. *Trends Plant Sci* **2**, 144–151 (1997).
- 354. Zhang, M. *et al.* Structural and functional coupling of HSP90- and SGT1-centred multiprotein complexes. *EMBO J* **27**, 2789–2798 (2008).
- 355. Stebbins, C. E. *et al.* Crystal structure of an HSP90–geldanamycin complex: targeting of a protein chaperone by an antitumor agent. *Cell* **89**, 239–250 (1997).
- 356. Dejonghe, W. & Russinova, E. Plant chemical genetics: from phenotype-based screens to synthetic biology. *Plant Physiol* **174**, 5–20 (2017).
- 357. Halder, V. & Russinova, E. Understanding the language of drugged plants. *Nat Chem Biol* **15**, 1025–1028 (2019).

8 Abstract

One of the major problems globally, is the loss of crops due to pathogens and pests^{1,2}. While an immune response also reduces the yield of the crop^{91,92,95,100,101}. Knowledge about these pathways is vital to maintain healthy crops in the future because plant immunity and growth are an intricate connected process¹²⁷.

Chemical biology has been shown to be an appealing method to tackle this problem 356,357 . Huang et al. (2016) discovered a chemical, Ro8-4304, that was able to rescue the small phenotype of an auto-immune mutant named $chs3-2D^{166}$. However, the immunity was also reduced. But since this chemical rescued one characteristic, we believed it to be a good starting point for chemical optimization.

In this thesis, first important aspects of the chemical rescue of Ro8-4304 were determined, incl. temperature dependency, optimal concentration, and the ideal time of treatment. Secondly, chemical optimization was used to identify the important parts of the molecular structure. Changes on the fluorine site, or the alcohol group in the middle of the molecule were more destructive for the fresh weight rescue in *chs3-2D* seedlings than changes on the benzamide site. From the synthesized analogues, one analogue (Ro-A03) was able to rescue the fresh weight of *chs3-2D* to similar levels as Ro8-4304. Additionally, defence marker gene expression, an infection assay and salicylic acid quantification showed that *chs3-2D* treated with this analogue still had a decent immunity. So, Ro-A03 was able to un-couple growth and immunity in the *chs3-2D* mutant.

Lastly, using literature research and a binding assay, we identified putative direct binding proteins. Considering pharmaceutical, genetic mutant data, and literature, we suggest that HSP90 is the most likely binding target of Ro8-4304. Binding of the chemical Ro8-4304 to HSP90 in the *chs3-2D* mutant reduces the amount of activated CHS3, because the correct folding of this NLR receptor cannot take place without the active form of HSP90. The un-coupling effect of Ro-A03 is probably due to a less strong binding affinity and therefore only a medium amount of HSP90 is rendered inactive. Additionally, we demonstrated that GTSFs and GLRs are vital for the action of Ro8-4304. However, currently it is unclear if this is due to direct binding, a transporter function or due to a general effect of these proteins on immunity.

9 German summary / Deutsche Zusammenfassung

Der Verlust von Ernten aufgrund von Krankheitserregern und Schädlingen ist weltweit eines der größten Probleme ^{1,2}. Ebenfalls verringert eine Immunreaktion auch den Ertrag der Ernte ^{91,92,95,100,101}. Das Wissen über diese Ertrag- und Ernteverlauf ist in der Zukunft entscheidend für die Erhaltung gesunder Nutzpflanzen, da Pflanzenimmunität und Wachstum ein kompliziert verbundener Prozess sind ¹²⁷.

Die chemische Biologie hat sich als attraktive Methode erwiesen, um dieses Problem zu bewältigen ^{356,357}. Huang et al. (2016) entdeckten eine Chemikalie, Ro8-4304, die in der Lage war, den kleinen Phänotyp einer Autoimmun-Mutante namens chs3-2D zu retten ¹⁶⁶. Allerdings wurde die Immunität dabei ebenfalls reduziert. Da diese Chemikalie jedoch eine Eigenschaft rettete, hielten wir sie für einen guten Ausgangspunkt für eine chemische Optimierung.

In dieser Thesis, wurden erstens wichtige Aspekte der chemischen Rettung von Ro8-4304 entschlossen, einschließlich Temperaturabhängigkeit, die optimale Konzentration und den idealen Zeitpunkt der Behandlung. Zweitens, die chemische Optimierung wurde genutzt, um die wichtigen Teile der Molekülstruktur zu identifizieren. Veränderungen an der Fluorstelle, oder der Alkoholgruppe in der Mitte des Moleküls, waren für die Rettung des Frischgewichts der chs3-2D-Sämlinge schädlicher als Veränderungen an der Benzamidstelle. Von den synthetisierten Analogon war ein Analoga (Ro-A03) in der Lage, das Frischgewicht von chs3-2D auf ein ähnliches Niveau wie Ro8-4304 zu bringen. Und zwar "Expression von Verteidigungsmarkergenen", ein "Infektionstest" und die "Quantifizierung von Salicylsäure" zeigten dass chs3-2D, die mit diesem Analoga behandelt wurden, immer noch über eine gute Immunität verfügten. Ro-A03 war in der Lage, Wachstum und Immunität in der chs3-2D-Mutante zu entkoppeln.

Schließlich, identifizierten wir mithilfe von Literaturrecherchen und einem Bindungstest direkt Mutmaßlich bindende Proteine. Unter Berücksichtigung der pharmazeutischen, genetischen Mutationsdaten und der Literatur legen wir nahe, dass HSP90 das wahrscheinlichste Bindungsziel von Ro8-4304 ist. Bindung der Chemikalie Ro8-4304 an HSP90 in der chs3-2D-Mutante reduziert die Menge an aktiviertem CHS3, weil die korrekte Faltung dieses NLR-Rezeptors ohne die aktive Form von HSP90 nicht stattfinden kann. Der Entkopplungseffekt von Ro-A03 ist wahrscheinlich auf eine weniger starke Bindungsaffinität zurückzuführen und daher wird nur eine mittlere Menge an HSP90 inaktiviert. Außerdem haben wir gezeigt, dass GTSFs und GLRs für die Wirkung von Ro8-4304 entscheidend sind. Derzeit ist jedoch unklar, ob dies auf eine direkte Bindung, eine Transporterfunktion oder auf eine allgemeine Wirkung dieser Proteine auf die Immunität.

10 Declaration of Oath

I hereby declare, on oath, that I have written the present dissertation by my own and have not used any help other than the acknowledged resources and aids.

Leimuiden

Martine Wilhelmina Maria Keijzer

11 Acknowledgment

"Life is like a forest, straight ahead is impossible."
- O. Popov

Finding my way through this forest (PhD adventure) wouldn't have been possible without some support. The assistance of family and friends gave me a map, compass, and sometimes an axe to find my way and accomplish this thesis. Therefore, I would like to thank them in this final piece of my work.

I would like to first and foremost thank my parents: Sjaak and Joke Keijzer. Without their love, encouragement, and financial support this work would not have been possible.

Secondly, my sister, Eveline Keijzer.

We may not always see eye to eye with each other, but you are always there for me when it counts; advising me when I need it the most. Helping me with difficult data sets.

But a family is bigger than just parents, and siblings.

Therefore, I would like to thank everyone who I consider my family.

The people that are still here, but also the people that are only present in loving memory.

Especially, Ben and Rob Keijzer. Grandmother Jans Keijzer-Koot, Grandmother and

Grandfather Leny and Piet Tak, Grandmother and Grandfather Bep, and Herman Leeuwis.

Ada and Wim Buskermolen, Angela and Ron van Haasteren.

Notably, I would like to thank Christoph and Angelique Williams for always inviting me into their loving home. Officially, we may not be family, but I will always consider you as part of my Hamburg family.

A thesis is not only achieved by the student, but also by the master.

Therefore, I would like to thank my doctor father Stefan Hoth for his continued support, supervision, and wisdom. So, that I could achieve this work.

During my time in the lab, I was assisted by many great people, especially Christiane Debus.

Without every one of you, this work wouldn't have been possible.

Thank you.

I would also like to thank the students that contributed to this thesis: Andrii Zinchenko, Merle Hartmann, Michael-Ruben Glagowski, and Robert Domènech Eres. I hope that you learned a lot during your stay at the lab, and I wish you a fruitful future.

Lastly, I would like to thank all the people playing table tennis at NTSV.
Especially, Brigitte Bublitz, Marianne Rittscher, Meike Sonntag-Woidt, Angelika Schwartz-Kämmle, Soraya Becker, and Sandra Metzger de Barona.
I enjoyed playing table tennis with you, and without this let-out I wouldn't have been able to beat this thesis.

Finally, I would like to say I am grateful to all the people involved. Even if your name might be omitted in this acknowledgment, your contribution will always linger.